On Frequency Synchronization in OFDM-based Systems

DISSERTATION

zur Erlangung des akademischen Grades eines

Doktor–Ingenieurs
(Dr.–Ing.)

der Fakultät für Ingenieurwissenschaften und Informatik
der Universität Ulm

von

WEI ZHANG

AUS MUDANJIANG, VR CHINA

1. Gutachter:	Prof. Dr.-Ing. Jürgen Lindner
2. Gutachter:	Prof. Dr.-Ing. Albrecht Rothermel
Amtierender Dekan:	Prof. Dr. rer. nat. Helmuth Partsch

Ulm, 27. April 2007

Acknowledgments

This doctoral thesis is the result of my research work at the Institute of Information Technology, University of Ulm.

First, I wish to express my special gratitude and appreciation to Prof. Dr.-Ing. Jürgen Lindner, for his kindness, allowing me to join his research group, supervising my thesis, and encouraging me to go further on the way to become a professional.

Next, I am grateful to Prof. Dr.-Ing. Albrecht Rothermel, Institute of Microelectronics, for acting as the co-referee.

I would like to thank all my past and current colleagues for their patience, assistance, and careful proof-reading of this thesis.

Finally, heartfelt gratefulness to my husband Yongchun. Without his continuous encouragement and support I could not have finished this work.

Wei Zhang

Neu-Ulm, Mai 2007

Contents

Chapter 1

Introduction

Wireless communication with mobile phones and wireless local area networks has become a part of the human life. Equipped with a wireless card, a laptop allows people to work at any place in the office. More and more wireless multimedia services are expected for the future. This creates an ever-increasing bandwidth demand. On the other hand, frequency is a finite resource. Thus, bandwidth efficient transmission techniques are urgently required.

Orthogonal frequency division multiplexing (OFDM) is a multi-carrier transmission method which allows a bandwidth efficient data transmission with low implementation complexity. Unfortunately, uncoded OFDM will suffer from the frequency selective behavior of radio channels, which may give rise to deep fading on some subcarriers. Error control coding can be used to cope with this problem. The resulting *coded* OFDM (COFDM) has been adopted by some standards as a technique in the physical layer, e.g., *digital audio broadcasting* (DAB), *digital video broadcasting - terrestrial* (DVB-T), and *wireless local area network* (WLAN). Furthermore, for a multiuser scenario, *orthogonal frequency division multiple access* (OFDMA) has been adopted in IEEE standard 802.11.16 as a multiple access technique.

However, the redundancy introduced by coding in turn reduces the bandwidth efficiency. Therefore, other solutions, like *multicarrier spread spectrum* (MC-SS), are proposed to improve the bandwidth efficiency. They can overcome the deep fading and improve the performance of OFDM by means of diversity. For instance, *multicarrier - code division multiplexing* (MC-CDM) spreads the transmit symbols over not fully correlated subcarriers to achieve a diversity gain. For multiuser scenarios, two variants of MC-CDM, i.e., *code division multiplexing - orthogonal frequency division multiple access* (CDM-OFDMA) and *multicarrier - code division multiple access* (MC-CDMA) can be applied.

One drawback of OFDM which cannot be overcome by MC-CDM is its sensitivity to frequency offset. For instance, in the case of BPSK, a frequency offset less than 2% of the subcarrier frequency spacing in OFDM is required, in order to keep the *signal to interference and noise ratio* (SINR) not less than 30dB. In the uplink transmission, interference caused by the frequency offsets may destroy the orthogonality among the users, even if the channel is ideal.

Essentially, this thesis deals with frequency synchronization in OFDM-based systems, and much attention is paid to the uplink transmission. Based on the study of the influence of *carrier frequency offset* (CFO) on OFDM and MC-CDM, we describe vector-valued transmission models for the uplink of OFDMA, CDM-OFDMA, and MC-CDMA in the presence of CFOs. Furthermore, we propose an uplink frequency synchronization scheme by using interference cancellation techniques, along with a modified frequency offset estimator suited for the uplink of OFDMA and CDM-OFDMA.

The outline of this thesis is as follows:

Chapter 2 describes the basic concepts required for a better understanding of this work. A description of the wireless radio channel is given first. Then, traditional multiplexing and the corresponding multiple access methods are introduced. The principles of *multicarrier modulation* (MCM) and OFDM are explained afterwards. We also give a brief overview of the synchronization errors in OFDM. The chapter ends with an introduction to two conventional vector equalizers: *zero-forcing* (ZF) equalizer and *linear minimum mean square error* (LMMSE) equalizer, based on a linear transmission model.

Chapter 3 starts with a particular description of the modeling process of OFDM over a time-invariant channel with a limited delay spread. This model has been introduced, e.g., in [22]. Nevertheless, we explain it here again because it is of particular importance for the derivation of the transmission model including the influence of frequency offset in the next chapter. Furthermore, the definitions, features, and vector-valued mathematical descriptions are investigated for each OFDM-based transmission scheme. Simplified models are derived for the uplink transmission of pure OFDMA and CDM-OFDMA.

The effects of carrier frequency offset on OFDM-based systems are studied in Chapter 4. Basically, in frequency domain the main impacts of a CFO on OFDM can be expressed by a matrix. Accordingly, a vector-valued model can be derived for OFDM in the presence of CFO, and thus for other systems based on it.

Frequency synchronization in the uplink is a challenge for OFDM-based systems. The traditional technique with adjusting a master frequency of a local oscillator is not directly suitable for an uplink receiver. The basic idea we proposed in this work is treating the frequency offset as part of a composite channel, and as a consequence, frequency offset compensation can be realized by means of interference cancellation techniques. Based on the proposed transmission models, this is performed in Chapter 5 under the assumption that all estimates of CFOs are perfectly known. Simulations are also made to compare the performance of CDM-OFDMA and MC-CDMA in some different scenarios.

Subsequently, in Chapter 6 we deal with the CFO estimation for OFDMA systems. A broad overview of the CFO estimators developed for OFDM is given first. Then, we develop a modified data-aided *maximum likelihood* (ML) estimator for CFO estimation in the uplink. To avoid the *multiuser interference* (MUI) and improve the estimation accuracy, this estimator restores the orthogonality among the users, before the estimation is performed. It should be noted that the frequency offset estimators developed for OFDMA can also be used for CDM-OFDMA.

The thesis ends with a summary, a final discussion of the results, and suggestions for future research.

Parts of this work have been published in [90], [91], [92], [93], and [94].

Chapter 2

Basic Concepts

2.1 Chapter Overview

This chapter introduces some basic concepts used in the following chapters which are required for the understanding of this work. We begin with a review of wireless radio channels in Section 2.2.

The importance of *multiple access* for communication systems is then explained in Section 2.3, together with the classification of different multiplexing and multiple access methods.

Orthogonal Frequency Division Multiplexing (OFDM) is first introduced in Section 2.4 as an efficient realization of multicarrier transmission. The basic principle, parameters and properties of OFDM are described.

Section 2.5 gives an overview of the synchronization errors encountered in OFDM. The impacts of timing errors and carrier phase errors on OFDM transmission are discussed briefly. More details about carrier frequency offset, the main topic of this work, will be found in Chapter 4.

Some conventional equalization methods are used in the subsequent chapters. For clarity, in Section 2.6 we explain how these equalization approaches work on a vector-valued transmission model.

2.2 The Wireless Radio Channel

The wireless radio channel is defined as the space between the antennas of the transmitter and the receiver. The special conditions under which the radio wave propagation takes place have significant impact on the performance of communication systems [65]. This section is intended to review the features of wireless radio channels, their mathematical description, and statistical properties. In the end, we give a typical multipath channel model for simulations run in the subsequent chapters.

2.2.1 Two Important Features

Two important features of the wireless radio channels have significant influence on the signal arriving at the receiver antenna: *multipath propagation* and *time variance.*

Multipath Propagation

In a typical wireless propagation channel, due to the existence of obstacles, the electromagnetic waves from the transmitter antenna can experience reflection, scattering, or diffraction before reaching receive antennas. In other words, the transmitted wave can arrive at the receiver through several different paths with possibly different propagation delay. Such phenomenon is called *multipath propagation*, which introduces the time spread into the signal that is transmitted through the channel. For this reason, at the receiver the received signal is the superposition of several replicas of the transmitted signal. Each replica has its specific amplitude weighting, time delay, and phase shift. These replicas can add constructively or destructively, dependent on their relative phase. As a result, the total power of the resulting received signals varies with the relative phase, which is a function of carrier frequency and the relative propagation delay. This variation in the receiver power is called *signal fading.* If the bandwidth of the transmitted signal is much smaller than the *coherence bandwidth* of the channel, the channel is thus called *flat fading* channel. In contrast to flat fading, *frequency selective fading* is caused if the bandwidth of the transmitted signal is much larger than the coherence bandwidth of the channel. In consequence different spectral components of the signal have different gains (frequency transfer functions), and *inter-symbol interference* (ISI) is induced.

Time variance

Time variance is an inherent feature of most wireless channels. It results not only from the position change of the transmitter and receiver, or an obstacle changing its position, but also from the time variation of the medium. In one word, the channel varies with time because of *mobility.* Accordingly, the amplitude as well as the phase of the received signals will also change with time. Mobility also leads to a shift of the received frequency, called *Doppler shift.* For instance, in a narrowband mobile channel, Doppler shift is a function of the carrier frequency f_c and the movement speed in the direction of wave propagation, given by

$$f_d = f_c \cdot \frac{v}{c} \cos \zeta, \tag{2.1}$$

where v is the velocity of movement, c is the velocity of light, and ζ represents the azimuthal angle between direction of wave and direction of relative receiver movement. The received frequency is therefore described as

$$f = f_c - f_d, \tag{2.2}$$

and distributed in the range $[f_c - f_{d\,\max},\ f_c + f_{d\,\max}]$, where $f_{d\,\max} = + f_c \cdot \frac{v_{\max}}{c}$. If there exist multiple paths, we need to know the power distribution of incident waves, i.e., the *Doppler power spectral density*, $S_D(f_d)$, which can be plotted as a function of f_d [41],

$$S_D(f_d) = \begin{cases} \frac{\text{const}}{\pi\sqrt{f_{d\,\max}^2 - f_d^2}} & \text{for } |\ f_d| \leq f_{d\,\max}, \\ 0 & \text{otherwise.} \end{cases}$$

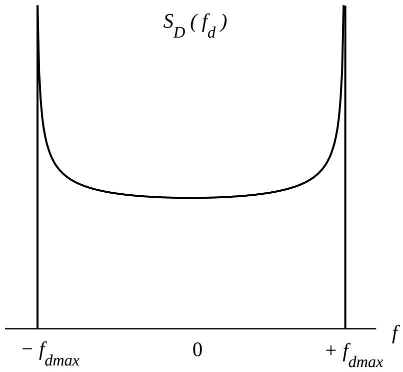

Figure 2.1: Jakes Doppler power spectrum.

An example of Doppler spectrum is plotted in Fig. 2.1.

Furthermore, if the channel impulse response (CIR) varies significantly in a symbol duration, or equivalently, in the frequency domain the *Doppler spread* B_D ($B_D = f_{d\,\max}$) is larger than the signal bandwidth, then the signal undergoes *fast fading;* By contrast, if B_D is much smaller than the signal bandwidth, the signal undergoes *slow fading*. In addition, the channel is considered time-invariant if the transmitter, the receiver, and the medium between them are static. Most wireless channels can be classified as *slowly* time-variant systems, also known as *quasi-static*.

In general, the time variations of the channel appear to be unpredictable to the user. Therefore, it is reasonable to characterize the time-variant multipath channel statistically [58]. In the following we give a tapped delay line model for the mathematical description of the channel.

2.2.2 Mathematical Description

Tapped Delay Line Model

By means of the time-variant channel impulse response, we can give a simple but comprehensive mathematical description of a time-variant multipath channel. The equivalent low-pass channel model is described as [49]

$$h(t,\tau) = \sum_{l=0}^{L-1} c_l(t) \cdot \delta(\tau - \tau_l(t)) = \sum_{l=0}^{L-1} |c_l(t)|\, e^{j\theta_l(t,\tau)} \delta(\tau - \tau_l(t)). \tag{2.3}$$

The parameters in (2.3) are described as follows:

- $\tau_l(t)$ time-variant propagation delay, $\tau_0(t)$ is assumed to be zero;
- $c_l(t)$ time-variant equivalent low-pass tap weighting;
- $|c_l(t)|$ amplitude of $c_l(t)$;

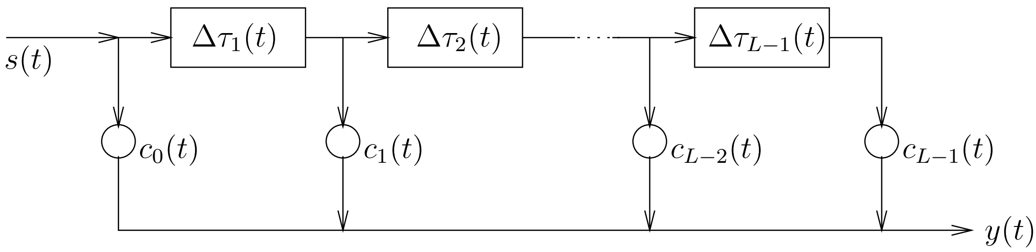

Figure 2.2: Tapped delay line model of the wireless channel.

- $\theta_l(t)$ time-variant phase of $c_l(t)$.

Fig. 2.2 illustrates such a channel model, where $\triangle\tau_l(t)$ represents the delay difference between $\tau_l(t)$ and $\tau_{l-1}(t)$. It is reasonable to suppose that signals via several different paths arrive at the receiver at the same time, i.e., have the same propagation delay. Equation (2.3) is therefore rewritten as

$$h(t,\tau) = \sum_{l=0}^{L-1}\sum_{k} a_{l,k}(t)\cdot\delta(\tau-\tau_l(t)) = \sum_{l=0}^{L-1}\sum_{k} |a_{l,k}(t)|\, e^{j\varphi_{l,k}(t)}\delta(\tau-\tau_l(t)). \tag{2.4}$$

Furthermore, if the autocorrelation functions of stochastic process $a_{l,k}(t)$ are independent of the absolute time t, and different weights $a_{l,k}(t)$ are mutually uncorrelated, i.e., the complex-valued tap weighting $a_{l,k}(t)$ is *wide sense stationary* (WSS), and *uncorrelated scattering* (US), channel model in (2.4) is called a WSSUS model.

If there exists no direct path between the transmitter and the receiver, we have a non-line-of-sight (NLOS) channel. In such a case any individual multipath component $a_{l,k}(t)$ can be modeled as a complex-valued Gaussian process, and in consequence the envelopes $|a_{l,k}(t)|$ at any instant t are Rayleigh distributed [59]. A Rayleigh distribution has a probability density function (PDF)

$$p(r) = \begin{cases} \frac{r}{\sigma^2}\exp\left[-\frac{r^2}{2\sigma^2}\right] & \text{for } \; r \geq 0, \\ 0 & \text{otherwise.} \end{cases} \tag{2.5}$$

The phase of $a_{l,k}(t)$ is uniformly distributed in the range of $(0, 2\pi)$. Moreover, $c_l(t)$ as well as $h(t,\tau)$ have the same statistical properties as $a_{l,k}(t)$. On the other hand, if there exists a line-of-sight (LOS) path, i.e., a dominant stationary non-faded path component, the envelope of $h(t,\tau)$, $|h(t,\tau)|$, has Ricean distribution. More details about the wireless channel can be seen in [58], [59], [49], [41], and [65].

2.2.3 Channel Model for Simulation

In digital communication systems, the received signals are normally (Dirac) sampled with a constant clock. The channel model in (2.3) is then simplified by

$$h(t,\tau) = \sum_{l=0}^{L-1} c_l(t)\cdot\delta(\tau-\tau_l), \qquad \tau_l = n\cdot\Delta\tau, \tag{2.6}$$

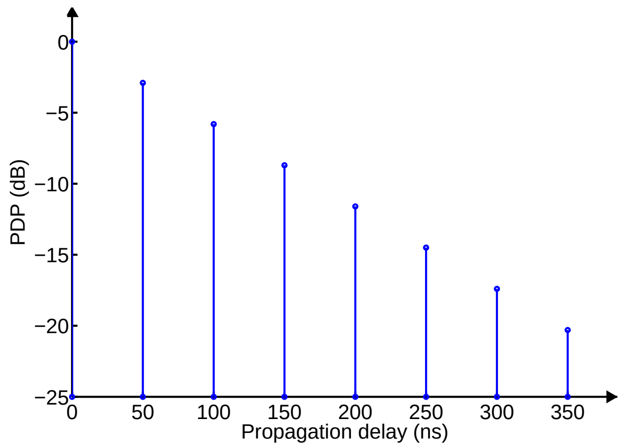

Figure 2.3: An indoor residential/office wireless channel model.

where $\frac{1}{\Delta\tau}$ is the sampling rate, and n is an integer. An one-path flat fading channel can be statistically modeled by $h(t) = c_0(t) \cdot \delta(t)$. If the channel is time-invariant, i.e., $c_0(t) = c_0$ being a constant, the channel is then an ideal channel; whereas for the time-variant case, we suppose $|c_0(t)|$ to be Rayleigh-distributed and the phase of $c_0(t)$ to be uniformly distributed. The latter assumption is also extended to multipath channels. We make use of an indoor residential/office model [1] for simulation, which is a time-variant eight-tap multipath channel with the power delay profile (PDP) given in table 1.1 and plotted in Fig. 2.3. Similarly, each tap has Rayleigh-distributed (absolute) amplitude and uniformly distributed phase.

tap	0	1	2	3	4	5	6	7
delay (ns)	0	50	100	150	200	250	300	350
average amplitude (dB)	0	-2.9	-5.8	-8.7	-11.6	-14.5	-17.4	-20.3

Table 1.1 An indoor residential/office wireless channel model.

In addition, in simulations an assumption, *block fading*, is often made. In case of block (vector) transmission, we use block fading to describe a slow fading effect where during transmission of one or several data blocks the channel stays constant, and between blocks the channel varies with time. Furthermore, a time-invariant two-path channel with CIR $\mathbf{h} = [1, 0.5]$ is often used in this work.

2.3 Multiplexing and Multiple Access

Multiplexing and *multiple access* refer to the sharing of a common transmission channel by a number of different users [56]. In general, multiplexing is the transmission of information from several sources, located at the same site, to several destinations over the same transmission channel. We emphasize 'sources' instead of 'users', since they are likely to belong to a single user. Multiple access, however, aims for containing multiple users in a communication system, where different users are located over a large geographical region, and share a common destination, like a base station (in a cellular radio network). For a given channel, the multiplexing can be done by

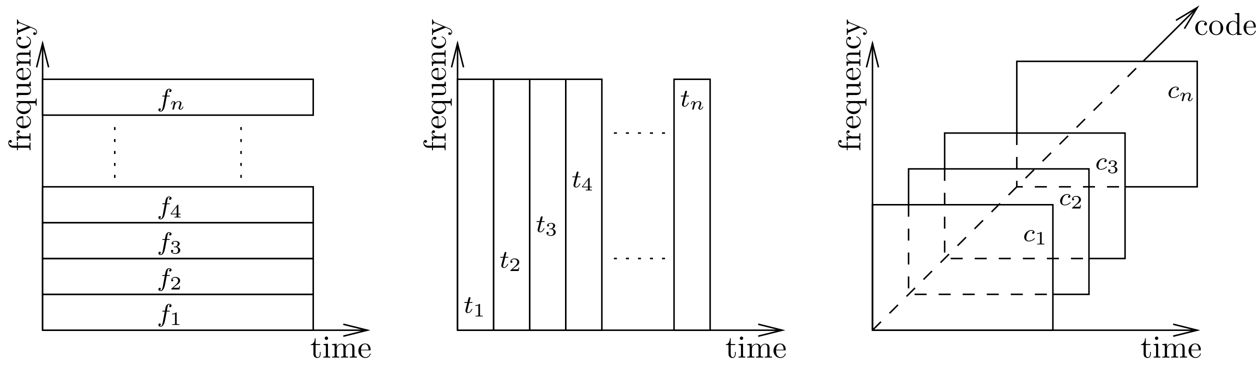

(a) FDM (b) TDM (c) CDM

Figure 2.4: Multiplexing techniques.

subdividing the channel capacity in to a number of portions (*channel division multiplexing*) and assigning a portion to each traffic source [56]. The channel division multiplexing can be done in different ways. Furthermore, each multiple access method has a corresponding multiplexing method, i.e.,

$$\textit{multiplexing method} \quad \Longleftrightarrow \quad \textit{multiple access method.}$$

FDM/FDMA One simple way to multiplex a channel is *frequency division multiplexing* (FDM) where the available channel bandwidth is subdivided into many non-overlapping sub-bands, which are so-called *frequency division channels,* as illustrated in Fig. 2.4(a). With FDM, signals in different sub-bands can be transmitted simultaneously over the same physical medium. Accordingly, in a *frequency division multiple access* (FDMA) system, each user accessing the base station is allocated a unique channel or sub-band. FDMA system is usually a narrowband system since the bandwidth of FDMA channels is relatively narrow. In addition, FDMA is not bandwidth efficient in that the channels are non-overlapping and once a channel is set to a specific user, it can not be used by other users even if it is not in use and stays idle.

TDM/TDMA With *time division multiplexing* (TDM) the radio spectrum is divided into time slots. Each time slot is a so-called *time division channel*, and each signal is transmitted one at a time in different time slots using the full frequency bandwidth, as shown in Fig. 2.4(b). In a *time division multiple access* (TDMA) system, an individual user is assigned one or several time slots on demand. Moreover, data transmission for users in such a system is not continuous but occurs in bursts. Such burst transmission results in larger overhead in TDMA for the synchronization as well as larger guard time as compared to FDMA.

CDM/CDMA By multiplying with a wideband signal, a narrowband signal is converted into a wideband noise-like signal before transmission. Such wideband signal is so-called spreading signal, which is a code sequence having a chip rate that is orders of the rate of the message. Simultaneously, transmitted narrowband signals are assigned by specific code sequences so that *Code division multiplexing* (CDM) is realized, see Fig. 2.4(c). Code sequences are carefully

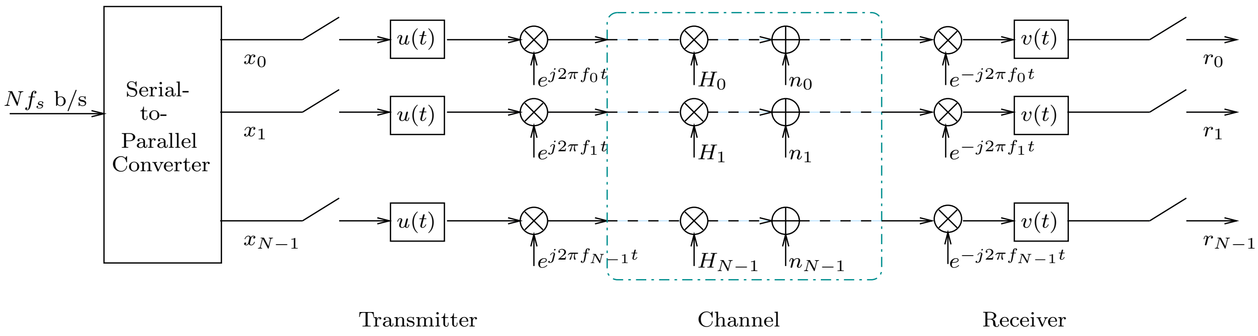

Figure 2.5: The basic principle of multicarrier modulation (MCM).

selected to ensure that each of them is orthogonal to or approximately orthogonal to others. A *code division multiple access* (CDMA) is inherently a wideband transmission system, where signals of different users overlap in both time and frequency, and are separated by using orthogonally coded spread spectrum modulation.

2.4 Multicarrier Modulation and OFDM

Multicarrier modulation (MCM) is a technique of data transmission by subdividing data into several (interleaved) data streams and using them to modulate parallel carriers. Therefore, it is a form of frequency division multiplexing (FDM) [7]. The basic principle of MCM is shown in Fig. 2.5. Transmit symbols of rate Nf_s b/s are first grouped into symbol blocks of length N, then serial-to-parallel converted, and finally modulated to a group of carriers with frequencies from f_0 to f_{N-1}. Due to parallel transmission, the symbol rate decreases to f_s and, thus, the transmission of an individual symbol is subject to the narrowband transmission and each symbol undergoes *non-frequency-selective* (flat) fading. To avoid interference from other carriers, guard band is required in a conventional FDM for keeping the orthogonality between the sub-bands. That means, sub-bands in terms of different carriers are non-overlapping. The corresponding transmit power spectra of a multicarrier (MC) system are like in Fig. 2.6(a). Such a system is not bandwidth-efficient because each of the signals must use a bandwidth equal to (if very sharp filters are implemented) or larger than Nyquist minimum, f_s, and steep bandpass filters are in demand [7].

To improve the bandwidth efficiency, a much narrower spacing of carriers is required, which can be achieved by a special MCM scheme, so-called *orthogonal frequency division multiplexing* (OFDM). OFDM was first proposed by Chang in 1966 [14]. In an OFDM system, carriers are allocated at the frequencies $f_n = nW/N$, where W represents the total available bandwidth, and n is an integer indicating carrier index, $0 \leq n \leq N-1$. For simplicity, we assume that $W = Nf_s$. Furthermore, if at the receiver the received signal is windowed by a rectangular window in the time domain, namely,

$$v(t) = \mathrm{rect}\left(\frac{t}{T_s}\right) \tag{2.7}$$

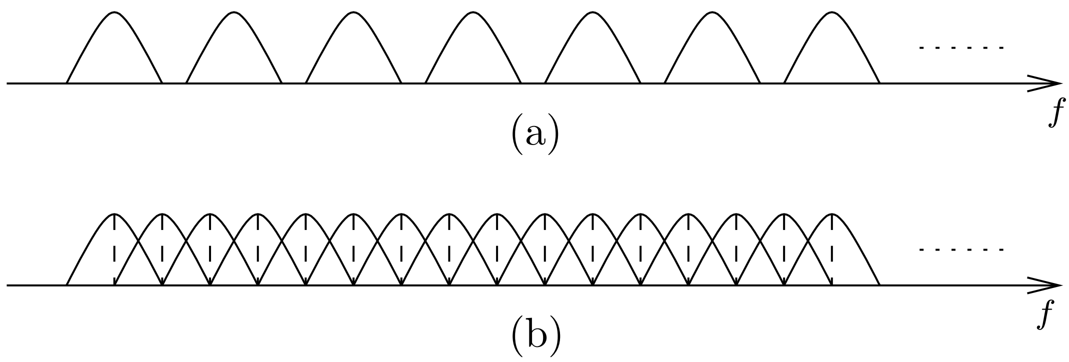

Figure 2.6: MCM transmit power spectra: conventional FDM (a) and OFDM (b).

with the spectrum of $\sin(x)/x$ shape

$$V(f) = T_s \cdot \mathrm{sinc}(\pi T_s f), \text{ where } \mathrm{sinc}(x) = \frac{\sin(x)}{x}, \tag{2.8}$$

then for each modulated carrier we have

$$\exp(j2\pi f_n t)\mathrm{rect}\left(\frac{t}{T_s}\right) \quad \Longleftrightarrow \quad T_s \cdot \mathrm{sinc}(\pi(T_s \cdot f - n)), \tag{2.9}$$

as shown in Fig. 2.7. $\mathrm{rect}(\cdot)$ denotes the rectangular function. It is easy to find that the carriers are mutually orthogonal, since during transmission of a symbol block the relationship

$$\int_{iT_s}^{(i+1)T_s} \exp(-j2\pi f_m t)\exp(j2\pi f_n t)dt = \delta_{mn} \tag{2.10}$$

holds, where δ_{mn} is Kronecker delta. Therefore, the spectra of different modulated carriers overlap, but at any carrier all other carriers have nulls in spectra. Making use of proper demodulation techniques on the receiving side, we can avoid the interference between carriers.

The MCM scheme in Fig. 2.5 is difficult to be implemented directly in practice, since the requirement for banks of subcarrier oscillators is not easy to be met. An alternative implementation is *discrete Fourier transform* (DFT) [84]. In a multicarrier system, the superposition of the baseband transmit signals at all frequencies can be expressed as

$$s(t) = \sum_{i=-\infty}^{+\infty} \sum_{n=0}^{N-1} x_{n,i} \exp(j2\pi f_n t) u(t - iT_s) \qquad T_s = \frac{1}{f_s}, \tag{2.11}$$

where $x_{n,i}$ represents the symbol transmitted at frequency f_n at time index i, and $u(t)$ is a rectangular function. Consider the transmission of one symbol block, e.g., $i = 0$. Substituting $f_n = nW/N$ into (2.11) and sampling $s(t)$ at instants $t = t_k = kT_s/N$, it yields

$$s_{k,0} = s(t_k) = \sum_{n=0}^{N-1} x_{n,0} \exp\left(j2\pi \frac{nk}{N}\right) \qquad 0 \le k < N. \tag{2.12}$$

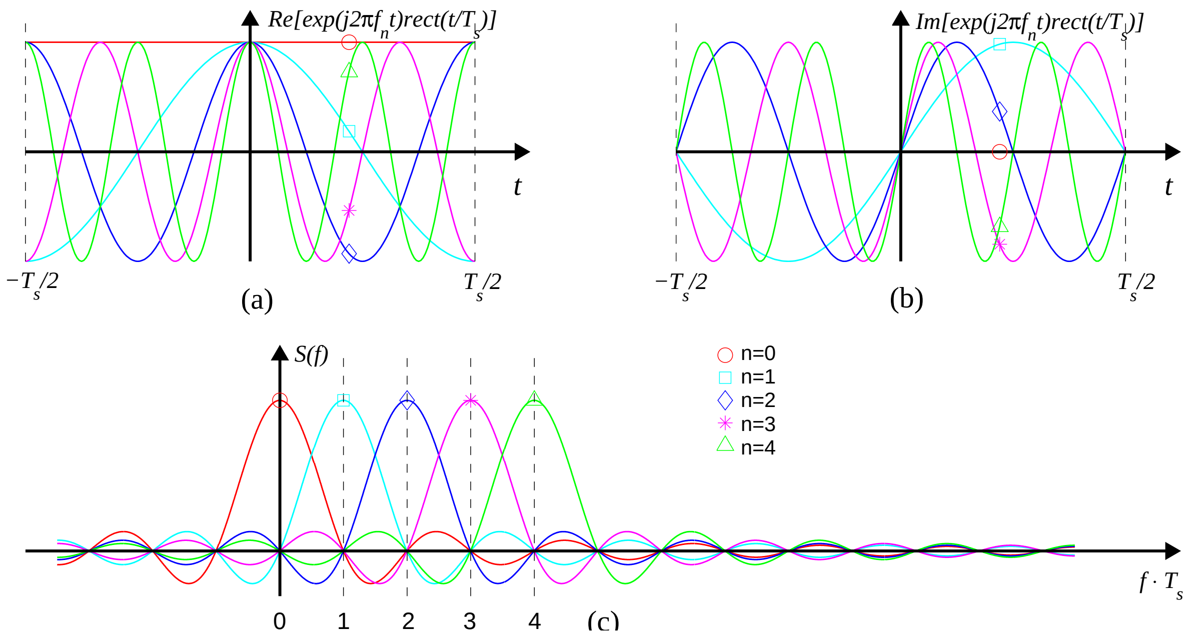

Figure 2.7: An example of time-domain illustration and spectra of OFDM signal.

Note that the expression on the right hand side (RHS) of (2.12) is the formula of *inverse* DFT (IDFT), except for lack of a scaling factor $1/N$. Consequently, any sample $s_{k,0}$ contains the components of all $x_{n,0}$.

Ignoring noise, channel attenuation and propagation delay, on the receiving side at the carrier f_m, the received demodulated signal can be expressed as

$$r_m(t) = s(t)\exp(-j2\pi f_m t) * v(t - iT_s). \tag{2.13}$$

Substituting (2.11) into (2.13), if the relationship in (2.10) holds, the resulting received symbol in the symbol interval $i = 0$ is then given by

$$\begin{aligned} r_{m,0} &= \int_{-\infty}^{\infty} s(\tau)\exp(-j2\pi f_m \tau) v(\tau) d\tau \\ &= \sum_{n=0}^{N-1} x_{n,0} \int_{-\infty}^{\infty} \mathrm{rect}\left(\frac{\tau}{T_s}\right)\exp(j2\pi f_n \tau)\exp(-j2\pi f_m \tau)\mathrm{rect}\left(\frac{\tau}{T_s}\right) d\tau \\ &= T_s x_{n,0}\delta_{mn}, \end{aligned} \tag{2.14}$$

where T_s is the energy of the rectangular window. Therefore, the transmit symbol is reconstructed at the receiver.

On the other hand, the reverse operation of (2.12) is given by

$$x_{n,0} = \frac{1}{N}\sum_{k=0}^{N-1} s_{k,0}\exp\left(-j2\pi\frac{nk}{N}\right) \qquad 0 \le n < N. \tag{2.15}$$

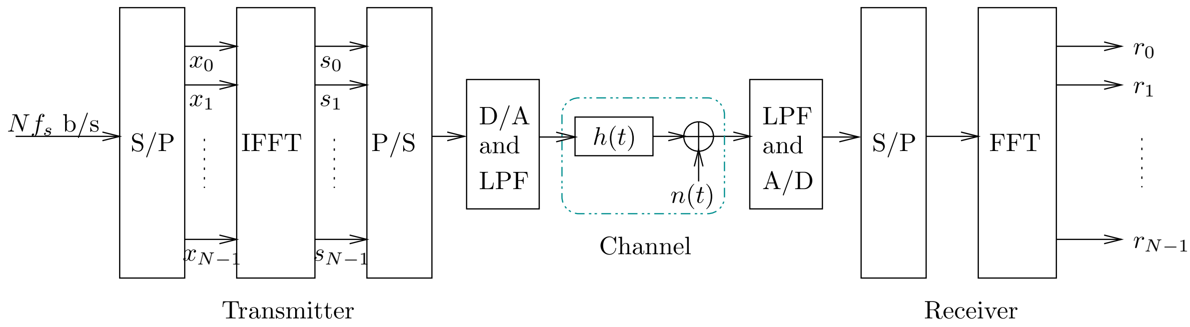

Figure 2.8: Block diagram of an OFDM transmission.

Accordingly, referring to (2.14) we have

$$r_{m,0} = T_s x_{m,0} = \frac{T_s}{N} \sum_{k=0}^{N-1} s_{k,0} \exp\left(-j2\pi \frac{mk}{N}\right) \qquad 0 \leq m < N. \tag{2.16}$$

Consequently, (2.12) and (2.16) imply that the generation of OFDM signals at the transmitter and the demodulation at the receiver can be performed efficiently by means of DFT, or *fast Fourier transformation* (FFT) when N is a power of 2. The block diagram of an OFDM transmission using FFT is shown in Fig. 2.8. A so-called *OFDM-symbol* is then made up of the ensemble of $s_{k,i}$, $0 \leq k < N$.

The investigation above is for an OFDM transmission over an ideal channel where $h(t) = c_0 \cdot \delta(t)$. As we have seen, orthogonal multiplexing is enabled during a symbol period $T_s = 1/f_s$, for the orthogonality condition in (2.10) is satisfied. This happens in the case of *additive white Gaussian noise* (AWGN) channel and in the case of a flat fading channel, $h(t) = c_0(t) \cdot \delta(t)$, as well. A time dispersive channel, however, would corrupt the orthogonality. To be specific, in the time domain ISI is introduced between OFDM-symbols, and in consequence *inter-carrier interference* (ICI) destroys the orthogonality between subcarriers in the frequency domain. The trick to eliminate ISI in the case of a linearly distorting channel is the introduction of a *guard interval* of a duration not less than the *maximum delay spread* of the linear channel. What's more, to maintain orthogonality, a *cyclic prefix* (CP) instead of an empty interval is used, which is able to remove ISI as well as ICI at the cost of extra transmit power. That is, we copy the last N_g samples of an OFDM-symbol and put them at the beginning of the symbol as a prefix. As a consequence, the linear convolution is converted into *cyclic convolution*. The latter one ensures the orthogonality between subcarriers. At the receiver this prefix will be discarded. If the maximum delay spread of the channel is not greater than N_g, the echoes of the last part of the previous symbol will fall into the duration of the prefix and be removed together with the prefix. The remaining samples are used for Fourier transform.

The time variance of the channel is likely to corrupt the orthogonality between subcarriers as well, e.g., in the case where the channel impulse response varies within the duration of an OFDM-symbol. Hence, OFDM is preferred to be implemented in a slow fading channel, which is considered constant at least during the transmission of an OFDM-symbol.

So far we have studied only the principle of OFDM modulation. More details will be found in the next chapter, where we will describe the OFDM transmission by a vector-valued transmission model. In addition, for clarity, from now on some notations are defined or redefined as:

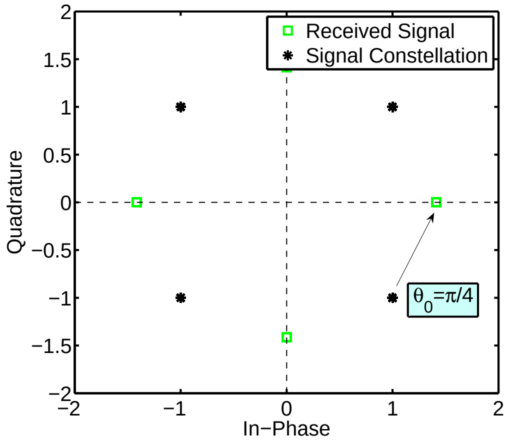

Figure 2.9: Influence of a constant phase offset on QPSK constellation.

- T_s, the full OFDM-symbol duration including prefix;
- N_s, the number of samples involved in an OFDM-symbol, $N_s = N_f + N_g$, where $N_f = N$, denoting the length of DFT, or the total number of subcarriers;
- T, the duration of a single sample, $T = T_s/N_s$.

2.5 Synchronization Errors in OFDM

In many wireless communication systems transmitters require a local oscillator (LO) for converting the transmit baseband signal to a radio frequency (RF) signal (passband signal), and receivers need a LO for the inverse conversion. The imperfections of LOs would lead to carrier phase errors. Furthermore, a precise clock signal is required in a digital communication system for symbol synchronization. The process of extracting such a clock signal at the receiver is called *timing recovery* [58]. Timing errors would occur either when the clock signal is not correctly recovered, or when sampling is not performed at precise sampling instants, e.g., in the case that there exists a time delay which is not exactly discovered. In general, these synchronization errors give rise to a performance degradation.

In this section we will have a look at the synchronization errors encountered in OFDM briefly. They are normally classified into two categories: carrier phase errors and timing errors. For simplicity, we assume that signals are transmitted over an ideal channel, and only synchronization errors have influence on the received OFDM-symbols.

2.5.1 Carrier Phase Errors

Let $s(t)$ represent the transmitted baseband signal in the time domain. Assuming that $s(t)$ is transmitted over an ideal channel, perfect timing is available at the receiver, and the carrier phase errors are the only reasons for performance loss, the received signal is therefore written as

$$y(t) = s(t)\exp(j\theta(t) + \theta_0), \tag{2.17}$$

where $\theta(t)$ represents the time-variant carrier phase error (CPE), and θ_0 the constant phase offset. The time-variant CPE can result either from the frequency dismatch between oscillators at the transmitter and receiver, f_ϵ, or from a time-variant phase noise, $\theta_\Delta(t)$.

Constant Phase Offset

The constant phase offset, θ_0, is introduced due to the phase dismatch between the transmitter and receiver carrier oscillators. In OFDM transmission, this constant phase offset leads to a rotation over an angle of θ_0 of the OFDM signals on all subcarriers, as illustrated in Fig. 2.9, but no ISI or ICI is induced. Such phase offset is carrier-independent and can be compensated at the receiver by multiplying by $\exp(-j\theta_0)$.

Phase Noise

The time-variant phase noise, $\theta_\Delta(t)$, is a random process which results from the fluctuation of the transmitter and receiver oscillators. Assuming that a free-running oscillator is used in the receiver, $\theta_\Delta(t)$ can be modeled as a Wiener process with zero mean and variance $2\pi\beta_\Delta|t|$, where β_Δ is two-side 3dB linewidth of the Lorentzian power density spectrum of the oscillator [76], [85]. The discrete-time expression for the Wiener phase noise process can be given by

$$\theta_\Delta(k+1) = \theta_\Delta(k) + w(k), \tag{2.18}$$

where $\theta_\Delta(k)$ denotes the phase noise process at sampling instant kT (like in the aforementioned system), and $w(k)$ is a Gaussian random variable (r.v.) with zero-mean and variance $4\pi\beta_\Delta T$.

Phase noise has two effects on an OFDM system: rotation of the symbols over all subcarriers by a common phase error (CPE) and the occurrence of ICI [85]. More studies on system performance degradation due to phase noise and approaches proposed to combat its impacts can be seen in [57], [73], and [76].

Carrier Frequency Offset

The carrier frequency offset (CFO), f_ϵ, is the frequency difference between the transmitter and receiver oscillators. Let Δf represent the subcarrier frequency spacing in an OFDM system. The CFO normalized to Δf is denoted by ϵ. In the presence of CFO, the carrier phase error increase linearly with time: $\theta(t) = 2\pi f_\epsilon t$. Furthermore, as shown in Fig. 2.10, only when $f_\epsilon = 0$ and the signal is sampled exactly at subcarrier frequencies, where the peak of a $sinc(x)$ function lies and spectra of other signals have null, no ICI is induced. A frequency offset would lead to amplitude reduction and phase rotation of the transmitted signal, as well as the ICI from other subcarriers. However, no ISI is introduced by CFO. In Chapter 4, we will study the effects of frequency offset in depth. It would be seen that a simple way to compensate for the performance loss due to CFO is multiplying the received time-domain signals by $\exp(-j2\pi f_\epsilon t)$.

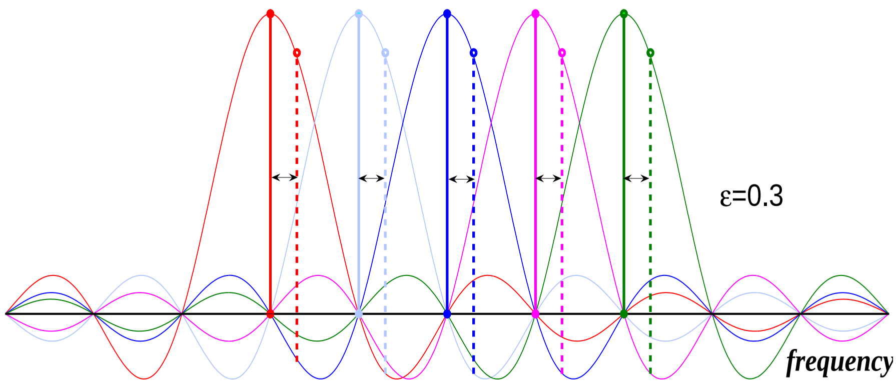

Figure 2.10: Influence of a carrier frequency offset.

Carrier Phase Jitter

Synchronization algorithms are usually used to estimate the constant phase offset and the CFO, and it is common to implement phase-locked local oscillator at the receiver (if continuous transmission is considered), in order to get rid of the frequency offset and phase offset, as well as the phase noise components falling within the bandwidth of the phase-locked loop (PLL) [68]. The residual phase error, $\varphi(t)$, so-called *carrier phase jitter*, can be modeled as a zero-mean stationary random process with jitter power spectral density $S_\varphi(f)$ and jitter variance σ_φ^2 [68]. In an OFDM system, the phase jitter has the same effect on the signals over all subcarriers, which appears to be a random carrier-independent rotation of the transmitted signals. With a small variance σ_φ^2, $\exp(j\varphi(t))$ can be approximately replaced by $1 + j\varphi(t)$. If the phase jitter varies rapidly as compared to average time of the equalizer in use, $\varphi(t)$ cannot be tracked. See [54], [16], and [57] for more information.

2.5.2 Timing Errors

Assume that the receiver has a free-running sampling clock independent of the carrier oscillator. In the presence of timing errors, if the received signal is sampled at time instant $t'_k = kT' - \nu T$, $T' = \Delta T + T$, it yields

$$y(t)|_{t=t'_k} = s(t - kT)|_{t=t'_k} = s(k\Delta T - \nu T), \tag{2.19}$$

where ν is constant time offset normalized to sample duration and $\nu > 0$. Furthermore, $\eta = \Delta T/T$, $|\Delta T| < T$, represents the normalized clock frequency offset between the transmitter and receiver sampling clocks. In the general case of continuous transmission, the time index should be $i(N_f + N_g) + k$ instead of k. For simplicity, we consider only transmission within one block.

Constant Time Offset

In a digital communication system, the arriving time of a signal at the receiver is uncertain and should be estimated. A constant time offset νT is a (backward) time delay that accounts for

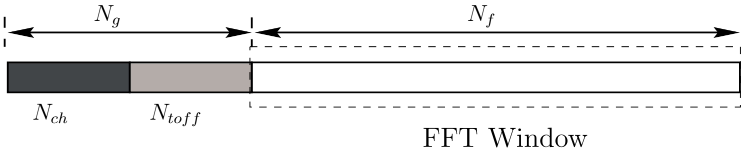

Figure 2.11: An OFDM-symbol with guard interval.

the constant time dismatch between the estimated and real propagation time of a signal from the transmitter to the receiver.

To investigate the effects of a constant time offset, we have to recall the guard interval used for OFDM. In the guard interval, there is a certain range that is not affected by the ISI caused by time dispersion of the channel. We denote the length of this range by N_{toff}, as shown in Fig. 2.11. As long as the FFT window starts from this range, the orthogonality between the different subcarriers will be maintained [89]. A constant time offset within this interval can just result in a phase rotation of symbol on each subcarrier. For instance, if signals on the subcarrier f_n, $f_n = n\Delta f$, is sampled at time instant $t'_k = kT - \nu T$, it yields then

$$\begin{aligned} \exp(j2\pi f_n(t-kT))|_{t=t'_k} &= \exp(j2\pi n\Delta f(kT - \nu T - kT)) \\ &= \exp\left(j2\pi n\Delta f \cdot \frac{-\nu}{N_f\Delta f}\right) \\ &= \exp\left(\frac{-j2\pi n\nu}{N_f}\right), \end{aligned} \tag{2.20}$$

where $\nu \leq N_{toff}$. It is seen that the phase rotation owing to a constant time offset, $\exp\left(\frac{-j2\pi n\nu}{N_f}\right)$, is carrier-dependent. Therefore, a constant time offset satisfying $\nu \leq N_{toff}$ does not lead to any interference. As the phase rotation can be compensated by an one-tap equalizer without noise enhancement, no performance degradation would arise. On the other hand, if ν is greater than N_{toff}, and then the beginning of the FFT window is out of the ISI free interval, the corresponding ISI will destroy the orthogonality between the subcarriers and introduce ICI [89]. See also [48], [66].

Clock Frequency Offset

Sampling clock errors include the clock phase error and the clock frequency error. The former has the effects similar to a constant time offset, and therefore it is treated as a kind of constant time offset [89]. The clock frequency error, on the other hand, is similar to carrier frequency offset, and can induce ICI. On a subcarrier f_n, a clock frequency offset gives rise to a carrier-dependent phase error, $\exp\left(\frac{j2\pi(N_f-1)n\eta}{N_f}\right) \approx \exp(j2\pi n\eta)$, and a carrier-dependent amplitude reduction $\frac{\sin\pi n\eta}{N_f \sin\left(\frac{\pi n\eta}{N_f}\right)} \approx \frac{\sin\pi n\eta}{\pi n\eta}$, of the signals of interest, as well as ICI with variance

$$\mathrm{var}(n\eta) = \frac{\pi^2}{3}(n\eta)^2. \tag{2.21}$$

Furthermore, the resulting absolute timing error, $k|\Delta T|$, increases linearly with time. Hence, an increasing misalignment between the time-domain samples at the transmitter and the receiver is introduced. For a continuous transmission, the periodical loss or duplication of samples is likely to take place, dependent on η has plus or negative sign. An OFDM system is very sensitive to clock frequency offset. Note that the attenuation of the desired signal and the ICI caused by clock frequency offset is different from those caused by carrier frequency offset. See also [67].

Timing Jitter

If synchronization algorithms are used to estimate and then adjust the sampling clock, i.e., the sampling clocks at the transmitter and receiver are synchronized, the OFDM system is affected only by timing jitter $\xi(t)$, which results from the imperfect synchronization. The terminology '*timing jitter*' is used to describe the disturbance to an ideal timing signal, and is defined as the time difference of the jittered and ideal signals as a function of phase, whereas terminology '*phase jitter*' describes the phase difference of two signals as a function of time [16]. A relationship (transformation) exists between phase jitter and time jitter (of the same synchronizer). Similar to phase jitter, a time jitter can be modeled as a zero-mean stationary random process with jitter spectrum $S_\xi(e^{j2\pi f T_s})$ and jitter variance σ_ξ^2. The timing jitter introduces a degradation dependent upon the carrier index [69].

2.6 Conventional Detection Techniques

2.6.1 The Vector-valued Transmission Model

In this section, we aim at reviewing some conventional equalization approaches based on a vector-valued transmission model

$$\mathbf{r} = \mathbf{H}_c\mathbf{x} + \mathbf{n}, \tag{2.22}$$

where $\mathbf{x} = [x_0, x_1, ..., x_{N-1}]^T$ denotes complex-valued transmit symbol vector that is constrained to an alphabet $\mathcal{A}_x$, $\mathbf{H}_c = [h_{ij}]_{N\times N}$ stands for a *known* channel matrix of full rank N and with complex-valued entries, $\mathbf{r} = [r_0, r_1, ..., r_{N-1}]^T$ is the received symbol vector, and $\mathbf{n} = [n_0, n_1, ..., n_{N-1}]^T$ represents a noise vector. The superscript $(\cdot)^T$ represents matrix transpose. The components of $\mathbf{n}$ are complex-valued independently distributed and uncorrelated Gaussian random variables with zero mean and variance σ_n^2, i.e., $\mathbf{n} \sim \mathcal{CN}(0, \sigma_n^2\mathbf{I})$. Furthermore, the transmit symbols in $\mathbf{x}$ are assumed to be independent and identically distributed (i.i.d) random variables (r.v.) with zero mean and variance σ_x^2. Therefore, the transmit vector $\mathbf{x}$ has mean $E[\mathbf{x}] = \mathbf{0}$ as well and the covariance matrix of $\mathbf{x}$ is given by

$$\mathbf{\Phi}_{\mathbf{xx}} = E\{(\mathbf{x} - E[\mathbf{x}])(\mathbf{x} - E[\mathbf{x}])^H\} = \sigma_x^2\mathbf{I}, \tag{2.23}$$

where superscript $(\cdot)^H$ represents the complex conjugate transposition (Hermitian). Some special cases of channel matrix are concerned as follows:

1. $\mathbf{H}_c = \mathbf{I}$, where $\mathbf{I}$ is the identity matrix. This implies the identical ideal subchannel for each element in $\mathbf{x}$ such that $\mathbf{r}$ is only a noisy version of $\mathbf{x}$;

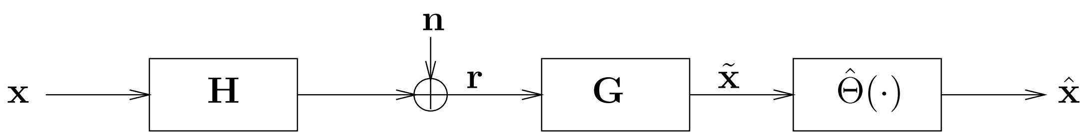

Figure 2.12: Data detection with a symbol-wise hard decision function $\hat{\Theta}(\cdot)$.

2. $\mathbf{H}_c$ is a diagonal matrix but $\mathbf{H}_c \neq \mathbf{I}$. This indicates that different subchannels are one-path channels experiencing different fading such that $\mathbf{r}$ is a faded and noisy version of $\mathbf{x}$, but components in $\mathbf{r}$ are orthogonal to each other.

In general, to recover $\mathbf{x}$ on the observation of $\mathbf{r}$ in a fading channel, data detection techniques should be implemented. Two types of detection techniques can be distinguished [30]:

- Single symbol detection, where one data symbol is detected, without taking into account the interference from other symbols;
- Vector or block detection, where knowledge about interference is exploited.

Data detection basically consists of two components: equalization and symbol decision. For a linear vector-valued transmission like in (2.22), the process of vector equalization can be modeled as a matrix $\mathbf{G} = [g_{ij}]_{N\times N}$ of size $N \times N$, and therefore the symbol vector before decision is given by

$$\tilde{\mathbf{x}} = \mathbf{G}\mathbf{r} = \mathbf{G}\mathbf{H}_c\mathbf{x} + \mathbf{G}\mathbf{n}, \tag{2.24}$$

as shown in Fig. 2.12. The decided symbol vector is obtained at the output of the symbol-wise decision function $\hat{\Theta}(\cdot)$

$$\hat{x} = \hat{\Theta}(\tilde{\mathbf{x}}). \tag{2.25}$$

The decision rule $\hat{\Theta}(\cdot)$ is called hard decision when the decided symbols are limited to the alphabet of $\mathbf{x}$ [20].

2.6.2 Vector Equalization

Vector (block) detection exploited the interference involved in the received signals. The interference can come from other users or simultaneously transmitted symbols of one user's own. Hereby the detection is performed under the observation of a block of received symbols.

Zero-forcing Vector Equalizer

The conditional PDF of the received signal is expressed as

$$p(\mathbf{r}|\mathbf{x}) = \frac{1}{(\pi\sigma_n)^N} \exp\left[-\frac{(\mathbf{r}-\mathbf{H}_c\mathbf{x})^H(\mathbf{r}-\mathbf{H}_c\mathbf{x})}{\sigma_n^2}\right]. \tag{2.26}$$

The ZF vector equalization aims to minimize the log-likelihood function

$$\Lambda(\mathbf{r}|\mathbf{x}) = (\mathbf{r} - \mathbf{H}_c\mathbf{x})^H(\mathbf{r} - \mathbf{H}_c\mathbf{x}) \tag{2.27}$$

with respect to $\mathbf{x}$. From Appendix A.1 the equalization matrix is given by

$$\mathbf{G} = (\mathbf{H}_c^H\mathbf{H}_c)^{-1}\mathbf{H}_c^H. \tag{2.28}$$

Therefore, interference can be totally eliminated by using the ZF vector equalization. The noise at the output of the ZF equalizer

$$\tilde{\mathbf{n}} = \mathbf{G}\mathbf{n} = (\mathbf{H}_c^H\mathbf{H}_c)^{-1}\mathbf{H}_c^H\mathbf{n} \tag{2.29}$$

with the covariance matrix

$$\mathbf{\Phi}_{\tilde{\mathbf{n}}\tilde{\mathbf{n}}} = E\left[(\mathbf{G}\mathbf{n})(\mathbf{G}\mathbf{n})^H\right] = \sigma_n^2(\mathbf{H}_c^H\mathbf{H}_c)^{-1}. \tag{2.30}$$

The noise variance of the individual symbols is denoted by the main diagonal of $\mathbf{\Phi}_{\tilde{\mathbf{n}}\tilde{\mathbf{n}}}$. In the case where $\mathbf{H}_c^H\mathbf{H}_c$ has near zero eigenvalues (frequency selective fading), i.e., when $\mathbf{H}_c^H\mathbf{H}_c$ is ill-conditioned, the variance of the additive noise $\sigma_{\tilde{n}}^2$ becomes very high relative to the energy of the transmitted symbols [20]. This fact is so-called *noise enhancement*. The resulting *signal to noise ratio* (SNR) is given by

$$SNR = \frac{\sigma_x^2}{\sigma_{\tilde{n}}^2}. \tag{2.31}$$

LMMSE Vector Equalizer

The *linear minimum mean square error* (LMMSE) equalization for vector detection takes into account the interference as well as the present SNR, which is realized by searching for the equalization matrix $\mathbf{G}$ that minimizes the mean square error $E[\|\mathbf{x} - \mathbf{G}\mathbf{r}\|^2]$ [33]. It yields

$$\mathbf{G} = (\mathbf{H}_c^H\mathbf{H}_c + \frac{\sigma_n^2}{\sigma_x^2}\mathbf{I})^{-1}\mathbf{H}_c^H = \mathbf{H}_c^H\left(\mathbf{H}_c\mathbf{H}_c^H + \frac{\sigma_n^2}{\sigma_x^2}\mathbf{I}\right)^{-1}. \tag{2.32}$$

The derivation of the equalization matrix is found in Appendix A.2. Note that in the case of very high SNRs, the solution of LMMSE equalizer and the solution of ZF equalizer coincide.

In the following chapters, the equalization methods described above will be implemented with respect to the different transmission schemes.

2.7 Summary

After introductions to wireless radio channels, as well as multiplexing and multiple access techniques, OFDM was first introduced in Section 2.4 as an efficient realization of the multicarrier modulation. The basic principle, parameters, and properties of OFDM were explained there.

A brief overview of synchronization errors encountered in OFDM has been given in Section 2.5. They are classified into two groups: carrier phase errors and timing errors. Their influence on OFDM has been introduced concisely.

Finally, in Section 2.6 two conventional equalization approaches, ZF and LMMSE, are described briefly. On the basis of a general vector-valued transmission model their use for vector detection was explained.

Chapter 3

Modeling of OFDM-based Systems

3.1 Chapter Overview

In this chapter we describe OFDM-based systems with vector-valued transmission models. Synchronous transmission is considered and, for the time being, we assume perfect synchronization for both downlink and uplink transmission. The influence of frequency offset will be investigated in the next chapter.

As the first step, a concise vector-valued expression of the *single-user* OFDM or *pure* OFDM transmission is described in Section 3.2. OFDM converts a wideband frequency selective fading channel into a set of parallel narrowband and flat fading subchannels. This simplifies the signal detection, but could cause that some subchannels experience deep fading. To make up for this drawback, *coded* OFDM (COFDM) is widely applied in practice, which is mentioned as well.

Orthogonal frequency division multiple access (OFDMA) is intuitively a multiple access technique that corresponds to OFDM in a multiuser scenario. Similar to conventional FDMA, a group of users share a common frequency band, or more exactly, all subcarriers in an OFDM structure, and a subset of subcarriers is assigned to an individual user. In Section 3.3, we model two typical OFDMA systems, *conventional* OFDMA (C-OFDMA) and *interleaved* OFDMA (I-OFDMA), according to two subcarrier assignment schemes. In C-OFDMA subcarrier assignment is based on sub-bands, whereas in I-OFDMA subcarriers with *maximum* frequency diversity are grouped for an individual user.

In Section 3.4 the combination of OFDM and the *spread spectrum* (SS) technique is investigated. This includes *multi-carrier - code division multiplexing* (MC-CDM), which is considered for a single user case, *code division multiplexing - orthogonal frequency division multiple access* (CDM-OFDMA), and *multi-carrier - code division multiple access (*MC-CDMA), where the latter two are considered for multiuser scenarios. Benefitting from spread spectrum techniques, *uncoded* MC-CDM outperforms OFDM in the case of frequency selective fading. For the same reason, CDM-OFDMA and MC-CDMA outperform OFDMA in the uncoded case.

3.2 Pure OFDM System

3.2.1 Vector-valued Transmission Model

The block diagram of an equivalent baseband OFDM transmission is illustrated in Fig. 3.1. On the transmitter side, $\mathbf{x}_i$ represents the transmit symbol vector in the time interval $[iT_S,(i+1)T_S]$, and $\mathbf{x}_i = [x_{0,i}, x_{1,i}, \ldots, x_{N_f-1,i}]^T$. N_f is the length of the symbol vector, T_s is the duration of one whole OFDM-symbol, and i denotes the discrete time vector index, $i = 0, 1, \ldots, \infty$. Like in Section 2.6.1, we assume that the components of $\mathbf{x}_i$ are PSK- or QAM-mapped, independent and identically distributed complex random variables with zero mean, i.e., $E[x_{m,i}] = 0$ and the variance $E[x_{m,i}x_{n,i}^*] = \sigma_x^2\delta_{mn}$. A N_f-point normalized IDFT is first performed on $\mathbf{x}_i$. The resulting time-domain symbols are expressed as

$$\dot{s}_{k,i} = \frac{1}{\sqrt{N_f}} \sum_{m=0}^{N_f-1} x_{m,i} e^{j\frac{2\pi mk}{N_f}}. \tag{3.1}$$

This operation can be described by the multiplication of the IDFT matrix $\mathbf{F}^{-1}$ and $\mathbf{x}_i$

$$\dot{\mathbf{s}}_i = \mathbf{F}^{-1}\mathbf{x}_i, \tag{3.2}$$

where $\dot{\mathbf{s}}_i = [\dot{s}_{0,i}, \dot{s}_{1,i}, \ldots, \dot{s}_{N_f-1,i}]^T$, and

$$\mathbf{F}^{-1} = \frac{1}{\sqrt{N_f}} \times \begin{pmatrix} 1 & 1 & 1 & \ldots & 1 \\ 1 & e^{j\frac{2\pi}{N_f}} & e^{j\frac{4\pi}{N_f}} & \ldots & e^{j\frac{2\pi}{N_f}(N_f-1)} \\ 1 & e^{j\frac{4\pi}{N_f}} & e^{j\frac{8\pi}{N_f}} & \ldots & e^{j\frac{4\pi}{N_f}(N_f-1)} \\ \vdots & \vdots & \vdots & \ddots & \vdots \\ 1 & e^{j\frac{2\pi}{N_f}(N_f-1)} & e^{j\frac{4\pi}{N_f}(N_f-1)} & \ldots & e^{j\frac{2\pi}{N_f}(N_f-1)^2} \end{pmatrix}. \tag{3.3}$$

Subsequently, $\dot{\mathbf{s}}_i$ is added by a cyclic prefix of length N_g, which is a replica of the last N_g elements of $\dot{\mathbf{s}}_i$, $\dot{s}_{N_f-N_g-1,i}, \ldots, \dot{s}_{N_f-1,i}$. This operation can be realized by a matrix-vector multiplication

$$\mathbf{s}_i = \mathbf{G}_{ap}\dot{\mathbf{s}}_i, \tag{3.4}$$

where $\mathbf{G}_{ap}$ has the form

$$\mathbf{G}_{ap} = \begin{pmatrix} \mathbf{0}_{N_g\times(N_f-N_g)} & \mathbf{I}_{N_g\times N_g} \\ \multicolumn{2}{c}{\mathbf{I}_{N_f\times N_f}} \end{pmatrix}. \tag{3.5}$$

In (3.5), $\mathbf{0}$ denotes a matrix with all zero entries. After parallel to serial conversion, the Dirac-sampled time-domain transmit symbols are filtered by the transmit filter $h_T(t)$, which is a bandlimited low-pass filter with cutoff frequency $f_g = \frac{1}{2\cdot\Delta t}$. Δt is the sampling time with $\Delta t = \frac{T_s}{N_f+N_g}$, which denotes also the single symbol duration T. The resulting signal $s(t)$ is expressed as

$$s(t) = \sum_{i=0}^{\infty} \sum_{k=0}^{N_s-1} s_{k,i} h_T(t-(iN_s+k)T). \tag{3.6}$$

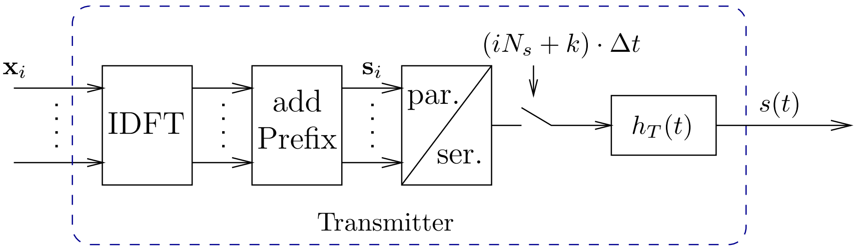

(a)

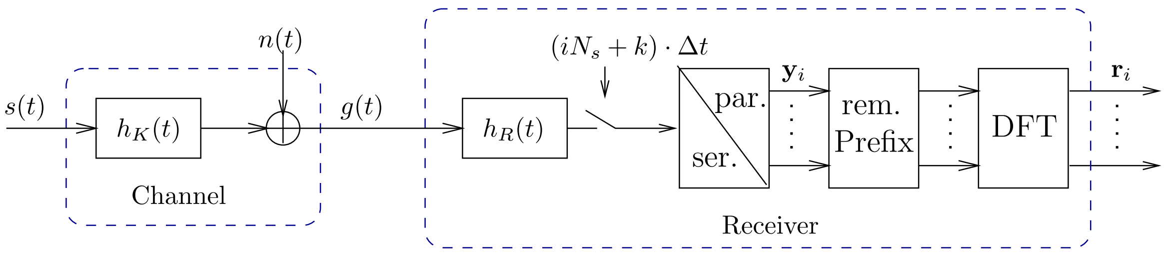

(b)

Figure 3.1: OFDM transmission in the equivalent low-pass domain.

$s(t)$ is then up-converted and transmitted over the time-invariant frequency-selective fading channel with impulse response $h_K(t)$.

In Fig. 3.1, $h_K(t)$ represents the impulse response of the low-pass equivalence of the physical channel. In general, $h_K(t)$ is assumed to be complex-valued. The output of the physical channel is disturbed by additive white Gaussian noise (AWGN) with two-side power spectral density (PSD) $\frac{N_0}{2}$. For a high frequency (HF) radio channel, band-pass filtering is performed at the receiver before down-conversion. The noise is therefore *band-pass white Gaussian*. Letting $n(t)$ denote the equivalent low-pass noise, it is then complex-valued with a PSD [58]

$$\Phi_{nn}(f) = \begin{cases} N_0, & \text{for } |f| \leq \frac{1}{2}B \\ 0, & \text{for } |f| > \frac{1}{2}B \end{cases} \tag{3.7}$$

and its autocorrelation function is

$$\phi_{nn}(\tau) = N_0 \frac{\sin \pi B \tau}{\pi \tau}. \tag{3.8}$$

B indicates the bandwidth of the band-pass filter. The limiting form of $\phi_{nn}(\tau)$ as B approaches infinity is

$$\phi_{nn}(\tau) = N_0 \delta(\tau). \tag{3.9}$$

The variance of $n(t)$ is defined as $\sigma_n^2 = \phi_{nn}(0) = N_0$.

Assuming the receiver is perfectly synchronized to the transmitter, the down-converted received signal $g(t)$ at the receiver is represented as

$$g(t) = \int_{-\infty}^{\infty} h_K(\tau) s(t - \tau) d\tau + n(t), \tag{3.10}$$

which is then filtered by receive filter $h_R(t)$ and Dirac sampled at $t = (iN_s + k) \cdot \Delta t$. $h_R(t)$ is assumed to be an ideal low-pass filter having the cutoff frequency $f_g = \frac{1}{2 \cdot \Delta t}$. The discrete-time equivalent low-pass channel impulse response results from the concatenation of $h_T(t)$, $h_K(t)$ and $h_R(t)$

$$h_l = h_T(t) * h_K(t) * h_R(t)|_{t=l \cdot \Delta t}, \tag{3.11}$$

where the time index i is ignored since the channel is time-invariant. The operator $*$ indicates the convolution operation. We denote the channel with a vector $\mathbf{h} = [h_0, h_1, \ldots, h_{L-1}]$. If $L > 1$, the channel is time dispersive and thus frequency selective. Consequently, the received time-domain discrete-time symbol $y_{k,i}$ is given by

$$y_{k,i} = \sum_{0}^{L-1} h_l s_{k-l,i} + \dot{n}_{k,i}, \tag{3.12}$$

where

$$\dot{n}_{k,i} = h_R(t) * n(t)|_{t=(iN_s+k) \cdot \Delta t}. \tag{3.13}$$

Assume that $B \geq \frac{1}{2\Delta t}$. Since $h_R(t)$ is an ideal low-pass filter, $\dot{n}_{k,i}$ is therefore a complex-valued white Gaussian random variable with variance $\sigma_n^2 = N_0$. The received symbol vector after serial to parallel conversion is denoted by $\mathbf{y}_i = [y_{0,i}, y_{1,i}, \ldots, y_{N_f+N_g-1,i}]$. Equation (3.12) also can be formulated as a matrix-vector convolution (see [22]):

$$\mathbf{y}_i = \sum_{i'=-\infty}^{\infty} \hat{\mathbf{H}}_{i'} \mathbf{s}_{i-i'} + \dot{\mathbf{n}}_i = \hat{\mathbf{H}}_i * \mathbf{s}_i + \dot{\mathbf{n}}_i, \tag{3.14}$$

where $\hat{\mathbf{H}}_i$ has the size $(N_f + N_g) \times (N_f + N_g)$. If the length of $\mathbf{h}$ is not greater than $N_f + 1$, the sequence of $\hat{\mathbf{H}}_i$ matrices consist of nonzero matrices for $i = 0$ and $i = 1$:

$$\hat{\mathbf{H}}_0 = \begin{pmatrix} h_0 & 0 & \ldots & 0 & \ldots & 0 \\ \vdots & h_0 & & \vdots & & \\ h_{L-1} & \vdots & \ddots & 0 & & \vdots \\ 0 & h_{L-1} & & h_0 & & \\ \vdots & & \ddots & \ddots & \ddots & 0 \\ 0 & \ldots & 0 & h_{L-1} & \ldots & h_0 \end{pmatrix}, \tag{3.15}$$

and

$$\hat{\mathbf{H}}_1 = \begin{pmatrix} 0 & \ldots & 0 & h_{L-1} & \ldots & h_1 \\ \vdots & & \vdots & 0 & \ddots & \vdots \\ 0 & \ldots & 0 & \vdots & & h_{L-1} \\ 0 & \ldots & 0 & 0 & \ldots & 0 \\ \vdots & & \ddots & \vdots & & \vdots \\ 0 & \ldots & 0 & 0 & \ldots & 0 \end{pmatrix}. \tag{3.16}$$

At the receiver, after the removal of the cyclic prefix for $\mathbf{y}_i$ and FFT demodulation, the frequency-domain received symbol vector $\mathbf{r}_i$ is given by

$$\mathbf{r}_i = \mathbf{F}\mathbf{G}_{pp}\mathbf{y}_i + \mathbf{n}_i \tag{3.17}$$

with

$$\mathbf{G}_{pp} = \begin{pmatrix} \mathbf{0}_{N_f\times N_g} & \mathbf{I}_{N_f\times N_f} \end{pmatrix} \tag{3.18}$$

and $\mathbf{n}_i = \mathbf{F}\mathbf{G}_{pp}\dot{\mathbf{n}}_i$. The noise sample $n_{k,i} \in \mathbf{n}_i$ is also complex-valued white Gaussian random variables with variance σ_n^2. In (3.17), $\mathbf{F}$ represents the normalized Fourier matrix with $F_{mn} = \frac{1}{\sqrt{(N_f)}}e^{-j\frac{2\pi}{N_f}(m-1)(n-1)}$ and $\mathbf{F}\mathbf{F}^{-1} = \mathbf{F}\mathbf{F}^H = \mathbf{I}$. Substituting (3.2), (3.4) and (3.14) in (3.17) yields

$$\mathbf{r}_i = \mathbf{F}\mathbf{G}_{pp}\hat{\mathbf{H}}_i\mathbf{G}_{ap}\mathbf{F}^{-1} * \mathbf{x}_i + \mathbf{n}_i. \tag{3.19}$$

If L is not greater than $N_g - 1$, then $\mathbf{G}_{pp}\hat{\mathbf{H}}_1\mathbf{G}_{ap}$ yields a zero matrix and the matrix resulting from

$$\mathbf{G}_{pp}\hat{\mathbf{H}}_0\mathbf{G}_{ap} = \begin{pmatrix} h_0 & 0 & \dots & 0 & h_{L-1} & \dots & h_1 \\ h_1 & h_0 & & \vdots & & \ddots & \vdots \\ \vdots & h_1 & \ddots & 0 & & & h_{L-1} \\ h_{L-1} & \vdots & \ddots & h_0 & \ddots & & 0 \\ 0 & h_{L-1} & & h_1 & \ddots & 0 & \vdots \\ \vdots & & \ddots & \vdots & & h_0 & 0 \\ 0 & \dots & 0 & h_{L-1} & \dots & h_1 & h_0 \end{pmatrix} \tag{3.20}$$

is circulant. According to the properties of circulant matrices, every circulant matrix can be diagonalized by the Fourier matrix $\mathbf{F}$, namely, $\mathbf{F}\mathbf{G}_{\mathbf{pp}}\hat{\mathbf{H}}_{\mathbf{0}}\mathbf{G}_{\mathbf{ap}}\mathbf{F}^{-\mathbf{1}}$ yields

$$\mathbf{G}_{pp}\hat{\mathbf{H}}_0\mathbf{G}_{ap} = \mathbf{F}^{-1}\mathbf{\Lambda}\mathbf{F}, \tag{3.21}$$

and $\mathbf{\Lambda}$ is a diagonal matrix with

$$\mathbf{\Lambda} = \mathrm{diag}\left\{\sqrt{N_f}\cdot\mathbf{F}\cdot[h_0, h_1, \dots, h_{L-1}, \mathbf{0}_{1\times N_f-L-1}]^T\right\}. \tag{3.22}$$

It is obvious that the elements on the main diagonal of $\mathbf{\Lambda}$ are the discrete channel transfer functions over N_f subcarriers. Hence, from (3.21)

$$\mathbf{F}\mathbf{G}_{pp}\hat{\mathbf{H}}_{\mathbf{0}}\mathbf{G}_{ap}\mathbf{F}^{-\mathbf{1}} = \mathbf{\Lambda}. \tag{3.23}$$

Accordingly, (3.19) simplifies to

$$\mathbf{r}_i = \mathbf{F}\mathbf{G}_{pp}\hat{\mathbf{H}}_i\mathbf{G}_{ap}\mathbf{F}^{-1}\cdot\delta(i) * \mathbf{x}_i + \mathbf{n}_i = \mathbf{\Lambda}\mathbf{x}_i + \mathbf{n}_i. \tag{3.24}$$

Normally, $\mathbf{H}$ is used to denote the channel transfer function matrix. Therefore, in the following we replace $\mathbf{\Lambda}$ by $\mathbf{H}$, and

$$\mathbf{r}_i = \mathbf{H}\mathbf{x}_i + \mathbf{n}_i \tag{3.25}$$

with $\mathbf{H}$ =diag$\{[H_0, H_1, ...H_{N_f-1}]\}$. A simplified block diagram is illustrated in Fig. 3.2 for OFDM transmission in the low-pass domain over time-invariant channel.

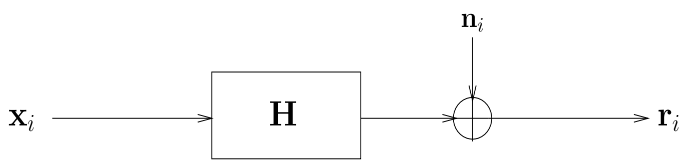

Figure 3.2: Simplifed OFDM transmission model in the equivalent low-pass domain.

3.2.2 Data Detection in OFDM Systems

As the channel transfer function matrix $\mathbf{H}$ is a diagonal matrix, i.e., symbols on individual subcarriers undergo flat fading, data detection can be realized by a bank of adaptive one-tap equalizers to combat the phase and amplitude distortions resulting from a fading channel. In such a case the equalization matrix $\mathbf{G}$ is a diagonal matrix with the weighting factors of these equalizers on the main diagonal.

Zero-forcing Equalization The symbol-by-symbol ZF equalizer applies the inverted channel coefficients

$$g_m = \frac{H_m^*}{|H_m|^2}, \tag{3.26}$$

where the superscript $(\cdot)^*$ represents the *complex conjugate* operation. The ZF equalizer totally recovers the desired symbols, except for the case where $|H_m| = 0$. The covariance matrix of $\tilde{\mathbf{n}}$ has the form

$$\mathbf{\Phi}_{\tilde{\mathbf{n}}\tilde{\mathbf{n}}} = \sigma_n^2 \begin{pmatrix} \frac{1}{|H_0|^2} & & & \mathbf{0} \\ & \frac{1}{|H_1|^2} & & \\ & & \ddots & \\ \mathbf{0} & & & \frac{1}{|H_{N_f-1}|^2} \end{pmatrix}, \tag{3.27}$$

and hence the output SNR with the ZF equalizer is given by

$$SNR = |H_m|^2 \frac{\sigma_x^2}{\sigma_n^2}. \tag{3.28}$$

Since $\mathbf{H}$ is a diagonal matrix, no noise enhancement occurs in this case. However, (3.28) shows that the SNR is *subcarrier-dependent*, provided that the channel is frequency selective.

In addition, note that the energy loss due to the insertion of the cyclic prefix has not been included in (3.28). As this energy loss is a constant factor and will be reflected as horizontal shift of the curves when *bit error rate* (BER) performance is evaluated, we ignore it in the following chapters.

LMMSE Equalization LMMSE equalizer for OFDM transmission has the equalization coefficients

$$g_m = \frac{H_m^*}{|H_m|^2 + \sigma_n^2/\sigma_x^2}, \tag{3.29}$$

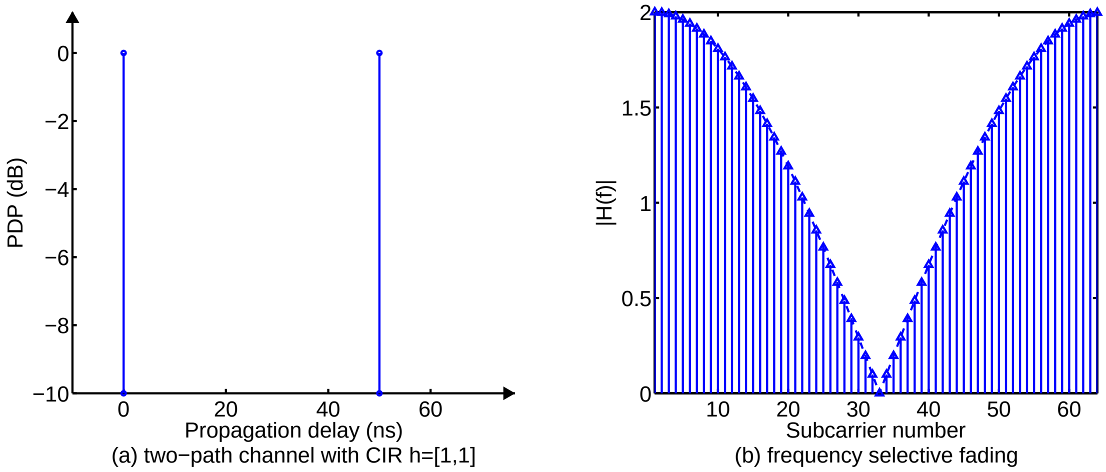

Figure 3.3: Two-path channel with 0 dB echos.

which minimize the quantity of $E[\|x_m - g_m r_m\|^2]$, where $r_m = H_m x_m + n_m$. In (3.29) an estimate of the actual variance of the noise, σ_n^2, is required for the computation of the MMSE equalization coefficients. To overcome the additional complexity due to the estimation of σ_n^2, a low-complexity suboptimal LMMSE equalization can be realized [30]. With suboptimal LMMSE equalization, the equalization coefficients are designed such that they perform optimally only in the most critical case in which successful transmission should be guaranteed. The variance σ_n^2 is chosen such that σ_n^2/σ_x^2 is equal to a threshold λ at which the optimal LMMSE equalization guarantees the maximum acceptable BER. With suboptimal LMMSE equalizer the equalization coefficients are given by

$$g_m = \frac{H_m^*}{|H_m|^2 + \lambda} \tag{3.30}$$

and require only information about H_m.

3.2.3 OFDM with Channel Coding and Interleaving

As studied in many contributions, e.g., [74], uncoded OFDM does not perform well in frequency selective channels, since a characteristic of frequency selective fading is that some frequencies are enhanced whereas others are attenuated. As a result, subcarriers with poor SNR will dominate the performance of the system. An extreme example is the channel with 0 dB echo (accordingly the existence of null subcarrier). As an example, in Fig. 3.3 the PDP of a two-path channel with $\mathbf{h} = [1, 1]$ and its frequency response in an OFDM system with 64 subcarriers are demonstrated. It is shown that the transfer function of subcarrier #31 equals zero. Information transmitted on this subcarrier will be lost if the transmission is uncoded, and therefore the average BER tends to be $\frac{1}{2} \cdot \frac{1}{64}$ as SNR approaches infinity, no matter what kind of equalization method is used. Thus, *error-correction coding* is expected to be implemented in practical OFDM systems to cope with the problems of multipath reception. The resulting system is so-called *coded* OFDM (COFDM). COFDM is able to deliver an acceptable bit error rate (BER) at a reasonably low SNR. Fig. 3.4 illustrated how OFDM benefits from coding, where a convolutional code of rate $R = 1/2$ is used. In addition, interleaving is utilized as well to reduce the risk of the successively

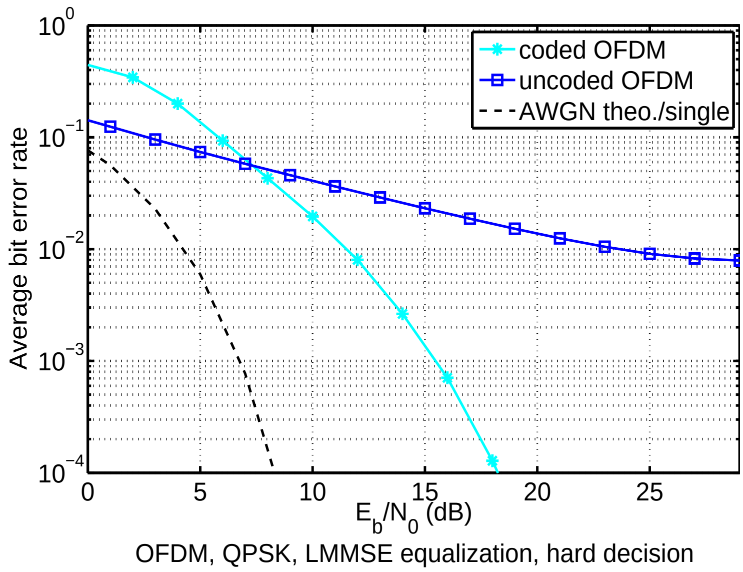

Figure 3.4: OFDM benefits from channel coding.

receiving faded-out signals when assigning successive symbols to adjacent subcarriers. More information can be obtained, e.g., in [2].

Another technique to deal with frequency selective behavior is diversity transmission. Based on OFDM, a bandwidth efficient diversity transmission is realized by using *code division multiplexing* (CDM) which spreads simultaneously transmitted symbols over all active subcarriers and separates different symbols by different spreading sequences. More details are given in Section 3.4.1.

3.3 Multiuser OFDM Systems

Multiple access techniques are required if we make use of OFDM in a multiuser scenario. As indicated in the previous chapter, TDMA and FDMA are two well-known techniques for resource management based on time-sharing and frequency-sharing, respectively. When combined with OFDM, they are called OFDM-TDMA and OFDM-FDMA, respectively. A more appropriate terminology for OFDM-FDMA is *orthogonal frequency division multiple access* (OFDMA). Both of them have been adopted by the IEEE standard as two options for transmission at the 2-11 GHz band [21], [3].

In OFDM-TDMA, one or several time slots are assigned to an individual user for data transmission, in which at least one whole OFDM-symbol can be transmitted. In other words, TDMA allocates OFDM-symbols to users, and symbols from different users are time-aligned. Different from OFDM-TDMA, OFDMA allocates subcarriers to users, and accommodates multiple users in a common channel at the same time. In OFDMA mode, all active subcarriers are divided into subsets of subcarriers, each subset is termed a subchannel. In the downlink, a subchannel may be intended for different (groups of) receivers (users); in the uplink, a transmitter (user) may be assigned one or several subchannels, and several transmitters (users) can transmit si-

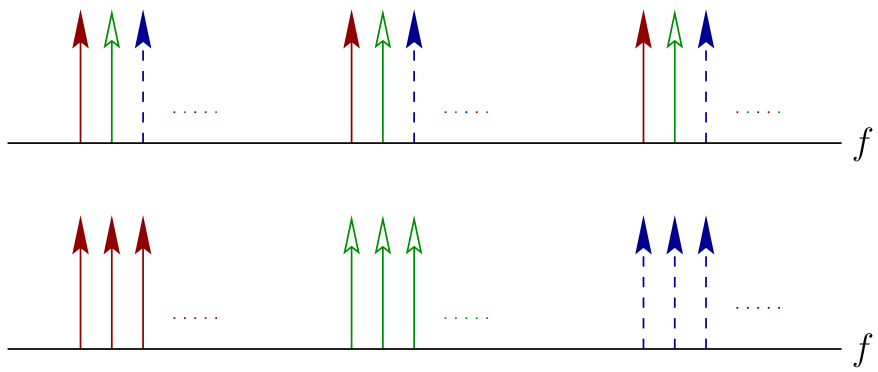

Figure 3.5: Two kinds of subcarrier division schemes: interleaved OFDMA (upper) and conventional OFDMA (lower).

multaneously [3]. If orthogonality among subcarriers is maintained, signals from different users will not interfere with each other.

In addition, OFDM can be combined with CDMA as well. We rank this into the combination of OFDM and spread spectrum techniques. Such a combination is termed as *multi-carrier spread spectrum* (MC-SS). According to different multiplexing and multiple access mode for which it is used, the resulting transmission schemes are defined as MC-CDM, CDM-OFDMA and MC-CDMA, respectively. They will be investigated in Section 3.4.

In this section, we will focus on OFDMA. As depicted in Fig. 3.5, basically two kinds of subcarrier partition schemes are developed: *conventional* OFDMA (C-OFDMA) based on subbands and *interleaved* OFDMA (I-OFDMA) based on subchannels which use subcarriers with *maximum* frequency diversity. To be specific, in conventional OFDMA adjacent subcarriers are chosen to construct a subchannel, whereas in interleaved OFDMA equidistant subcarriers are grouped to a subchannel. The vector-valued transmission of these two OFDMA schemes will be developed in the following, for both downlink and uplink transmission. Moreover, we will compare and analyze the performance of both systems as well.

For simplicity, synchronous transmission is assumed in the uplink, although it is hardly achievable. A synchronization policy of OFDMA systems will be introduced in Section 6.3.1 in detail.

3.3.1 Downlink Transmission Model of OFDMA

Consider an OFDMA system with N_f subcarriers. Assuming all subcarriers are in use and have been divided into K subchannels, each subchannel is then made up of P subcarriers, thus $PK = N_f$. Note that K is also the maximum number of users. Some parameters are defined as follows:

- $\mathbf{x}_i^{(k)}$: transmit symbol vector of user k at time index i;
- $\mathbf{H}_i^{(k)}$: channel transfer function matrix of user k at time index i, or simply $\mathbf{H}^{(k)}$ if channel is time-invariant;

- $\mathbf{x}_i$: the overall transmit symbol vector consisting of symbols from all active users at time index i;
- $\mathbf{V}^{(k)}$: the user-specific subchannel division matrix for user k, which specifies the subcarriers belonging to the individual user and is therefore a diagonal matrix.

The downlink transmission of OFDMA can be modeled as

$$\mathbf{r}_{i,\mathrm{DL}}^{(k)} = \mathbf{V}^{(k)}\mathbf{H}_{\mathrm{DL}}^{(k)}\mathbf{x}_i + \mathbf{n}_i^{(k)} = \mathbf{V}^{(k)}\mathbf{H}_{\mathrm{DL}}^{(k)}\mathbf{x}_i^{(k)} + \mathbf{n}_i^{(k)}, \tag{3.31}$$

where subscript $[\cdot]_{\mathrm{DL}}$ indicates downlink. Note that the definitions of $\mathbf{x}_i^{(k)}$ and $\mathbf{V}^{(k)}$ are different in conventional OFDMA and interleaved OFDMA.

Conventional OFDMA Assume a set of transmit symbols $[X_{0,i}^{(k)}, ..., X_{p,i}^{(k)}, ..., X_{P-1,i}^{(k)}]$ is transmitted to user k, where $0 \leq p < P$ and $0 \leq k < K$. In conventional OFDMA, the components of $\mathbf{x}_i^{(k)}$ are given by

$$x_{m,i}^{(k)} = \begin{cases} X_{p,i}^{(k)}, & \text{for } m = k \times P + p \\ 0, & \text{otherwise} \end{cases}, \tag{3.32}$$

where $0 \leq m \leq N_f - 1$. Furthermore, the entries on the main diagonal of $\mathbf{V}^{(k)}$ are defined as

$$V_{jj}^{(k)} = \begin{cases} 1, & \text{for } kP \leq j < (k+1)P \\ 0, & \text{otherwise} \end{cases}. \tag{3.33}$$

Interleaved OFDMA On the other hand, in interleaved OFDMA, $\mathbf{x}_i^{(k)}$ and $\mathbf{V}^{(k)}$ are redefined as

$$x_{m,i}^{(k)} = \begin{cases} X_{p,i}^{(k)}, & \text{for } m = p \times K + k \\ 0, & \text{otherwise} \end{cases}, \tag{3.34}$$

and

$$V_{jj}^{(k)} = \begin{cases} 1, & \text{for } \ j = pK + k \\ 0, & \text{otherwise} \end{cases}, \tag{3.35}$$

respectively. The definitions of $\mathbf{V}^{(k)}$ in (3.33) and (3.35) ensure that each subcarrier is assigned to only one user. Hence, whether in conventional OFDMA or interleaved OFDMA the overall transmit symbol vector $\mathbf{x}_i$ is the superposition of signals from all active users

$$\mathbf{x}_i = \sum_{k=0}^{K-1} \mathbf{x}_i^{(k)}, \tag{3.36}$$

and in turn $\mathbf{x}_i^{(k)}$ can be obtained from $\mathbf{x}_i$

$$\mathbf{x}_i^{(k)} = \mathbf{V}^{(k)}\mathbf{x}_i, \tag{3.37}$$

as described in (3.31). In addition, note that at a terminal receiver not only the signals transmitted over desired subchannels are received, but also the signals over subchannels of other users. We denote this *overall* received symbol vector by $\mathbf{r}_{i,\mathrm{DL}}$ and at the receiver of user k we have

$$\mathbf{r}_{i,\mathrm{DL}} = \mathbf{H}_{\mathrm{DL}}^{(k)}\mathbf{x}_i + \mathbf{n}_i, \tag{3.38}$$

and, as given in (3.31), the symbols associated with this specific user are extracted from $\mathbf{r}_{i,\mathrm{DL}}$ by

$$\mathbf{r}_{i,\mathrm{DL}}^{(k)} = \mathbf{V}^{(k)}\mathbf{r}_{i,\mathrm{DL}}. \tag{3.39}$$

The noise vector $\mathbf{n}_i^{(k)}$ in (3.31)

$$\mathbf{n}_i^{(k)} = \mathbf{V}^{(k)}\mathbf{n}_i. \tag{3.40}$$

Components in $\mathbf{n}_i$ are assumed to be complex-valued white Gaussian random variables.

3.3.2 Uplink Transmission Model of OFDMA

Under the assumption of perfect synchronization in the uplink, the received symbol vector at the base station (BS) receiver, $\mathbf{r}_{i,\mathrm{UL}}$, can be represented as

$$\mathbf{r}_{i,\mathrm{UL}} = \sum_{k=0}^{K-1}\mathbf{H}_{\mathrm{UL}}^{(k)}\mathbf{x}_i^{(k)} + \mathbf{n}_i = \sum_{k=0}^{K-1}\mathbf{H}_{\mathrm{UL}}^{(k)}\mathbf{V}^{(k)}\mathbf{x}_i + \mathbf{n}_i = \sum_{k=0}^{K-1}\bar{\mathbf{H}}_{\mathrm{UL}}^{(k)}\mathbf{x}_i + \mathbf{n}_i = \bar{\mathbf{H}}_{\mathrm{UL}}\mathbf{x}_i + \mathbf{n}_i, \tag{3.41}$$

where $\bar{\mathbf{H}}_{\mathrm{UL}}^{(k)} = \mathbf{H}_{\mathrm{UL}}^{(k)}\mathbf{V}^{(k)}$. It is obvious that $\bar{\mathbf{H}}_{\mathrm{UL}}^{(k)}$ only consists of the discrete transfer functions of the subcarriers assigned to user k, and other diagonal entries of $\bar{\mathbf{H}}_k$ are set to be zero, so that

$$\bar{\mathbf{H}}_{\mathrm{UL}} = \sum_{k=0}^{K-1}\bar{\mathbf{H}}_{\mathrm{UL}}^{(k)} = \sum_{k=0}^{K-1}\mathbf{H}_{\mathrm{UL}}^{(k)}\mathbf{V}^{(k)} \tag{3.42}$$

can be seen as a combined uplink channel matrix. $\mathbf{x}_i$ is a vector consisting of transmit symbols of all active users, as defined in (3.36). Equations (3.41) and (3.42) indicate that if perfect synchronization is available, the uplink transmission model of OFDMA can be simplified to be like a simple OFDM transmission. Fig. 3.6 shows the block diagram of uplink transmission of an OFDMA system.

3.3.3 Comparison of Conventional and Interleaved OFDMA

Coherence Bandwidth Before comparing conventional OFDMA with interleaved OFDMA, we first recall the *frequency selective behavior* of multipath channels. In Section 2.2.1, it is mentioned that frequency selective fading is caused if the bandwidth of the transmitted signal is much larger than the coherence bandwidth of the channel. As defined in [59], the *coherence bandwidth*, B_c, is a statistical measurement of the range of frequency over which the channel

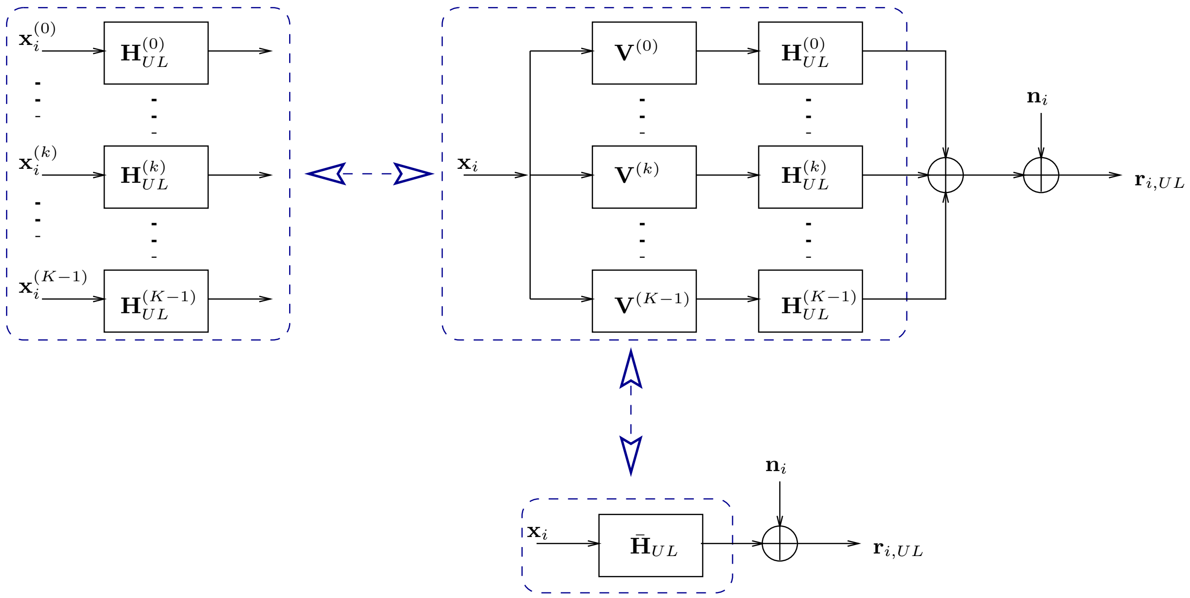

Figure 3.6: Uplink transmission of OFDMA.

can be considered "flat". In other words, the coherence bandwidth is the range of frequencies over which two frequency components have a strong potential for amplitude correlation. For a given channel with channel impulse response (CIR) $h(t,\tau)$, the *power delay profile* (PDP) of the channel, $P_h(\tau)$, is calculated by [49]

$$P_h(\tau) = \int_{-\infty}^{\infty} |h(t,\tau)|^2 dt. \tag{3.43}$$

The *mean excess delay* is the normalized first-order moment of the PDP, for a discrete time PDP there is

$$\bar{\tau} = \frac{\sum_{\tau=0}^{L-1} P_h(\tau)\tau}{P_m}, \tag{3.44}$$

where P_m is the zeroth-order moment of PDP, i.e., time-integrated power

$$P_m = \sum_{\tau=0}^{L-1} P_h(\tau) \tag{3.45}$$

The *rms delay spread* is the normalized second-order central moment of PDP and is defined as

$$\sigma_\tau = \sqrt{\bar{\tau^2} - (\bar{\tau})^2}, \tag{3.46}$$

where $\bar{\tau^2}$ is the normalized second-order moment

$$\bar{\tau^2} = \frac{\sum_{\tau=0}^{L-1} P_h(\tau)\tau^2}{P_m}. \tag{3.47}$$

Furthermore, as described in [59], the coherence bandwidth B_c is a defined relation derived from the rms delay spread. If the coherence bandwidth is defined as the bandwidth over which

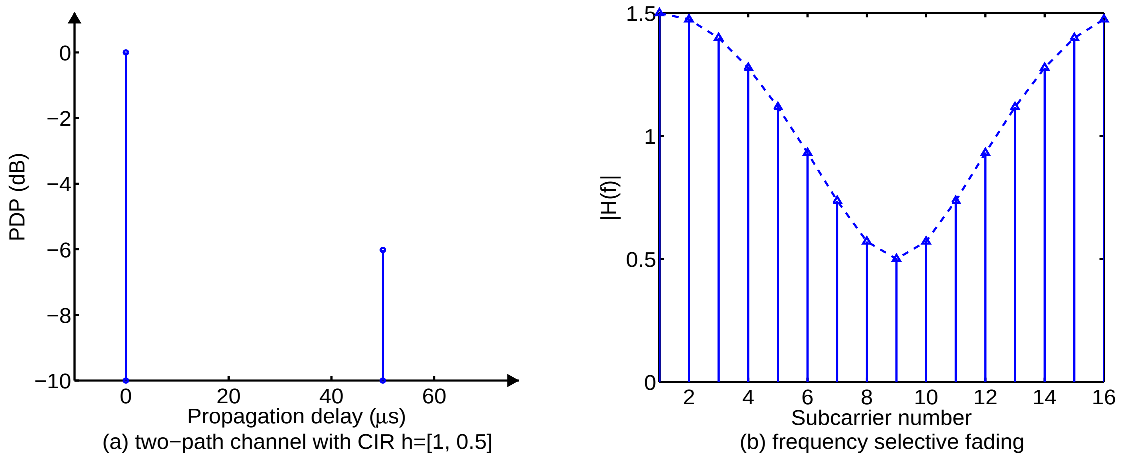

Figure 3.7: Two path channel with discrete CIR $h = [1, 0.5]$: power delay profile (left) and frequency selective behavior (right).

the frequency correlation function is above 0.9, then the coherence bandwidth for a given PDP is approximately

$$B_c|_{0.9} = \frac{1}{50\sigma_\tau}. \tag{3.48}$$

If the definition is relaxed and the correlation function is above 0.5, the coherence bandwidth is approximately

$$B_c|_{0.5} = \frac{1}{5\sigma_\tau}. \tag{3.49}$$

Using the equations above, the coherence bandwidth of a given channel can be easily calculated. For instance, Fig. 3.7(a) depicts the PDP a two-path channel with CIR $h = [1, 0.5]$ and tap delay $\tau_0 = 0$ and $\tau_1 = 50\mu s$. The coherence bandwidths with respect to (3.48) and (3.49) are approximately $B_c|_{0.9} = 1KHz$ and $B_c|_{0.5} = 10KHz$, respectively. Assuming $T = \tau_1 = 50\mu s$ is the symbol duration, the baseband bandwidth is then given by $B = 1/T = 20KHz$. As compared to coherence bandwidth, signals transmitted over this channel apparently undergo frequency selective fading. If OFDM with 16 subcarriers is implemented, the subcarrier spacing is $B/16 = 1.25KHz$ and thus signals over each subcarrier experience flat fading. In the meantime, adjacent subcarriers are strongly correlated with respect to amplitude. The frequency selective behavior of the channel is demonstrated in Fig. 3.7(b).

Influence of Frequency Selective Fading on Conventional and Interleaved OFDMA

In conventional OFDMA, adjacent subcarriers are assigned to an individual user. If the channel is frequency selective, subcarriers in one subchannel may simultaneously undergo deep fading due to the amplitude correlation, which will lead to a severe performance loss for the user using this subchannel. In contrast, in interleaved OFDMA the distance of subcarriers in a subchannel may be longer than the coherence bandwidth of the channel and thus experience independent fading. It is well known that these independent subcarriers are unlikely to fade simultaneously, so that an acceptable system performance is available for each user.

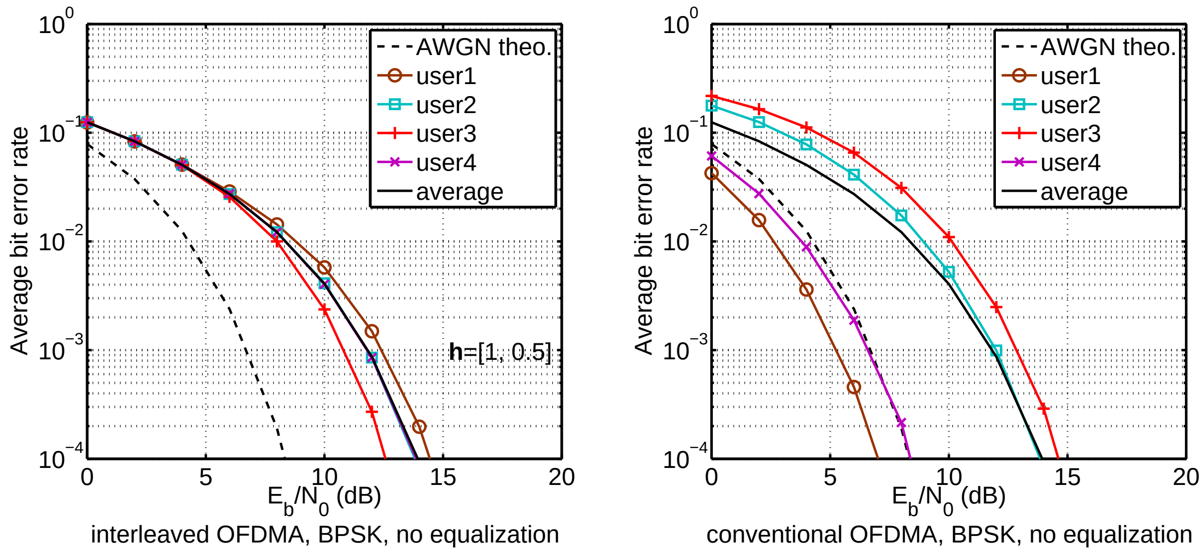

Figure 3.8: OFDMA transmission over two-path channel: interleaved OFDMA (left) and conventional OFDMA (right).

As an example, we made the simulations for the downlink transmission of an uncoded OFDMA system with four users over the two-path channel given in Fig. 3.7. Fig. 3.8 depicts the average BER performance for each user. As shown, with interleaved OFDMA all users attain similar performance; whereas with conventional OFDMA user #3 has a bad performance owing to deep fading, and user #1 and #4 have better performance due to the channel gain. As a consequence, when conventional OFDMA is used, subchannels should be assigned carefully such that each user can benefit from the channel instead of suffering from the loss. It is likely to come true since the channels may differ from user to user in a multiuser system.

3.3.4 Adaptive Subcarrier Assignment

Conventional and interleaved OFDMA are fixed assignment strategies for frequency (subcarriers) sharing. In recent years *adaptive* OFDMA subcarrier assignment has been under study. It is based on the fact that subcarriers fade differently from user to user, i.e., signals from different users experience independent fading. Therefore, system performance differs greatly using different allocation schemes. If an intelligent subcarrier allocation scheme is employed, it ensures that the majority of subcarriers allocated to each user perceive gain (relative to mean) rather than attenuation. However, the *channel state information* (CSI) of channels is required at the transmitter, which undoubtedly complicates the receiver structure. Algorithms for *dynamic subcarrier allocation* have been investigated in many contributions [38], [88]. For instance, in [38] one method is proposed to realize a judicious subcarrier assignment by maximizing the throughput of the system.

In addition, note that no matter what kind of allocation scheme is used, one subcarrier can be allocated to only one user. That means the transmission models in (3.31) and (3.41) are valid for all allocation schemes, and only the user-specific subchannel division matrix $\mathbf{V}^{(k)}$ has to be adjusted according to the adopted subcarrier allocation scheme.

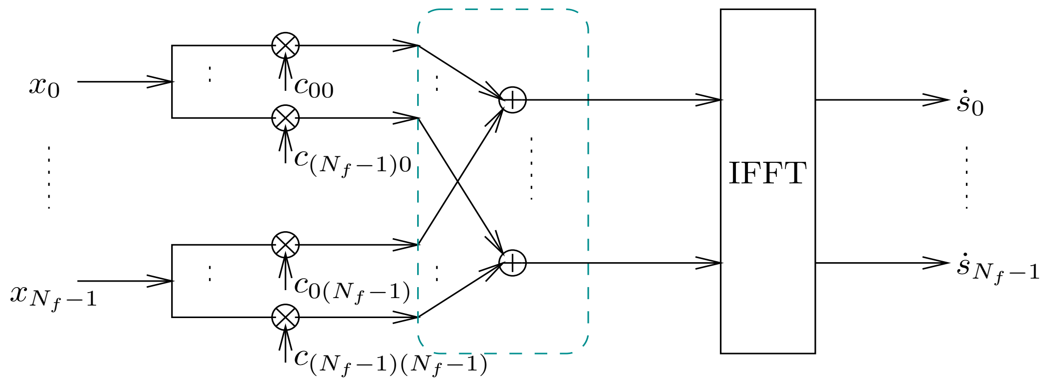

Figure 3.9: Spreading in MC-CDM : an scheme where each symbol is spread over all subcarriers.

3.4 Combination of OFDM and Spread Spectrum

In this section, we study *multi-carrier spread spectrum* (MC-SS) transmission based on OFDM, CDM and their corresponding multiple access techniques, and then form the resultant systems with a vector-valued transmission model.

MC-SS aims to compensate for the poor performance of uncoded OFDM systems in frequency selective fading channels by exploiting the frequency diversity in OFDM. Three transmission schemes are considered in the following:

- **MC-CDM** *Multi-Carrier Code Division Multiplexing* is considered as a single user transmission scheme. In MC-CDM, simultaneously transmitted symbols of a *single* user are spread over multiple subcarriers. In general, to distinguish different symbols over the same subchannel, each symbol is spread by a unique code sequence. MC-CDM can also be implemented in a multiple access scenario if combined with TDMA.
- **CDM-OFDMA** *Code Division Multiplexing - Orthogonal Frequency Division Multiple Access* is a variant of MC-CDM used in a multiple access environment on the basis of OFDMA. In CDM-OFDMA, different users access the BS receiver by sharing the subchannels, and simultaneously transmitted symbols of an individual user are spread over the subcarriers in the assigned subchannel.
- **MC-CDMA** *Multi-Carrier Code Division Multiple Access* is another variant of MC-CDM applied in a multiple access environment on the basis of CDMA. In MC-CDMA, all active users can make use of all available bandwidth simultaneously, and are distinguished from each other by different spreading codes. Moreover, simultaneously transmitted symbols of each individual user can be either spread over all available subcarriers and separated by different codes, or distinguished by distinct subchannels with the same spreading code.

3.4.1 MC-CDM

MC-CDM, or OFDM-CDM, is an intuitive realization of MC-SS. Referring to the subcarrier allocation scheme for OFDMA, MC-CDM can be realized by spreading each data symbol over

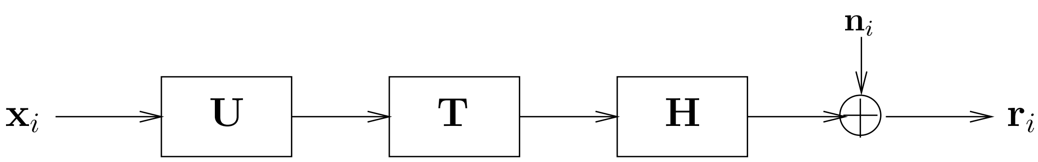

Figure 3.10: Simplified MC-CDM transmission.

(1) all available subcarriers (defined as full spreading); (2) a subchannel made up of adjacent subcarriers (defined as sub-band spreading); (3) a subchannel made up of interleaved subcarriers (defined as interleaved spreading). We begin with the first case where maximum frequency diversity is achieved.

Consider the transmission of a symbol vector $\mathbf{x}_i = [x_{0,i}, x_{1,i}, \ldots, x_{N_f-1,i}]^T$ at time index i. Assuming all subcarriers are available for each individual symbol, as shown in Fig. 3.9, a symbol $x_{j,i}$, $x_{j,i} \in \mathbf{x}_i$, is multiplied by a spreading sequence $\mathbf{c}_j = [c_{0j}, c_{1j}, ..., c_{(N_f-1)j}]^T$, and the resulting spread signals, $c_{0j}x_{j,i}, c_{1j}x_{j,i}, ..., c_{(N_f-1)j}x_{j,i}$, are transmitted simultaneously over different subcarriers. The signal on each subcarrier is then the superposition of weighted replica of $x_{j,i}$, $j = 0, 1, ..., N_f - 1$. For example, on the mth subcarrier, $\dot{x}_{m,i} = c_{m0}x_{0,i} + c_{m1}x_{1,i} + ... + c_{m(N_f-1)}x_{N_f-1,i} = \sum_{j=0}^{N_f-1} c_{mj}x_{j,i}$. Note that each symbol in $\mathbf{x}_i$ has a unique spreading sequence such that it can be separated from others at the receiver. Therefore, the spread transmit symbol vector is defined as

$$\dot{\mathbf{x}}_i = \mathbf{U}\mathbf{x}_i, \tag{3.50}$$

where the spreading matrix $\mathbf{U}$ is of the form

$$\mathbf{U} = \begin{bmatrix} \mathbf{c}_0, & ..., & \mathbf{c}_j, & ..., & \mathbf{c}_{N_f-1} \end{bmatrix}_{N_f \times N_f}. \tag{3.51}$$

In order to avoid extra interference and preserve channel capacity, we want to make use of the spreading sequences with orthogonality, i.e.,

$$\mathbf{U}^H\mathbf{U} = \mathbf{I}, \tag{3.52}$$

which ensures that after despreading $(\mathbf{U}^H)$, the signals can be recovered without loss, provided that there exist no channel distortion and noise. Fig. 3.10 illustrates the basic block diagram of an uncoded MC-CDM transmission. The received symbol vector at the output of the DFT is given by

$$\mathbf{r}_i = \mathbf{H}\mathbf{U}\mathbf{x}_i + \mathbf{n}_i, \tag{3.53}$$

where $\mathbf{r}_i$ is the corrupted version of the spread symbol vector $\dot{\mathbf{x}}_i$. On the other hand, if we spread each symbol just over a subchannel in OFDM and a fixed subcarrier allocation scheme is used, the spreading matrix $\mathbf{U}$ is then a block diagonal matrix of the form

$$\mathbf{U} = \begin{pmatrix} \mathbf{W}_0 & & & & \mathbf{0} \\ & \ddots & & & \\ & & \mathbf{W}_q & & \\ & & & \ddots & \\ \mathbf{0} & & & & \mathbf{W}_{Q-1} \end{pmatrix}_{N_f \times N_f}. \tag{3.54}$$

$\mathbf{W}_q$ is a square matrix of size $N_Q \times N_Q$, and $N_Q = \frac{N_f}{Q}$ is the number of subcarriers in a subchannel. Accordingly, (3.53) is modified to be

$$\mathbf{r}_i = \mathbf{HTUx}_i + \mathbf{n}_i, \tag{3.55}$$

where $\mathbf{T}$ is a permutation matrix which allocate the signals spread by $\mathbf{U}$ to the associated subchannels, and $\mathbf{T}^H\mathbf{T} = \mathbf{I}$. In the case of full spreading and sub-band spreading, $\mathbf{T} = \mathbf{I}$ is an identity matrix. Specially, if equidistant subcarriers are taken for a subchannel, $\mathbf{T}$ works as an interleaver. In addition, for the latter case all $\mathbf{W}_q$, $0 \leq q \leq Q-1$, which are defined as spreading submatrices, could be identical or different, since symbols can be separated by distinct subchannels. But within a subchannel, each symbol has a unique spreading sequence.

Selection of Spreading Code in MC-CDM

The spreading sequences satisfying (3.52) are preferred to reduce the interference. One candidate of such sequences is Fourier matrix. As shown in (3.3), either row sequences or column sequences are orthogonal to one another, and $\mathbf{F}^H\mathbf{F} = \mathbf{F}^{-1}\mathbf{F} = \mathbf{I}$ fulfills the requirement in (3.52). In principle, implementation of Fourier spreading reduces the peak-to-average power ratio (PAPR) in an OFDM-based system. However, Fourier transformation has been applied to OFDM as a modulation technique. If Fourier spreading is over *all* IDFT subcarriers, the system turns to be a single carrier system for a serial transmission with cyclic extension. On the other hand, if a spreading scheme as in (3.54) is used and equidistant interleaved subcarriers are selected for a subchannel, the joint implementation of DFT spreading (over subchannels) and IDFT of the modulation can be replaced by a number of small IDFTs plus rotation of transmitted symbols in the complex plane [9], which reduces the computational complexity of the system.

Hadamard-Walsh matrices are most commonly used in MC-SS as orthogonal spreading matrices. These matrices are real-valued and are built of chips that belong to the set {-1,+1}. For the size of the transform being a power of two, the matrices are easily constructed using a recursive matrix operation

$$V_\gamma = \begin{bmatrix} V_{\gamma-1} & V_{\gamma-1} \\ V_{\gamma-1} & -V_{\gamma-1} \end{bmatrix}, \tag{3.56}$$

where V_γ is the $2^\gamma \times 2^\gamma$ Hadamard matrix formed by using the Hadamard matrix $V_{\gamma-1}$, and the initial matrix V_1 is given by

$$V_1 = \begin{bmatrix} 1 & 1 \\ 1 & -1 \end{bmatrix}. \tag{3.57}$$

Note that in order to satisfy (3.52), the Hadamard matrix should be normalized before being used as the spreading matrix or submatrix.

In addition, in some contributions [66], *random sequences, e.g., pseudo-noise* (PN) *sequences*, are used as spreading sequences as well. However, since random sequences are not orthogonal, *multiuser interference* (MUI) occurs as soon as two users are active, even in the case of an ideal channel.

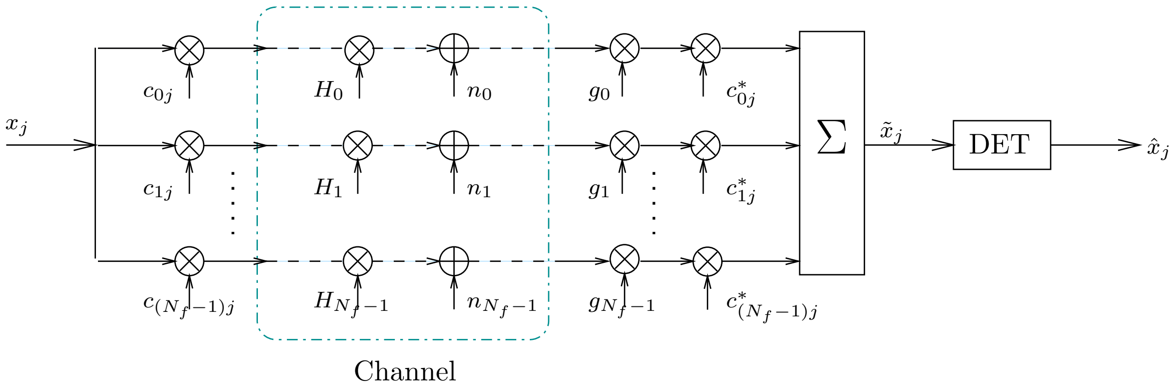

Figure 3.11: Diversity transmission with MC-CDM.

Diversity Transmission with MC-CDM

An OFDM transmission provides a number of parallel flat fading subchannels without mutual interference. For a given WSSUS channel model, statistical fading of these parallel multiplexing channels is characterized by the Rayleigh distribution [9]. It is well known that Rayleigh fading channels exhibit a poor bit error performance in the case of uncorrelated transmission [58]. Therefore, it is reasonable to apply CDM in order to achieve a diversity gain at the receiver. For each transmitted symbol, MC-CDM can be regarded as a weighted diversity transmission in *frequency domain*. As shown in Fig. 3.11, a symbol x_j is weighted by a spreading sequence and then spread over all available subcarriers. All subcarriers are disturbed by respective additive white Gaussian noise of identical variance, and undergo flat Rayleigh fading. On the receiving side, the weights g^*_m and c^*_{mj} perform an *equal gain combining* (EGC) or a *maximum ratio combining* (MRC) (g^*_m and c^*_{mj}) of all received signals and yields a corrupted version of x_j, $\tilde{x}_j$, which is then passed to the detector. The two combining techniques are introduced as follows.

Equal Gain Combining *Equal gain combining* (EGC) only compensates for the phase rotations caused by the channel. The coefficients on each subcarrier are given by

$$g_m = \frac{H^*_m}{|H_m|}, \; m = 1, ..., N. \tag{3.58}$$

The noise components, $\tilde{n}_m = g_m n_m$, have the same statistical properties as n_m.

Maximum Ratio Combining *Maximum ratio combining* (MRC) compensates for the phases, and weighs the received symbols according to their *output* SNR. The coefficients are the complex conjugate of the corresponding channel transfer function

$$g_m = H^*_m. \tag{3.59}$$

This operation is equivalent to *matched filtering* (MF).

When using diversity transmission and reception, the performance improvement depends on the *independence* of the fading characteristics of the channels (subcarriers). Consequently, in order to obtain the optimal diversity, *uncorrelated* subcarriers should be grouped for diversity transmission. For this reason, spreading based on sub-band sometimes will not fulfill this condition due to the possible correlation between adjacent subcarriers. In contrast, MC-CDM with full spreading and interleaved spreading meet the requirement and may provide a better diversity performance.

Furthermore, in comparison to simple diversity transmission over OFDM subcarriers, MC-CDM retains bandwidth efficiency if the number of the multiplexed symbols are identical to the number of subcarriers.

Interference due to Frequency Selective Behavior of the Channel

Extend the transmission in Fig. 3.11 to all symbols in a transmit vector $\mathbf{x}_i$ of length N_f at time index i. If matched filtering is implemented, after despreading it yields

$$\tilde{\mathbf{x}}_i = \mathbf{U}^H\mathbf{T}^H\mathbf{H}^H\mathbf{H}\mathbf{T}\mathbf{U}\mathbf{x}_i + \mathbf{U}^H\mathbf{T}^H\mathbf{H}^H\mathbf{n}_i. \tag{3.60}$$

Note that even if an orthogonal spreading matrix is used, owing to multipath propagation, the orthogonality among the transmitted symbols will be destroyed by the frequency selective behavior of the channel, and interference will be introduced. Accordingly, an individual symbol in vector $\tilde{\mathbf{x}}_i$ is expressed as

$$\tilde{x}_{j,i} = \underbrace{\frac{1}{N_f}\sum_{m=0}^{N_f-1}|H_m|^2\cdot x_{j,i}}_{\text{signal of interest}} + \underbrace{\sum_{m=0}^{N_f-1}\sum_{n=0,n\neq j}^{N_f-1}|H_m|^2 c_{mj}^* c_{mn} x_{n,i}}_{\text{interference}} + \underbrace{\sum_{m=0}^{N_f-1} H_m^* c_{mj}^* n_{m,i}}_{\text{noise}}. \tag{3.61}$$

Let $\mathbf{R}$ =$\mathbf{HTU}$ represent the equivalent transmission channel matrix. The correlation matrix of $\mathbf{R}$ is then

$$\mathbf{R}^H\mathbf{R}=\mathbf{U}^H\mathbf{T}^H\mathbf{H}^H\mathbf{H}\mathbf{T}\mathbf{U}. \tag{3.62}$$

Furthermore, assuming $E[|H_m|^2] = |H|^2$, an estimate of $E[|H_m|^2]$ results from the sample mean of the $|H_m|^2$

$$|\hat{H}|^2 = \frac{1}{N_f}\sum_{m=0}^{N_f-1}|H_m|^2. \tag{3.63}$$

As a consequence, the diagonal entries of the correlation matrix $\mathbf{R}^H\mathbf{R}$ are identical. For instance, Fig. 3.13(a) illustrates the correlation matrix $\mathbf{R}^H\mathbf{R}$ for a MC-CDM system, and the *histogram* of diagonal entries is depicted in Fig. 3.13(b) which verifies the analysis in (3.63). The off-diagonal entries, or the crosstalk between code division subchannels, stand for the interference from other symbols. The correlation matrix of the corresponding transfer function matrix, $\mathbf{H}^H\mathbf{H}$, is shown in Fig. 3.12. Furthermore, Figs. 3.14 and 3.15 demonstrate the cases of sub-band spreading and interleaved fading. The estimation of $|H|^2$ is performed within the defined subchannels such that different results are shown: in sub-band spreading, the channel gain (here we consider the code division subchannel) is subchannel dependent, i.e., suffers from the amplitude correlation of the adjacent OFDM-subcarriers. Note that the interference in both cases is limited in the subchannel.

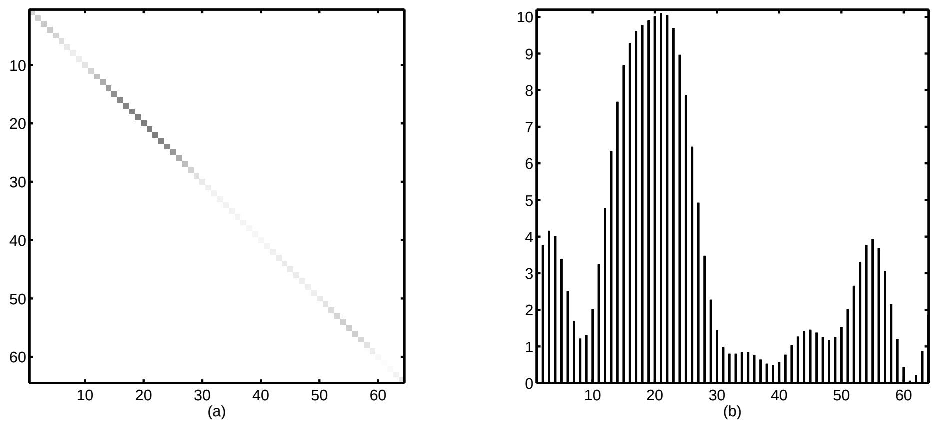

Figure 3.12: Power distribution of the equivalent OFDM channel matrix of a frequency selective fading channel (left), and the histogram of diagonal entries (right).

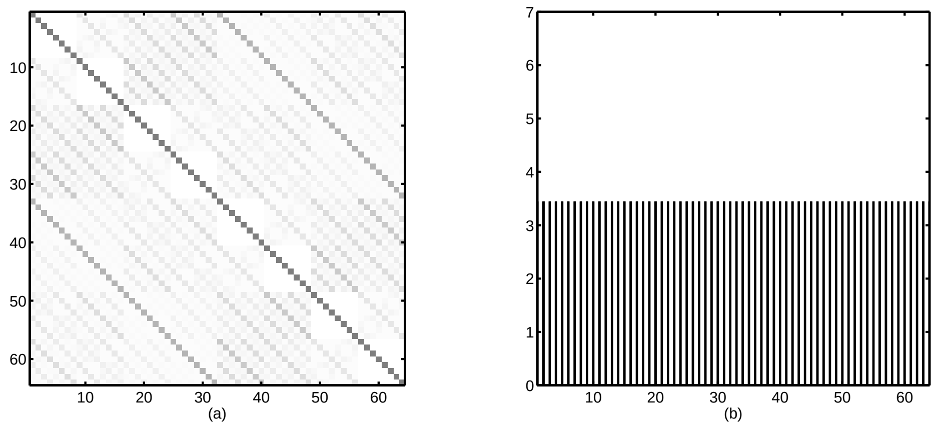

Figure 3.13: MC-CDM with full spreading.

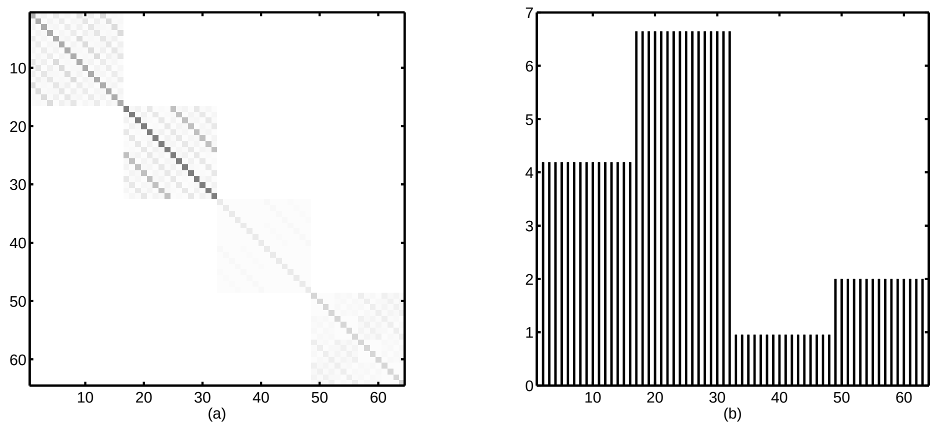

Figure 3.14: MC-CDM with sub-band spreading.

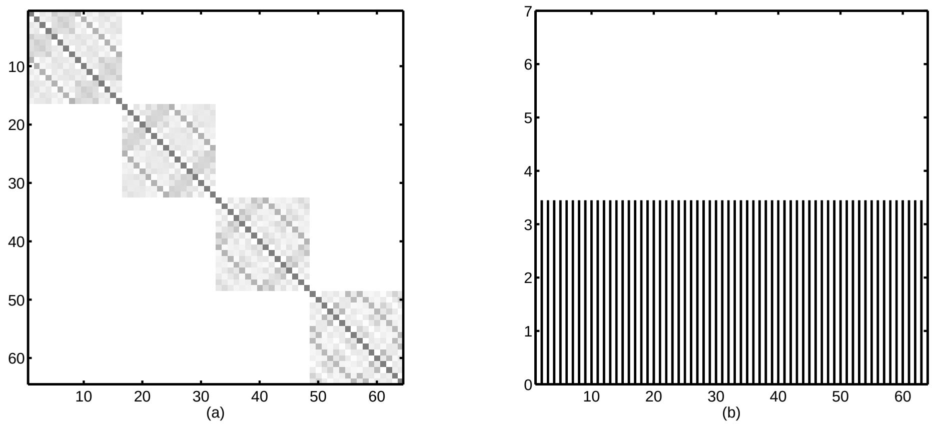

Figure 3.15: MC-CDM with interleaved spreading.

Vector Detection for MC-CDM The interference in MC-CDM has to be dealt with. We prefer to implement vector detection at the receiver to recover the transmitted signals, and suppress the interference. According to (3.55), the equalization matrices are given by (2.28) and (2.32), respectively, with

$$\mathbf{H}_c = \mathbf{R} = \mathbf{HTU}. \tag{3.64}$$

In addition, in Fig. 3.16 we give an example to show how the system benefits from the diversity gain offered by MC-CDM, as compared to OFDM with error-correction fading. The same simulation environment is taken as in Fig. 3.4.

3.4.2 CDM-OFDMA

To apply MC-CDM in a multiple access scenario, we can use Code Division Multiplexing - Orthogonal Frequency Division Multiple Access (CDM-OFDMA) or Multi-Carrier Code Division Multiple Access (MC-CDMA). In a CDM-OFDMA system, one or several subchannels are assigned to an individual user such that users are separated in frequency. Within a subchannel, the user spreads transmit symbols over subcarriers, and therefore symbols of an individual user have to be separated by different spreading sequences (or codewords). We first consider the form of the spreading matrix in CDM-OFDMA. Let $\mathbf{U}$ represent the *overall* spreading matrix and $\mathbf{U}^{(k)}$ denote the user-specific spreading matrix of user k. $\mathbf{U}^{(k)}$ is of the form

$$\mathbf{U}^{(k)} = \begin{pmatrix} 0 & & & \mathbf{0} \\ & \ddots & & \\ & & \mathbf{W}_k & \\ & & & \ddots \\ \mathbf{0} & & & 0 \end{pmatrix}_{N_f \times N_f} \qquad 0 \leq k \leq K-1, \tag{3.65}$$

where $\mathbf{W}_k$ is called the user-specific spreading submatrix of size $P \times P$, K is the maximum number of users, and $PK = N_f$. Consequently, $\mathbf{U} = \sum_{k=0}^{K-1} \mathbf{U}^{(k)}$ is a block diagonal matrix

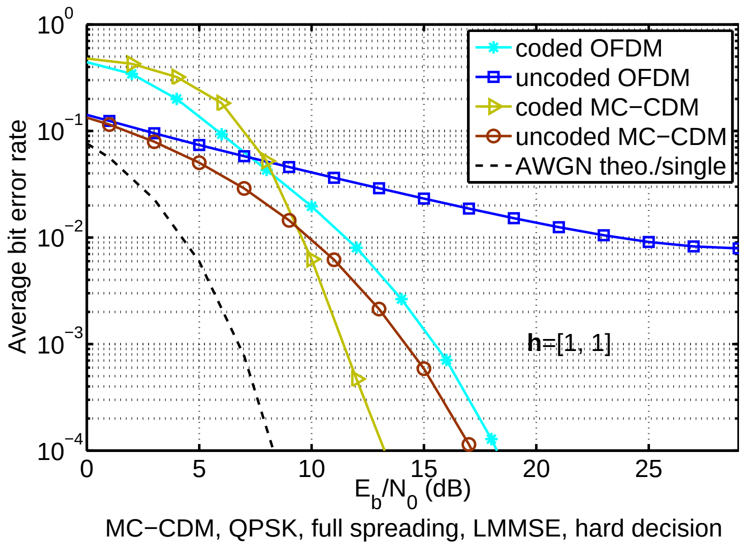

Figure 3.16: Diversity gain in MC-CDM.

with $\{\mathbf{W}_k\}_{k=0}^{K-1}$ on the main diagonal, like in (3.54). For any l and k, $0 \leq l, k < K$, $\mathbf{W}_l$ and $\mathbf{W}_k$ can be either the same or distinct. Both conventional and interleaved OFDMA can be taken as basis for CDM-OFDMA, and in consequence we have the so-called conventional CDM-OFDMA (C-CDM-OFDMA) and interleaved CDM-OFDMA (I-CDM-OFDMA), respectively.

Downlink Transmission

For downlink transmission, the received *overall* symbol vector after DFT generally can be written as

$$\mathbf{r}_{i,\mathrm{DL}} = \mathbf{H}_{\mathrm{DL}}^{(k)} \mathbf{T}_c \mathbf{U} \mathbf{x}_i + \mathbf{n}_i, \tag{3.66}$$

where the overall transmit vector $\mathbf{x}_i$ is defined in (3.36). $\mathbf{T}_c$ is a permutation matrix that maps the spread signals of different users to the respective subchannels. $\mathbf{T}_c$ is an identity matrix if C-CDM-OFDMA is taken and an interleaver if I-CDM-OFDMA is taken. Furthermore, it should be pointed out that in CDM-OFDMA, the transmit symbol vector of user k at time index i, $\mathbf{x}_i^{(k)}$, is defined in (3.32). In a frequency selective channel, due to the interference within the subchannel of an individual user (so-called *self-interference*, SI), vector detection is required to recover the transmit symbols. Nevertheless, the computational complexity can be reduced by extracting the received signals of user k from the corresponding subchannel, i.e.,

$$\mathbf{r}_{i,\mathrm{DL}}^{(k)} = \mathbf{V}^{(k)} \mathbf{T}_c^H \mathbf{r}_{i,\mathrm{DL}},$$

and then processing the non-zero symbols in $\mathbf{r}_{i,\mathrm{DL}}^{(k)}$ further. $\mathbf{V}^{(k)}$ is defined in (3.33). This scheme is applicable because there exists no MUI under the assumption of perfect synchronization.

Uplink Transmission

Assuming a synchronous transmission is available in the uplink, the general description for the uplink transmission is expressed as

$$\begin{aligned}\mathbf{r}_{i,\mathrm{UL}} &= \sum_{k=0}^{K-1} \mathbf{H}_{\mathrm{UL}}^{(k)} \mathbf{T}_c \mathbf{U}^{(k)} \mathbf{x}_i^{(k)} + \mathbf{n}_i \\ &= \sum_{k=0}^{K-1} \mathbf{H}_{\mathrm{UL}}^{(k)} \mathbf{T}_c \mathbf{U}^{(k)} \mathbf{x}_i + \mathbf{n}_i. \end{aligned} \tag{3.67}$$

Referring to (3.65) and (3.33),

$$\mathbf{U}^{(k)} = \mathbf{V}^{(k)} \mathbf{U}. \tag{3.68}$$

Further, since subchannels belonging to different users are not overlapping, a combined uplink channel transfer function matrix can be defined as

$$\bar{\mathbf{H}}_{\mathrm{UL}} = \sum_{k=0}^{K-1} \mathbf{H}_{\mathrm{UL}}^{(k)} \mathbf{T}_c \mathbf{V}^{(k)}, \tag{3.69}$$

which is equivalent to the definition in (3.42). As a consequence, (3.67) can be simplified to

$$\mathbf{r}_{i,\mathrm{UL}} = \bar{\mathbf{H}}_{\mathrm{UL}} \mathbf{U} \mathbf{x}_i + \mathbf{n}_i. \tag{3.70}$$

Obviously, (3.70) has an expression similar to (3.66). This implies that, on the assumption that perfect synchronization is available in the uplink and the channels are time-invariant or slowly faded (e.g., block-wise faded), only the channel gain on each subcarrier is required, and therefore, the transmission model is simplified significantly. Furthermore, no MUI is introduced in a CDM-OFDMA system, since the orthogonality among the subchannels is kept.

3.4.3 MC-CDMA

In the case of CDM-OFDMA, only a group of subcarriers are assigned to an individual user, and users are separated in frequency. In the case of MC-CDMA, instead, all active subcarriers are available for an individual user, and user separation is accomplished by assigning different spreading sequences to different users. Furthermore, all three spreading schemes for MC-CDM can be applied in MC-CDMA. If full spreading is taken, the *overall* spreading matrix is of the form similar to that in (3.51), and the user-specific spreading matrix of user k, $\mathbf{U}^{(k)}$, can be defined as

$$\mathbf{U}^{(k)} = \begin{bmatrix} \mathbf{0}, & \ldots, & \mathbf{c}_{k,0}, & \ldots, & \mathbf{c}_{k,P-1}, & \ldots, & \mathbf{0} \end{bmatrix}_{N_f \times N_f}, \tag{3.71}$$

where we assume that a maximum of P different sequences are used by each user, and $PK = N_f$. Namely, P represents the maximum number of symbols which are permitted to be transmitted by each user. Note that in the case of full spreading, the maximum number of users could be N_f if $P = 1$. For convenience, in the following we allocate the spreading sequences of one user in row direction of $\mathbf{U}^{(k)}$ in an interleaved way, and accordingly, the transmit symbol vector of user k at time index i, $\mathbf{x}_i^{(k)}$, is defined in (3.34).

Furthermore, if sub-band or interleaved spreading is taken, $\mathbf{U}^{(k)}$ is then defined as

$$\mathbf{U}^{(k)} = \begin{pmatrix} \mathbf{W}_{k,0} & \mathbf{0} & \dots & \mathbf{0} \\ \mathbf{0} & \mathbf{W}_{k,1} & \dots & \mathbf{0} \\ \mathbf{0} & \vdots & \ddots & \vdots \\ \mathbf{0} & \mathbf{0} & \dots & \mathbf{W}_{k,P-1} \end{pmatrix}_{N_f \times N_f}, \tag{3.72}$$

where $\mathbf{W}_{k,p}$ stands for the user-specific spreading submatrix of user k on the pth subchannel. $\mathbf{W}_{k,p}$ is a $K \times K$ matrix with a spreading sequence of user k on column k and zeros on other columns. For any p and q, $\mathbf{W}_{k,p}$ and $\mathbf{W}_{k,q}$ can be identical or different, but $\mathbf{W}_{l,p}$ and $\mathbf{W}_{k,q}$ must be different for any $l \neq k$. For both (3.71) and (3.72) $\mathbf{U} = \sum_{k=0}^{K-1} \mathbf{U}^{(k)}$ holds.

Downlink Transmission

The downlink transmission model of MC-CDMA is similar to that of CDM-OFDMA:

$$\mathbf{r}_{i,\mathrm{DL}} = \mathbf{H}_{\mathrm{DL}}^{(k)} \mathbf{T}_m \mathbf{U} \mathbf{x}_i + \mathbf{n}_i, \tag{3.73}$$

where $\mathbf{x}_i = \sum_{k=0}^{K-1} \mathbf{x}_i^{(k)}$. Similary, in the case of full spreading and sub-band spreading, $\mathbf{T}_m = \mathbf{I}$; whereas in the case of interleaved spreading, $\mathbf{T}_m$ permutes the spread signals of each symbol over the subcarriers in an interleaved way. However, it is worth noting that the definitions of $\mathbf{U}$ and $\mathbf{x}_i$ differ in MC-CDMA and CDM-OFDMA, and $\mathbf{T}_m$ distinguishes itself from $\mathbf{T}_c$ in the case of interleaved spreading as well.

In a multipath propagation scenario, the frequency selective fading will destroy the orthogonality between the spreading sequences, and thus lead to the MUI as well as SI. In consequence, to suppress the interference, vector detection is required in MC-CDMA systems for the downlink transmission. In addition, since signals of each user are spread over the total bandwidth, the matrix size cannot be reduced.

Uplink Transmission

The uplink transmission model is described as

$$\begin{aligned} \mathbf{r}_{i,\mathrm{UL}} &= \sum_{k=0}^{K-1} \mathbf{H}_{\mathrm{UL}}^{(k)} \mathbf{T}_m \mathbf{U}^{(k)} \mathbf{x}_i^{(k)} + \mathbf{n}_i \\ &= \sum_{k=0}^{K-1} \mathbf{H}_{\mathrm{UL}}^{(k)} \mathbf{T}_m \mathbf{U}^{(k)} \mathbf{x}_i + \mathbf{n}_i. \end{aligned} \tag{3.74}$$

Since each user occupies all available subcarriers, a simplified expression cannot be found for the uplink transmission of MC-CDMA. Nevertheless, (3.74) also can be expressed in a vector-matrix multiplication form

$$\mathbf{r}_{i,\mathrm{UL}} = \bar{\mathbf{H}}_{\mathrm{UL}} \bar{\mathbf{U}}_{\mathrm{UL}} \mathbf{x}_i + \mathbf{n}_i, \tag{3.75}$$

where the composite channel transfer function matrix

$$\bar{\mathbf{H}}_{\mathrm{UL}} = \left[\begin{array}{ccccc} \mathbf{H}_{\mathrm{UL}}^{(0)}\mathbf{T}_m & \dots & \mathbf{H}_{\mathrm{UL}}^{(k)}\mathbf{T}_m & \dots & \mathbf{H}_{\mathrm{UL}}^{(K-1)}\mathbf{T}_m \end{array} \right]_{N_f \times (N_f K)}, \tag{3.76}$$

and the spreading matrix

$$\bar{\mathbf{U}}_{\mathrm{UL}} = \begin{bmatrix} \mathbf{U}^{(0)} \\ \vdots \\ \mathbf{U}^{(k)} \\ \vdots \\ \mathbf{U}^{(K-1)} \end{bmatrix}_{(N_f K) \times N_f}. \tag{3.77}$$

It is clear that channel state information (CSI) of all active users is required for coherent detection. This undoubtedly creates a great demand for the channel estimation in the uplink.

3.5 Summary

This chapter contributes to modeling of synchronous OFDM-based systems with vector-valued transmission models, on the assumption that perfect synchronization is available in both, downlink and uplink. Furthermore, the channel is assumed to be time-invariant, at least during the transmission of one OFDM-symbol.

A simple vector-valued equivalent low-pass transmission model has been derived for OFDM in Section 3.2. OFDM offers a bandwidth efficient data transmission by converting a wideband frequency selective fading channel into a set of parallel narrowband flat fading subchannels. In consequence simple one-tap equalizers can be used for data detection. However, OFDM suffers from the deep fading on some subcarriers, which results from the frequency selective behavior of a time dispersive channel. To cope with this problem, error-correction coding has been implemented in practical OFDM systems. Another solution to this problem is MC-CDM.

MC-CDM can overcome the deep fading in OFDM by means of diversity. The performance improvement depends on the independence of the fading characteristics of the subcarriers. Three spreading schemes are proposed for MC-CDM: full spreading, interleaved spreading, and sub-band spreading. The maximum frequency diversity can be achieved by MC-CDM with full spreading.

For multiuser scenarios, OFDMA, CDM-OFDMA, and MC-CDMA can be adopted as multiple access techniques. Two transmission schemes with fixed subcarrier assignment have been proposed for OFDMA: conventional OFDMA based on sub-bands, and interleaved OFDMA based on subchannels which use subcarriers with maximum frequency diversity. Conventional OFDMA and interleaved CDM-OFDMA are defined accordingly.

CDM-OFDMA and MC-CDMA are two variants of MC-CDM. Intuitively, the former is based on OFDMA, and the latter is based on CDMA. This leads to their differences in system structure, parameter estimation, and so on. For instance, in the case of frequency selective fading, in CDM-OFDMA the orthogonality among the users remains, and thus an individual user suffers only from SI, whereas in MC-CDMA he will suffer from both SI and MUI.

Similar to pure OFDMA, a simplified vector-valued transmission model can be formed for CDM-OFDMA uplink, and in principle, vector detection is needed only by each individual user. In contrast, when modeling the uplink transmission of MC-CDMA, no simplification can be made, and the channel state information of all users are required for multiuser detection.

Chapter 4

Influence of Frequency Offsets on OFDM-based Systems

4.1 Chapter Overview

Many studies have shown that one of the principal disadvantages of OFDM is its sensitivity to frequency offset [4], [50], [72], [66]: that is either a *carrier frequency offset* (CFO), f_ϵ, which is the frequency difference between transmitter and receiver local oscillator; or the *Doppler shift* due to the relative motion of transmitter and receiver. Throughout this work Doppler shift is treated as a characteristic of wireless mobile channels, and has been investigated in Chapter 2. This chapter restricts our attention to the influence of carrier frequency offset on OFDM-based systems.

In an OFDM system, a carrier frequency offset has threefold effects. First of all, a CFO will lead to amplitude reduction and phase rotation of the desired signals. Secondly, crosstalk between subcarriers, i.e., *inter-carrier interference* (ICI), is introduced. Finally, a phase error increases linearly with time, or, more exactly, with the indices of the symbol vectors. Moreover, in the case of multiple access, the ICI will further give rise to MUI, even in the absence of channel attenuation.

In this chapter, the vector-valued transmission models derived in Chapter 3 are modified for the case where a frequency offset is present. Such models allow us to analyze the effects of CFO in a convenient way, and make it possible to deal with the corrupted received signals with vector detection techniques.

The chapter is organized as follows. In Section 4.2 the sensitivity of pure OFDM to a CFO is investigated in detail. A matrix describing the first two effects of CFO is derived independent of the channel transfer function matrix. Subsequently, Section 4.3 extends our investigation to a multiple access scenario, OFDMA, where we will find that MUI caused by ICI affects the conventional and interleaved OFDMA differently. The impacts of CFO on MC-CDM, as well as the transmission schemes for multiuser scenarios, CDM-OFDMA and MC-CDMA, are studied in Section 4.4.

For simplicity, perfect timing synchronization is assumed throughout the chapter, even for the uplink transmission. Consideration for time offset only is given for OFDM. A synchronization policy which concerns the asynchrony in the uplink will be addressed later in Chapter 6.

4.2 OFDM Systems in the Presence of Carrier Frequency Offset

Consider the equivalent baseband transmission of an OFDM system in the presence of a carrier frequency offset f_ϵ, as shown in Fig. 4.1. The absolute value of f_ϵ, $|f_\epsilon|$, is either an integer multiple or a fraction of Δf, or the sum of them. If normalizing f_ϵ to the subcarrier frequency spacing Δf, the resulting normalized CFO in general can be expressed as

$$\epsilon = \frac{f_\epsilon}{\Delta f} = \delta + \varepsilon, \tag{4.1}$$

where δ is an integer and $\varepsilon \in (-0.5, +0.5)$.

The influence of an integer CFO on OFDM is different from the influence of a fractional CFO. In the event that $\delta \neq 0$ and $\epsilon = 0$, symbols transmitted on a certain subcarrier, e.g., subcarrier m, will shift to another subcarrier m_δ,

$$m_\delta = m + \delta \mod N_f - 1. \tag{4.2}$$

If δ is unknown at the receiver, then information can not be recovered from the received symbols such that the resulting *bit error rate* (BER) will be 0.5. Nonetheless, no ICI is caused by an integer CFO.

4.2.1 Transmission Model

As shown in Fig. 4.1, on the receiving side the received signal after down-conversion can be written as

$$g(t) = \exp(j2\pi f_\epsilon t)\cdot h_K(t) * s(t) + n(t), \tag{4.3}$$

with

$$s(t) = \sum_{i=0}^{\infty} \sum_{k=0}^{N_s-1} s_{k,i}\delta(t - (iN_s + k)T) * h_T(t). \tag{4.4}$$

Suppose that the bandwidth of receive filter is large and able to tolerate the frequency offset. The signal after the receive filter is then given by

$$\begin{aligned} y(t) &= h_R(t) * g(t) \\ &= h_R(t) * \exp(j2\pi f_\epsilon t)\cdot h_K(t) * s(t) + h_R(t) * n(t) \\ &= \exp(j2\pi f_\epsilon t)\cdot h(t) * \sum_{i=0}^{\infty} \sum_{k=0}^{N_s-1} s_{k,i}\delta(t - (iN_s + k)T) + h_R(t) * n(t). \end{aligned} \tag{4.5}$$

In order to derive a transmission model for OFDM transmission with CFO, two steps have to be taken: first the one-shot transmission of a symbol vector is considered, and then the successive

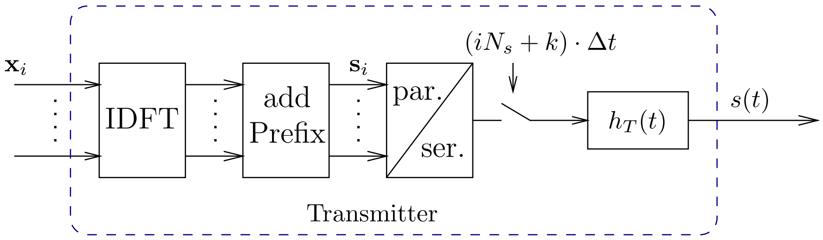

(a)

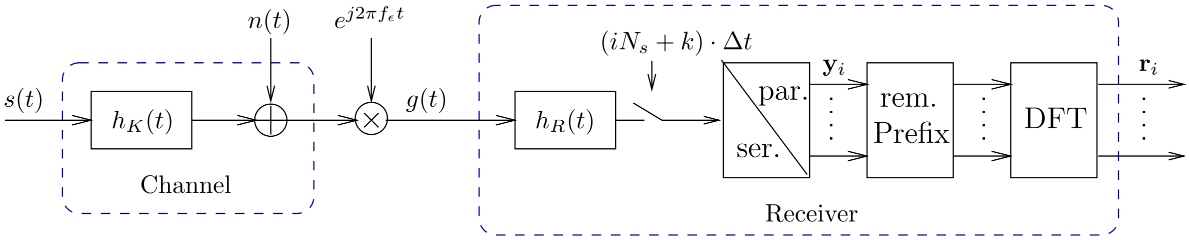

(b)

Figure 4.1: An OFDM system in the presence of carrier frequency offset.

data transmission. Assume a single symbol vector is transmitted, e.g., at $i = 0$. Ignoring the distortion of noise and sampling at the time instants $t = t_k = kT$, $T = 1/(N_f \Delta f)$, it yields

$$y_{k,0} = \exp\left(\frac{j2\pi\epsilon k}{N_f}\right) \sum_{0}^{L-1} s_{k-l,0} h_l + \dot{n}_{k,0}, \qquad 0 \leq k < N_s,\ N_s = N_f + N_g. \tag{4.6}$$

h_l is defined in (3.11). By means of a vector of length N_s, the effects of ϵ with respect to the time domain symbols y_k can be expressed as

$$\mathbf{e} = \left[1, \exp\left(j2\pi\epsilon\frac{1}{N_f}\right), \ldots, \exp\left(j2\pi\epsilon\frac{N_f + N_g - 1}{N_f}\right)\right]. \tag{4.7}$$

Referring to (4.6), in the presence of a CFO, the vector-valued transmission model in (3.19) has to be rewritten as

$$\mathbf{r}_0 = \mathbf{F}\mathbf{G}_{pp}\mathbf{E}\hat{\mathbf{H}}_0\mathbf{G}_{ap}\mathbf{F}^{-1}\mathbf{x}_0 + \mathbf{n}_0, \tag{4.8}$$

where $\mathbf{E}$ is a diagonal matrix with $\mathbf{e}$ on the main diagonal

$$\mathbf{E} = \mathrm{diag}\left\{\mathbf{e}\right\} = \begin{pmatrix} 1 & & & & \mathbf{0} \\ & \ddots & & & \\ & & \exp\left(j2\pi\epsilon\frac{k}{N_f}\right) & & \\ & & & \ddots & \\ \mathbf{0} & & & & \exp\left(j2\pi\epsilon\frac{N_f+N_g-1}{N_f}\right) \end{pmatrix}_{(N_f+N_g)\times(N_f+N_g)}. \tag{4.9}$$

Now we want to transform $\mathbf{F}\mathbf{G}_{pp}\mathbf{E}\hat{\mathbf{H}}_0\mathbf{G}_{ap}\mathbf{F}^{-1}$ into some form such that the relationship between the channel transfer function matrix and effects of a CFO can be embodied (in the frequency

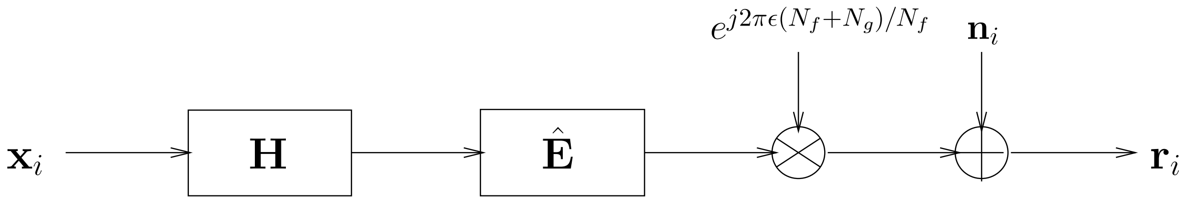

Figure 4.2: A simplified OFDM transmission model in the presence of CFO in the equivalent low-pass domain.

domain). For this reason, we try to find a matrix $\hat{\mathbf{E}}$ that satisfies

$$\hat{\mathbf{E}}\mathbf{F}\mathbf{G}_{pp} = \mathbf{F}\mathbf{G}_{pp}\mathbf{E}. \tag{4.10}$$

Right-multiplying both sides of (4.10) by $\mathbf{G}_{ap}\mathbf{F}^{-1}$ yields

$$\hat{\mathbf{E}}\mathbf{F}\mathbf{G}_{pp}\mathbf{G}_{ap}\mathbf{F}^{-1} = \mathbf{F}\mathbf{G}_{pp}\mathbf{E}\mathbf{G}_{ap}\mathbf{F}^{-1}.$$

Since $\mathbf{G}_{pp}\mathbf{G}_{ap} = \mathbf{I}$ and $\mathbf{F}\mathbf{F}^{-1} = \mathbf{I}$, we obtain then

$$\hat{\mathbf{E}} = \mathbf{F}\mathbf{G}_{pp}\mathbf{E}\mathbf{G}_{ap}\mathbf{F}^{-1}. \tag{4.11}$$

Substituting (4.10) into (4.8), it yields

$$\mathbf{r}_0 = \hat{\mathbf{E}}\mathbf{F}\mathbf{G}_{pp}\hat{\mathbf{H}}_0\mathbf{G}_{ap}\mathbf{F}^{-1}\mathbf{x}_0 + \mathbf{n}_0 = \hat{\mathbf{E}}\mathbf{H}\mathbf{x}_0 + \mathbf{n}_0. \tag{4.12}$$

Obviously, the result in (4.12) meets our requirement, and the matrix $\hat{\mathbf{E}}$ stands for the impacts of a CFO in the frequency domain. More details about $\hat{\mathbf{E}}$ will be introduced in Section 4.2.2.

In the following, we extend the study to the successive transmission of multiple symbol vectors. It can be seen that apart from the effects reflected in the matrix $\hat{\mathbf{E}}$, the CFO also leads to a phase increment between the received signals at a rate of $2\pi\epsilon\left(1+\frac{N_g}{N_f}\right)$/vector, provided that the frequency offset is not compensated during the transmission. To be specific, for the ith received symbol vector, an additional instantaneous phase error is induced by frequency offset, which is calculated by $2\pi i\epsilon(N_f+N_g)/N_f \bmod 2\pi$, where i denotes the vector index. Defining $\theta = 2\pi\epsilon(N_f+N_g)/N_f$, in the case of successive transmission the received vector can be expressed as

$$\mathbf{r}_i = \exp\left(j2\pi i\epsilon\left(1+\frac{N_g}{N_f}\right)\right)\hat{\mathbf{E}}\mathbf{H}\mathbf{x}_i + \mathbf{n}_i = \exp(j\theta i)\hat{\mathbf{E}}\mathbf{H}\mathbf{x}_i + \mathbf{n}_i, \quad i = 0,1,...,\infty \tag{4.13}$$

Additionally, in a sense $\exp(j\theta i)\hat{\mathbf{E}}\mathbf{H}$ can be viewed as a composite channel matrix between the transmit vector $\mathbf{x}_i$ and the received vector $\mathbf{r}_i$, and consequently $\exp(j\theta i)$ represents part of the phase characteristics of the composite channel. Even if $\mathbf{H}$ is time-invariant, this composite channel will vary with time (or exactly, vector index i) due to the CFO. But during the transmission of a vector, the channel keeps constant. According to (4.13), the block diagram of a simplified OFDM transmission model with CFO is shown in Fig. 4.2.

4.2.2 The Influence of Carrier Frequency Offset on OFDM

A brief view of the influence of an integer CFO has been made before. In the following we restrict our discussion to a fractional CFO, i.e., $\epsilon = \varepsilon \in (-0.5, +0.5)$. We begin with the full details of the matrix $\hat{\mathbf{E}}$. The time-variant phase error $i\theta$ is studied then. Afterwards, *signal to interference and noise ratio* (SINR) and performance degradation due to frequency offset are investigated. In the end, some timing errors are considered together with carrier frequency offset.

Details of Matrix $\hat{\mathbf{E}}$

Recall that $\hat{\mathbf{E}} = \mathbf{F}\mathbf{G}_{pp}\mathbf{E}\mathbf{G}_{ap}\mathbf{F}^{-1}$. To simplify the expression, let us replace $\mathbf{G}_{pp}\mathbf{E}\mathbf{G}_{ap}$ by $\dot{\mathbf{E}}$. It yields then

$$\begin{aligned}\dot{\mathbf{E}} = \mathbf{G}_{pp}\mathbf{E}\mathbf{G}_{ap} &= \mathrm{diag}\left\{\left[\exp\left(j2\pi\epsilon\frac{N_g}{N_f}\right), \ldots, \exp\left(j2\pi\epsilon\frac{N_f+N_g-1}{N_f}\right)\right]\right\} \\ &= \exp\left(j2\pi\epsilon\frac{N_g}{N_f}\right) \times \mathrm{diag}\left\{\left[1, \ldots, \exp\left(j2\pi\epsilon\frac{N_f-1}{N_f}\right)\right]\right\},\end{aligned} \tag{4.14}$$

which is a $N_f \times N_f$ diagonal matrix. The first product term on the RHS of (4.14), $\exp\left(j2\pi\epsilon\frac{N_g}{N_f}\right)$, represents a constant phase shift caused by the CFO. Further calculating $\hat{\mathbf{E}} = \mathbf{F}\dot{\mathbf{E}}\mathbf{F}^{-1}$, the resulting matrix is a square matrix of the form

$$\hat{\mathbf{E}} = \begin{pmatrix} S_0 & S_1 & \cdots & S_{N_f-2} & S_{N_f-1} \\ S_{-1} & S_0 & \cdots & S_{N_f-3} & S_{N_f-2} \\ \vdots & \vdots & \ddots & \vdots & \vdots \\ S_{-N_f+2} & S_{-N_f+3} & \cdots & S_0 & S_1 \\ S_{-N_f+1} & S_{-N_f+2} & \cdots & S_{-1} & S_0 \end{pmatrix}_{N_f \times N_f}, \tag{4.15}$$

where

$$\begin{aligned} S_{m'-m} &= \frac{1}{N_f}\exp\left(\frac{j2\pi\epsilon N_g}{N_f}\right)\sum_{q=0}^{N_f-1}\exp\left(\frac{j2\pi q(m'-m+\epsilon)}{N_f}\right) \\ &= \frac{1}{N_f}\exp\left(\frac{j2\pi\epsilon N_g}{N_f}\right)\frac{\sin\pi(m'-m+\epsilon)}{\sin\pi\left(\frac{m'-m+\epsilon}{N_f}\right)} \\ &\times \exp\left(j\pi\frac{(N_f-1)(m'-m+\epsilon)}{N_f}\right), \end{aligned} \tag{4.16}$$

and

$$\begin{aligned} S_0 &= \frac{1}{N_f}\exp\left(\frac{j2\pi\epsilon N_g}{N_f}\right)\sum_{q=0}^{N_f-1}\exp\left(\frac{j2\pi q\epsilon}{N_f}\right) \\ &= \frac{1}{N_f}\exp\left(\frac{j2\pi\epsilon N_g}{N_f}\right)\exp\left(\frac{j\pi\epsilon(N_f-1)}{N_f}\right)\frac{\sin\pi\epsilon}{\sin\left(\frac{\pi\epsilon}{N_f}\right)}. \end{aligned} \tag{4.17}$$

In (4.16) and (4.17), q, m' and m represent the sampling clock index (counting from the first signal after the prefix), the carrier index at the transmitter and the carrier index at the receiver, respectively. For $m' = m$, S_0 stands for the influence of the CFO on the desired symbol on each subcarrier. Note that all entries on the main diagonal of $\hat{\mathbf{E}}$ are identical. This implies that in OFDM, a carrier frequency offset has the same effects on the desired symbols of all subcarriers. If $\epsilon \neq 0$, the desired symbols have an amplitude reduction of $\frac{\sin \pi\epsilon}{N_f \sin\left(\frac{\pi\epsilon}{N_f}\right)}$ and a phase rotation of $\phi_0 = \frac{\pi\epsilon(2N_g+N_f-1)}{N_f}$, and the larger the CFO, the more severely the amplitude decreases. Conversely, as $\epsilon \to 0$, it yields

$$\lim_{\epsilon \to 0} \frac{1}{N_f} \frac{\sin \pi\epsilon}{\sin\left(\frac{\pi\epsilon}{N_f}\right)} = 1, \tag{4.18}$$

such that no attenuation occurs.

For $m' \neq m$, on the other hand, $S_{m'-m}$ represents the crosstalk from subcarrier m' to subcarrier m. The corresponding ICI is the product of $S_{m'-m}$ and the value of the transmit symbol on subcarrier m', provided that there exits no channel distortion, i.e., $\mathbf{H}$ is an identity matrix. Moreover, it follows from (4.16) that

$$\frac{\sin \pi(m'-m+\epsilon)}{N_f \sin \pi\left(\frac{m'-m+\epsilon}{N_f}\right)} = \frac{(-1)^{m'-m}\sin(\pi\epsilon)}{N_f \sin \pi\left(\frac{m'-m+\epsilon}{N_f}\right)}. \tag{4.19}$$

The magnitude of the interference is therefore quantified by

$$\left|\frac{\sin \pi(m'-m+\epsilon)}{N_f \sin \pi\left(\frac{m'-m+\epsilon}{N_f}\right)}\right| = \left|\frac{\sin \pi\epsilon}{N_f \sin \pi\left(\frac{m'-m+\epsilon}{N_f}\right)}\right|, \tag{4.20}$$

which is dependent on the absolute value of $m'-m$, if ϵ is given. It can be seen that for $|m'-m| < N_f/2$, the smaller the difference between m' and m, the larger the quantity in (4.20), whereas for $|m'-m| > N_f/2$, the larger the difference of m' and m, the larger the quantity in (4.20). It is because, for convenience, in this work the FFT transform is performed from 0 to $N_f - 1$. Namely, instead of being in the middle of the frequency spectrum (of a low-pass filter), the zero-frequency together with positive frequencies is shifted horizontally to the left, and the negative frequencies are shifted to the right and allocated by means of a modulus operation, mod N_f. As a consequence, the normalized frequency $\# -1$ is shifted to $\# N_f - 1$, and $\#-2$ to $\# N_f - 2$, and so on. The $N_f - 1$th subcarrier is in fact next to the 0th subcarrier, such that ICI from this subcarrier is one of the greatest. Hence, a conclusion can be drawn that the signal on one subcarrier is mainly affected by the crosstalk from the nearby subcarriers. To give an example, Fig. 4.3 illustrates the normalized *envelope* distribution of the entries of $\hat{\mathbf{E}}$ with $N_f = 16$, $N_g = 4$, and $\epsilon = 0.3$.

Moreover, the phase rotation of each interference component is given by

$$\begin{aligned}\phi_{m'-m} &= \frac{(2N_g + N_f - 1)\pi\epsilon + (N_f - 1)(m'-m)\pi}{N_f} \\ &= \phi_0 + \left(1 - \frac{1}{N_f}\right)(m'-m)\pi.\end{aligned} \tag{4.21}$$

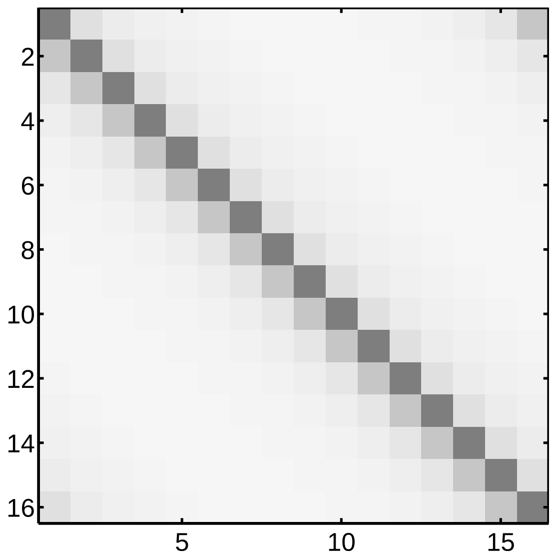

Figure 4.3: Normalized envelope distribution of $\hat{\mathbf{E}}$, with $N_f = 16$, $N_g = 4$, and $\epsilon = 0.3$.

If N_f is large enough, i.e.,

$$\lim_{N_f \to \infty} 1 - \frac{1}{N_f} = 1,$$

it yields then

$$\phi_{m'-m} \approx \phi_0 + (m' - m)\pi, \tag{4.22}$$

and

$$\begin{aligned} \exp(j\phi_{m'-m}) &= \cos\phi_{m'-m} + j\sin\phi_{m'-m} \\ &\approx (-1)^{m'-m}\exp(j\phi_0). \end{aligned} \tag{4.23}$$

Substituting (4.19) and (4.23) into (4.16) yields

$$\begin{aligned} S_{m'-m} &\approx \frac{(-1)^{m'-m}\sin(\pi\epsilon)}{N_f \sin\pi\left(\frac{m'-m+\epsilon}{N_f}\right)} \cdot (-1)^{m'-m}\exp(j\phi_0) \\ &= \exp(j\phi_0)\frac{\sin(\pi\epsilon)}{N_f \sin\pi\left(\frac{m'-m+\epsilon}{N_f}\right)}. \end{aligned} \tag{4.24}$$

It can be seen that under the assumption of $|\epsilon| < 0.5$, the following relationships hold

$$\begin{cases} \frac{\sin(\pi\epsilon)}{N_f \sin\pi\left(\frac{m'-m+\epsilon}{N_f}\right)} < 0 & \text{for } \epsilon > 0 \text{ and } m' < m, \text{ or, for } \epsilon < 0 \text{ and } m' > m, \\ \frac{\sin(\pi\epsilon)}{N_f \sin\pi\left(\frac{m'-m+\epsilon}{N_f}\right)} > 0 & \text{for } \epsilon > 0 \text{ and } m' > m, \text{ or, for } \epsilon < 0 \text{ and } m' < m. \end{cases} \tag{4.25}$$

It indicates that the entries in the upper triangle part and the lower triangle part will have different sign, if the phase shift ϕ_0 can be compensated. As an example, Fig. 4.4 depicts how

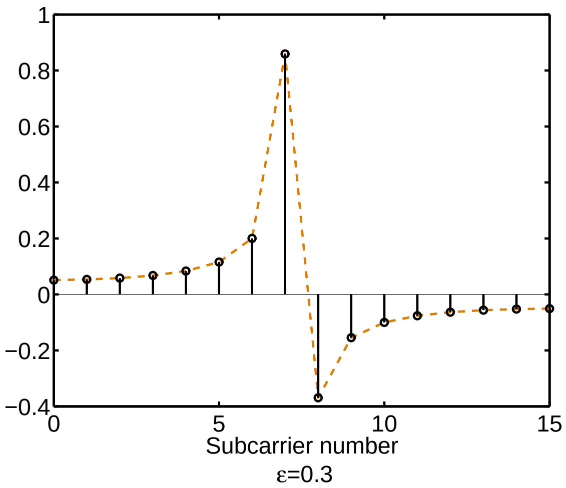

Figure 4.4: Effects of carrier frequency offset on an individual subcarrier: an example to testify (4.25) for $\epsilon = 0.3$ (left) and $\epsilon = -0.3$ (right), with $N_f = 16$, $N_g = 4$ and $m' = 7$.

the value of $\frac{\sin(\pi\epsilon)}{N_f \sin\pi\left(\frac{m'-m+\epsilon}{N_f}\right)}$ varies with m when m' is given, i.e., how the signal transmitted on some subcarrier interferes with signals over other subcarriers. We assume an OFDM system with $N_f = 16$ and $N_g = 4$, and specify the subcarrier $m' = 7$. It is shown that the desired signal on subcarrier $m = m' = 7$ is attenuated, and the subcarriers near to it obtain more interference. In addition, the analysis in (4.25) is verified.

Furthermore, comparing (4.17) with (4.24), we can find that the product term $\exp(j\phi_0)$ appears in both equations. If the phase offset ϕ_0 could be corrected, the matrix left will be approximately real-valued.

Effects of the Time-Variant Phase Error

In addition to the influence of $\hat{\mathbf{E}}$, the time-variant phase error $i\theta = 2\pi i\epsilon(1 + \frac{N_g}{N_f})$ caused by CFO is also of importance. That is because, even if ϵ is small and the performance loss caused by $\hat{\mathbf{E}}$ is tolerable, the cumulative phase rotation $i\theta$ with some i may lead to a wrong decision and hence severe performance degradation, especially in the case of PSK and QAM mapping. Together with the phase rotation involved in $\hat{\mathbf{E}}$, at vector index i the received symbol vector has an overall instantaneous phase error

$$\theta_{r,i} = i\theta + \phi_0 \mod 2\pi \tag{4.26}$$

by reason of the CFO ϵ. Fig. 4.5 illustrates the QPSK constellation and the phase rotation of three received symbol vectors over an ideal channel with a CFO $\epsilon = 0.02$. It seems that after the transmission of some symbols a wrong decision is likely to be made. Except for the phase rotation, it is also shown that received symbols are distorted by ICI, so that symbols from an identical alphabet cannot focus on the same position in the map.

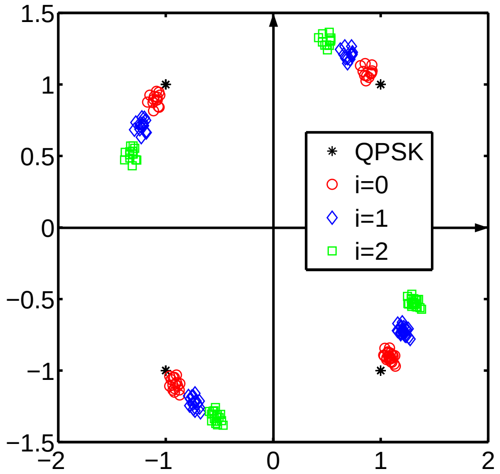

Figure 4.5: Time-variant phase rotation due to frequency offset in OFDM, with $N_f = 64$, $N_g = 16$, and $\varepsilon = 0.02$.

Signal to Interference and Noise Ratio

Referring to (4.13), each element of $\mathbf{r}_i$ can be expressed as

$$r_{m,i} = \underbrace{\exp(j\theta i) S_0 H_m x_{m,i}}_{\text{desired signal}} + \underbrace{\exp(j\theta i) \sum_{m'=0, m' \neq m}^{N_f-1} S_{m'-m} H_{m'} x_{m',i}}_{\text{ICI}} + \underbrace{n_{m,i}}_{\text{noise component}}, \quad m = 0, ..., N_f - 1. \tag{4.27}$$

The second term on the RHS of (4.27) shows that if data are transmitted through a fading channel, on each subcarrier the ICI from some other subcarrier will be weighted by the transfer function at that frequency. In the following, we will investigate the *signal to interference and noise ratio* (SINR) for AWGN channels and frequency selective fading channels with a CFO, respectively.

AWGN Channel with CFO If an AWGN channel is assumed, i.e., $\mathbf{H} = \mathbf{I}$, then $\mathbf{r}_i = \exp(j\theta i)\hat{\mathbf{E}}\mathbf{x}_i + \mathbf{n}_i$, and $r_{m,i}$ is simplified to be

$$r_{m,i} = \exp(j\theta i) S_0 x_{m,i} + \exp(j\theta i) \sum_{m'=0, m' \neq m}^{N_f-1} S_{m'-m} x_{m',i} + n_{m,i}. \tag{4.28}$$

Letting $I_{ICI,0}^{(m)}$ denote the ICI on the subcarrier m, it is expressed as

$$I_{ICI,0}^{(m)} = \exp(j\theta i) \sum_{m'=0, m' \neq m}^{N_f-1} S_{m'-m} x_{m',i}, \tag{4.29}$$

where the subscript "0" means that the transmission is conditioned on an ideal or an AWGN channel. Since we have assumed that the transmit symbols are independent and identically distributed (i.i.d) complex random variables (r.v.) with zero mean and variance σ_x^2, the power of ICI is thus calculated by

$$E[|I_{ICI,0}^{(m)}|^2] = E\left[\left|\sum_{m'=0,m'\neq m}^{N_f-1} S_{m'-m}x_{m',i}\right|^2\right] = \sum_{m'=0,m'\neq m}^{N_f-1} |S_{m'-m}|^2\sigma_x^2. \tag{4.30}$$

Note that

$$\sum_{m'=0}^{N_f-1} |S_{m'-m}|^2 = 1 \quad \text{for } \forall\ m = 0, 1, ..., N_f - 1. \tag{4.31}$$

Consequently, the *signal to interference ratio* (SIR) in an ideal channel, SIR_0, can be obtained by

$$SIR_0 = \frac{|S_0|^2\sigma_x^2}{E\left[\left|I_{ICI,0}^{(m)}\right|^2\right]} = \frac{|S_0|^2}{\sum_{m'=0,m'\neq m}^{N_f-1} |S_{m'-m}|^2} = \frac{|S_0|^2}{(1-|S_0|^2)}. \tag{4.32}$$

Furthermore, because the noise component in (4.28) is assumed to be an i.i.d complex Gaussian r.v. with zero mean and variance σ_n^2, the SINR in an AWGN channel, $SINR_0$, is given by

$$SINR_0 = \frac{|S_0|^2\sigma_x^2}{E\left[\left|I_{ICI,0}^{(m)}\right|^2\right] + \sigma_n^2} = \frac{|S_0|^2}{\sum_{m'=0,m'\neq m}^{N_f-1} |S_{m'-m}|^2 + 1/\gamma_0} = \frac{|S_0|^2}{(1-|S_0|^2)+1/\gamma_0}, \tag{4.33}$$

where

$$\gamma_0 = \frac{\sigma_x^2}{\sigma_n^2} \tag{4.34}$$

is the SNR in an AWGN channel.

Frequency Selective Channel with CFO On the other hand, if signals undergo frequency selective fading, the power of the desired symbol and the power of the ICI are given by

$$E[|\exp(j\theta i)S_0H_m x_{m,i}|^2] = E[|H_m|^2]|S_0|^2\sigma_x^2 \tag{4.35}$$

and

$$E[|I_{ICI}^{(m)}|^2] = E\left[\left|\sum_{m'=0,m'\neq m}^{N_f-1} S_{m'-m}H_{m'}x_{m',i}\right|^2\right] = \sum_{m'=0,m'\neq m}^{N_f-1} |S_{m'-m}|^2 E[|H_{m'}|^2]\sigma_x^2, \tag{4.36}$$

respectively. The average SIR is therefore expressed as

$$SIR = \frac{E[|H_m|^2]|S_0|^2}{\sum_{m'=0,m'\neq m}^{N_f-1} E[|H_{m'}|^2]|S_{m'-m}|^2}. \tag{4.37}$$

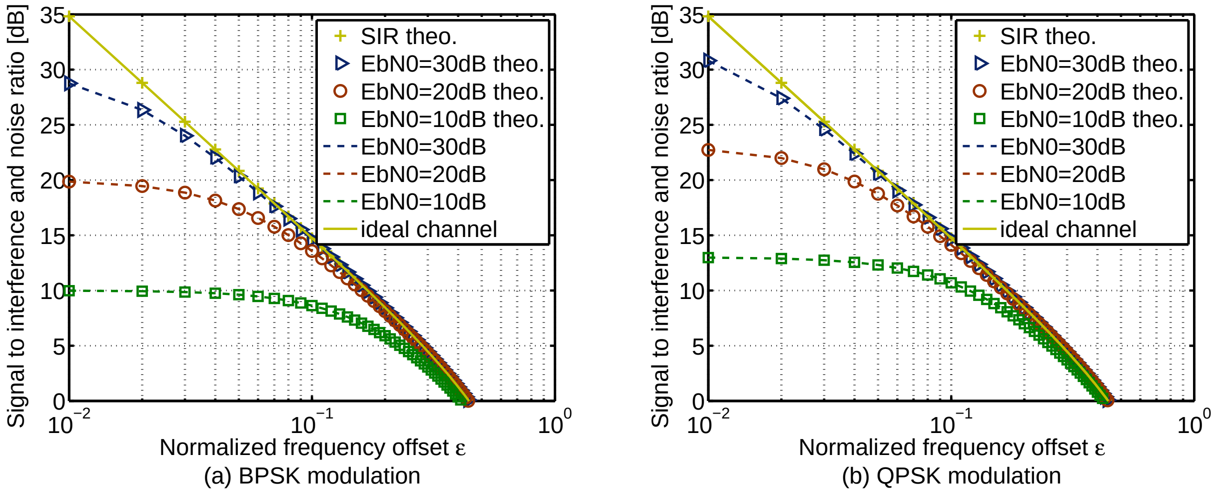

Figure 4.6: SINR varies with the normalized frequency offset.

Letting $E[|H_m|^2] = |H|^2$ represent the average channel gain, then

$$SIR = SIR_0 = \frac{|S_0|^2}{(1 - |S_0|^2)}. \tag{4.38}$$

As a consequence, the average SINR is given by

$$SINR = \frac{|H|^2 |S_0|^2 \sigma_x^2}{\sum_{m'=0, m' \neq m}^{N_f - 1} |H|^2 |S_{m'-m}|^2 \sigma_x^2 + \sigma_n^2} = \frac{|S_0|^2}{(1 - |S_0|^2) + 1/\gamma}, \tag{4.39}$$

where γ represents the average SNR at the output of a fading channel

$$\gamma = \frac{|H|^2 \sigma_x^2}{\sigma_n^2} = |H|^2 \gamma_0. \tag{4.40}$$

Fig. 4.6 depicts how the average SINR (SIR if noise-free) varies with carrier frequency offset in an OFDM system. We assume an uncoded transmission over an ideal channel as well as AWGN channels. As shown, the SINR decreases dramatically with the increase of ϵ, and the upper bound is given by the SIR curve. The simulation results coincide with the theoretical analysis in (4.33).

Furthermore, the corresponding uncoded BER performance is depicted in Fig. 4.7. Note that in simulations the time-variant phase error is not taken into account. In addition, only hard decision is used for data detection. As shown, the BER degrades rapidly with ϵ. When comparing the simulation results for BPSK and QPSK modulation, we can see that at a given BER of 10^{-3}, the former can tolerate a larger CFO than the latter. This means, data transmission with high-level modulation will suffer much more from a CFO.

From theoretical analysis and simulations, we can conclude that OFDM is very sensitive to CFO, and hence efficient CFO estimators and compensation approaches are required, in order to reduce the performance degradation caused by CFO. It also implies that a one-tap equalizer will not work well, if ϵ has a relative large value and is not compensated before FFT.

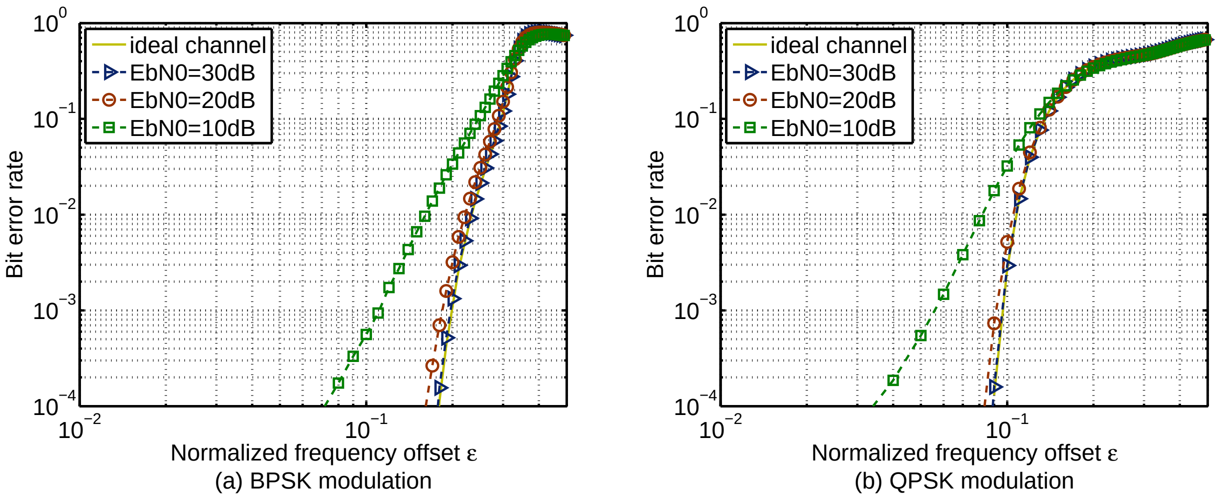

Figure 4.7: Bit error rate performance of an uncoded OFDM system with CFO in ideal and AWGN channels: $N_f = 64$, $N_g = 16$.

4.2.3 The Influence of Timing Errors

The investigation above have been made on the assumption that perfect timing is available. In this subsection we want to give some consideration for the situation with two timing errors: constant time offset and clock frequency offset.

Constant Time Offset

If a constant time offset and a CFO are present in an OFDM system at the same time, the received signal $y(t)$ will be sampled at time instants $t'_k = kT - \nu T$, $T = 1/(N_f \Delta f)$, and in the time domain we will obtain

$$\begin{aligned} \exp(j2\pi f_\epsilon t)|_{t=t'_k} &= \exp\left(\frac{j2\pi\epsilon(k-\nu)}{N_f}\right) \\ &= \exp\left(\frac{j2\pi\epsilon k}{N_f}\right)\exp\left(\frac{-j2\pi\epsilon\nu}{N_f}\right). \end{aligned} \tag{4.41}$$

The joint influence of ϵ and ν is described by the second product term on the RHS of (4.41), $\exp\left(\frac{-j2\pi\epsilon\nu}{N_f}\right)$. That is to say, besides its effects revealed in Section 2.5.2, a constant time offset ν causes a additional phase shift $\theta_\nu = -2\pi\epsilon\nu/N_f$. Such a phase shift is common to all subcarriers, and cannot distinguish itself from the *constant phase offset* (CPO) between the transmitter and receiver oscillators. Therefore, it can be easily compensated together with the CPO.

Clock Frequency Offset

If a clock frequency offset is present along with a CFO, the received signals will be sampled at time instants $t'_k = k(T + \Delta T)$. Referring to (2.20), in time domain it yields then

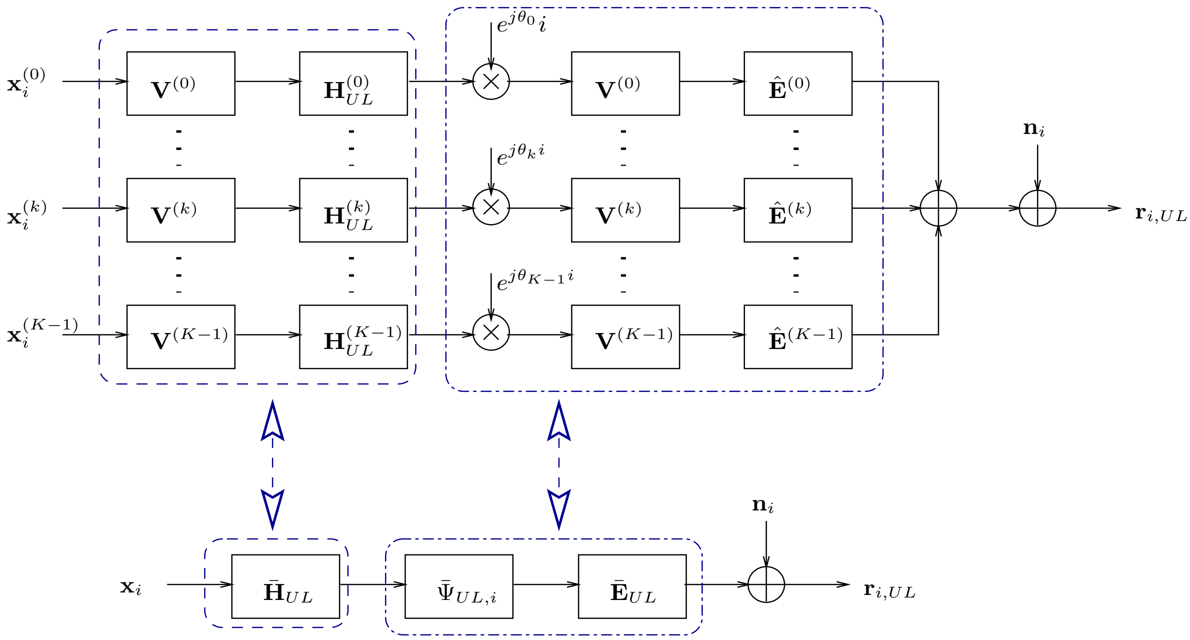

Figure 4.8: Uplink transmission with frequency offsets.

$$
\begin{aligned}
\exp(j2\pi f_{\epsilon} t)|_{t=t'_k} &= \exp\left(\frac{j2\pi\epsilon k(1+\eta)}{N_f}\right) \\
&= \exp\left(\frac{j2\pi\epsilon k}{N_f}\right)\exp\left(\frac{j2\pi\epsilon k\eta}{N_f}\right).
\end{aligned}
\tag{4.42}
$$

The second product term on the RHS of (4.42), $\exp\left(\frac{j2\pi\epsilon k\eta}{N_f}\right)$, stands for the joint influence of ϵ and η. Apparently, $\epsilon\eta$ can be regarded as an additional frequency offset such that it affects the OFDM system in a similar way: giving rise to amplitude reduction and phase rotation of the desired symbols, ICI as well as the time-variant phase error. How clock frequency offset alone affects an OFDM system has been discussed in Section 2.5.

4.3 Multiuser OFDM Systems in the Presence of Carrier Frequency Offset

4.3.1 Downlink Transmission

For the downlink transmission of an OFDMA system in the presence of frequency offset, at the receiver of user k the *overall* received symbol vector $\mathbf{r}_{i,\mathrm{DL}}$ is expressed as

$$
\mathbf{r}_{i,\mathrm{DL}} = \exp(j\theta_k i)\hat{\mathbf{E}}^{(k)}\mathbf{H}_{\mathrm{DL}}^{(k)}\mathbf{x}_i + \mathbf{n}_i \tag{4.43}
$$

with

$$
\theta_k = 2\pi\epsilon_k\left(1+\frac{N_g}{N_f}\right), \tag{4.44}
$$

where ϵ_k represents the normalized CFO of user k. In a multiuser scenario, ICI comes not only from the subcarriers of the user k, but also from the subcarriers of other active users. Therefore, ICI can generally be classified into two categories:

- Self-interference (SI): ICI caused by the CFO of one user's own;
- Multiuser interference (MUI): ICI caused by CFOs of other users.

Furthermore, as studied in the previous section, ICI from the adjacent subcarriers is much stronger than those from the remote subcarriers. In consequence, in conventional OFDMA (C-OFDMA) signals of a certain user are mainly interfered with by SI, and only the marginal subcarriers in a subchannel are affected badly by MUI. In contrast, in interleaved OFDMA (I-OFDMA) signals of a certain user are mainly disturbed by MUI instead of SI.

4.3.2 Uplink Transmission

In the downlink, signals arriving at a mobile station experience the identical channel (perhaps have different distortion because of frequency selective fading), have the same frequency offset and time delay. In the uplink, however, due to the multiple access, signals from different users will perhaps undergo different channels, and have different arriving time as well as different carrier frequency offsets (CFOs). Assume that perfect timing is available and CFO is the only synchronization error. The *overall* uplink transmission model in the presence of multiple CFOs can be described as

$$\mathbf{r}_{i,\mathrm{UL}} = \sum_{k=0}^{K-1} \exp(j\theta_k i)\hat{\mathbf{E}}^{(k)}\mathbf{H}_{\mathrm{UL}}^{(k)}\mathbf{x}_i^{(k)} + \mathbf{n}_i = \bar{\mathbf{E}}_{\mathrm{UL}}\bar{\Psi}_{i,\mathrm{UL}}\bar{\mathbf{H}}_{\mathrm{UL}}\mathbf{x}_i + \mathbf{n}_i, \tag{4.45}$$

where $\mathbf{x}_i^{(k)}$ is defined in (3.32) for C-OFDMA and in (3.34) for I-OFDMA, respectively. The relationship between $\mathbf{x}_i = \sum_{k=0}^{K-1}\mathbf{x}_i^{(k)}$ and $\mathbf{x}_i^{(k)} = \mathbf{V}^{(k)}\mathbf{x}_i$ holds, where $\mathbf{V}^{(k)}$ is defined either in (3.33) or in (3.35), according to the OFDMA scheme applied. $\bar{\mathbf{E}}_{\mathrm{UL}}$ and $\bar{\Psi}_{i,\mathrm{UL}}$ are defined by

$$\bar{\mathbf{E}}_{\mathrm{UL}} = \sum_{k=0}^{K-1} \bar{\mathbf{E}}^{(k)}, \tag{4.46}$$

$$\bar{\mathbf{E}}^{(k)} = \hat{\mathbf{E}}^{(k)}\mathbf{V}^{(k)}, \tag{4.47}$$

and

$$\bar{\Psi}_{i,\mathrm{UL}} = \sum_{k=0}^{K-1} \bar{\Psi}_i^{(k)}, \tag{4.48}$$

$$\bar{\Psi}_i^{(k)} = \exp(j\theta_k i)\mathbf{V}^{(k)}, \tag{4.49}$$

respectively. $\bar{\mathbf{E}}^{(k)}$, $\bar{\mathbf{E}}_{\mathrm{UL}}$, $\bar{\Psi}_i^{(k)}$, and $\bar{\Psi}_{i,\mathrm{UL}}$ are all square matrices of size $N_f \times N_f$. It is worth noting that $\bar{\Psi}_{i,\mathrm{UL}}$ lies in the right to $\bar{\mathbf{E}}_{\mathrm{UL}}$. It is because the definitions in (4.46) and (4.48) result from the derivation

$$\exp(j\theta_k i)\hat{\mathbf{E}}^{(k)}\mathbf{H}_{\mathrm{UL}}^{(k)}\mathbf{V}^{(k)}\mathbf{x}_i = \hat{\mathbf{E}}^{(k)}\mathbf{V}^{(k)}\exp(j\theta_k i)\mathbf{V}^{(k)}\mathbf{H}_{\mathrm{UL}}^{(k)}\mathbf{V}^{(k)}\mathbf{x}_i = \bar{\mathbf{E}}^{(k)}\bar{\Psi}_i^{(k)}\bar{\mathbf{H}}_{\mathrm{UL}}^{(k)}\mathbf{x}_i. \tag{4.50}$$

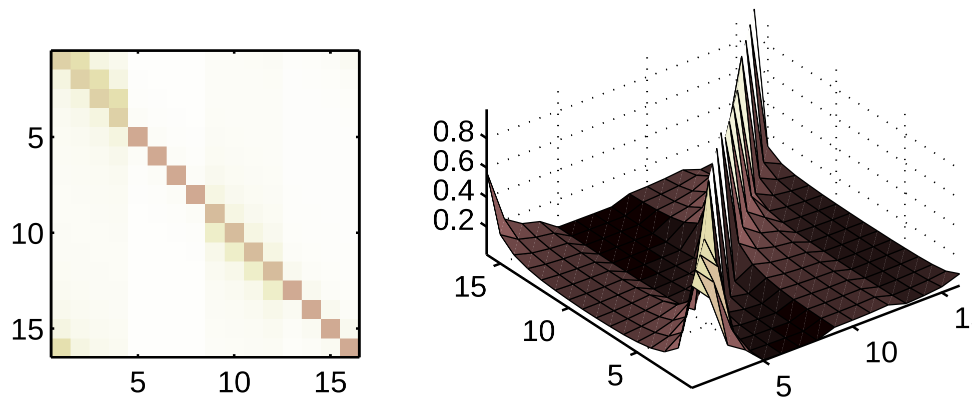

Figure 4.9: Equivalent overall uplink channel matrix for a conventional OFDMA system with CFOs [-0.45 0.05 0.30 -0.10] and an ideal channel.

We cannot transform $\mathbf{V}^{(k)}$ to the left of $\hat{\mathbf{E}}^{(k)}$, since $\hat{\mathbf{E}}^{(k)}$ is not a diagonal matrix. On the other hand, in (4.45) the effects of CFOs and the channels are separated into two independent matrices, $\bar{\mathbf{E}}_{\mathrm{UL}}$ and $\bar{\mathbf{H}}_{\mathrm{UL}}$, such that we can exploit them respectively.

Furthermore, on a certain subcarrier m assigned to user k, the received symbol can be written as

$$\begin{aligned} r_{m,i}^{(k)} &= \underbrace{\exp(j\theta_k i) S_0^{(k)} H_m^{(k)} x_{m,i}^{(k)}}_{\text{signal of interest}} + \underbrace{\sum_{m' \in \mathcal{G}_k, m' \neq m} \exp(j\theta_k i) S_{m'-m}^{(k)} H_{m'}^{(k)} x_{m',i}^{(k)}}_{\text{SI}} \\ &+ \underbrace{\sum_{k'=0, k' \neq k}^{K-1} \sum_{m' \in \mathcal{G}_{k'}} \exp(j\theta_{k'} i)) S_{m'-m}^{(k')} H_{m'}^{(k')} x_{m',i}^{(k')}}_{\text{MUI}} + \underbrace{n_{m,i}}_{\text{noise}}, \end{aligned} \tag{4.51}$$

and consequently, the SINR is given by

$$SINR_{OFDMA} = \frac{\left|S_0^{(k)}\right|^2 E\left[\left|H_m^{(k)}\right|^2\right]}{\sum_{m' \in \mathcal{G}_k, m' \neq m} \left|S_{m'-m}^{(k)}\right|^2 E\left[\left|H_{m'}^{(k)}\right|^2\right] + \sum_{k'=0, k' \neq k}^{K-1} \sum_{m' \in \mathcal{G}_{k'}} \left|S_{m'-m}^{(k')}\right|^2 E\left[\left|H_{m'}^{(k')}\right|^2\right] + 1/\gamma_0}. \tag{4.52}$$

Assuming $E\left[\left|H_m^{(k)}\right|^2\right] = E\left[\left|H_{m'}^{(k')}\right|^2\right] = |H|^2$, (4.52) can be simplified to be

$$SINR_{OFDMA} = \frac{\left|S_0^{(k)}\right|^2}{\sum_{m' \in \mathcal{G}_k, m' \neq m} \left|S_{m'-m}^{(k)}\right|^2 + \sum_{k'=0, k' \neq k}^{K-1} \sum_{m' \in \mathcal{G}_{k'}} \left|S_{m'-m}^{(k')}\right|^2 + 1/\gamma}. \tag{4.53}$$

From Fig. 4.9 to Fig. 4.12 we give examples to demonstrate the *envelope* distribution, $\left|\bar{\mathbf{E}}_{\mathrm{UL}} \bar{\mathbf{H}}_{\mathrm{UL}}\right|$, of the equivalent overall uplink channel matrices for a C-OFDMA and an I-OFDMA system,

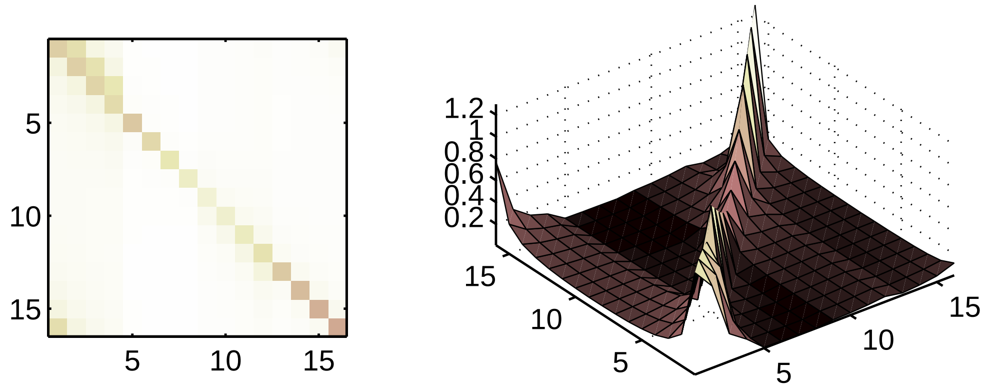

Figure 4.10: Equivalent overall uplink channel matrix for a conventional OFDMA system with CFOs [-0.45 0.05 0.30 -0.10] and a multipath channel with tap weight [1, 0.5].

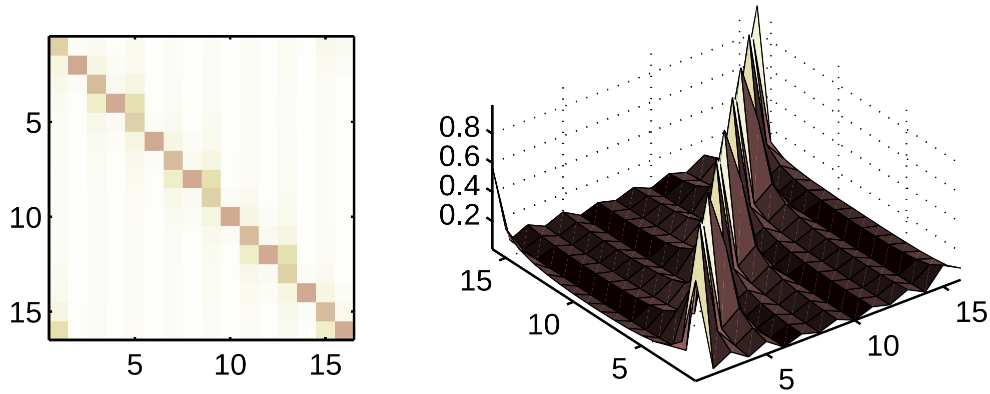

Figure 4.11: Equivalent overall uplink channel matrix for an interleaved OFDMA system with CFOs [-0.45 0.05 0.30 -0.10] and an ideal channel.

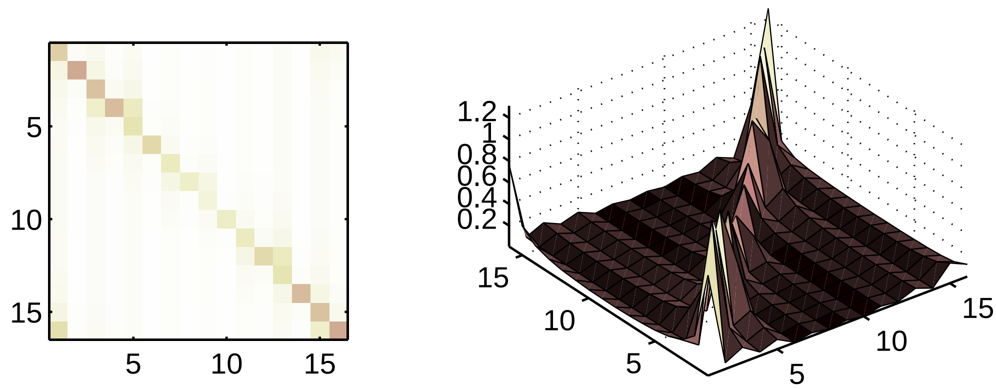

Figure 4.12: Equivalent overall uplink channel matrix of an interleaved OFDMA system with CFOs [-0.45 0.05 0.30 -0.10] and a multipath channel with tap weignt [1, 0.5].

respectively, in cases of an ideal channel and a two-path channel. The presence of carrier frequency offsets is assumed for both cases. It can be seen that

- The entries on the main diagonal are associated with the desired symbols on each subcarrier, and the off-diagonal entries are crosstalk between subcarriers;
- In principle, signals transmitted on a certain subcarrier are mainly affected by ICI from the adjacent subcarriers, and therefore in conventional OFDMA SI is dominating. In contrast, in interleaved OFDMA MUI is dominating;
- The distortion of the desired symbols as well as the amount of ICI depends on CFOs and the channel characteristics.

Phase Shift in the Uplink

Equation (4.51) shows that in the uplink transmission, signals from different users will rotate at different rates, if multiple frequency offsets are present. Fig. 4.13 illustrates signal phase rotations in the uplink of an OFDMA system with four active users. Ideal channels with CFOs $\epsilon = [0.02, -0.02, 0.05, -0.05]$ are assumed. At time index $i = 1$, it is shown that the received symbols of different users are shifted mainly in terms of their corresponding CFOs, and signals of a certain user k have an overall phase shift $\theta_k + \phi_k$ with $\phi_k = \pi\epsilon_k(2N_g + N_f - 1)/N_f$. Such a phase rotation with some i will result in wrong decisions of symbols, and thus performance degradation. Furthermore, the scattering of the received symbols is caused by SI and MUI. It can also be seen that the larger the CFO, the more scattering the symbols experience. Fig. 4.13(b) verifies that in a C-OFDMA system SI is dominating, whereas Fig. 4.13(a) shows that in an I-OFDMA system, MUI is dominant such that the symbols with a small CFO are also scattered significantly.

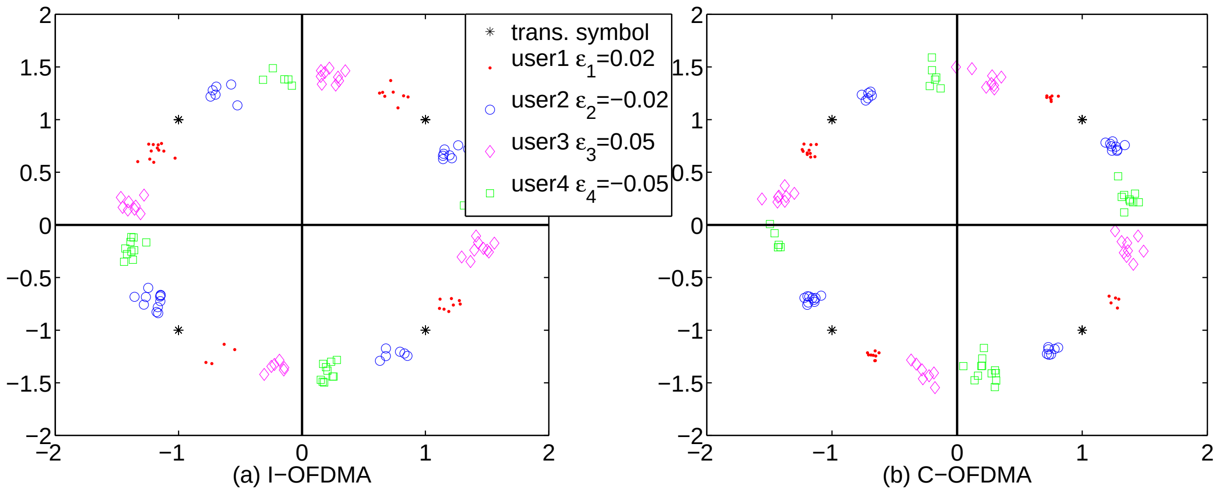

Figure 4.13: Phase rotations in the uplink of OFDMA systems with four users, and $\epsilon = [0.02, -0.02, 0.05, -0.05]$.

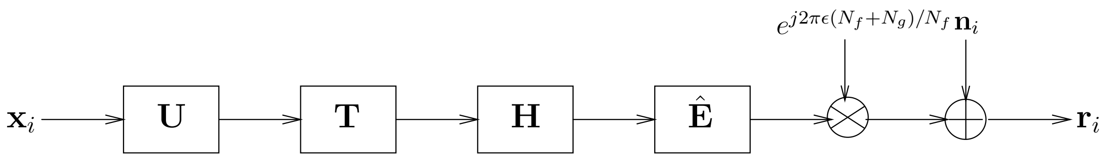

Figure 4.14: A simplified transmission model of MC-CDM in the presence of carrier frequency offset.

Influence of Constant Time Offsets

In wireless communication systems, signals from the mobile stations located at different positions may arrive at the base station with different propagation delays, which may be constant if the mobile station does not move during the transmission. These propagation delays can therefore be modeled as constant time offsets. Because a constant time offset will result in a frequency independent phase shift on the associated subcarriers, on the assumption that the total length of maximum time offset $\nu_{\max}$ and maximum delay spread τ_{L-1} is not greater than $N_g + 1$, (4.45) can then be rewritten as

$$\mathbf{r}_{i,\mathrm{UL}} = \sum_{k=0}^{K-1} \exp\left(\frac{j2\pi\epsilon_k\nu_k}{N_f}\right) \exp(j\theta_k i)\hat{\mathbf{E}}^{(k)}\mathbf{H}_{\mathrm{UL}}^{(k)}\mathbf{x}_i^{(k)} + \mathbf{n}_i, \tag{4.54}$$

where ν_k denotes the time offset of user k. Apparently, even if perfect knowledge of ϵ_k, ν_k and $\mathbf{H}_{\mathrm{UL}}^{(k)}$ is available, one-tap equalizers cannot totally compensate for the signal distortion.

4.4 Multi-carrier Spread Spectrum in the Presence of Carrier Frequency Offset

Like OFDM, all MC-SS transmission schemes based on OFDM are sensitive to CFO. Again we begin with the single user case: MC-CDM.

4.4.1 MC-CDM

As demonstrated in Fig. 4.14, the transmission model of a MC-CDM system with frequency offset can be expressed as

$$\mathbf{r}_i = \exp(j\theta i)\hat{\mathbf{E}}\mathbf{HTU}\mathbf{x}_i + \mathbf{n}_i. \tag{4.55}$$

In terms of the spread transmit symbol vector, $\dot{\mathbf{x}}_i = \mathbf{U}\mathbf{x}_i$, $\mathbf{r}_i$ is the corrupted version of $\dot{\mathbf{x}}_i$ going through an OFDM system. Although time dispersion of the channel destroys the orthogonality among spreading sequences, and vector detection is preferred for MC-CDM, to simplify the investigation of the effects of frequency offset on MC-CDM, we take into account a simple

$$\mathbf{r}_i \longrightarrow \boxed{\mathbf{H}^H} \longrightarrow \boxed{(\mathbf{H}^H\mathbf{H})^{-1}} \longrightarrow \boxed{\mathbf{T}^H} \longrightarrow \boxed{\mathbf{U}^H} \longrightarrow \tilde{\mathbf{x}}_i$$

Figure 4.15: Effects of CFO on MC-CDM with *zero forcing* equalization: model.

case where only one-tap ZF equalization and despreading are performed on $\mathbf{r}_i$. As shown in Fig. 4.15, it yields consequently

$$\begin{aligned}\tilde{\mathbf{x}}_i &= \mathbf{U}^H\mathbf{T}^H(\mathbf{H}^H\mathbf{H})^{-1}\mathbf{H}^H\mathbf{r}_i\\ &= \mathbf{U}^H\mathbf{T}^H(\mathbf{H}^H\mathbf{H})^{-1}\mathbf{H}^H\exp(j\theta i)\hat{\mathbf{E}}\mathbf{H}\mathbf{T}\mathbf{U}\mathbf{x}_i + \mathbf{U}^H\mathbf{T}^H(\mathbf{H}^H\mathbf{H})^{-1}\mathbf{H}^H\mathbf{n}_i.\end{aligned}\tag{4.56}$$

As $\mathbf{U}$ is a unitary matrix, the resulting noise samples, $\mathbf{U}^H\mathbf{T}^H(\mathbf{H}^H\mathbf{H})^{-1}\mathbf{H}^H\mathbf{n}_i$, are uncorrelated Gaussian random variables as well. Subsequently, the impacts of CFO will be exploited for MC-CDM with full spreading, sub-band spreading and interleaved spreading, respectively.

MC-CDM with Full Spreading

In the case of full spreading, it follows from (4.56) that on the receiving side, a received symbol after despreading can be described as

$$\begin{aligned}\tilde{x}_{l,i} &= \underbrace{\exp(j\theta i)\mathbf{c}_l^H\overbrace{(\mathbf{H}^H\mathbf{H})^{-1}\mathbf{H}^H}^{\text{ZF equalizer}}\hat{\mathbf{E}}\mathbf{H}\mathbf{c}_l x_{l,i}}_{\text{desired signal}}\\ &\quad \underbrace{+\exp(j\theta i)\sum_{l'=0,l'\neq l}^{N_f-1}\mathbf{c}_l^H(\mathbf{H}^H\mathbf{H})^{-1}\mathbf{H}^H\hat{\mathbf{E}}\mathbf{H}\mathbf{c}_{l'}x_{l',i}}_{\text{crosstalk}} + \underbrace{\mathbf{c}_l^H(\mathbf{H}^H\mathbf{H})^{-1}\mathbf{H}^H\mathbf{n}_i}_{\text{noise}}\\ &= \exp(j\theta i)(S_0 + \sum_{m=0}^{N_f-1}\sum_{m'=0,m'\neq m}^{N_f-1}S_{m'-m}c_{ml}^*c_{m'l}\frac{H_m^*H_{m'}}{|H_m|^2})x_{l,i}\\ &\quad + \exp(j\theta i)\sum_{l'=0,l'\neq l}^{N_f-1}\sum_{m=0}^{N_f-1}\sum_{m'=0}^{N_f-1}S_{m'-m}c_{ml}^*c_{m'l'}\frac{H_m^*H_{m'}}{|H_m|^2}x_{l',i} + \sum_{m=0}^{N_f-1}c_{ml}^*\frac{H_m^*}{|H_m|^2}n_{m,i}.\end{aligned}\tag{4.57}$$

We first consider the transmission over an AWGN channel, i.e., $\mathbf{H} = \mathbf{I}$. The second term in (4.57) is then decoupled into

$$\begin{aligned}\sum_{l'=0,l'\neq l}^{N_f-1}\mathbf{c}_l^H\hat{\mathbf{E}}\mathbf{c}_{l'}x_{l',i} &= \underbrace{\sum_{l'=0,l'\neq l}^{N_f-1}\mathbf{c}_l^H\text{diag}\{\hat{\mathbf{E}}\}\mathbf{c}_{l'}x_{l',i}}_{0} + \sum_{l'=0,l'\neq l}^{N_f-1}\mathbf{c}_l^H(\hat{\mathbf{E}}-\text{diag}\{\hat{\mathbf{E}}\})\mathbf{c}_{l'}x_{l',i}\\ &= \sum_{l'=0,l'\neq l}^{N_f-1}\sum_{m=0}^{N_f-1}\sum_{m'=0,m'\neq m}^{N_f-1}S_{m'-m}c_{ml}^*c_{m'l'}\frac{H_m^*H_{m'}}{|H_m|^2}x_{l',i},\end{aligned}\tag{4.58}$$

and (4.57) is rewritten as

$$\tilde{x}_{l,i} = \exp(j\theta i)S_0 x_{l,i} + \exp(j\theta i)\sum_{m=0}^{N_f-1}\sum_{m'=0,m'\neq m}^{N_f-1} S_{m'-m}c_{ml}^* c_{m'l}x_{l,i}$$
$$+ \exp(j\theta i)\sum_{l'=0,l'\neq l}^{N_f-1}\sum_{m=0}^{N_f-1}\sum_{m'=0,m'\neq m}^{N_f-1} S_{m'-m}c_{ml}^* c_{m'l'}x_{l',i} + \sum_{m=0}^{N_f-1} c_{ml}^* n_{m,i}. \tag{4.59}$$

Referring to (4.30), and as $c_{ml}^* c_{ml} = \frac{1}{N_f}$ and $E[x_{l,i}^* x_{l',i}] = \sigma_x^2 \delta_{ll'}$, the SINR in an AWGN channel can be given by

$$\begin{aligned}
SINR_{\text{MC-CDM, 0}} &= \frac{|S_0|^2 + \frac{1}{N_f^2}\sum_{m=0}^{N_f-1}\sum_{m'=0,m'\neq m}^{N_f-1}|S_{m'-m}|^2\sigma_x^2}{\frac{1}{N_f^2}\sum_{l'=0,l'\neq l}^{N_f-1}\sum_{m=0}^{N_f-1}\sum_{m'=0,m'\neq m}^{N_f-1}|S_{m'-m}|^2\sigma_x^2 + \sigma_n^2} \\
&= \frac{|S_0|^2 + \frac{1}{N_f^2}\sum_{m=0}^{N_f-1}(\sum_{m'=0}^{N_f-1}|S_{m'-m}|^2 - |S_0|^2)}{\frac{1}{N_f^2}\sum_{l'=0,l'\neq l}^{N_f-1}\sum_{m=0}^{N_f-1}(\sum_{m'=0}^{N_f-1}|S_{m'-m}|^2 - |S_0|^2) + \sigma_n^2} \\
&= \frac{|S_0|^2 + \frac{1}{N_f^2}\sum_{m=0}^{N_f-1}(1 - |S_0|^2)}{\frac{(N_f-1)N_f}{N_f^2}(1 - |S_0|^2) + \frac{1}{\gamma_0}} \\
&= \frac{|S_0|^2 + (1 - |S_0|^2)/N_f}{\frac{(N_f-1)}{N_f}(1 - |S_0|^2) + 1/\gamma_0} \\
&\approx \frac{|S_0|^2}{(1 - |S_0|^2) + 1/\gamma_0}.
\end{aligned} \tag{4.60}$$

This result is approximately equal to the $SINR_0$ for a pure OFDM system. Moreover, in the absence of CFO, we have

$$|S_0|_{\epsilon=0} = 1,$$

and then

$$SINR_{\text{MC-CDM, 0}}|_{\epsilon=0} = \gamma_0. \tag{4.61}$$

On the other hand, in the case of a frequency selective fading channel, if one-tap ZF equalizer is implemented to compensate for the degradation caused by channel distortion, the SINR will be

$$SINR_{\text{MC-CDM, ZF}} = \frac{|S_0|^2\sigma_x^2 + \frac{1}{N_f^2}\sum_{m=0}^{N_f-1}\sum_{m'=0,m'\neq m}^{N_f-1}|S_{m'-m}|^2\sigma_x^2}{\frac{1}{N_f^2}\sum_{l'=0,l'\neq l}^{N_f-1}\sum_{m=0}^{N_f-1}\sum_{m'=0,m'\neq m}^{N_f-1}|S_{m'-m}|^2\sigma_x^2 + \frac{\sigma_n^2}{N_f}\sum_{m=0}^{N_f-1}\frac{1}{E[|H_m|^2]}}. \tag{4.62}$$

Assuming $E[|H_{m'}|^2] = |H|^2$, we have then

$$SINR_{\text{MC-CDM, ZF}} = \frac{|S_0|^2 + (1 - |S_0|^2)/N_f}{\frac{N_f-1}{N_f}(1 - |S_0|^2) + \frac{\sigma_n^2}{|H|^2\sigma_x^2}} \approx \frac{|S_0|^2}{(1 - |S_0|^2) + 1/\gamma}, \tag{4.63}$$

which approximately coincides with the SINR in (4.39) for OFDM.

MC-CDM with Sub-band Spreading

In the case of sub-band spreading, $\mathbf{U}$ is defined in (3.54), where the spreading submatrices $\mathbf{W}_q$, $q = 0, ..., Q-1$, are of size $N_Q \times N_Q$ and $N_Q = N_f/Q$. Therefore, referring to (4.57), the received despread symbol $\tilde{x}_{l,i}$, with $l = d + q \times N_Q$, $0 \leq d < N_Q$, is expressed as

$$\begin{aligned}
\tilde{x}_{l,i} &= \tilde{x}_{d+q\times N_Q,i} \\
&= \exp(j\theta i)\mathbf{c}_l^H(\mathbf{H}^H\mathbf{H})^{-1}\mathbf{H}^H\hat{\mathbf{E}}\mathbf{H}\mathbf{c}_l x_{l,i} \\
&+ \exp(j\theta i)\sum_{l'=0,l'\neq l}^{N_f-1}\mathbf{c}_l^H(\mathbf{H}^H\mathbf{H})^{-1}\mathbf{H}^H\hat{\mathbf{E}}\mathbf{H}\mathbf{c}_{l'}x_{l',i} + \mathbf{c}_l^H(\mathbf{H}^H\mathbf{H})^{-1}\mathbf{H}^H\mathbf{n}_i \\
&= \exp(j\theta i)S_0 x_{d+q\times N_Q,i} + \exp(j\theta i)\sum_{p=0}^{N_Q-1}\sum_{p'=0,p'\neq p}^{N_Q-1}S_{p'-p} \\
&\times c^*_{(p+q\times N_Q)(d+q\times N_Q)}c_{(p'+q\times N_Q)(d+q\times N_Q)}\frac{H^*_{p+q\times N_Q}H_{p'+q\times N_Q}}{\left|H_{p+q\times N_Q}\right|^2}x_{d+q\times N_Q,i} \\
&+ \exp(j\theta i)\sum_{d'=0,d'\neq d}^{N_Q-1}\sum_{p=0}^{N_Q-1}\sum_{p'=0}^{N_Q-1}S_{p'-p} \\
&\times c^*_{(p+q\times N_Q)(d+q\times N_Q)}c_{(p'+q\times N_Q)(d'+q\times N_Q)}\frac{H^*_{p+q\times N_Q}H_{p'+q\times N_Q}}{\left|H_{p+q\times N_Q}\right|^2}x_{d'+q\times N_Q,i} \\
&+ \exp(j\theta i)\sum_{q'=0,q'\neq q}^{Q-1}\sum_{d'=0}^{N_Q-1}\sum_{p=0}^{N_Q-1}\sum_{p'=0}^{N_Q-1}S_{(p'+q'\times N_Q)-(p+q\times N_Q)} \\
&\times c^*_{(p+q\times N_Q)(d+q\times N_Q)}c_{(p'+q'\times N_Q)(d'+q'\times N_Q)}\frac{H^*_{p+q\times N_Q}H_{p'+q'\times N_Q}}{\left|H_{p+q\times N_Q}\right|^2}x_{(d'+q'\times N_Q),i} \\
&+ \sum_{p=0}^{N_Q-1}\frac{H^*_{p+q\times N_Q}}{\left|H_{p+q\times N_Q}\right|^2}c^*_{(p+q\times N_Q)l}n_{p+q\times N_Q,i}.
\end{aligned} \tag{4.64}$$

Further, if the spreading submatrices are identical, i.e., $c^*_{ml}c_{ml} = c^*_{(p+q\times N_Q)(d+q\times N_Q)}c_{(p+q\times N_Q)(d+q\times N_Q)} = c^*_{w,pd}c_{w,pd} = \frac{1}{N_Q}$, where $c_{w,pd}$ denotes the code chip in W_q at the position of pth row and dth column, a simplified expression yields then

$$\begin{aligned}
\tilde{x}_{l,i} &= \tilde{x}_{d+q\times N_Q,i} \\
&= \exp(j\theta i)(S_0 + \sum_{p=0}^{N_Q-1}\sum_{p'=0,p'\neq p}^{N_Q-1}S_{p'-p}c^*_{pd}c_{p'd}\frac{H^*_{p+q\times N_Q}H_{p'+q\times N_Q}}{\left|H_{p+q\times N_Q}\right|^2})x_{d+q\times N_Q,i} \\
&\underbrace{+ \exp(j\theta i)\sum_{d'=0,d'\neq d}^{N_Q-1}\sum_{p=0}^{N_Q-1}\sum_{p'=0}^{N_Q-1}S_{p'-p}c^*_{pd}c_{p'd'}\frac{H^*_{p+q\times N_Q}H_{p'+q\times N_Q}}{\left|H_{p+q\times N_Q}\right|^2}x_{d'+q\times N_Q,i}}_{\text{crosstalk inside subchannel } q} \\
&\underbrace{+ \exp(j\theta i)\sum_{q'=0,q'\neq q}^{Q-1}\sum_{d'=0}^{N_Q-1}\sum_{p=0}^{N_Q-1}\sum_{p'=0}^{N_Q-1}S_{(p'+q'\times N_Q)-(p+q\times N_Q)}c^*_{pd}c_{p'd'}\frac{H^*_{p+q\times N_Q}H_{p'+q'\times N_Q}}{\left|H_{p+q\times N_Q}\right|^2}x_{(d'+q'\times N_Q),i}}_{\text{crosstalk outside subchannel } q}
\end{aligned}$$

$$+\underbrace{\sum_{p=0}^{N_Q-1}\frac{H^*_{p+q\times N_Q}}{\left|H_{p+q\times N_Q}\right|^2}c^*_{(p+q\times N_Q)l}n_{p+q\times N_Q,i}}_{\text{noise}}. \tag{4.65}$$

The corresponding $SINR_{\text{MC-CDM, 0}}$ is different from that in the case of full spreading and is given by

$$SINR_{\text{MC-CDM, 0}}|_{W_q}=\frac{|S_0|^2\,\sigma_x^2+P_{\text{sv}}\sigma_x^2}{P_{I_{\text{in}}}\sigma_x^2+P_{I_{\text{out}}}\sigma_x^2+\sigma_n^2}=\frac{|S_0|^2+P_{\text{sv}}}{P_{I_{\text{in}}}+P_{I_{\text{out}}}+1/\gamma_0}, \tag{4.66}$$

where

$$P_{\text{sv}}=\frac{1}{N_Q^2}\sum_{p=0}^{N_Q-1}\sum_{p'=0,p'\neq p}^{N_Q-1}|S_{p'-p}|^2 \tag{4.67}$$

represents the variance of the diagonal entries,

$$P_{I_{\text{in}}}=\frac{1}{N_Q^2}\sum_{d'=0,d'\neq d}^{N_Q-1}\sum_{p=0}^{N_Q-1}\sum_{p'=0,p'\neq p}^{N_Q-1}|S_{p'-p}|^2=(N_Q-1)\,P_{\text{sv}} \tag{4.68}$$

the interference from the transmit symbols transmitted on the desired subchannel, and

$$\begin{aligned}P_{I_{\text{out}}}&=\frac{1}{N_Q^2}\sum_{q'=0,q'\neq q}^{Q-1}\sum_{d'=0}^{N_Q-1}\sum_{p=0}^{N_Q-1}\sum_{p'=0}^{N_Q-1}\left|S_{(p'+q'\times N_Q)-(p+q\times N_Q)}\right|^2\\&=\frac{1}{N_Q}\sum_{q'=0,q'\neq q}^{Q-1}\sum_{p=0}^{N_Q-1}\sum_{p'=0}^{N_Q-1}\left|S_{(p'+q'\times N_Q)-(p+q\times N_Q)}\right|^2\end{aligned} \tag{4.69}$$

the interference from other subchannels. Unfortunately, (4.66) cannot be simplified further, since

$$\sum_{p=0}^{N_Q-1}\sum_{p'=0}^{N_Q-1}|S_{p'-p}|^2\neq 1.$$

Furthermore, according to (4.65), the noise component will have zero mean and variance

$$\frac{1}{N_Q}\sum_{p=0}^{N_Q-1}\frac{\sigma_n^2}{E\left[\left|H_{p+q\times N_Q}\right|^2\right]}=\frac{\sigma_n^2}{|H_{W_q}|^2}, \tag{4.70}$$

where $E[\left|H_{p+q\times N_Q}\right|^2]=|H_{W_q}|^2$ is assumed for subchannel q. This is because the adjacent subcarriers of OFDM are usually correlated such that subchannels based on sub-bands will have a different average channel gain, and the resultant noise components will be multivariate. Moreover, at the receiver the $SINR_{\text{MC-CDM, ZF}}$ associated with the subchannel q is given by

$$SINR_{\text{MC-CDM, ZF}}|_{W_q}=\frac{|S_0|^2+P_{\text{sv}}}{P_{I_{\text{in}}}+P_{I_{\text{out}}}\left|H_{W_{q'}}\right|^2/|H_{W_q}|^2+1/(|H_{W_q}|^2\gamma_0)}. \tag{4.71}$$

Namely, in MC-CDM with sub-band spreading, $SINR_{\text{MC-CDM, ZF}}$ is subchannel-dependent. However, this results not from frequency offset but from channel characteristics as well as the spreading scheme.

MC-CDM with Interleaved Spreading

In the case of interleaved spreading, on the other hand, equidistant subcarriers are chosen for spreading, such that $E\left[|H_{p'\times Q+q}|^2\right] = |H|^2$ can be assumed, and after despreading it yields

$$\begin{aligned}
\tilde{x}_{l,i} &= \tilde{x}_{d+q\times N_Q,i} \\
&= \exp(j\theta i)(S_0 + \sum_{p=0}^{N_Q-1}\sum_{p'=0,p'\neq p}^{N_Q-1} S_{\underbrace{(p'\times Q+q)-(p\times Q+q)}_{(p'-p)\times Q}} c^*_{pd}c_{p'd}\frac{H^*_{p\times Q+q}H_{p'\times Q+q}}{|H_{p\times Q+q}|^2})x_{d+q\times N_Q,i} \\
&\underbrace{+\exp(j\theta i)\sum_{d'=0,d'\neq d}^{N_Q-1}\sum_{p=0}^{N_Q-1}\sum_{p'=0}^{N_Q-1} S_{\underbrace{(p'\times Q+q)-(p\times Q+q)}_{(p'-p)\times Q}} c^*_{pd}c_{p'd'}\frac{H^*_{p\times Q+q}H_{p'\times Q+q}}{|H_{p\times Q+q}|^2}x_{d'+q\times N_Q,i}}_{\text{crosstalk inside subchannel } q} \\
&\underbrace{+\exp(j\theta i)\sum_{q'=0,q'\neq q}^{Q-1}\sum_{d'=0}^{N_Q-1}\sum_{p=0}^{N_Q-1}\sum_{p'=0}^{N_Q-1} S_{\underbrace{(p'\times Q+q')-(p\times Q+q)}_{(p'-p)\times Q+(q'-q)}} c^*_{pd}c_{p'd'}\frac{H^*_{p\times Q+q}H_{p'\times Q+q'}}{|H_{p\times Q+q}|^2}x_{(d'+q'\times N_Q),i}}_{\text{crosstalk outside subchannel } q} \\
&+\sum_{p=0}^{N_Q-1}\frac{H^*_{p\times Q+q}}{|H_{p\times Q+q}|^2}c^*_{(p+q\times N_Q)l}n_{p\times Q+q,i}.
\end{aligned} \tag{4.72}$$

The resulting $SINR_{\text{MC-CDM, }0}|_{W_q}$ and $SINR_{\text{MC-CDM, }ZF}|_{W_q}$ are expressed as

$$SINR_{\text{MC-CDM, }0}|_{W_q} = \frac{|S_0|^2 + P_{\text{sv, inter}}}{P_{I_{\text{in, inter}}} + P_{I_{\text{out, inter}}} + 1/\gamma_0}, \tag{4.73}$$

and

$$SINR_{\text{MC-CDM, ZF}}|_{W_q} = \frac{|S_0|^2 + P_{\text{sv, inter}}}{P_{I_{\text{in, inter}}} + P_{I_{\text{out, inter}}} + 1/(|H|^2\gamma_0)} = \frac{|S_0|^2 + P_{\text{sv, inter}}}{P_{I_{\text{in, inter}}} + P_{I_{\text{out, inter}}} + 1/\gamma}, \tag{4.74}$$

respectively. Note that they are independent of the subchannels, and $P_{\text{sv, inter}}$, $P_{I_{\text{in, inter}}}$ and $P_{I_{\text{out, inter}}}$ are defined as

$$P_{\text{sv, inter}} = \frac{1}{N_Q^2}\sum_{p=0}^{N_Q-1}\sum_{p'=0,p'\neq p}^{N_Q-1}\left|S_{(p'-p)\times Q}\right|^2, \tag{4.75}$$

$$P_{I_{\text{in, inter}}} = \frac{N_Q-1}{N_Q^2}\sum_{p=0}^{N_Q-1}\sum_{p'=0,p'\neq p}^{N_Q-1}\left|S_{(p'-p)\times Q}\right|^2 = (N_Q-1)\,P_{\text{sv, inter}}, \tag{4.76}$$

and

$$P_{I_{\text{out, inter}}} = \frac{1}{N_Q}\sum_{q'=0,q'\neq q}^{Q-1}\sum_{p=0}^{N_Q-1}\sum_{p'=0}^{N_Q-1}\left|S_{(p'-p)\times Q+(q'-q)}\right|^2, \tag{4.77}$$

respectively.

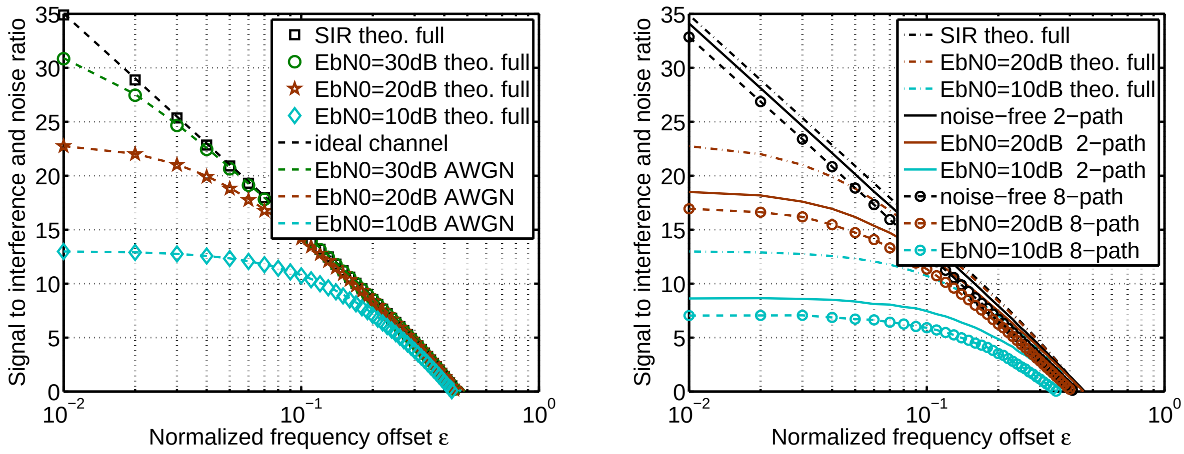

(a) QPSK, AWGN channel (b) QPSK, multipath channel

Figure 4.16: Effects of CFO on MC-CDM with *zero forcing* equalization: SIR and SINR.

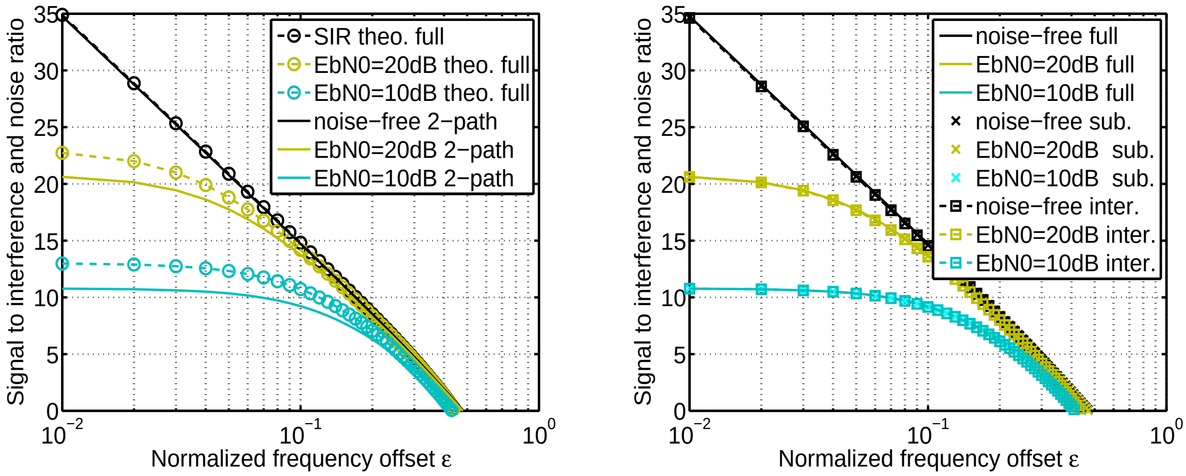

(a) QPSK, **h**=[0.8944, 0.4472] (b) QPSK, **h**=[0.8944, 0.4472]

Figure 4.17: Effects of CFO on MC-CDM with *zero forcing* equalization: SIR and SINR, transmission over a two-path channel $\mathbf{h} = [0.8944, 0.4472]$.

In Fig. 4.16 simulation results are given for an MC-CDM system with full spreading and $N_f = 64$. The channels we used for simulations include AWGN channels, two-path Rayleigh fading channels, and eight-path Rayleigh fading channels given in Section 2.2.3. For the sake of comparison, in all simulations channels are normalized. As depicted in Fig. 4.16, simulation results for AWGN channels coincide with the theoretical curves, whereas in the case of multipath propagation, simulation results are dependent on the channel characteristics: less than 1dB SIR loss occurs in the case of two-path Rayleigh fading channels, and about 2dB SIR loss in the case of eight-path Rayleigh fading channels. Furthermore, the actual SNR, γ, is strongly affected by the channel characteristics such that the SINR curves for the eight-path fading channels are far away from the theoretical curves, which has been derived under the assumption of an average channel gain $|H|^2$.

Simulation results for a two-path channel with CIR $\mathbf{h} = [0.8944, 0.4472]$ are shown in Fig. 4.17,

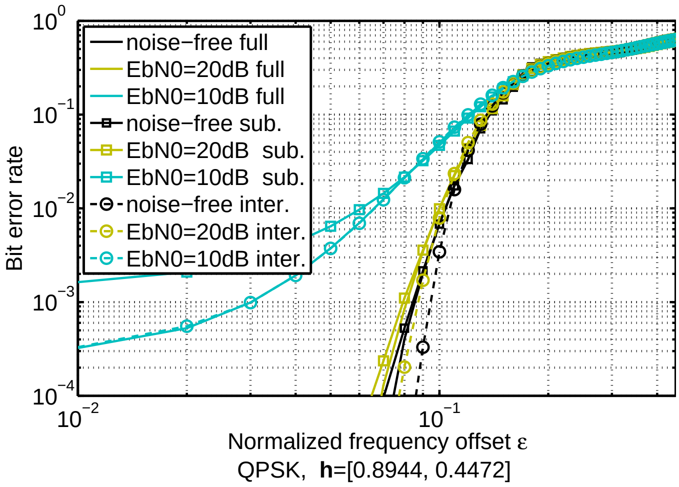

Figure 4.18: MC-CDM with full spreading: Effect of CFO on BER performance, transmission over a two-path channel $\mathbf{h} = [0.8944, 0.4472]$.

where different spreading schemes are considered. It is worth noting that the average SIR as well as SINR are almost identical for the three spreading schemes. This is because in all cases, $|S_0|^2$ dominates the power of the desired signals and the total power of interference, and the noise power does not change when a unitary spreading matrix is used. Fig. 4.18 depicts the corresponding BER performance degradation with CFO. Basically, without consideration of the time-variant phase rotation caused by CFO, at a given BER of 10^{-4} and a given SNR of 20dB, the tolerable normalized CFO is about $\epsilon = 0.07$.

4.4.2 CDM-OFDMA

As a variant of MC-CDM applied in a multiple access scenario, CDM-OFDMA also suffers from the time dispersion of the channel. Nevertheless, under the assumption of perfect synchronization, in CDM-OFDMA users are separated in frequency and therefore no MUI occurs. If a CFO is present, however, the resulting ICI will further destroy the orthogonality between subchannels and lead to MUI.

Downlink Transmission

In the presence of a CFO, the *overall* received symbol vector at the receiver of user k can be described as

$$\mathbf{r}_{i,\mathrm{DL}} = \exp(j\theta_k i)\hat{\mathbf{E}}^{(k)}\mathbf{H}_{\mathrm{DL}}^{(k)}\mathbf{T}_c\mathbf{U}\mathbf{x}_i + \mathbf{n}_i, \tag{4.78}$$

The parameters $\mathbf{H}_{\mathrm{DL}}^{(k)}$, $\mathbf{T}_c$, $\mathbf{U}$, and $\mathbf{x}_i$ are defined in Section 3.4.2. Referring to MC-CDM with sub-band spreading and interleaved spreading, in CDM-OFDMA interference inside a subchannel (belonging to a certain user) can be classified into SI, while the interference outside a subchannel can be classified into MUI.

Uplink Transmission

In the presence of frequency offsets, the uplink transmission of CDM-OFDMA can be expressed as

$$\mathbf{r}_{i,\mathrm{UL}} = \sum_{k=0}^{K-1} \exp(j\theta_k i)\hat{\mathbf{E}}^{(k)}\mathbf{H}_{\mathrm{UL}}^{(k)}\mathbf{T}_c\mathbf{U}^{(k)}\mathbf{x}_i^{(k)} + \mathbf{n}_i = \bar{\mathbf{E}}_{\mathrm{UL}}\bar{\Psi}_{i,\mathrm{UL}}\bar{\mathbf{H}}_{\mathrm{UL}}\mathbf{U}\mathbf{x}_i + \mathbf{n}_i, \tag{4.79}$$

where $\bar{\mathbf{E}}_{\mathrm{UL}}$, $\bar{\Psi}_{i,\mathrm{UL}}$, and $\bar{\mathbf{H}}_{\mathrm{UL}}$ are all square matrices of size $N_f \times N_f$, and defined in (4.46), (4.48), and (3.69), respectively. Thanks to the modeling in (4.79) as well as the analysis for MC-CDM, we can easily find out that for any individual user, in the uplink SI is associated with the transmit symbols, the CFO and the subchannel characteristics of the user's own, whereas the amount of MUI depends on transmit symbols, CFOs and the subchannel characteristics of other users.

4.4.3 MC-CDMA

In MC-CDMA, user separation is accomplished by different spreading sequences, or different spreading codes.

Downlink Transmission

Referring to (3.73), The downlink transmission model of MC-CDMA with a CFO can be written as

$$\mathbf{r}_{i,\mathrm{DL}} = \exp(j\theta_k i)\hat{\mathbf{E}}^{(k)}\mathbf{H}_{\mathrm{DL}}^{(k)}\mathbf{T}_m\mathbf{U}\mathbf{x}_i + \mathbf{n}_i. \tag{4.80}$$

If sub-band spreading or interleaved spreading is in use, different from CDM-OFDMA, in MC-CDMA the crosstalk inside a subchannel would be MUI. Moreover, the crosstalk from other subchannels may be caused either by the identical user or by other users, so that they are a mixture of SI and MUI. In the case of full spreading, if assuming the system is fully loaded, i.e., each user has only one spreading sequence, then no SI but only MUI occurs.

Uplink Transmission

The uplink transmission model can be expressed as

$$\begin{aligned}\mathbf{r}_{i,\mathrm{UL}} &= \sum_{k=0}^{K-1} \exp(j\theta_k i)\hat{\mathbf{E}}^{(k)}\mathbf{H}_{\mathrm{UL}}^{(k)}\mathbf{T}_m\mathbf{U}^{(k)}\mathbf{x}_i^{(k)} + \mathbf{n}_i \\ &= \sum_{k=0}^{K-1} \exp(j\theta_k i)\hat{\mathbf{E}}^{(k)}\mathbf{H}_{\mathrm{UL}}^{(k)}\mathbf{T}_m\mathbf{U}^{(k)}\mathbf{x}_i + \mathbf{n}_i.\end{aligned} \tag{4.81}$$

Furthermore, defining

$$\bar{\mathbf{E}}_{\mathrm{UL}} = \left[\begin{array}{ccccc} \hat{\mathbf{E}}^{(0)} & \ldots & \hat{\mathbf{E}}^{(k)} & \ldots & \hat{\mathbf{E}}^{(K-1)} \end{array}\right]_{N_f\times(N_f K)}, \tag{4.82}$$

and

$$\bar{\Psi}_{i,\mathrm{UL}} = \mathrm{Diag}\left\{\begin{bmatrix} \Psi_i^{(0)} & \ldots & \Psi_i^{(k)} & \ldots & \Psi_i^{(K-1)} \end{bmatrix}_{N_f \times (N_f K)}\right\} \tag{4.83}$$

with

$$\Psi_i^{(k)} = \exp(j\theta_k i)\mathbf{I}_{N_f \times N_f}, \tag{4.84}$$

a vector-matrix multiplication form of (4.81) is therefore given by

$$\mathbf{r}_{i,\mathrm{UL}} = \bar{\mathbf{E}}_{\mathrm{UL}}\bar{\Psi}_{i,\mathrm{UL}}\mathrm{Diag}\{\bar{\mathbf{H}}_{\mathrm{UL}}\}\bar{\mathbf{U}}_{\mathrm{UL}}\mathbf{x}_i + \mathbf{n}_i, \tag{4.85}$$

where $\bar{\mathbf{H}}_{\mathrm{UL}}$ and $\bar{\mathbf{U}}_{\mathrm{UL}}$ are defined in (3.76) and (3.77), respectively. $\mathrm{Diag}\{\cdot\}$ represents an operation of forming a block diagonal matrix. As we are unable to separate users before despreading, each component in $\mathbf{r}_{i,\mathrm{UL}}$ is the superposition of signals from all users. Even if ideal channels are assumed, referring to (4.59), CFOs alone can lead to MUI. Moreover, the power of MUI from different users will be different, because with different ϵ_k the value of $S_0^{(k)}$ will be different. On the other hand, if signals experience frequency selective fading, ICI due to a CFO is further weighted by the channel coefficients, which complicates the components of MUI. This also happens in CDM-OFDMA. But for the latter case, from (4.79) we know that in some situations only a composite uplink channel needs to be estimated. And, since CDM-OFDMA is on the basis of OFDMA, it is possible to use the parameter estimation methods in OFDMA. In MC-CDMA, unfortunately, full channel state information of each user is required, and, since after despreading these information may be erased, parameter estimation in the uplink would be a tough task.

4.5 Summary

In this chapter, we have analyzed the effects of carrier frequency offset on OFDM-based systems. The vector-valued transmission models have been modified for the scenario with CFO.

The derivation of the matrix $\hat{\mathbf{E}}$ is one of the most important contributions in this work. The matrix $\hat{\mathbf{E}}$ contains all the impacts of a fractional frequency offset on a frequency-domain OFDM symbol vector, except for the phase rotation with time (vector index). The diagonal entries are of the same value, which give rise to amplitude reduction and phase rotation of the desired symbols. The off-diagonal entries, on the other hand, represent the crosstalk (ICI) between subcarriers caused by a CFO. Furthermore, analysis shows that the signal on an individual subcarrier is mainly affected by the crosstalk from the adjacent subcarriers. In an AWGN channel with a CFO, the SIR depends upon the power of a diagonal entry, $|S_0|^2$. As $|S_0|^2$ decreases rapidly with CFO, the SIR goes down quickly. In a fading channel, the ICI will be weighted by the channel coefficients.

A CFO also results in a phase increment θ between two received vectors. The cumulative phase rotation $i\theta$ with some i may lead to a wrong decision and hence severe performance degradation.

In the case of OFDMA, ICI from the identical user is classified into self-interference (SI), and that from other users is classified into multiuser interference (MUI). In conventional OFDMA the SI is dominating, whereas in interleaved OFDMA the MUI is dominating. Moreover, in the uplink signals from different users will rotate at different rates, because multiple frequency offsets are present in general.

The impacts of a CFO on MC-CDM has been considered for a simple situation where only one-tap ZF equalization and despreading are performed on received symbols. It is found that $|S_0|^2$ is still a dominating factor in the resulting SINR.

In CDM-OFDMA, ICI caused by CFO will destroy the orthogonality between subchannels and lead to MUI. Furthermore, if the channel is frequency selective, the ICI is further weighted by the channel coefficients, which will complicate the components of MUI. This happens in MC-CDMA as well.

Chapter 5

Frequency Offset Compensation

5.1 Chapter Overview

After the study of the influence of carrier frequency offset (CFO), the subsequent problem we have to solve is how to estimate and correct the frequency offset, or in other words, how to establish the frequency synchronization in an OFDM-based system. This chapter is devoted to the compensation methods, while CFO estimation will be considered in the next chapter. Throughout the chapter we ignore the estimation error, and assume that a perfect estimate of the carrier frequency offset is available for the compensation.

In an OFDM-based system, at a terminal receiver a single CFO can be compensated by multiplying a reverse phase factor $\exp(-j2\pi\epsilon(iN_s + k)/N_f)$ at time instant $(iN_s + k)T$. This method is suitable to a burst transmission, such as WLAN. On the other hand, in the case of continuous transmissions, like DAB, a basic frequency synchronization approach that makes use of a *phase-locked loop* (PLL) can be implemented at the receiver, which aims to adjust the local oscillator to synchronize with the carrier frequency of the received signals. A PLL is impractical in burst transmission, however, since the transmission will be finished before the synchronization is set up.

The disadvantage of these two methods is that they are not appropriate to frequency synchronization at the base station (BS). It is because at the BS the correction of one user's frequency would misalign the other users [51]. One solution to this synchronization problem is performing only time and frequency estimation at the BS, whereas adjustment of the synchronization parameters is performed on the user's side, based on instructions transmitted on the inverse control channel. This method simplifies the synchronization in the uplink. Especially in the scenario where users access to the BS not at the same time, all active users other than the new coming one are assumed to be synchronized, and thus the synchronization problem can be treated like in the single user case. However, an extra traffic overhead is introduced by feeding back the estimated carrier frequency offsets to the transmitter side.

Another solution, on the other hand, is to compensate for the effects of frequency offsets on the receiving side. On the basis of the vector-valued transmission model given in Chapter 4, frequency compensation can be realized solely or together with data detection. The former concept is suited for systems with a relatively simple structure, such as pure OFDMA; the latter is then preferred in CDM-OFDMA and MC-CDMA. A more complicated receiver structure is expected in this case, in order to meet the requirement that the system performance should be as close as possible to the case where the transmitter and receiver are frequency synchronized.

In the following, firstly in Section 5.2 frequency compensation by performing *matrix inversion* of the frequency offset matrix is investigated for OFDM and OFDMA. We also propose a complexity-reduced scheme to alleviate the computational burden. The *least squares* (LS) and *minimum mean square error* (MMSE) criteria are then used in Section 5.3 to reconstruct the orthogonal signals in the frequency domain from one received symbol vector. A trade-off between system performance and computational complexity can be achieved in OFDMA, but unfortunately not in MC-CDMA. The uplink BER performance of these systems are shown and compared in Section 5.4.

It should be pointed out that the implementation of frequency compensation approaches is conditioned on the information of all parameters, including the channel state information (CSI), the value of CFOs, the SNR, and so on. Besides, we assume that the frequency offset of each user does not exceed half of a subcarrier spacing. This assumption is reasonable, because the coarse downlink frequency synchronization can be applied before the user terminal accesses the communication network.

5.2 Frequency Offset Compensation by Matrix Inversion

In a pure OFDM system or a downlink transmission of other OFDM-based systems, the easiest way to compensate for the loss of orthogonality due to CFO is multiplying by a reverse factor before FFT demodulation at the receiver. Its counterpart in the frequency domain will be considered subsequently. In Chapter 4, the vector-valued model for an OFDM transmission in the presence of a CFO has been given by

$$\mathbf{r}_i = \exp(j\theta i)\hat{\mathbf{E}}\mathbf{H}\mathbf{x}_i + \mathbf{n}_i, \quad i = 0, 1, 2, ..., \tag{5.1}$$

where $\exp(j\theta i)$ and $\hat{\mathbf{E}}$,

$$\hat{\mathbf{E}} = \mathbf{F}\mathbf{G}_{pp}\mathbf{E}\mathbf{G}_{ap}\mathbf{F}^{-1} = \mathbf{F}\dot{\mathbf{E}}\mathbf{F}^{-1}, \tag{5.2}$$

represent the effects of frequency offset in frequency domain. $\dot{\mathbf{E}} = \mathbf{G}_{pp}\mathbf{E}\mathbf{G}_{ap}$ is an $N_f \times N_f$ diagonal matrix with the diagonal entries given by

$$\left[\exp\left(j2\pi\epsilon\frac{N_g}{N_f}\right), \ldots, \exp\left(j2\pi\epsilon\frac{N_f + N_g - 1}{N_f}\right)\right].$$

As $\dot{\mathbf{E}}$ is inherently invertible, i.e., it is of full rank, $\hat{\mathbf{E}}$ is thus invertible as well, and the inverse matrix of $\hat{\mathbf{E}}$ is given by

$$\hat{\mathbf{E}}^{-1} = \left(\mathbf{F}\dot{\mathbf{E}}\mathbf{F}^{-1}\right)^{-1} = \mathbf{F}\dot{\mathbf{E}}^{-1}\mathbf{F}^{-1} = \mathbf{F}\dot{\mathbf{E}}^{H}\mathbf{F}^{H} = \hat{\mathbf{E}}^{H}, \tag{5.3}$$

i.e., $\hat{\mathbf{E}}$ is a unitary matrix. As a result, frequency offset compensation in the frequency domain can be performed by means of *matrix inversion* or *matched filtering* of $\hat{\mathbf{E}}$. Together with reversing the instantaneous phase, we get

$$\tilde{\mathbf{r}}_i = \exp(-j\theta i)\hat{\mathbf{E}}^{-1}\mathbf{r}_i = \exp(-j\theta i)\hat{\mathbf{E}}^{H}\mathbf{r}_i = \mathbf{H}\mathbf{x}_i + \exp(-j\theta i)\hat{\mathbf{E}}^{H}\mathbf{n}_i. \tag{5.4}$$

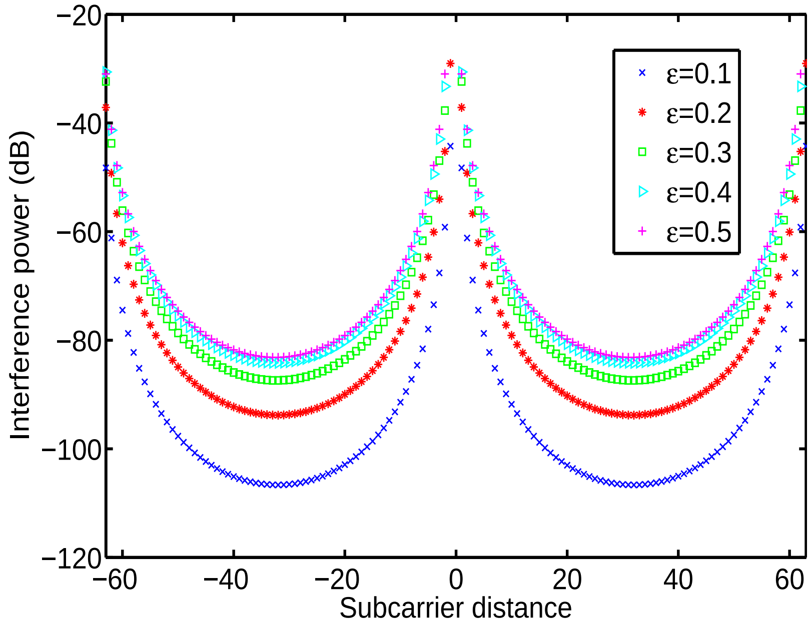

Figure 5.1: The interference power of a subcarrier on other subcarriers.

The noise components in $\tilde{\mathbf{n}}_i$, $\tilde{\mathbf{n}}_i = \exp(-j\theta i)\hat{\mathbf{E}}^H \mathbf{n}_i$, are uncorrelated because

$$\mathbf{\Phi}_{\tilde{\mathbf{n}}_i\tilde{\mathbf{n}}_i} = E\left[\left(\hat{\mathbf{E}}^H\mathbf{n}\right)\left(\hat{\mathbf{E}}^H\mathbf{n}\right)^H\right] = \sigma_n^2 E\left[\hat{\mathbf{E}}^H\hat{\mathbf{E}}\right] = \sigma_n^2\mathbf{I}. \tag{5.5}$$

In comparison to its time domain counterpart, the frequency domain compensation method in (5.4) is not *cost efficient*. To reduce the computational complexity, we try to simplify the matrix $\hat{\mathbf{E}}$ by replacing some off-diagonal entries (interference) with zeros. This idea comes from the ICI analysis in Chapter 4. Let $|I_{m,m'}|^2$ represent the normalized power of the ICI from the subcarrier m' to subcarrier m, and assume the ICI is caused only by CFO. Referring to (4.16) and (4.20), $|I_{m,m'}|^2$ is then equal to $|S_{m'-m}|^2$

$$|I_{m,m'}|^2 = |S_{m'-m}|^2 = \left|\frac{\sin(\pi\epsilon)}{N_f \sin\pi(\frac{m'-m+\epsilon}{N_f})}\right|^2. \tag{5.6}$$

That means, for a given subcarrier, the power of the interference from a certain subcarrier depends only on the index distance between these two subcarriers and the value of ϵ. In Fig. 5.1, the distribution of $|I_{m,m'}|^2$ versus subcarrier distance $m'-m$ for different CFO is plotted (with FFT of point $N_f = 64$). As shown, the power distribution of ICI is approximately symmetric about $|m'-m| = N_f/2$: for $|m'-m| < N_f/2$, $|I_{m,m'}|^2$ decreases as the distance between these two subcarriers increases, whereas for $|m'-m| > N_f/2$, $|I_{m',m}|^2$ increases with $|m'-m|$. In a practical system, a threshold μ can be introduced as a design parameter. For the subcarrier group $\{m : \mu < |m'-m| < N_f - \mu\}$, the ICI is neglected and the interference component $I_{m,m'}$ is accordingly set to zero. In consequence, the interference into subcarrier m is localized to its neighboring subcarrier group $\{m : |m'-m| \leq \mu\}$ and remote subcarrier group $\{m : N_f - \mu \leq |m'-m| \leq N_f - 1\}$. From (4.15), we see that the remote subcarrier group lies in the lower-left and upper-right triangle areas of size μ.

To avoid a terminological ambiguity, we replace $\hat{\mathbf{E}}$ by $\mathbf{\Pi}$ for the time being. The interference localization introduced above will separate $\mathbf{\Pi}$ into two parts: $\mathbf{\Pi}=\mathbf{\Pi}_I+\mathbf{\Pi}_n$. The entries in $\mathbf{\Pi}_I$ are determined by

$$\mathbf{\Pi}_I(m,m') = \begin{cases} S_{m'-m} & \text{if } |m'-m| \leq \mu \text{ or } N_f-\mu \leq |m'-m| \leq N_f-1; \\ 0 & \text{otherwise.} \end{cases} \tag{5.7}$$

The system model for OFDM can be rewritten as

$$\mathbf{r}_i = \exp(j\theta i)\mathbf{\Pi}_I\mathbf{H}\mathbf{x}_i + \exp(j\theta i)\mathbf{\Pi}_n\mathbf{H}\mathbf{x}_i+\mathbf{n}_i=\exp(j\theta i)\mathbf{\Pi}_I\mathbf{H}\mathbf{x}_i + \bar{\mathbf{n}}_i, \tag{5.8}$$

where $\bar{\mathbf{n}}_i=\exp(j\theta i)\mathbf{\Pi}_n\mathbf{H}\mathbf{x}_i+\mathbf{n}_i$. The residual interference represented by $\mathbf{\Pi}_n\mathbf{H}\mathbf{x}_i$ is treated as noise, thus the system noise level will increase. The frequency compensation can therefore be realized by means of matrix inversion of $\mathbf{\Pi}_I$

$$\tilde{\mathbf{r}}_i = \exp(-j\theta i)\mathbf{\Pi}_I^{-1}\mathbf{r}_i = \mathbf{H}\mathbf{x} + \exp(-j\theta i)\mathbf{\Pi}_I^{-1}\bar{\mathbf{n}}_i. \tag{5.9}$$

A similar implementation has been proposed by Cao in [13], where normalized power of ICI is approximately given by

$$|I_{m,m'}|^2 \approx \left|\frac{\sin(\pi\epsilon)}{\pi(m'-m+\epsilon)}\right|^2. \tag{5.10}$$

Equation (5.10) holds for $\frac{m'-m+\epsilon}{N_f} \ll 1$, since $\sin(x) \approx x$ when $x \ll \pi$. Fig. 5.2 shows the interference power distribution according to (5.10). As compared with Fig. 5.1, the effect of the remote subcarrier groups are ignored. Therefore, the entries of $\mathbf{\Pi}_I$ according to (5.10) are given by

$$\mathbf{\Pi}_I(m,m') = \begin{cases} S_{m'-m} & \text{if } |m'-m| \leq \mu; \\ 0 & \text{otherwise.} \end{cases} \tag{5.11}$$

Although with (5.11) the computational complexity will be further reduced, the total noise level will ascend more rapidly and give rise to system performance degradation. The numerical simulation and performance comparison will be given in Section 5.4. In addition, it should be mentioned that frequency compensation by means of matrix inversion is inefficient for OFDM, as compared with the time domain compensation method. However, it can be applied in the uplink of OFDMA systems.

Application to OFDMA and CDM-OFDMA Uplink

According to (4.45) in Chapter 4, at the BS of an OFDMA system, the received symbol vector at time index i is expressed as

$$\mathbf{r}_{i,\mathrm{UL,OFDMA}} = \bar{\mathbf{E}}_{\mathrm{UL}}\bar{\Psi}_{i,\mathrm{UL}}\bar{\mathbf{H}}_{\mathrm{UL}}\mathbf{x}_i + \mathbf{n}_i. \tag{5.12}$$

Note that $\bar{\mathbf{E}}_{\mathrm{UL}}^H\bar{\mathbf{E}}_{\mathrm{UL}}\neq\mathbf{I}$ except when the frequency offsets of different users are the same. Nonetheless, $\bar{\mathbf{E}}_{\mathrm{UL}}$ is still invertible. Therefore, to compensate for the frequency offsets, we prefer to perform matrix inversion rather than matched filtering

$$\tilde{\mathbf{r}}_{i,\mathrm{UL,OFDMA}} = \left(\bar{\mathbf{E}}_{\mathrm{UL}}\bar{\Psi}_{i,\mathrm{UL}}\right)^{-1}\mathbf{r}_{i,\mathrm{UL,OFDMA}} = \bar{\mathbf{H}}_{\mathrm{UL}}\mathbf{x}_i+ \left(\bar{\mathbf{E}}_{\mathrm{UL}}\bar{\Psi}_{i,\mathrm{UL}}\right)^{-1}\mathbf{n}_i, \tag{5.13}$$

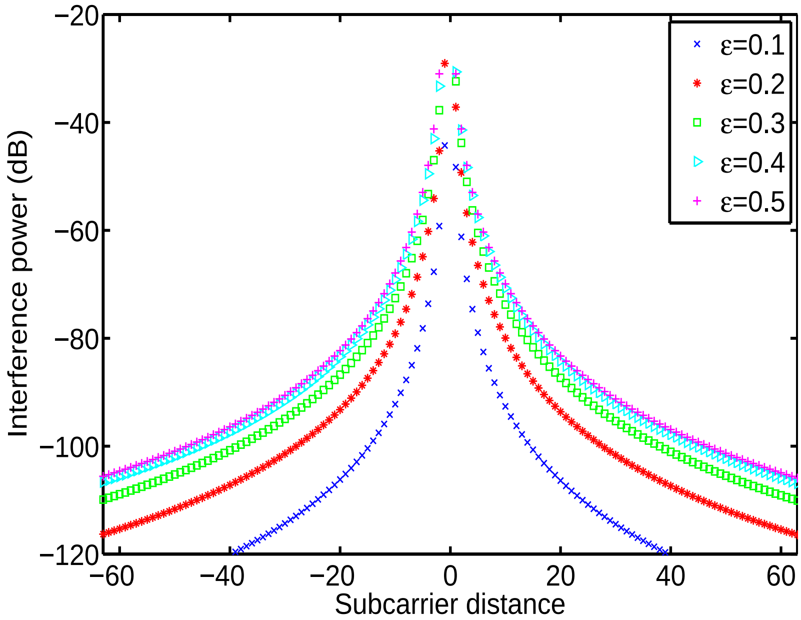

Figure 5.2: The interference power of a subcarrier on other subcarriers according to 5.10.

but the noise $\tilde{\mathbf{n}}_i = \left(\bar{\mathbf{E}}_{\mathrm{UL}}\bar{\Psi}_{i,\mathrm{UL}}\right)^{-1}\mathbf{n}_i$ is colored since

$$\mathbf{\Phi}_{\tilde{\mathbf{n}}_i\tilde{\mathbf{n}}_i} = \sigma_n^2\mathbf{\Phi}_{\bar{\mathbf{E}}_{\mathrm{UL}}\bar{\mathbf{E}}_{\mathrm{UL}}} \neq \sigma_n^2\mathbf{I}. \tag{5.14}$$

Similarly, the frequency compensation by using matrix inversion can also be applied for CDM-OFDMA

$$\begin{aligned}\tilde{\mathbf{r}}_{i,\mathrm{UL,CDM\text{-}OFDMA}} &= \left(\bar{\mathbf{E}}_{\mathrm{UL}}\bar{\Psi}_{i,\mathrm{UL}}\right)^{-1}\mathbf{r}_{i,\mathrm{UL,CDM\text{-}OFDMA}} \\ &= \bar{\mathbf{H}}_{\mathrm{UL}}\mathbf{T}_c\mathbf{U}\mathbf{x}_i + \left(\bar{\mathbf{E}}_{\mathrm{UL}}\bar{\Psi}_{i,\mathrm{UL}}\right)^{-1}\mathbf{n}_i.\end{aligned} \tag{5.15}$$

However, matrix inversion is not applicable to MC-CDMA, since in (4.82) the matrix $\bar{\mathbf{E}}_{\mathrm{UL}}$ is not a square matrix. Instead, the pseudoinverse is considered in this case. Yet, this is inconvenient because $\bar{\mathbf{E}}_{\mathrm{UL}}$ as well as $\bar{\Psi}_{i,\mathrm{UL}}$ are large scale matrices in MC-CDMA in comparison to those in OFDMA or CDM-OFDMA.

5.3 Frequency Offset Compensation by ZF Approach and LMMSE Approach

Frequency compensation also can be achieved by using *least square error* (LS) criterion and *minimum mean square error* (LMMSE) criterion. The details of these two approaches are shown in Appendix A. The first criterion minimizes the total interference power in one OFDMA block, which results in *least squares* (LS) or *zero-forcing* (ZF) method. The symbol vector after frequency compensation can be expressed as

$$\tilde{\mathbf{r}}_{i,\mathrm{UL,OFDMA}} = (\Gamma_i^H\Gamma_i)^{-1}\Gamma_i^H\mathbf{r}_{i,\mathrm{UL,OFDMA}} = \bar{\mathbf{H}}_{\mathrm{UL}}\mathbf{x}_i + (\Gamma_i^H\Gamma_i)^{-1}\Gamma_i^H\mathbf{n}_i, \tag{5.16}$$

where $\Gamma_i = \bar{\mathbf{E}}_{\mathrm{UL}}\bar{\Psi}_{i,\mathrm{UL}}$. However, as

$$(\Gamma_i^H \Gamma_i)^{-1}\Gamma_i^H = \Gamma_i^{-1}(\Gamma_i^H)^{-1}\Gamma_i^H = \Gamma_i^{-1},$$

ZF approach is equivalent to matrix inversion in the case of square matrices. In the ZF approach no probabilistic assumption is made about the received symbols or about the noise. If the first two moments of the joint PDF $p(\mathbf{r}_i, \bar{\mathbf{H}}_{\mathrm{UL}}\mathbf{x}_i)$ are known, then the LMMSE method can be used

$$\tilde{\mathbf{r}}_{i,\mathrm{UL,OFDMA}} = (\Gamma_i^H \Gamma_i + \sigma_n^2 \mathbf{\Phi}_{\bar{\mathbf{x}}_i\bar{\mathbf{x}}_i}^{-1})^{-1}\Gamma_i^H \mathbf{r}_{i,\mathrm{UL,OFDMA}} \tag{5.17}$$

where $\mathbf{\Phi}_{\bar{\mathbf{x}}_i\bar{\mathbf{x}}_i}^{-1}$ is the inverse of the covariance matrix of the signals $\bar{\mathbf{x}}_i$, $\bar{\mathbf{x}}_i = \bar{\mathbf{H}}_{\mathrm{UL}}\mathbf{x}_i$, and

$$\begin{aligned}\mathbf{\Phi}_{\bar{\mathbf{x}}_i\bar{\mathbf{x}}_i} &= E[(\bar{\mathbf{H}}_{\mathrm{UL}}\mathbf{x}_i)(\bar{\mathbf{H}}_{\mathrm{UL}}\mathbf{x}_i)^H] = \sigma_x^2 E\left[\bar{\mathbf{H}}_{\mathrm{UL}}\bar{\mathbf{H}}_{\mathrm{UL}}^H\right] \\ &= \sigma_x^2 \mathrm{diag}\left\{E[|\bar{H}_0|^2], E[|\bar{H}_1|^2], ..., E[|\bar{H}_{N_f-1}|^2]\right\}.\end{aligned} \tag{5.18}$$

Apparently, $\mathbf{\Phi}_{\bar{\mathbf{x}}_i\bar{\mathbf{x}}_i}^{-1}$ depends on the channel characteristics of all users. Both approaches can also be implemented in CDM-OFDMA, provided that frequency offsets and the impulse responses of the channels are known.

Joint Equalization

If the concatenation of spreading, the physical channel, the frequency offset, and other signal processing steps between the transmit vector $\mathbf{x}_i$ and the received vector $\mathbf{r}_i$ are viewed as an equivalent channel, then we can combine the frequency compensation and equalization together. This is much more suitable for CDM-OFDMA and MC-CDMA due to the system complexity. Rewriting the ZF and LMMSE approaches for the joint equalization in the uplink transmission, we get

$$\tilde{\mathbf{x}}_{i,\mathrm{ZF}} = (\mathbf{R}_i^H \mathbf{R}_i)^{-1}\mathbf{R}_i^H \mathbf{r}_i = \mathbf{x}_i + \tilde{\mathbf{n}}_{i,\mathrm{ZF}}, \tag{5.19}$$

$$\tilde{\mathbf{x}}_{i,\mathrm{LMMSE}} = \left(\mathbf{R}_i^H \mathbf{R}_i + \frac{\sigma_n^2}{\sigma_x^2}\mathbf{I}\right)^{-1} \mathbf{R}_i^H \mathbf{r}_i \approx \mathbf{x}_i + \tilde{\mathbf{n}}_{i,\mathrm{LMMSE}}. \tag{5.20}$$

The equivalent channel matrices of different systems are defined as

$$\mathbf{R}_{i,\mathrm{OFDMA}} = \bar{\mathbf{E}}_{\mathrm{UL}}\bar{\Psi}_{i,\mathrm{UL}}\bar{\mathbf{H}}_{\mathrm{UL}}, \tag{5.21}$$

$$\mathbf{R}_{i,\mathrm{CDM\text{-}OFDMA}} = \bar{\mathbf{E}}_{\mathrm{UL}}\bar{\Psi}_{i,\mathrm{UL}}\bar{\mathbf{H}}_{\mathrm{UL}}\mathbf{U}, \tag{5.22}$$

and

$$\mathbf{R}_{i,\mathrm{MC\text{-}CDMA}} = \bar{\mathbf{E}}_{\mathrm{UL}}\bar{\Psi}_{i,\mathrm{UL}}\mathrm{Diag}\{\bar{\mathbf{H}}_{\mathrm{UL}}\}\bar{\mathbf{U}}_{\mathrm{UL}}. \tag{5.23}$$

In the next section, the BER performance of CDM-OFDMA and MC-CDMA will be compared.

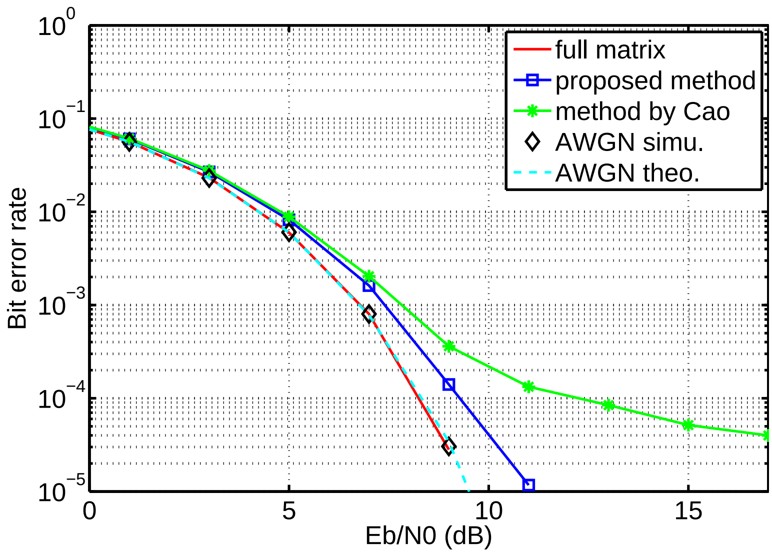

Figure 5.3: Bit error rate performance of matrix inversion for $\epsilon = 0.2$ and $\mu = 5$, QPSK mapping.

5.4 Simulation Results

Again, we use Monte Carlo simulations to evaluate the performance of the proposed algorithms. In simulations, the OFDM structure used for all transmission schemes is assumed having 64 subcarriers, i.e., $N_f = 64$ and $N_g = 16$. Furthermore, if only frequency offset compensation is taken into account, the simulation will be made only for transmission over AWGN channels, in order to avoid the extra performance degradation due to channel imperfection. In the case of joint equalization, when the eight-path Rayleigh fading channels introduced in Section 2.2.3 is applied, for the sake of comparison each realization of the channel (even for each individual user in the uplink) is normalized. In some simulations, a coded transmission is taken into account, where information bits are encoded by a conventional code (131,171) of rate $R = 1/2$. In addition, in a multiuser scenario, four users are always assumed in the uplink transmission. And, if not otherwise mentioned, the transmit symbols are chosen from a QPSK signal modulation.

5.4.1 Frequency Offset Compensation in OFDM Using Frequency-domain Algorithms

Fig. 5.3 compares the frequency offset compensation in OFDM over an AWGN channel by using matrix inversion. The frequency offset and the threshold are set to be $\epsilon = 0.2$ and $\mu = 5$, respectively. It is shown that the inverse operation with the full matrix totally compensates for the frequency offset. At a BER of 10^{-4}, the simplified method proposed above gives a performance loss less than 1 dB, whereas the method proposed by Cao leads to a performance loss more than 1.5 dB. Furthermore, an error floor occurs as E_b/N_0 increases.

Performance comparison with different values of ϵ and μ is plotted in Fig. 5.4. At a given μ, performance loss increases with the CFO. Comparing the left and the right figures, we can see that when using full matrix the simulation results always coincide with the AWGN curve, while for the other two approaches, the BER performance becomes bad as the value of μ decreases. The proposed method in (5.7) provides a better performance than the method by Cao. Nevertheless, with a small threshold and a large CFO, e.g., when $\mu = 5$ and $\epsilon = 0.45$, both approaches fail to suppress the effects of the CFO and to recover the frequency synchronization.

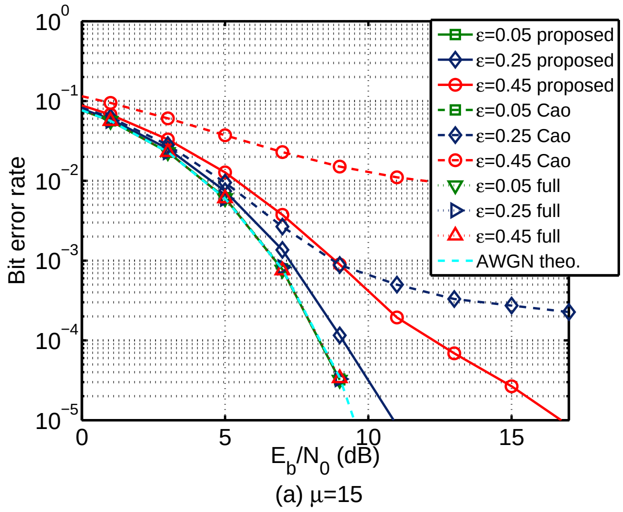

Figure 5.4: Bit error rate performance with different values of ϵ and μ.

5.4.2 Frequency Offset Compensation in OFDMA Uplink

In simulations for the uplink transmission of an uncoded OFDMA system, signals from different users are assumed to have different CFOs, and the CFOs are uniformly distributed in the range of $[-0.35, +0.35]$. We define the largest value in this range as the *maximum frequency offset*, denoted by $\epsilon_{\max}$. In this case $\epsilon_{\max} = 0.35$. Furthermore, to get an average performance, in each simulation new CFOs are chosen. Fig. 5.5 illustrates the performance of frequency compensation by means of ZF approach and LMMSE approach, respectively, where μ is set to be 15.

In Fig. 5.5, we can observe that a different BER performance is obtained by the two OFDMA schemes. If the full matrix is used for compensation, at a lower E_b/N_0 C-OFDMA outperforms I-OFDMA, but at a higher SNR, e.g., as $E_b/N_0 > 10$dB, in the case of ZF I-OFDMA outperforms C-OFDMA. The same conclusion can be drawn for complexity-reduction methods. Nevertheless, an error floor occurs when either method (5.7) or (5.11) is applied. In addition, similar to OFDM, the simplified method in (5.7) provides a better performance. Finally, it can be seen that the LMMSE approach outperforms the ZF approach at low SNR. Therefore, in the following only the LMMSE approach is considered.

Compensation with Different μ

The choice of the threshold μ is of importance when we attempt to reduce the computational complexity. As an example, Fig. 5.6 compares the BER performance when a different μ is

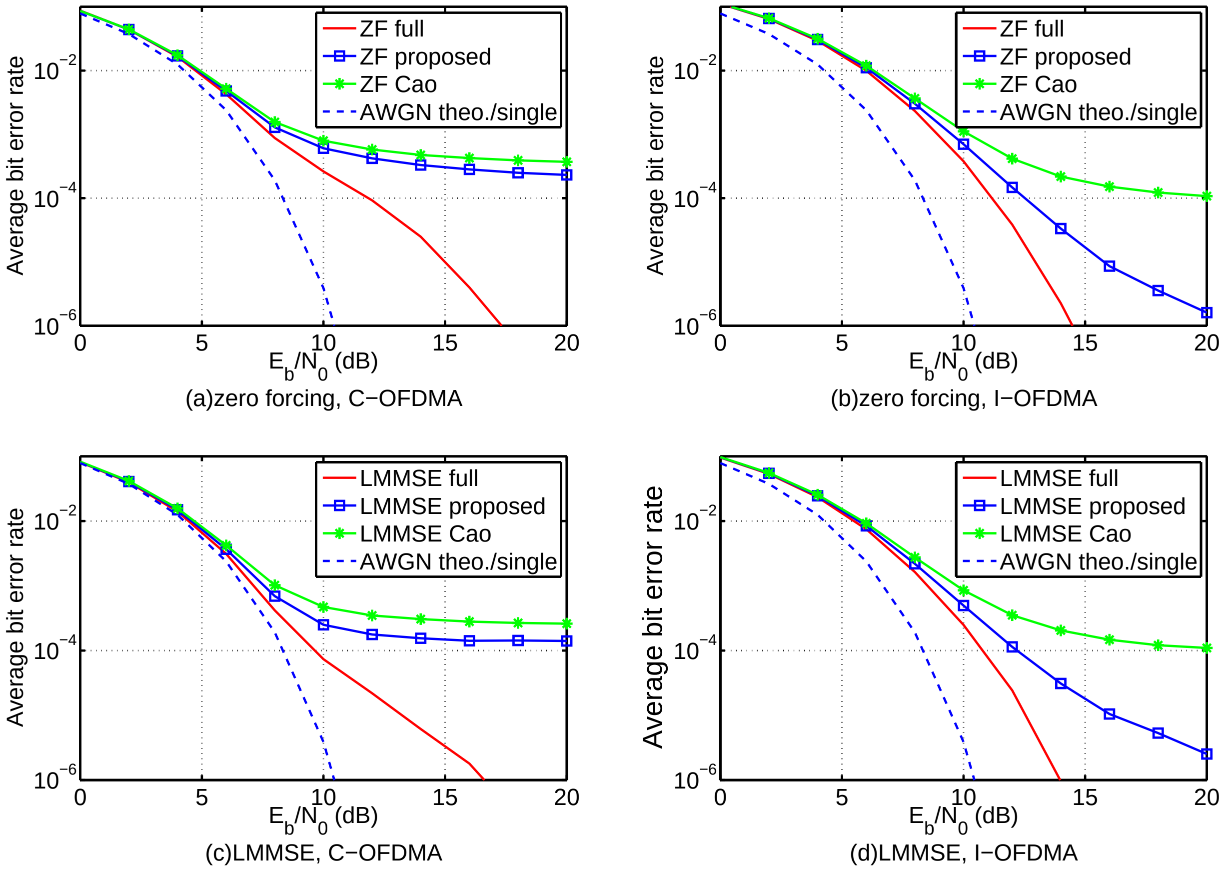

Figure 5.5: Performance comparison of frequency offset compensation methods for uncoded OFDMA ($\mu = 15$, $\epsilon_{\max} = 0.35$).

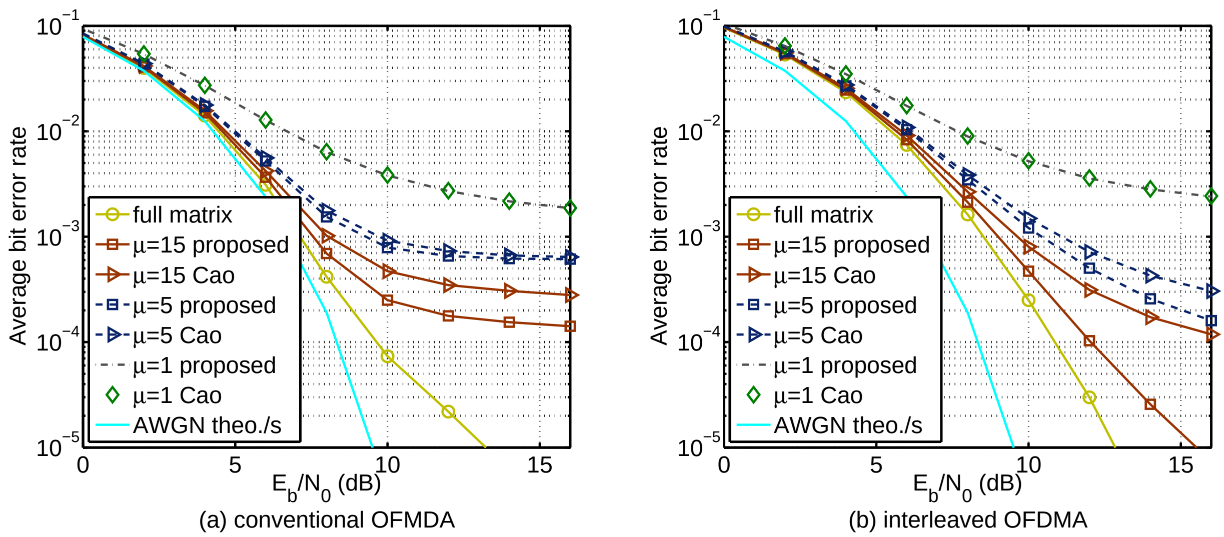

Figure 5.6: Frequency offset compensation by LMMSE approach for uncoded OFDMA over an AWGN channel with different threshold μ ($\epsilon_{\max} = 0.35$).

chosen. It is shown that setting $\mu = 5$ can fulfill a requirement of BER$< 10^{-3}$ at $E_b/N_0 = 10$dB for C-OFMDA, and at $E_b/N_0 = 11$dB for I-OFMDA, under the condition that $\epsilon_{\max} = 0.35$. The choice of μ depends on the range in which the frequency offsets are distributed. To achieve a given BER performance, the larger the $\epsilon_{\max}$, the larger the threshold μ should be set.

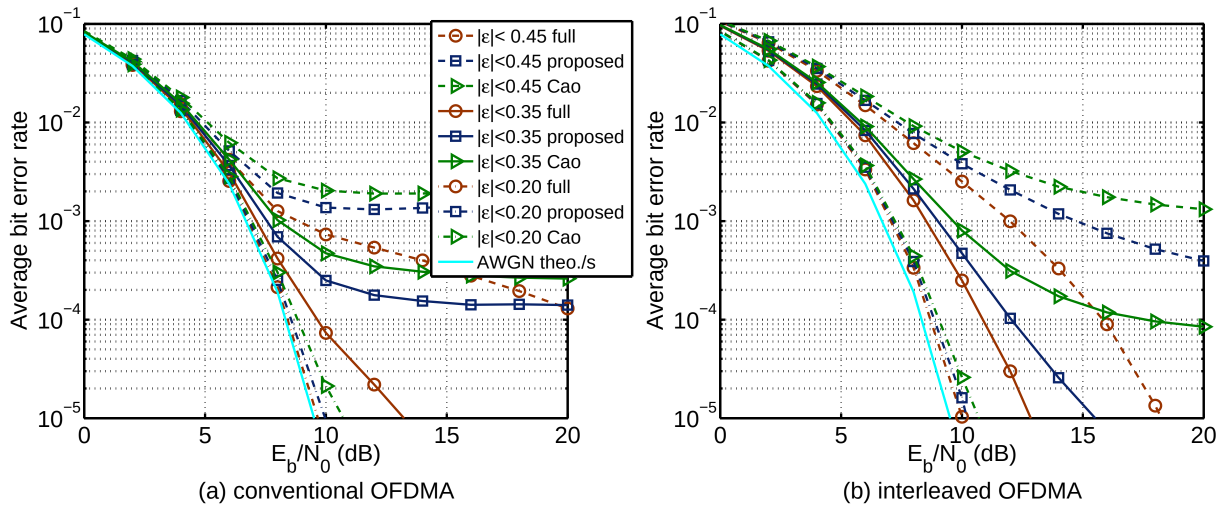

Figure 5.7: Frequency offset compensation by LMMSE approach for uncoded OFDMA over an AWGN channel with different maximum frequency offset $\epsilon_{\max}$ ($\mu = 15$).

Compensation with Different Maximum Frequency Offset $\epsilon_{\max}$

Fig. 5.7 further verifies the impact of the distribution of frequency offsets on the compensation performance. If the $\epsilon_{\max}$ is relatively small, e.g., in the case of $\epsilon_{\max} = 0.20$, the performance degradation caused by CFO can be mostly compensated for by using the LMMSE approach. However, with the increase of $\epsilon_{\max}$, the performance gets worse.

Joint Compensation of Frequency Offsets and Frequency Selective Fading Channels

We now extend our sight to a more practical scenario where multipath propagation further deteriorates the transmission. Joint equalization is implemented to cope with the effects of frequency offsets and frequency selective fading. In Fig. 5.8 we compare only the case without frequency offsets and with the maximum frequency offset $\epsilon_{\max} = 0.45$. It is not surprising to see that in the absence of CFOs, the same average BER performance is obtained in both C-OFDMA and I-OFDMA in the case of an uncoded transmission. As shown in Fig. 5.9, if a coded transmission is considered, benefitting from interleaving, a much better performance is obtained by I-OFDMA when having no CFOs. In the presence of CFOs, however, the extra performance loss is small in C-OFDMA but significant in I-OFDMA. This is because, in the case of I-OFDMA, MUI is possible to be enhanced by the channel coefficients of other users, so that a worse uncoded performance is obtained. In the case of a coded transmission and the full $\bar{\mathbf{E}}_{\mathrm{UL}}$ matrix, I-OFDMA has a slightly better performance than C-OFDMA. But unfortunately, the matrix simplification methods do not work well in this case. It is because, on one hand,

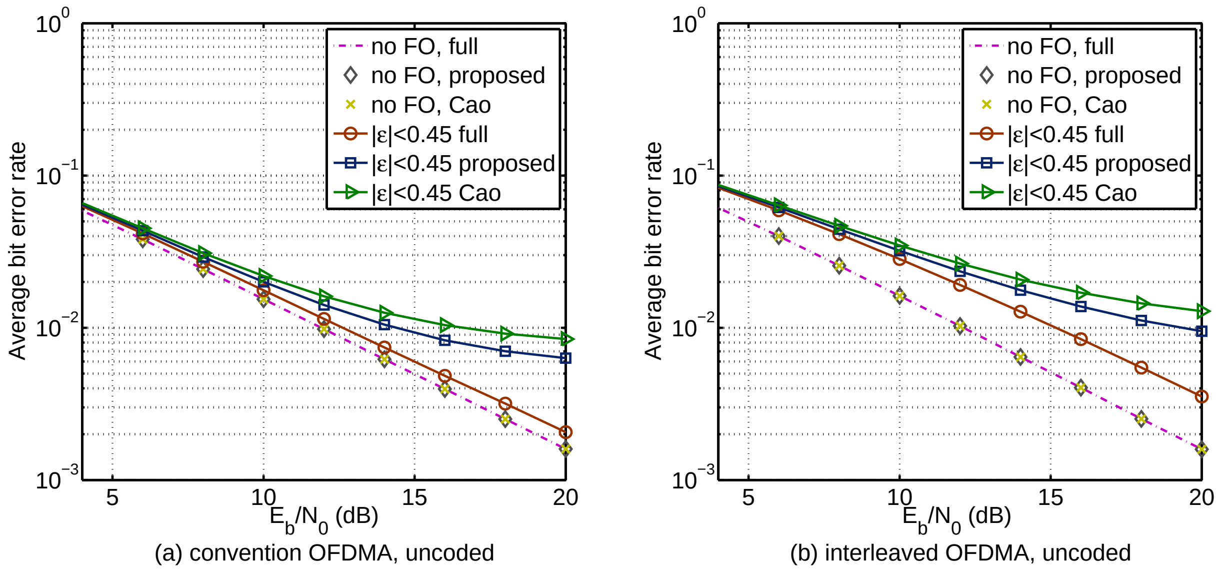

Figure 5.8: Joint compensation of frequency offsets and frequency selective fading channels: uncoded ($\mu = 15$).

the CFOs are distributed in a large range; on the other hand, the weighting by the channel coefficients will change the distribution of the interference, and thus the reasonableness of the $\mathbf{\Pi}_I$ matrix.

5.4.3 Comparison of CDM-OFDMA and MC-CDMA in the Uplink

In the previous chapters, two transmission schemes have been defined for CDM-OFDMA: conventional and interleaved CDM-OFDMA. For MC-CDMA, three transmission schemes can be distinguished by (1) fully-spread MC-CDMA, representing MC-CDMA with full spreading; (2) interleaved MC-CDMA, representing MC-CDMA with interleaved spreading; (3) non-interleaved spreading, representing MC-CDMA with sub-band spreading. In the following, we will compare their performance in the uplink.

The LMMSE equalizer in (5.20) is taken for vector equalization. It should be mentioned that for BPSK transmission, the LMMSE vector equalization can be modified to

$$\tilde{\mathbf{x}}_{i,\,\mathrm{LMMSE}} = \left(\mathrm{Re}\left\{ \mathbf{R}_i^H \mathbf{R}_i \right\} + \frac{\sigma_n^2}{2\sigma_x^2}\mathbf{I} \right)^{-1} \mathrm{Re}\left\{ \mathbf{R}_i^H \mathbf{r}_i \right\}. \tag{5.24}$$

This implies that only the real part is useful for the data detection. In addition, since the simplified matrix $\mathbf{\Pi}_I$ is not appropriate for the case of joint equalization, only the full $\bar{\mathbf{E}}_{\mathrm{UL}}$ matrix is used in simulations.

As we know, the unitary matrices have been used as the spreading matrices in all CDM-OFDMA and MC-CDMA transmission schemes. For this reason, if no distortion results from channel impairment or from imperfect synchronization, i.e., additive white Gaussian noise is the only factor which degrades the system performance, all aforementioned transmission schemes have the same average BER performance which coincide with the theoretical AWGN curve for a

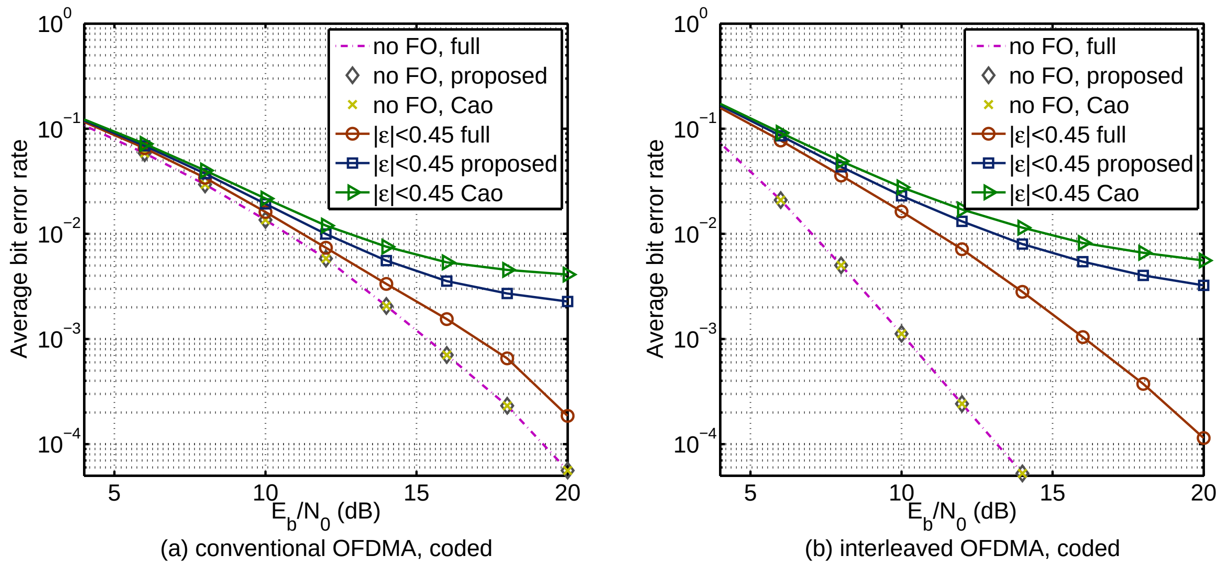

Figure 5.9: Joint compensation of frequency offsets and frequency selective fading channels: coded ($\mu = 15$).

single user. In Figs. 5.10 and 5.13, this curve has a legend 'AWGN, simulation for all'. We take this curve as a reference for evaluating the performance degradation caused by the multipath channels or/and the CFOs.

The performance comparison is made from three aspects:

- The Influence of the carrier frequency offsets on different systems. It is evaluated by assuming an uplink transmission over AWGN channels;
- The impacts of the frequency selective fading on different systems. An eight-path Rayleigh fading channel model is used for simulations, and additionally the block fading is assumed;
- The joint influence of the carrier frequency offsets and the frequency selective fading.

Moreover, it should be noted that in the following simulations, we focus on the average performance of all users.

Transmission with QPSK

Transmission over AWGN Channels Only the influence of CFOs is considered in this subsection. In Simulations, we set $\epsilon_{\max} = 0.45$, i.e., the CFOs of different users are uniformly distributed in the range of $[-0.45, +0.45]$. To obtain a average performance, the CFO of each user is changed block by block, where each block consists of 32 *overall* symbol vectors, and 2000 block is used for simulation. Furthermore, it should be noted that phase rotation due to the CFO can not be ignored, such that the $\bar{\Psi}_{i,\mathrm{UL}}$ matrix will change vector by vector.

The simulation results for uncoded transmission of different scheme are shown in Fig. 5.10. Apparently, the curves are much different from each other. In fact, it is not easy to give reasons

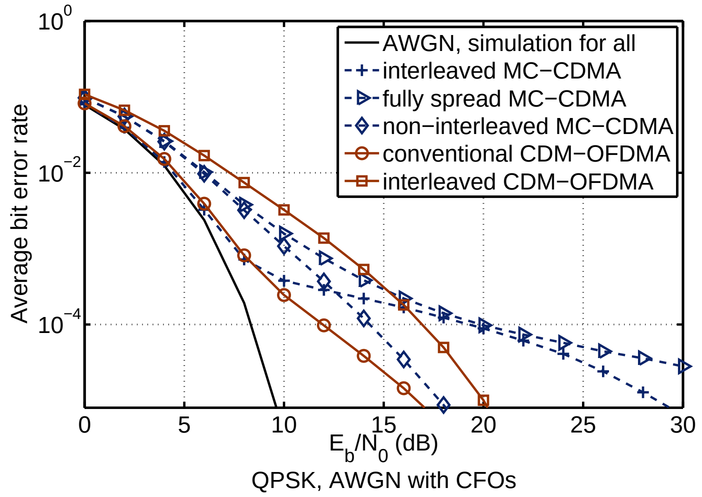

Figure 5.10: Uncoded BER performance over AWGN channels with CFOs: QPSK, $\epsilon_{\max} = 0.45$.

to them, for the uplink structures of these systems are too complicated. We consider then a simple scenario, where all users have the same CFO. Under this assumption, according to the definitions of uplink models in Sections 4.4.2 and 4.4.3, the $\bar{\mathbf{E}}_{\mathrm{UL}}$ will be a full $\hat{\mathbf{E}}$ matrix in CDM-OFDMA, and in MC-CDMA will be made up of K identical $\hat{\mathbf{E}}$ matrices. When matched filtering is used (a step in LMMSE), since $\hat{\mathbf{E}}$ is a unitary matrix, the interference caused by the CFO will be totally eliminated, and thus the resulting BER performance should be identical to the theoretical AWGN curve. A simulation we have made for this scenario, and the results have verified the analysis above. Therefore, to some extent we can believe the correctness of the programmes for simulation, and thus the results shown in Fig. 5.10.

It can be seen that in general, when LMMSE equalization is in use, conventional CDM-OFDMA is most robust to the CFOs. In contrast, interleaved CDM-OFDMA is more sensitive to CFOs than conventional CDM-OFDMA. For instance, at a given average BER of 10^{-4}, the former has about 5dB performance loss in comparison to the latter. The performance of non-interleaved MC-CDMA is in between. For the other two schemes, the curve of fully-spread MC-CDMA varies with E_b/N_0 slowly but smoothly, whereas interleaved MC-CDMA has a surprising result: at a lower E_b/N_0, its curve approximately overlaps with the curve of conventional CDM-OFDMA, but as $E_b/N_0 > 8$dB, the performance of uncoded interleaved MC-CDMA suddenly becomes poor. As compared with other systems, performance of fully-spread MC-CDMA has the worst BER performance at a higher E_b/N_0.

Transmission over Multipath Channels In the case of multipath channels, before discussing the uplink performance, we give some results for the downlink transmission over an eight-path Rayleigh fading channel. It is shown in Fig. 5.11 that interleaved CDM-OFDMA and fully-spread MC-CDMA have the similar performance, which is much better than other schemes'. At a given average BER of 10^{-4}, conventional CDM-OFDMA, interleaved and non-interleaved MC-CDMA have 5.7dB, 8.7dB and 11.2dB performance loss, respectively, in comparison to interleaved CDM-OFDMA.

In the uplink, block Rayleigh fading is assumed in simulations. Fig. 5.12(a) depicts the resulting BER performance of all transmission schemes in the absence of the CFOs. The uplink

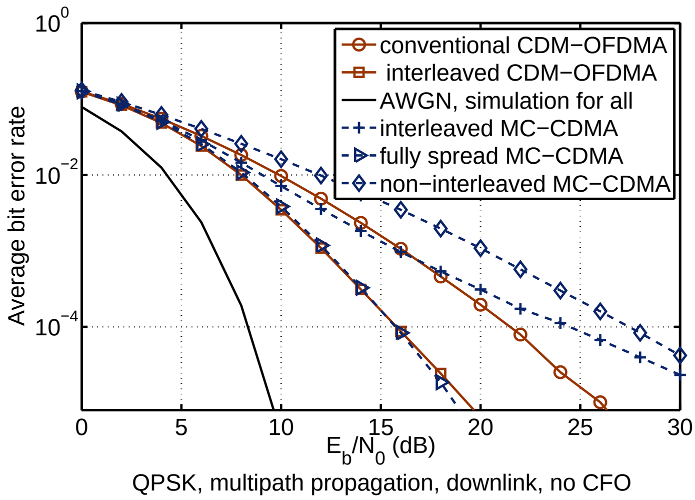

Figure 5.11: Uncoded BER performance over 8-path channels without CFOs: downlink transmission.

performance of fully-spread MC-CDMA and both CDM-OFDMA schemes are similar to those in the downlink, whereas the uplink performance of interleaved and non-interleaved MC-CDMA becomes worse, especially the former one, whose curve has nearly overlapped over the curve of the latter one.

Simulation results for joint influence of the frequency selective fading and the carrier frequency offsets on the uplink performance are given in Fig. 5.12(b). Extra performance loss is introduced in most of the schemes, as compared with the cases without CFO. In general, performance change of different schemes is basically in accord with the previous investigation for CFO alone. For instance, because of the CFOs, the curves of interleaved CDM-OFDMA and fully-spread MC-CDMA shift more than 5dB to the right (at an average BER of 10^{-4}), whereas the curve of conventional CDM-OFDMA has moved just a little to the right. As a consequence, these three schemes have very close performance. Moreover, interleaved MC-CDMA has a slightly better performance than non-interleaved MC-CDMA in the range of E_b/N_0 for which we have simulated. The uplink uncoded performance of both MC-CDMA schemes are however much worse than the others.

Transmission with BPSK

Transmission over AWGN Channels Fig. 5.13 depicts the uncoded BER performance of different transmission schemes with CFOs in the case of BPSK. The uncoded performance of most of schemes other than fully-spread MC-CDMA is in accord with that in the case of QPSK. Furthermore, when comparing the two modulation schemes, we can see that with BPSK the performance of all schemes has been improved significantly. This first of all verified the analysis in the previous chapter that BPSK transmission has relatively less sensitivity to CFO than QPSK transmission. Secondly, LMMSE equalizer in (5.24) has been implemented for BPSK transmission, in which the imaginary part of the correlation matrix of the equivalent channel matrix, as well as the imaginary part of the received signals after matched filtering, are omitted before the equalization. This operation reduces the total amount of interference,

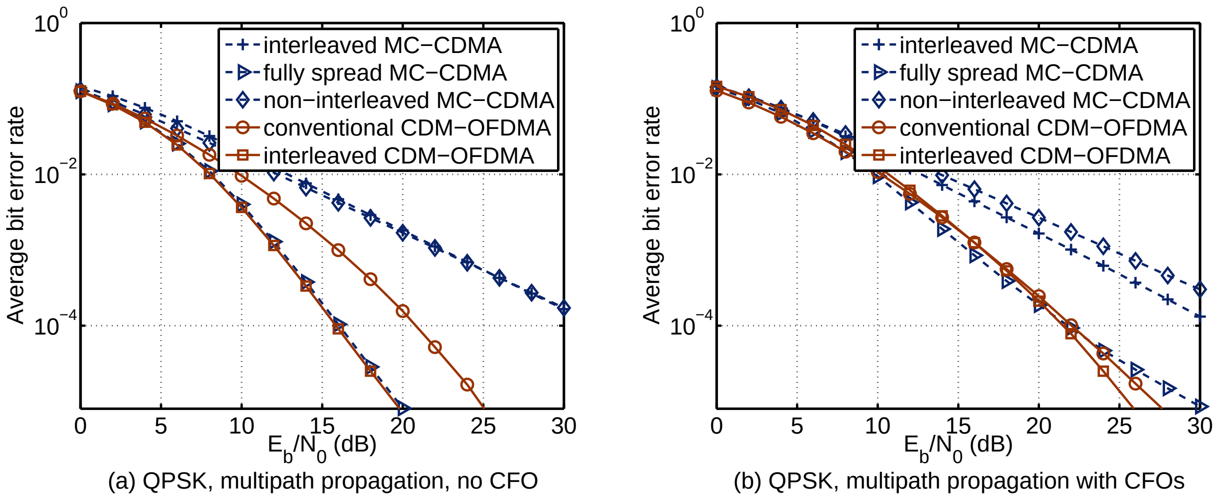

Figure 5.12: Uncoded BER performance over 8-path channels with and without CFOs: QPSK, $\epsilon_{\max} = 0.45$.

and thus improves the performance of BPSK transmission. It may also be the reason to the performance improvement of fully-spread MC-CDMA, whose curve goes down more rapidly than the associated curve in Fig. 5.10.

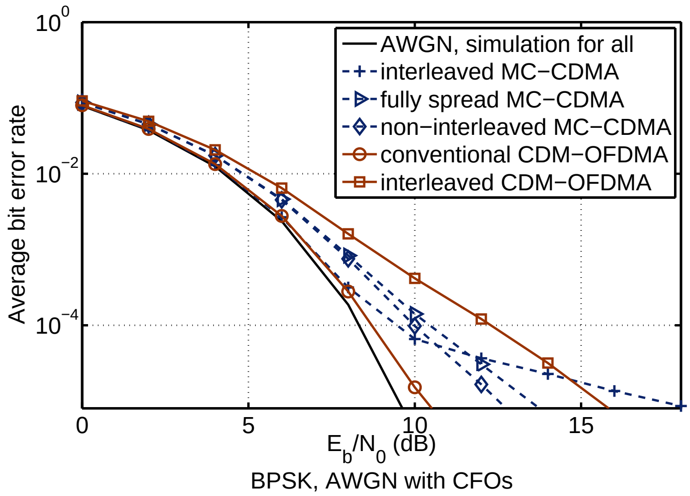

Figure 5.13: Uncoded BER performance over AWGN channels with CFOs: BPSK, $\epsilon_{\max} = 0.45$.

Transmission over Multipath Channels The same reason may also be used to explain the performance change when transmitting over multipath channels. Simulation results for this case are given in Fig. 5.14. If the performance degradation caused by the frequency selective fading alone, as shown in Fig. 5.14(a), the performance of all MC-CDMA schemes becomes better than in the case of QPSK. A significant performance improvement is achieved by interleaved MC-CDMA, which, along with spread MC-CDMA, outperforms interleaved CDM-OFDMA. But the performance of two CDM-OFDMA schemes is not improved, by contrast, even a slightly performance loss happened to conventional CDM-OFDMA.

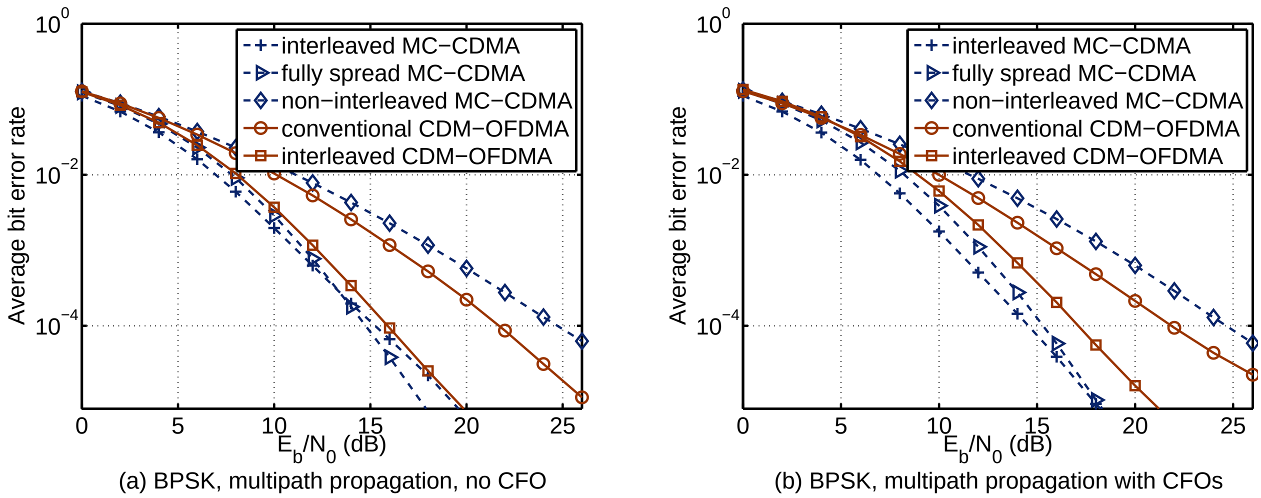

Figure 5.14: Uncoded BER performance over 8-path channels with and without CFOs: BPSK, $\epsilon_{\max} = 0.45$.

If CFOs are present, like in the case of QPSK, all transmission schemes other than interleaved MC-CDMA have the extra performance loss. The form of their curves changes according to the results in Fig. 5.13. For example, the curve of interleave CDM-OFDMA has shifted beyond the curve of fully-spread MC-CDMA, as it has been strongly affected by the CFOs. The result of interleaved MC-CDMA is questionable, however. It may be because in this case the joint influence of the complex-valued channel (coefficients) and the CFOs leads to that in interleaved MC-CDMA, the interference distributes in a specially way, such that more interference in the imaginary part can be discarded, and thus the performance is improved.

When comparing the uncoded uplink performance of all the schemes, some results can be found as follows. In the absence of CFOs, with QPSK transmission interleaved CDM-OFDMA and fully-spread MC-CDMA have provided the best performance, whereas with BPSK transmission interleaved MC-CDMA will also acceptable. In the presence of CFOs, with QPSK transmission fully-spread MC-CDMA and both CDM-OFDMA schemes are available, whereas with BPSK transmission fully-spread and interleaved MC-CDMA, as well as interleaved CDM-OFDMA would be recommended. However, two factors have to be considered when we chose a transmission schemes for the uplink: first, the ability to allow the adaptive modulation; second, the complexity of parameter estimations. Because uplink parameter estimation (e.g. CIRs, CFOs) is much rougher task for MC-CDMA than for CDM-OFDMA, and conventional CDM-OFDMA is not suitable for BPSK transmission, it follows that interleaved CDM-OFDMA is the only one which fulfills the conditions above. It should be noted that this is just a conclusion which is drawn from the insufficient evidences. Other conditions, e.g., performance in the cases of coded transmission, other equalizers, and high-level mapping (e.g. 16QAM), should also be taken into account. Those are not included in this work, but will be considered in the future.

5.5 Summary

This chapter is devoted to the frequency offset compensation in an OFDM-based system, especially for the uplink. The task can be accomplished on the basis of the vector-valued transmission model developed in the previous chapter. For transmission schemes with a relatively simple structure, such as pure OFDMA, separate frequency compensation can be performed, whereas for CDM-OFDMA and MC-CDMA, joint equalization is expected to cope with the interference caused by both CFOs and the distortion of the dispersive channels. Moreover, throughout this chapter an assumption is made that a perfect estimate of the carrier frequency offset is available for the compensation step, so is the estimate of the CIR, when it is required. Besides, we have assumed that the maximum frequency offset does not exceed half of a subcarrier frequency spacing.

The chapter started with an analysis of the matrix $\hat{\mathbf{E}}$. One fact is found that $\hat{\mathbf{E}}$ is a unitary matrix, and thus in OFDM frequency offset compensation can be performed in the frequency domain by means of matrix inversion or matched filtering of $\hat{\mathbf{E}}$. Similarly, the combined matrix $\bar{\mathbf{E}}_{\mathrm{UL}}$ in the uplink model of an OFDMA system is invertible as well. However, since $\bar{\mathbf{E}}_{\mathrm{UL}}^{H}\bar{\mathbf{E}}_{\mathrm{UL}}\neq\mathbf{I}$ except when the frequency offsets of different users are the same, matched filtering is not preferred for uplink frequency offset compensation. Frequency compensation can also be achieved by using ZF and LMMSE approaches. As shown, ZF approach is equivalent to matrix inversion in the case of square matrices.

By the analysis of the matrix $\hat{\mathbf{E}}$, we also proposed a method to reduce the computational complexity when performing matrix inversion. A new matrix $\mathbf{\Pi}_I$ can be created by replacing some off-diagonal entries (interference) of $\hat{\mathbf{E}}$ with zeros. A threshold μ has been introduced as a design parameter. To generate $\mathbf{\Pi}_I$ from $\hat{\mathbf{E}}$, the entries that are localized to the neighboring of the main diagonal with an index distance not more than μ and the entries that lies in the lower-left and upper-right triangle areas of size μ are taken, while other entries are replaced with zeros. This method is then taken for OFDMA systems. The idea was first proposed in [13]. The modification we have made, however, is based on the investigation in the last chapter, and has provided an improvement in performance, as shown in simulations. Nevertheless, a full matrix $\bar{\mathbf{E}}_{\mathrm{UL}}$ is preferred to be used when the values of the frequency offsets are distributed in a relatively large range.

The second part of this chapter has dealt with the frequency compensation in the cases of MC-CDMA and CDM-OFDMA. It has been performed jointly with cancellation of the interference introduced by the fading channels. We have focussed on the uncoded uplink performance over AWGN channels and multipath channels, with BPSK and QPSK transmission, in the absence and presence of carrier frequency offsets.

In general, fully-spread MC-CDMA and interleaved CDM-OFDMA provide a better performance if data are transmitted over multipath channels. Furthermore, the former slightly outperforms the latter in the case of BPSK. However, if the complexity of parameter estimations is under consideration, CDM-OFDMA instead of MC-CDMA is preferred to be applied in the uplink.

Chapter 6

Frequency Offset Estimation in Multiuser OFDM Systems

6.1 Chapter Overview

This chapter deals with the frequency offset estimation for multiuser OFDM (OFDMA) systems. To give a general impression, we start with the CFO estimation in OFDM, which is equivalent to the CFO estimation in the downlink of a multiuser OFDM system. Then, in Section 6.3 the consideration of CFO estimation for OFDMA uplink is given.

Much effort has been put into the development of efficient CFO estimation algorithms. These algorithms basically can be categorized into two main classes: *data-aided* (DA) and *non-data-aided* (NDA) algorithms. Data-aided algorithms take advantage of the knowledge of reference signals, e.g., in a form of training symbols and/or pilot tones; whereas a non-data-aided algorithm, or blind algorithm, only relies on the received information signals [55], i.e., no pilots are required in these algorithms. A common family of NDA algorithms for CFO estimation originates from the redundancy of *cyclic prefix* (CP) in OFDM, which provides sufficient information to perform synchronization, see, e.g., [80]. Besides this, the inherent orthogonality among OFDM subcarriers also offers the opportunity of frequency offset estimation [42], [78]. Approaches making use of null subcarrier have also been proposed, e.g., in [55].

Multiuser uplink synchronization is more difficult than synchronization in a broadcast or downlink scenario for a couple of reasons [79]. First, if the oscillator at BS receiver is adjusted to be synchronized with one user, other users that are misaligned with this user will not synchronize with the BS. To solve this problem, in [79] a synchronization policy is proposed, in which time offsets as well as frequency offsets are estimated in the uplink, but corrected in the downlink. In such a case a feedback control channel is necessary for all active users. This policy is also adopted in [51]. Second, estimation of frequency offsets is a more crucial task in a multiuser scenario. On one hand, the estimation accuracy will possibly be affected by the reduction of the number of subcarriers assigned to an individual user. For instance, the performance of the CFO estimator in [79], degrades for this reason. On the other hand, accurate estimation requires orthogonality among users, but the orthogonality will be destroyed if there exist multiple carrier frequency offsets. In [51], with aforementioned synchronization policy, the assumption of the control channel makes it possible that all the users, except for the new coming one, are synchronized with the BS. In consequence, CFO estimation in the uplink is simplified to be for a single user.

In this chapter, however, we adopt another synchronization policy in which no downlink control channel is needed. Instead, a quasi-synchronous mechanism is assumed, and the correction of frequency offsets are realized jointly by means of vector equalization, as studied in the previous chapter. Furthermore, the CFO of the new coming user will be estimated in the presence of CFOs of other users.

The chapter is organized as follows. Section 6.2 will focus on CFO estimation in OFDM. In Subsection 6.2.1, data-aided algorithms are developed for estimation of a fractional as well as an integer CFO. Data-aided *maximum likelihood* (ML) estimator is of the most importance, and will be considered in both time and frequency domain. Subsection 6.2 will deal with NDA algorithms, where a brief overview of CP-based as well as subspace-based blind algorithms will be given. In Section 6.3, CFO estimation in the uplink is considered. The synchronization policy will be explained in Subsection 6.3.1, and in Subsection 6.3.2 the direct application of the frequency domain ML estimator will be found. Unfortunately, CFO estimation suffers from MUI. To improve estimation accuracy, a modified ML frequency estimator will be proposed for the uplink receiver, based on the compensation algorithms developed in the last chapter.

6.2 Frequency Offset Estimation in OFDM

Frequency offset estimation is indispensably required in OFDM-based systems because of the severe performance degradation caused by frequency synchronization error. In an OFDM system, the frequency offset estimation is usually composed of two steps: *frequency acquisition* and *frequency tracking*. If the local oscillators at the transmitter and receiver are free-running, the absolute value of f_ϵ could possibly be greater than the subcarrier frequency spacing Δf. As defined in (4.1), we have

$$f_\epsilon = \delta\Delta f + \varepsilon\Delta f, \tag{6.1}$$

where δ is an integer and $\varepsilon \in (-0.5, +0.5)$. In general, in the *frequency acquisition* step, both δ and ε are considered, whereas in the *frequency tracking* step, f_ϵ will be a small fraction of Δf, and therefore $\delta = 0$.

6.2.1 Data-Aided Frequency Offset Estimation

In an OFDM system, frequency offset estimation can be performed either in the time domain or in the frequency domain. We begin with a maximum likelihood CFO estimator which is developed for the time-domain training sequences.

Maximum Likelihood (ML) Frequency Offset Estimation in Time Domain

In the time domain, CFO estimation for OFDM can also be realized by implementing the algorithm proposed for a single carrier system, since in a practical OFDM system, signals are carried at a single carrier frequency. Furthermore, a preamble is usually used in a burst transmission for synchronization and channel estimation. In the IEEE standard 802.11a for WLAN, for example, repeated short training sequences are used in the preamble for coarse frequency synchronization. In the following, we will propose a ML estimator based on such an assignment.

Let $\mathbf{b} = [b_0, ..., b_{L_b-1}]$ represent a short training sequence, where L_b is the length of $\mathbf{b}$. The selection of L_b satisfies the condition that N_f is a multiple of L_b, i.e., there is an integer L_s, $L_s = N_f/L_b$. Furthermore, let $\mathbf{y}_0, ..., \mathbf{y}_{L_s-1}$ denote the received training sequence. In a noise-free scenario, in the presence of CFO, the symbols in two successively received vectors have the relationship

$$y_{l_b,l_s+1} = e^{j\beta} y_{l_b,l_s} \quad 0 \leq l_b < L_b \text{ and } 0 \leq l_s < L_s, \tag{6.2}$$

where β is the phase difference between two vectors, $\beta = 2\pi f_\epsilon L_b T$, and $\beta \in (-\pi, \pi)$ is assumed. A frequency offset estimate is therefore given by

$$f_\epsilon = \frac{\beta}{2\pi L_b T}, \tag{6.3}$$

or equivalently

$$\delta + \epsilon = \frac{\beta L_s}{2\pi}. \tag{6.4}$$

In a multipath channel, on the other hand, assume that the *maximum delay spread* of the channel, L, is less than αL_b, $\alpha \in [1, L_s - 3]$. To avoid estimation inaccuracy caused by the channel dispersion, we only choose the received training sequence starting from $\alpha + 1$, i.e.,

$$\hat{f}_\epsilon = \frac{1}{2\pi L_b T} \tan^{-1} \left[\frac{\mathrm{Im}\left(\sum_{l_s=\alpha+1}^{L_s-2} \mathbf{y}_{l_s}^H \mathbf{y}_{l_s+1} \right)}{\mathrm{Re}\left(\sum_{l_s=\alpha+1}^{L_s-2} \mathbf{y}_{l_s}^H \mathbf{y}_{l_s+1} \right)} \right]. \tag{6.5}$$

Equation (6.4) implies that the maximum estimation range of this method is $\pm L_s/2$, and the estimation accuracy depends on the values of L_b and α. To enlarge the estimation range, we can shorten the period's duration L_b, at the cost of decreased estimation accuracy. Nonetheless, any offset beyond the predetermined estimation range ($\pm L_s/2$) can not be tracked. It should be pointed out that under the same assumption, the estimation accuracy can be improved by using other approaches [53], at the expense of computational complexity.

Maximum Likelihood (ML) Frequency Offset Estimation in Frequency Domain

ML Estimator for Fractional Frequency Offset As we know, the received frequency-domain symbol vector at time index i is given by

$$\mathbf{r}_i = \exp(j\theta i)\hat{\mathbf{E}}\mathbf{H}\mathbf{x}_i + \mathbf{n}_i, \tag{6.6}$$

where $\theta = 2\pi\epsilon(1 + \frac{N_g}{N_f})$. The received symbol on subcarrier m can be expressed as

$$\begin{aligned} r_{m,i} &= \exp(j\theta i) \sum_{m'=0}^{N_f-1} S_{m'-m} H_{m'} x_{m',i} + n_{m,i} \\ &= \exp(j\theta i) \sum_{m'=0}^{N_f-1} S_{m'-m} H_{m'} x_{m',i} (1 + v_{m,i}), \end{aligned} \tag{6.7}$$

where the variable $v_{m,i}$ is defined as

$$v_{m,i} = \frac{n_{m,i} \exp(-j\theta i)}{\sum_{m'=0}^{N_f-1} S_{m'-m} H_{m'} x_{m',i}}, \tag{6.8}$$

and has zero mean, i.e.,

$$E[v_{m,i}] = 0. \tag{6.9}$$

Assume ϵ to be a fraction of subcarrier frequency spacing Δf , and $|\theta| < \pi$. If

$$E\left[|v_{m,i}|^2\right] = \frac{\sigma_n^2}{E\left[\left|\sum_{m'=0}^{N_f-1} S_{m'-m} H_{m'} x_{m',i}\right|^2\right]} \ll 1, \tag{6.10}$$

i.e., SNR$\gg$ 1, we have then

$$1 + v_{m,i} \approx 1 + j\,\mathrm{Im}\{v_{m,i}\}, \tag{6.11}$$

since $\mathrm{Re}\{v_{m,i}\} \ll 1$, and

$$\arg(1 + v_{m,i}) \approx \mathrm{Im}\{v_{m,i}\}, \tag{6.12}$$

since $\tan(\sigma) \approx \sigma$ if $\sigma \ll 1$.

The successively received symbols on the same subcarrier, e.g. $r_{m,i}$ and $r_{m,i+1}$, differ only in phase, provided that the channel is time-invariant and noiseless, and the same symbol vector is transmitted. Assume that $\mathbf{a} = [a_1, ..., a_{N_f-1}]$ is a training symbol vector, and the components in $\mathbf{a}$ have zero mean and the correlation function $E[a_j a_k^*] = \sigma_a^2 \delta_{jk}$. Furthermore, we define a new variable $z_{m,i}$, $z_{m,i} = r_{m,i+1} r_{m,i}^*$. If $\mathbf{a}$ is transmitted twice at time indices i and $i+1$, according to (6.7) we have

$$\begin{aligned} z_{m,i} &= r_{m,i+1} r_{m,i}^* \\ &= \exp(j\theta) \left| \sum_{m'=0}^{N_f-1} S_{m'-m} H_{m'} a_{m'} \right|^2 + n_{m,i}^* r_{m,i+1} + r_{m,i}^* n_{m,i+1} - n_{m,i}^* n_{m,i+1}. \end{aligned} \tag{6.13}$$

Therefore, on each subcarrier, the estimation of ϵ turns to recover a normalized frequency of single complex sinusoid in uncorrelated Gaussian noise. Obviously, (6.13) is valid for all subcarriers in an OFDM system. The mean of $z_{m,i}$ is then derived by

$$\begin{aligned}
E[z_{m,i}] &= E[r_{m,i+1}r^*_{m,i}] \\
&= E\left[\exp(j\theta)\left|\sum_{m'=0}^{N_f-1} S_{m'-m}H_{m'}a_{m'}\right|^2\right] \\
&+ \underbrace{E[n^*_{m,i}r_{m,i+1}]}_{=0} + \underbrace{E[r^*_{m,i}n_{m,i+1}]}_{=0} - \underbrace{E[n^*_{m,i}n_{m,i+1}]}_{=0} \\
&= \exp(j\theta)\sigma_a^2 \sum_{m'=0}^{N_f-1} |S_{m'-m}|^2 \, E\left[|H_{m'}|^2\right] \\
&= \exp(j\theta)|H|^2\sigma_a^2,
\end{aligned} \tag{6.14}$$

where $E[|H_m|^2] = |H|^2$ is assumed and $\sum_{m'=0}^{N_f-1} |S_{m'-m}|^2 = 1$. As a consequence, an estimate of θ is obtained by calculating the argument of $E[z_{m,i}]$

$$\hat{\theta} = \arg(E[z_{m,i}]). \tag{6.15}$$

On the other hand, if the condition in (6.10) is fulfilled, (6.13) can be rewritten as

$$\begin{aligned}
z_{m,i} &= r_{m,i+1}r^*_{m,i} \\
&= \exp(j\theta)\left|\sum_{m'=0}^{N_f-1} S_{m'-m}H_{m'}a_{m'}\right|^2 (1+v_{m,i+1})(1+v_{m,i})^*.
\end{aligned} \tag{6.16}$$

According to (6.7), (6.11) and (6.12), the argument of $z_{m,i}$ in (6.16) can be expressed as

$$\Delta_m = \arg(z_{m,i}) = \theta + \mathrm{Im}\{v_{m,i+1}\} - \mathrm{Im}\{v_{m,i}\}. \tag{6.17}$$

The real-valued noise component w_m, $w_m = \mathrm{Im}\{v_{m,i+1}\} - \mathrm{Im}\{v_{m,i}\}$, is Gaussian of zero mean,

$$E[w_m] = 0. \tag{6.18}$$

The correlation function is given by

$$E[w_{m+l}w^*_m] = \begin{cases} \frac{\sigma_n^2}{\sigma_a^2|H|^2}, & l = 0 \\ 0, & l \neq 0 \end{cases} \tag{6.19}$$

because

$$\begin{aligned}
E[w_m w^*_m] &= E[(\mathrm{Im}\{v_{m,i+1}\} - \mathrm{Im}\{v_{m,i}\})^2] = 2E[(\mathrm{Im}\{v_{m,i}\})^2] \\
&= \frac{2\times\sigma_n^2/2}{\sigma_a^2 \sum_{m'=0}^{N_f-1}\left|S_{m'-N_f+1}\right|^2 E\left[|H_{m'}|^2\right]} = \frac{\sigma_n^2}{\sigma_a^2\,|H|^2}.
\end{aligned} \tag{6.20}$$

Accordingly, the covariance matrix $\mathbf{\Phi_{ww}}$ takes on the diagonal form

$$\mathbf{\Phi_{ww}} = \begin{pmatrix} \frac{\sigma_n^2}{\sigma_a^2|H|^2} & 0 & \cdots & 0 \\ 0 & \frac{\sigma_n^2}{\sigma_a^2|H|^2} & 0 & \vdots \\ \vdots & 0 & \ddots & 0 \\ 0 & \cdots & 0 & \frac{\sigma_n^2}{\sigma_a^2|H|^2} \end{pmatrix} = \frac{\sigma_n^2}{\sigma_a^2\,|H|^2}\mathbf{I}_{N_f\times N_f}. \tag{6.21}$$

The problem turns to estimate θ on the observations Δ_m, $m = 0, 1, ..., N_f - 1$. The maximum likelihood estimate (MLE) of θ is found by minimizing the log-likelihood function

$$\Lambda = (\boldsymbol{\Delta} - \theta\mathbf{1})^T \boldsymbol{\Phi}_{\mathbf{ww}}^{-1} (\boldsymbol{\Delta} - \theta\mathbf{1}), \tag{6.22}$$

where $\boldsymbol{\Delta} = [\Delta_0, \Delta_1, \ldots, \Delta_{N_f-1}]^T$, and $\mathbf{1} = [1, 1, \ldots, 1]^T$. The solution of this problem is well known and is

$$\hat{\theta} = \frac{\mathbf{1}^T \boldsymbol{\Phi}_{\mathbf{ww}}^{-1} \boldsymbol{\Delta}}{\mathbf{1}^T \boldsymbol{\Phi}_{\mathbf{ww}}^{-1} \mathbf{1}}. \tag{6.23}$$

Frequency offset estimator in (6.23) is a *minimum variance unbiased* (MVU) estimator of θ as well. From (6.21) and (6.23) it yields

$$\hat{\theta} = \frac{1}{N_f} \sum_{m=0}^{N_f-1} \arg\{z_{m,i}\} = \frac{1}{N_f} \sum_{m=0}^{N_f-1} \arg\left\{r_{m,i+1} r_{m,i}^*\right\}. \tag{6.24}$$

Note that this estimator is conditioned on the assumption of a high average SNR, and the argument of $z_{m,i}$ being in the range of $(-\pi, \pi)$. It follows from (6.24) that

$$2\pi(1 + \frac{N_g}{N_f})\hat{\epsilon} = \frac{1}{N_f} \sum_{m=0}^{N_f-1} \arg\left\{r_{m,i+1} r_{m,i}^*\right\}. \tag{6.25}$$

An alternative of (6.25) is then

$$2\pi(1 + \frac{N_g}{N_f})\hat{\epsilon} = \arg\left\{\frac{1}{N_f} \sum_{k=0}^{N_f-1} r_{k,i+1} r_{k,i}^*\right\} = \arg\left\{\mathbf{r}_{i+1}^T \mathbf{r}_i^*\right\} = \arg\left\{\mathbf{r}_i^H \mathbf{r}_{i+1}\right\}. \tag{6.26}$$

Consequently, the ML estimator of ϵ is given by

$$\hat{\epsilon} = \frac{1}{2\pi} \frac{N_f}{N_g + N_f} \tan^{-1} \frac{\mathrm{Im}(\mathbf{r}_{i+1}^T \mathbf{r}_i^*)}{\mathrm{Re}(\mathbf{r}_{i+1}^T \mathbf{r}_i^*)} = \frac{1}{2\pi} \frac{N_f}{N_g + N_f} \tan^{-1} \frac{\mathrm{Im}(\mathbf{r}_i^H \mathbf{r}_{i+1})}{\mathrm{Re}(\mathbf{r}_i^H \mathbf{r}_{i+1})}. \tag{6.27}$$

This is similar to the algorithm indicated in [50], except that the estimation range of $\hat{\epsilon}$ is scaled by $\frac{N_f}{N_g+N_f}$, apparently depending on the length of guard interval. The maximum estimation range $(-0.5, 0.5)$ is achieved when $N_g = 0$.

Statistical Properties Substituting (6.17) into (6.24), and calculating the expectation of $\hat{\theta}$, we obtain

$$E\left[\hat{\theta}\right] = \frac{1}{N_f} \sum_{m=0}^{N_f-1} E\left[\Delta_m\right] = \theta, \tag{6.28}$$

and equivalently $E\left[\hat{\epsilon}\right] = \epsilon$, i.e.,

$$E\left[\hat{\epsilon} - \epsilon | \epsilon\right] = 0. \tag{6.29}$$

Therefore, for small errors, the estimate is conditionally unbiased. This is in accord with what we mentioned above that the ML estimator in (6.24) is also a MVU estimator of θ.

The variance of the estimate $\hat{\theta}$ and $\hat{\epsilon}$ are given by

$$\mathrm{var}\left[\hat{\theta}|\theta\right] = \frac{1}{\mathbf{1}^T \mathbf{\Phi}_{\mathbf{ww}}^{-1} \mathbf{1}} = \frac{\sigma_n^2}{N_f \sigma_a^2 |H|^2} = \frac{1}{N_f \gamma_a}, \tag{6.30}$$

and

$$\mathrm{var}\left[\hat{\epsilon}|\epsilon\right] = \frac{1}{(2\pi)^2} \frac{N_f^2}{(N_g + N_f)^2} \frac{1}{N_f \gamma_a}, \tag{6.31}$$

respectively. Note that $\gamma_a = \sigma_a^2 |H|^2 / \sigma_n^2$ is the average SNR, and on the RHS of (6.30), N_f in the last product term stands for the total number of subcarriers used for estimation. This implies that the performance of the estimator depends on the number of training symbols and γ_a. What's more, for a given OFDM system (where N_f and N_g are given), under the assumption that $E[|H_m|^2] = |H|^2$, the minimum variance in (6.31) is also the Cramer-Rao lower bound (CRLB) of the estimator. Since

$$\frac{\sigma_a^2}{\sigma_n^2} = \frac{E_b}{N_0} \log_2(M)$$

for the PSK-mapped symbols, referring to [33], the CRLB is calculated by

$$\mathrm{CRLB} = \frac{1}{(2\pi)^2} \frac{N_f^2}{(N_g + N_f)^2} \frac{N_0 / E_b}{N_f |H|^2 \log_2(M)}, \tag{6.32}$$

where M is the cardinality of the alphabet. In Fig. 6.1, Monte Carlo simulations are implemented to evaluate the performance of the estimator in several OFDM systems. 1000 simulations are run to get an average MSE. The training symbols are QPSK-mapped. The 8-path channel model introduced in Chapter 2 is used. For the sake of comparison, the total energy of the multipath channel is normalized such that $E[|H_m|^2] = |H|^2 = 1$. In each simulation, a new Rayleigh realization of the channel and a new frequency offset are assumed. The latter is uniformly selected in the range of $(-0.3, 0.3)$. It is shown that wether in AWGN channels or in multipath channels, the estimator is efficient in that it attains the CRLB. This data-aided ML frequency offset estimator is apparently appropriate for fine frequency offset estimation.

Frequency Tracking by Using Pilot Subcarriers In an OFDM system, during data transmission, pilot subcarriers can be used for frequency tracking. Consider a situation where only one pilot subcarrier is assigned. For a given subchannel m and a given pilot symbol X_P, we rewrite (6.7) and (6.16) as

$$\begin{aligned} r_{m,i+1} &= \exp(j\theta i) S_0 H_m X_P + \underbrace{\exp(j\theta i) \sum_{m'=0, m' \neq m}^{N_f - 1} S_{m'-m} H_{m'} x_{m',i}}_{\mathrm{ICI}} + n_{m,i} \\ &= \exp(j\theta i) S_0 H_m X_P + I_{ICI}^{(m)} + n_{m,i} \end{aligned} \tag{6.33}$$

and

$$z_{m,i} = r_{m,i+1} r_{m,i}^* = \exp(j\theta) \left|S_0\right|^2 \left|H_m\right|^2 \left|X_P\right|^2 (1 + v_{m,i+1})(1 + v_{m,i})^*. \tag{6.34}$$

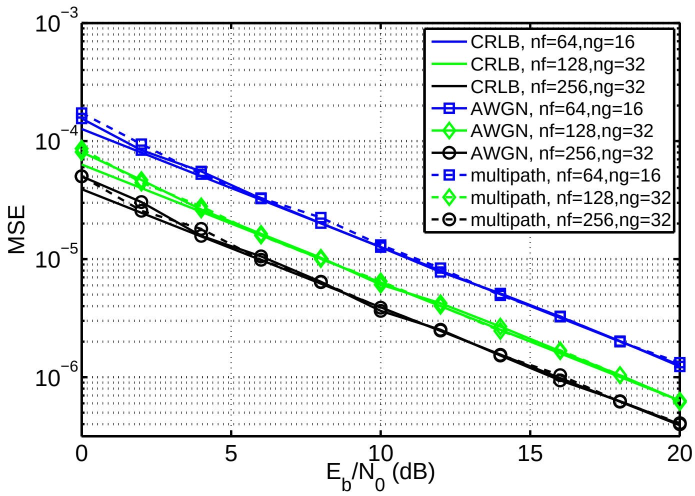

Figure 6.1: The performance of frequency-domain ML estimator.

Note that unlike in (6.8), $v_{m,i}$ is defined as

$$v_{m,i} = \frac{I_{ICI}^{(m)} \exp(-j\theta i)}{S_0 H_m X_P} + \frac{n_{m,i} \exp(-j\theta i)}{S_0 H_m X_P}, \tag{6.35}$$

If ICI is treated as the complex Gaussian noise, since $E[I_{ICI}^{(m)}] = 0$, from (6.35) it follows that

$$\operatorname{var}(v_{m,i}) = \frac{E\left[\left|I_{ICI}^{(m)}\right|^2\right] + \sigma_n^2}{\left|S_0\right|^2 E\left[\left|H_m\right|^2\right] \left|X_P\right|^2}, \tag{6.36}$$

where $E\left[\left|I_{ICI}^{(m)}\right|^2\right]$ is defined in (4.36). Obviously, the variance of $v_{m,i}$ depends on the SINR. This restricts the estimation range of CFO to be small in that a large CFO will give rise to large ICI, and therefore a lower SIR, which will badly affect the estimation accuracy. The frequency offset estimation is based on the observation of N_P concessively received pilot symbols $r_{P,0}, ..., r_{P,N_P-1}$. Without loss of generality, we ignore the time index i. Similar to (6.27), a frequency offset estimator can be given by

$$\hat{\epsilon} = \frac{1}{2\pi} \frac{N_f}{N_g + N_f} \tan^{-1} \frac{\operatorname{Im}\left(\mathbf{r}_{P,2}^T \mathbf{r}_{P,1}^*\right)}{\operatorname{Re}\left(\mathbf{r}_{P,2}^T \mathbf{r}_{P,1}^*\right)}, \tag{6.37}$$

where $\mathbf{r}_{P,1}^T = \{r_{P,l}\}_{l=0}^{N_P-2}$ and $\mathbf{r}_{P,2}^T = \{r_{P,l}\}_{l=1}^{N_P-1}$. The estimate $\hat{\epsilon}$ is the sample mean over $N_P - 1$ measurements $\frac{1}{2\pi} \frac{N_f}{N_g+N_f} \arg(z_{m,l})$, $l = 0, ..., N_P - 2$. This estimator is sub-optimal, however, as it neglects the noise in (6.17), which is correlated and whose covariance matrix takes on the tridiagonal form

$$\mathbf{\Phi}_{\mathbf{ww}} = \frac{E\left[\left|I_{ICI}^{(m)}\right|^2\right] + \sigma_n^2}{2\left|S_0\right|^2 E[\left|H_m\right|^2] \left|X_P\right|^2} \begin{pmatrix} 2 & -1 & 0 & 0 & \cdots & 0 \\ -1 & 2 & -1 & 0 & \cdots & 0 \\ \cdots & \cdots & \cdots & \cdots & \cdots & \cdots \\ 0 & 0 & \cdots & \cdots & -1 & 2 \end{pmatrix}_{(N_P-1)\times(N_P-1)}. \tag{6.38}$$

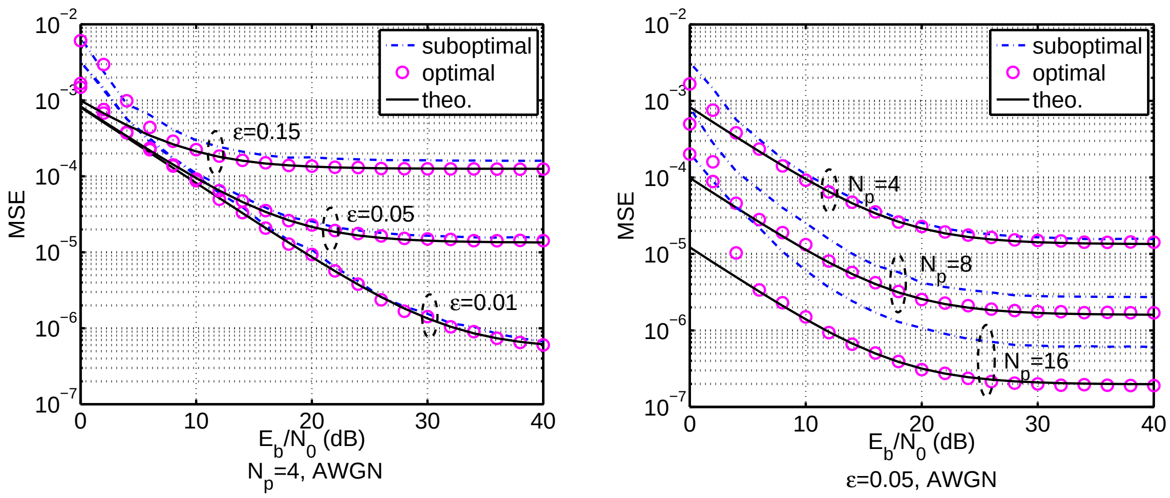

Figure 6.2: Performance of the estimator for frequency tracking in AWGN channel with $N_f = 64$ and $N_g = 16$. Comparison of different frequency offsets (left) and comparison of different number of pilot symbols (right).

Referring to [32], the variance of the estimate $\hat{\theta}$ is given by

$$\mathrm{var}(\hat{\theta}) = \frac{1}{\mathbf{1}^T \mathbf{\Phi}_{\mathbf{ww}}^{-1} \mathbf{1}} = \frac{6}{N_P(N_P^2 - 1)} \frac{E\left[\left|I_{ICI}^{(m)}\right|^2\right] + \sigma_n^2}{|S_0|^2 \, E\left[|H_m|^2\right] |X_P|^2}. \tag{6.39}$$

The optimal ML estimator of θ is

$$\hat{\theta} = \frac{\mathbf{1}^T \mathbf{\Phi}_{\mathbf{ww}}^{-1} \mathbf{\Delta}}{\mathbf{1}^T \mathbf{\Phi}_{\mathbf{ww}}^{-1} \mathbf{1}} = \sum_{l=0}^{N_P-2} w_l \arg(r_{P,l+1} r_{P,l}^*) \tag{6.40}$$

with

$$w_l = \frac{\frac{3}{2} N_P}{N_A^2 - 1} \left\{ 1 - \left[\frac{l - \left(\frac{N_P}{2} - 1\right)}{\frac{N_P}{2}} \right]^2 \right\}. \tag{6.41}$$

Accordingly, the optimal ML estimator of ϵ is

$$\hat{\epsilon} = \frac{1}{2\pi} \frac{N_f}{N_g + N_f} \sum_{l=0}^{N_P-2} w_l \arg(r_{P,l+1} r_{P,l}^*). \tag{6.42}$$

Furthermore, if $|X_P|^2 = \sigma_x^2$, and $E[|H_m|^2] = |H|^2$, from (6.39) we then have

$$\begin{aligned} \mathrm{var}(\hat{\epsilon}) &= \frac{1}{(2\pi)^2} \frac{N_f^2}{(N_g + N_f)^2} \frac{6}{N_P(N_P^2 - 1)} \frac{\sum_{m'=0, m' \neq m}^{N_f-1} |S_{m'-m}|^2 + 1/\gamma}{|S_0|^2} \\ &= \frac{1}{(2\pi)^2} \frac{N_f^2}{(N_g + N_f)^2} \frac{6}{N_P(N_P^2 - 1)} (SINR)^{-1}, \end{aligned} \tag{6.43}$$

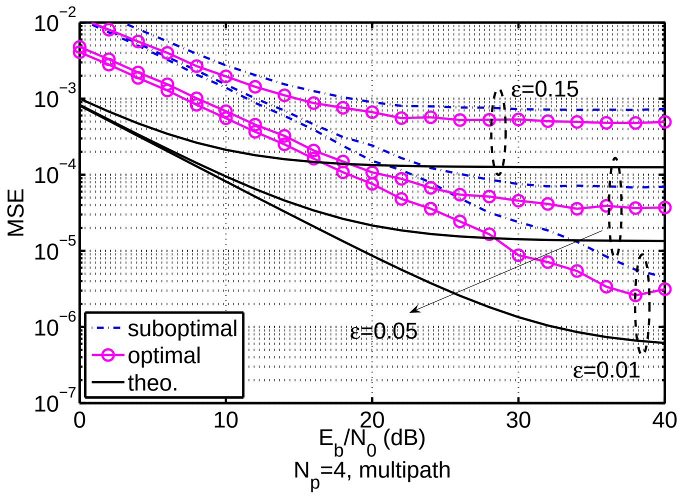

Figure 6.3: Frequency tracking in AWGN channel with $N_f = 64$ and $N_g = 16$.

where $\gamma = |H|^2 \sigma_x^2 / \sigma_n^2$, and $SINR$ is defined in (4.39). It follows from (6.43) that for a given OFDM system, the variance of the estimate is inversely proportional to the SINR. As SINR decreases with the increase of ϵ, the frequency estimators in (6.37) and (6.42) in consequence can have good performance only when the value of ϵ is small. Moreover, the number of the observations, N_P, affects the performance as well. It is shown in the right of Fig. 6.2 that the more pilot symbols are used, the better the performance.

The efficiency of the estimators can also be compared by simulation results. The optimal estimator in (6.42) is efficient, for its simulation results coincide with the theoretical curves, whereas the estimator in (6.37) is suboptimal since its curves diverge away from theoretical curves as N_P increases. However, with small N_P both estimators have the similar performance.

The simulations for multipath channels are demonstrated in Fig. 6.3. Simulation is run 100000 times to obtain a smooth curve. The MSE performance is apparently worse than in an AWGN channel. This is because the estimator is severely *channel-dependent* with respect to the assigned pilot subcarrier. Hence, this estimator is only practicable for tracking very small frequency offset.

Estimation of an Integer Frequency Offset An integer CFO, δ, can also be estimated with frequency domain training symbols, provided that they are well assigned. Before δ is estimated, the fractional CFO should be compensated. ICI will disappear after this manipulation, but subcarrier shift caused by an integer CFO still remains. The idea to estimate δ is based on the condition that the training symbols are selected in a random way, and have the correlation function $E[a_j a_k^*] = \sigma_a^2 \delta_{jk}$. To achieve this goal, we can make use of PN sequence in both the real and imaginary part of the training symbols, the resulting complex-valued training sequence $\mathbf{a}$, $\mathbf{a} = [a_0, a_1, ..., a_{N_f-1}]$, has an autocorrelation function

$$E[\mathbf{a}_d^H \mathbf{a}] = \begin{cases} 2N_f & \text{for} \quad d = 0 \\ N_f - 1 & \text{for} \quad d = -1, 1 \\ 2 & \text{otherwise} \end{cases}, \tag{6.44}$$

where $\mathbf{a}_d$ is the cyclically shifted version of $\mathbf{a}$. In an AWGN channel, the number of shifted subcarriers can be calculated by finding $\hat{d}$ which maximizes

$$I(d) = \frac{\left|\mathbf{a}_d^H \mathbf{r}_i\right|^2}{\left|\mathbf{r}_i^H \mathbf{r}_i\right|^2}. \tag{6.45}$$

The estimation range of this method is $N_f - 1$ if necessary. This method works well in AWGN channels. However, in multipath channels its performance is poor, as the frequency selective fading will change the statistical property of $\mathbf{r}_i$ and give rise to a wrong solution. An appropriate design for training sequence as well as cost metric is necessary, which can be found, e.g., in [61].

6.2.2 Non-Data-Aided (Blind) Frequency Offset Estimation

In OFDM, NDA or blind frequency offset estimation algorithms are partitioned into three classes: CP-based algorithms, null-subcarrier-based algorithms, and resolution subspace methods, such as MUSIC and ESPRIT.

CP-Based Algorithms

The redundant information contained within the cyclic prefix enables frequency offset estimation without pilots [80], [34]. Assuming that data transmission takes place over an AWGN channel, and an OFDM symbol vector, $\mathbf{y} = [y_0, y_1, \ldots, y_{N_s-1}]$, $N_s = N_f + N_g$, is observed at the receiver side before FFT, the autocorrelation function of the observation vector can be expressed as

$$E[y_k^* y_{k+n}] = \begin{cases} \sigma_s^2 + \sigma_n^2 & n = 0, \\ \sigma_s^2 \exp(j2\pi\epsilon) & n = N_f, \\ 0 & \text{otherwise.} \end{cases} \tag{6.46}$$

Only the repeated symbols in CP satisfy the second term on the RHS of (6.46). Similar to the data-aided ML frequency offset estimation in Section 6.2.1, we obtain a sample mean estimate of ϵ

$$\hat{\epsilon} = \frac{1}{2\pi} \tan^{-1} \frac{\operatorname{Im}\left(\sum_{k=0}^{N_g-1} y_k^* y_{k+N_f}\right)}{\operatorname{Re}\left(\sum_{k=0}^{N_g-1} y_k^* y_{k+N_f}\right)}. \tag{6.47}$$

Unfortunately, several drawbacks cannot be avoided by CP-based algorithms. First, algorithms based on CP apparently suffer from time dispersion of the channel. The symbols distorted by interference from the previous OFDM-block will reduce the estimation accuracy and should not be used for estimation. This requires that the length of the CP must be greater than the maximum delay spread, i.e., $N_g > L$. On the other hand, the accuracy of the frequency estimator depends on the length of CP and SNR, even when the channel is time non-dispersive. But the insertion of CP aims to cope with the multipath propagation, and it reduces the bandwidth efficiency. It is not necessary to insert a CP in a flat fading channel, whereas in a multipath fading channel, the extra numbers of CP for frequency offset estimation will reduce the bandwidth efficiency further. In fact, the CP used here is like the pilot symbols.

Subspace-Based Algorithms

Subspace-based algorithms take advantage of the inherent othorgonality among OFDM subcarriers [42], [78]. As $\mathbf{F}$ is a unitary matrix, its columns form an orthonormal basis of $C^{n\times n}$. Let $\{\mathbf{u}_m\}, m = 1, ..., N_f$, represent the column vectors of $\mathbf{F}$. The inner product of any two columns of $\mathbf{F}$ is zero, i.e.,

$$\langle \mathbf{u}_m, \mathbf{u}_n \rangle = 0 \text{ for } m \neq n. \tag{6.48}$$

This property contributes to the subspace-based algorithms for frequency offset estimation.

The prerequisite to applying these algorithms is that the number of the actually used subcarriers must be less than the total number of subcarriers. In other words, at least one *virtual* subcarrier exists during the transmission. This requirement basically can be met in practice, e.g., in WLAN only 52 of 64 subcarriers are used for data transmission. For this reason, subspace-based algorithms also can be categorized into null-subcarrier-based algorithms.

From the previous chapter, we know that a received symbol vector can be expressed in form of vector transmission as

$$\mathbf{y}_i = \exp\left(j2\pi i\epsilon\left(1+\frac{N_g}{N_f}\right)\right)\dot{\mathbf{E}}\mathbf{F}_Q^H\mathbf{H}\mathbf{x}_i + \mathbf{n}_i, \quad i = 0, ..., \infty. \tag{6.49}$$

where the CP is discarded, $\dot{\mathbf{E}} = \mathbf{G}_{pp}\mathbf{E}\mathbf{G}_{ap}$, and $\mathbf{F}_Q^H$ stands for a submatrix of IDFT matrix $\mathbf{F}^H$, in which only the columns associated with the used subcarriers are taken, and other columns are set to zero, implying that their corresponding subcarriers carrying no signals. According to the property of the normalized DFT matrix, if $\mathbf{u}_{\tilde{q}}$ is a column vector of $\mathbf{F}^H$ but not in $\mathbf{F}_Q^H$, then in the absence of frequency offset, i.e., $\epsilon = 0$,

$$\mathbf{u}_{\tilde{q}}^H\mathbf{F}_Q^H\mathbf{H}\mathbf{x}_i = 0. \tag{6.50}$$

In the presence of a frequency offset, if ignoring the noise, (6.49) can be rewritten as

$$\begin{aligned}\mathbf{y}_i &= \operatorname{diag}\left\{\left[1,\ldots,\exp(j2\pi\epsilon\frac{N_f-1}{N_f})\right]\right\}\mathbf{F}_Q^H\underbrace{\mathbf{H}\mathbf{x}_i\exp\left(j2\pi i\epsilon\left(1+\frac{2N_g}{N_f}\right)\right)}_{\tilde{\mathbf{x}}_i}\\ &= \operatorname{diag}\left\{\left[1,\ldots,\exp(\frac{j2\pi\epsilon}{N_f}(N_f-1))\right]\right\}\mathbf{F}_Q^H\tilde{\mathbf{x}}_i.\end{aligned} \tag{6.51}$$

A cost function then can be formulated as

$$\begin{aligned}J(z) &= \frac{1}{L_{\tilde{q}}}\sum_{i=0}^{L_{\tilde{q}}-1}\sum_{\tilde{q}}\left|\mathbf{u}_{\tilde{q}}^H\mathbf{Z}^{-1}\mathbf{y}_i\right|^2 \\ &= \sum_{\tilde{q}}\mathbf{u}_{\tilde{q}}^H\mathbf{Z}^{-1}\left(\frac{1}{L_{\tilde{q}}}\sum_{i=0}^{L_{\tilde{q}}-1}\mathbf{y}_i\mathbf{y}_i^H\right)\left(\mathbf{Z}^{-1}\right)^H\mathbf{u}_{\tilde{q}} \\ &= \sum_{\tilde{q}}\mathbf{u}_{\tilde{q}}^H\mathbf{Z}^{-1}\mathbf{\Phi}_{\mathbf{YY}}\left(\mathbf{Z}^{-1}\right)^H\mathbf{u}_{\tilde{q}},\end{aligned} \tag{6.52}$$

where $\mathbf{Z} \stackrel{\text{def}}{=} \text{diag}\left\{\left[1, z, z^2, \ldots, z^{(N_f-1)}\right]\right\}$ and

$$\mathbf{\Phi_{YY}} = \frac{1}{L_{\tilde{q}}}\mathbf{Y}_i\mathbf{Y}_i^H = \frac{1}{L_{\tilde{q}}}\sum_{i=0}^{L_{\tilde{q}}-1}\mathbf{y}_i\mathbf{y}_i^H. \tag{6.53}$$

Note that $L_{\tilde{q}}$ is not more than the total number of virtual subcarriers. Clearly, from (6.50), $J(z)$ is zero when $z = \exp(j2\pi\epsilon/N_f)$. In the presence of noise, the frequency offset is estimated as the minima of $J(z)$ [42]. This is so-called MUSIC-like (*MUltiple SIgnal Classification*) algorithm for frequency offset estimation. MUSIC method is one of the parametric methods for linear spectra. Another subspace-based algorithm used for OFDM, ESPRIT (*Estimation of Signal Parameters by Rotational Invariance Techniques*), is proposed in [78]. More knowledge of spectral analysis can be found, e.g., in [71].

Consistency of the Frequency Offset Estimation One drawback of subspace-based estimators is their *dependence on the channel.* They are able to work well in a flat fading channel with a reasonable SNR. In a frequency selective fading channel, however, subspace-based estimators are possibly channel-dependent, and suffer from the subcarriers with the transfer function of near-zero value, which may cause lack of identifiability of the CFO. The estimators therefore turn to be inconsistent, and no matter how many data blocks are used, the resulting CFO estimator is not guaranteed to converge to the true ϵ [45]. In other words, the channel dependence of the estimator lead to the ambiguous estimates. In an attempt to solve this ambiguity, [45] discards the use of consecutive null subcarriers and distributes the null subcarriers to nonconsecutive subcarriers. Unfortunately, this method is limited by two facts. One is that, in some scenario, the pattern of channel nulls resulted from the frequency selective fading is similar to the inserted null subcarriers, thus no consistent estimate can be obtained. It is also impractical to apply this null subcarrier distribution scheme, for the guard band is usually adopted for the purpose of avoiding the *adjacent channel interference* (ACI), as shown in HIPERLAN/2 and the IEEE standard 802.11a [37].

The inconsistency can occur in other estimators, too. For instance, performance of ML estimator based on pilot subcarriers is also *channel-dependent.* If the pilot subcarriers have small channel gain as compared to other subcarriers, the total amount of the ICI will be strong and therefore improves the inconsistency of the estimation. Hence, to avoid an inconsistent estimate, estimation algorithms should be chosen carefully.

6.3 Frequency Offset Estimation for the Uplink of OFDMA Systems

6.3.1 Synchronization Policy

Frequency synchronization is a tough task in the uplink of an OFDMA system. As mentioned earlier, frequency offset estimation at the BS receiver generally is a multiple parameter estimation problem associated with multiple users. Nevertheless, synchronization policy for a given

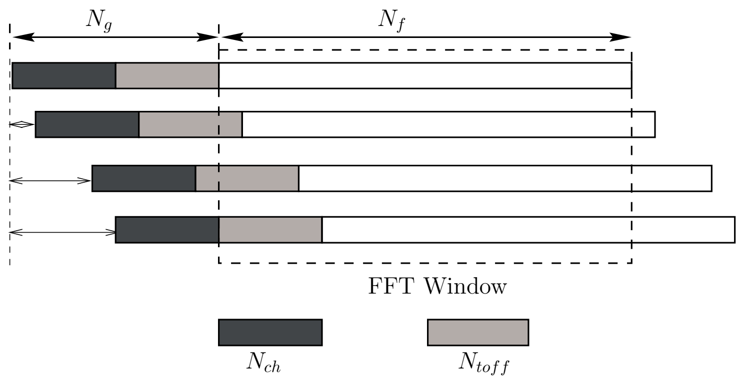

Figure 6.4: Quasi-synchronous mechanism.

system plays an important role as well. In the following, we first have a brief look at the synchronization mechanisms taken for OFDMA systems, and then discuss the possible synchronization policies.

Asynchronous Mechanism

In asynchronous systems, the time offset may be not small with respect to the duration of an OFDM symbol, and thus it is not advisable to incorporate the unknown time offset as part of the channel, because an excessively long cyclic prefix has to be introduced. Hence, in asynchronous systems, the time offsets should be estimated separately, and the length of cyclic prefix is kept as short as possible. Similarly, frequency offsets may be larger than half of subcarrier frequency spacing Δf. This obviously raises the difficulties in synchronization.

Quasi-synchronous Mechanism

Quasi-synchronism is usually assumed for the uplink of a multiple access system. In quasi-synchronous (QS) systems, the users try to synchronize with the BS before a connection. Usually a common time reference is available for both MS and BS. For instance, the BS periodically sends synchronization information to the MS. In such a case, the residual time offset is usually small, and it may be incorporated as part of the known channel response [5]. This demands the guard interval to be longer than necessary (the maximum delay spread) and thus entails a small efficiency loss, but it simplifies the synchronization task. And, a coarse CFO estimation can be accomplished at the MS, such that only residual frequency offsets are required to be dealt with at the BS. Therefore, in the rest of this work, we assume that a quasi-synchronous mechanism is in use. Specially, as shown in Fig. 6.4, we assume that the total duration of the guard interval N_g can be partitioned into two parts: N_{cp}, being not less than the maximum delay spread of the channel, and N_{toff}, being not less than the maximum time offset.

Another problem that has to be considered is the frequency correction policy. It is well known that the correction of one user's frequency (and/or timing) can not be done by adjusting oscillator and clock at the BS, since this operation will misalign the other users. Therefore, a widely accepted synchronization policy is that *estimation* is performed at the BS, whereas *adjustment* of the synchronization parameters is made at the user's side. A control channel is thus required to feedback the instructions, which leads to extra overhead. Based on this policy, it is reasonable to make a further assumption for a scenario where all the active users but one are already synchronized. This reduces the multiple parameter (frequency offset) estimation to a simple case: only one frequency needs to be estimated. Such an assumption is used in [51].

To decrease the overhead paid for the feedback control channel, a joint compensation scheme at the BS can be taken for QS systems. In such a case, the interference caused by synchronization mismatch as well as channel impairment are coped with jointly by means of multiuser detection, under the condition that all parameters are estimated and known. As a main synchronization task, frequency offsets of all active users have to be estimated. In the rest of this chapter, we will adopt this correction policy, base on a reasonable assumption that only the CFO of the new coming user has to be estimated, while CFOs of all the other users are known.

6.3.2 Frequency Offset Estimation in the Uplink

Consider a quasi-synchronous OFDMA system where the coarse frequency synchronization and oscillator adjustment have been made at the users' receiver. In the uplink, the residual frequency offsets would exist due to the oscillator frequency mismatch (estimation error). It is reasonable to assume that these frequency offsets are fractions of subcarrier frequency spacing, i.e., in the range of $(-0.5, 0.5)$ or smaller. Therefore, users can be roughly separated after FFT by different subchannels assigned to them. Subcarrier misalignment would not happen since there exist no integer frequency offsets. Furthermore, we assume that users access the BS sequentially such that only one CFO should be estimated at a time. Because there is no feedback control channel, the problem is restricted to estimate the CFO of the new coming user, in the presence of SI and MUI.

To minimize the influence of SI and the imperfect propagation channel, we use the data-aided ML frequency estimator introduced in Section 6.2.1. To be specific, a repeated frequency-domain training sequence is arranged at the beginning of the transmit blocks of the new coming user, while the other users transmit the data at the same time. At the BS receiver after FFT, the two received training sequence can be extracted from the subchannels belonging to the new coming user. Like in Section 6.2.1, the channel is assumed to be constant for the time being. Let k, $\mathbf{r}_i$ and $\mathbf{r}_{i+1}$ represent the user number of the incoming user, and the received symbol vector at time indices i and $i+1$, respectively. The time index i is set for all users according to the initial access of the first user. This seems not to be true for the users which have accessed the BS subsequently, since their access time should be counted on their own. Nonetheless, a common time reference is welcome, for the time ambiguity in a mathematical expression can then be avoided. On the other hand, from (4.45) we know that the instantaneous phase only depends on the index i and CFO, which can be unwrapped by differential multiplication. As a consequence, we use i as a common time reference.

As the first step, we consider the direct implementation of ML estimator at the BS. Let $\mathbf{a}=[a_0, ..., a_{N_A-1}]$ represent the training sequence used for FO estimation of user k, where N_A is the length of $\mathbf{a}$, and also the number of subcarriers belonging to a user. Training symbols in $\mathbf{a}$ satisfy $E[a_j a_l^*] = \sigma_a^2 \delta_{jl}$. On the receiving side, a received training symbol on subcarrier m,

$m \in \mathcal{G}_k$, is then expressed as

$$
\begin{aligned}
r_{m,i}^{(k)} &= \exp(j\theta_k i) S_0^{(k)} H_m^{(k)} a_{N_m} + \sum_{m' \in \mathcal{G}_k, m' \neq m} \exp(j\theta_k i) S_{m'-m}^{(k)} H_{m'}^{(k)} a_{N_{m'}} \\
&+ \underbrace{\sum_{k' \neq k} \sum_{m' \in \mathcal{G}_{k'}} \exp(j\theta_{k'} i) S_{m'-m}^{(k')} H_{m'}^{(k')} x_{m',i}^{(k')}}_{\text{MUI}} + n_{m,i}.
\end{aligned} \tag{6.54}
$$

The first two terms on the RHS of (6.54) will contribute to frequency offset estimation. Similar to (6.27), the estimate of ϵ_k is given by

$$
\hat{\epsilon}_k = \frac{1}{2\pi} \frac{N_f}{N_g + N_f} \tan^{-1} \frac{\mathrm{Im}(\mathbf{r}_i^{(k)H} \mathbf{r}_{i+1}^{(k)})}{\mathrm{Re}(\mathbf{r}_i^{(k)H} \mathbf{r}_{i+1}^{(k)})}. \tag{6.55}
$$

Statistical Properties of the Estimate

Recalling the ML estimator in (6.27), it is not difficult to come to the conclusion that $E[\hat{\epsilon}_k] = \epsilon_k$, namely the estimator is unbiased. The variance of the estimator is then given by

$$
\mathrm{var}(\hat{\epsilon}_k) = \frac{1}{(2\pi)^2} \frac{N_f^2}{(N_g + N_f)^2} \frac{1}{N_A} \frac{\sum_{k' \neq k} \sum_{m' \in \mathcal{G}_k} \left| S_{m'-m}^{(k')} \right|^2 E\left[\left| H_{m'}^{(k')} \right|^2 \right] \sigma_x^2 + \sigma_n^2}{\sum_{m' \in \mathcal{G}_k} \left| S_{m'-m}^{(k)} \right|^2 E\left[\left| H_{m'}^{(k)} \right|^2 \right] \sigma_a^2}. \tag{6.56}
$$

Assuming $\sigma_x^2 = \sigma_a^2$, for an AWGN channel (6.56) is simplified to be

$$
\mathrm{var}(\hat{\epsilon}_k) = \frac{1}{(2\pi)^2} \frac{N_f^2}{(N_g + N_f)^2} \frac{1}{N_A} \frac{\sum_{k' \neq k} \sum_{m' \in \mathcal{G}_{k'}} \left| S_{m'-m}^{(k')} \right|^2 + 1/\gamma_0}{\sum_{m' \in \mathcal{G}_k} \left| S_{m'-m}^{(k)} \right|^2}. \tag{6.57}
$$

The variance of the estimator is therefore affected by the following factors:

- The sum $\sum_{m' \in \mathcal{G}_k} \left| S_{m'-m}^{(k)} \right|^2$. It is determined by the value of ϵ_k, and of which $\left| S_0^{(k)} \right|^2$ is of the most importance.
- The ratio between $\sum_{m' \in \mathcal{G}_k} \left| S_{m'-m}^{(k)} \right|^2$ and $\sum_{k' \neq k} \sum_{m' \in \mathcal{G}_{k'}} \left| S_{m'-m}^{(k')} \right|^2$. In (6.57) it represents the SIR.
- Channel gain of each subcarrier. It depends upon the channel characteristics of different users, and affects the actual SIR and SNR.
- The distribution of the subchannels. In interleaved OFDMA, a pilot subcarrier will be strongly affected by the MUI from the nearby subcarriers, whereas in conventional OFDMA only the subcarriers near the margin may interfere severely. Therefore, the accuracy of ML estimator will be reduced in I-OFDMA.

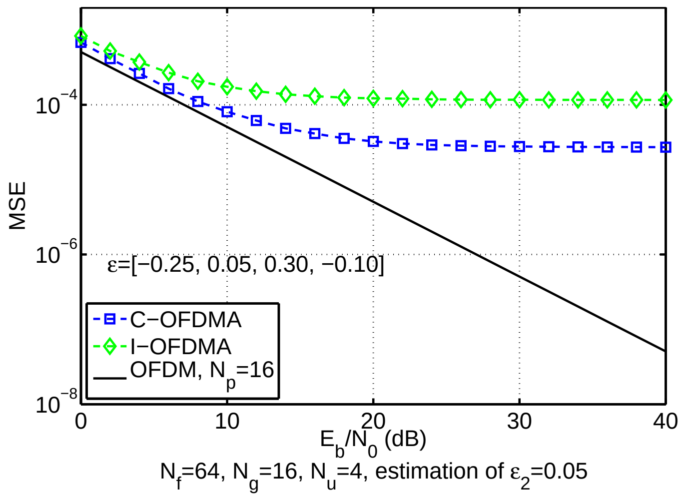

Figure 6.5: An example of CFO estimation for a incoming user in an AWGN channel, in the presence of MUI .

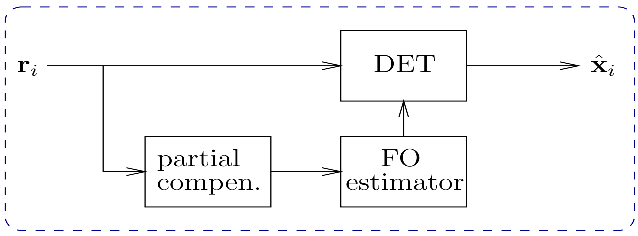

Figure 6.6: Frequency synchronization scheme.

Simulation results in Fig. 6.5 verify the above conclusions. Compared with the single user case in OFDM, the ML estimator in (6.55) offers a poor performance when it is directly implemented in a multiuser situation where MUI is present. It is shown that for a given scenario, a relatively better MSE performance can be obtained with C-OFDMA. Moreover, an error floor arises due to MUI, i.e., the estimation accuracy will not increase with SNR. Therefore, to improve the estimation accuracy, we have to find a way to overcome the influence of MUI and restore the orthogonality among users.

Modified ML Frequency Estimator

Assume that before a new MS is accessing, the CFOs of all current users have been estimated and thus are known. These information can then be used to cope with MUI. To accomplish this task, we can take advantage of CFO compensation approaches introduced in the previous chapter. The estimation of the new coming CFO can be performed with the following steps:

- Picking up $\mathbf{r}_i$ and $\mathbf{r}_{i+1}$, which include the pilot symbols of the new coming user, and information data of other users;
- Making use of the known CFOs to form $\bar{\mathbf{E}}_{\mathrm{UL}}$, $\bar{\Psi}_{i,\mathrm{UL}}$, and $\bar{\Psi}_{i+1,\mathrm{UL}}$. The unknown CFO is set to be zero;

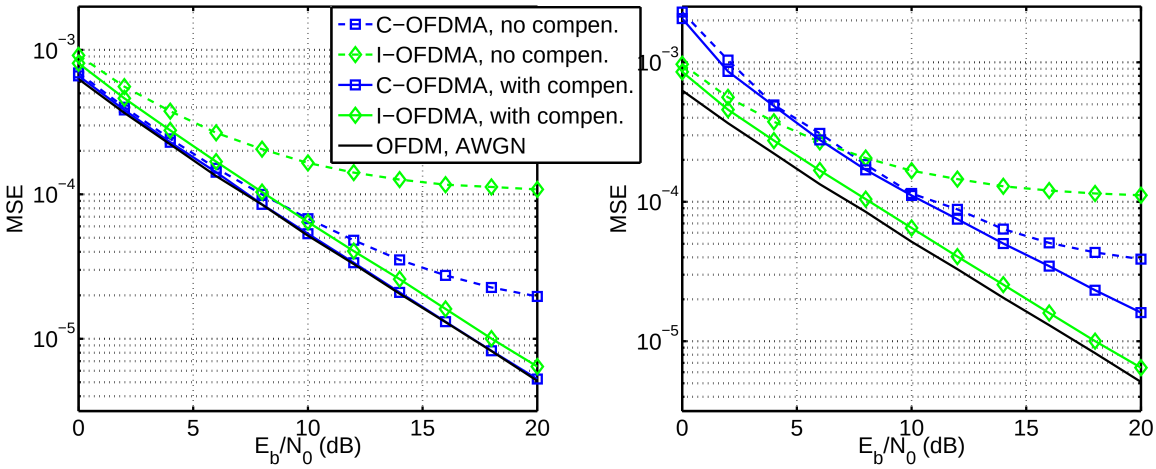

(a) AWGN (b) multipath propagation

Figure 6.7: Performance of the modified ML frequency offset estimator.

- Suppressing MUI by using LMMSE equalizer introduced in (5.17). ICI caused by the unknown CFO will remain;
- Estimating the unknown CFO with the ML frequency offset estimator given in (6.55).

The corresponding modified estimator is shown in Fig. 6.6. The estimate of ϵ_k can then be used for the vector detection together with estimates of other CFOs. Fig. 6.7 illustrates the performance of this modified CFO estimator. As a contrast, simulations are also made for pure OFDM with a CFO, where pilot subcarriers of the same number are used, and no data are transmitted over other subcarriers. The parameters of OFDMA are assumed like in Fig. 6.5. CFOs are supposed to be uniformly distributed in the range of $(-0.3, 0.3)$.

Some conclusions can be drawn when comparing Fig. 6.5 with Fig. 6.7. Firstly, without compensation, the estimation accuracy is badly limited by MUI, especially in I-OFDMA. Secondly, in an AWGN channel, with partial frequency compensation, the performance of the modified frequency offset estimator approaches the performance in a single user case. The curve for C-OFDMA even attains the best performance. Finally, it can be seen that because C-OFDMA is subchannel-dependent, in the case of multipath channels, the performance of the ML estimator is worse than that in an AWGN channel. In contrast, the curves for I-OFDMA retain the similar performance in both situation.

In general, thanks to the introduction of compensation step, the orthogonality between users is roughly recovered, so that the estimation is carried out in a nearly MUI-free scenario, and thus a good performance is obtained. This benefit is however accompanied by the cost of computational complexity.

6.3.3 Frequency Tracking by Using Pilot Subcarrier

Looking back at the frequency tracking scheme in Section 6.2.1, we now consider its implementation in the uplink. If the mth subcarrier is set to be pilot subcarrier of user k, according to

(4.51), the received pilot signal is then given by

$$r_{m,i}^{(k)} = e^{j\theta_k i} S_0^{(k)} H_m^{(k)} X_P^{(k)} + SI_i + MUI_i + n_{m,i}. \tag{6.58}$$

The estimate $\hat{\epsilon}_k$ can be calculated by (6.37) or (6.42) with N_P successively received pilot symbols.

Similar to the downlink, at a high average SNR we have

$$E\left[\hat{\epsilon}_k - \epsilon_k | \epsilon_k, X_P^{(k)}\right] = 0, \tag{6.59}$$

and

$$\text{var}\left(\hat{\epsilon}_k\right) = \frac{1}{(2\pi)^2} \frac{N_f^2}{(N_g + N_f)^2} \frac{6}{N_P(N_P^2 - 1)} \frac{\left|I_{SI}^{(k)}\right|^2 + \left|I_{MUI}^{(k)}\right|^2 + \sigma_n^2}{P_m^{(k)}}, \tag{6.60}$$

where

$$\begin{aligned} P_m^{(k)} &= \left|S_0^{(k)}\right|^2 E\left[\left|H_m^{(k)}\right|^2\right] \left|X_P^{(k)}\right|^2, \\ \left|I_{SI}^{(k)}\right|^2 &= \sum_{m' \in \mathcal{G}_k, m' \neq m} \left|S_{m'-m}^{(k)}\right|^2 E\left[\left|H_{m'}^{(k)}\right|^2\right] \sigma_x^2, \\ \left|I_{MUI}^{(k)}\right|^2 &= \sum_{k'=1, k' \neq k}^{K} \sum_{m' \in \mathcal{G}_{k'}} \left|S_{m'-m}^{(k')}\right|^2 E\left[\left|H_{m'}^{(k')}\right|^2\right] \sigma_x^2. \end{aligned} \tag{6.61}$$

If $\left|X_P^{(k)}\right|^2 = \sigma_x^2$, in the case of an AWGN channel, the variance of $\hat{\epsilon}_k$ is given by

$$\begin{aligned} \text{var}\left(\hat{\epsilon}_k\right) = & \frac{1}{(2\pi)^2} \frac{N_f^2}{(N_g + N_f)^2} \frac{6}{N_P(N_P^2 - 1)} \\ & \times \frac{\sum_{m' \in \mathcal{G}_k, m' \neq m} \left|S_{m'-m}^{(k)}\right|^2 + \sum_{k' \neq k} \sum_{m' \in \mathcal{G}_{k'}} \left|S_{m'-m}^{(k')}\right|^2 + 1/\gamma}{\left|S_0\right|^2}. \end{aligned} \tag{6.62}$$

Simulations are made for both conventional and interleaved OFDMA, as plotted in Fig. 6.8. The values of CFOs are limited in $[-0.15, +0.15]$. It is shown that even in an AWGN channel, the average MSE performance of $\hat{\epsilon}_k$ suffers from SI and MUI, so that an error floor appears as $E_b/N_0 > 20$dB. In summary, the performance of frequency tracking by using a single pilot subcarrier is poor whether in a scenario of broadcasting or multiple access.

In contrast, ML frequency offset estimator in (6.27) and its modified version are robust to frequency selective fading and can offer a better performance. Furthermore, since an acceptable performance can be obtained either in the uplink of C-OFDMA or I-OFDMA, as shown in Fig. 6.7, the modified frequency offset estimator will be applicable to an adaptive OFDMA system. It is expected to be implemented for CDM-OFDMA as well.

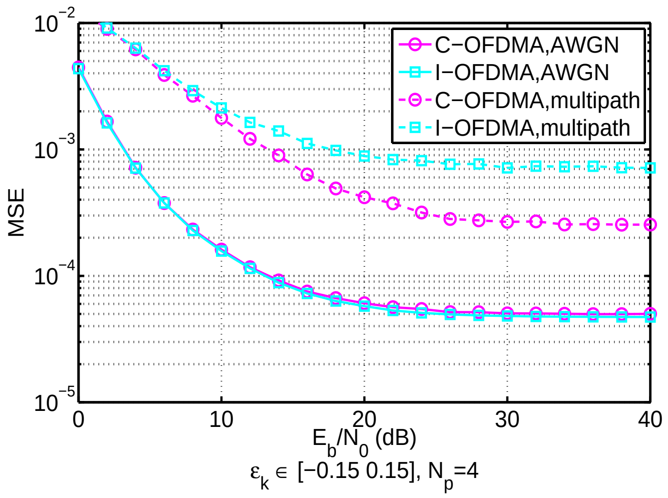

Figure 6.8: Frequency tracking in the uplink.

6.4 Summary

In this chapter, frequency offset estimation in OFDMA systems has been considered under some assumptions. Firstly, a quasi-synchronous system is adopted. This means a coarse CFO estimation can be performed in the downlink receiver, and thus only the residual CFOs have to be estimated in the uplink. Secondly, we assume that in the uplink receiver frequency offset compensation can be performed by means of vector equalization. Therefore, no feedback control channel is needed, and the estimation of the CFO of each user has to be performed in the presence of CFOs of other users. Furthermore, a reasonable assumption is made that different users access the BS sequentially, such that only the CFO of the incoming user should be estimated at a time.

To give a general impression, in Section 6.2 CFO estimation algorithms for the pure OFDM are developed first. Note that all of them can be implemented in the downlink of an OFDMA system. These algorithms can be categorized in different ways. According to whether training symbols are used or not, we can distinguish data-aided algorithms from non-data-aided algorithms. On the other hand, according to that an algorithm is implemented before or after Fourier transform, the algorithms can be classified into time-domain algorithms and frequency-domain algorithms. In addition, the estimation ranges of different CFO estimators are not identical. Some of them can estimate a CFO larger than the subcarrier frequency spacing, whereas others are only useful for estimation of a fractional CFO. An integer CFO can also be estimated separately. To get a reliable estimation, the channel is assumed to be time-invariant during the CFO estimation.

When comparing the CFO estimation algorithms which are developed for the pure OFDM, it can be found that the one-shot data-aided ML estimator using all available subcarriers is robust to multipath propagation and can provide a good performance for the fine CFO estimation in that it attains the Cramer-Rao lower bound (CRLB). Nevertheless, a direct implementation of this estimation in the uplink receiver is not recommended. It is because the estimation accuracy will be strongly affected by the MUI results from the CFOs of other users, which will lead to an error floor in MSE performance, as shown in Subsection 6.3.2.

To eliminate the MUI and restore the orthogonality among users, we can implement the frequency compensation approaches proposed in last chapter, under the condition that CFOs of all active users other than the incoming one are known. The unknown CFO is set to be zero in the compensation step. Then, CFO estimation can be applied for the new coming user. The resulting estimator including the compensation step can be regarded as a modification of the ML estimator derived for the single user case. Because the orthogonality among users is approximately restored, this modified ML estimator provides a good performance both in AWGN and multipath channels.

Furthermore, comparing the performance of this modified ML estimator in conventional OFDMA and interleaved OFDMA, we can find out that in the case of multipath channels, for conventional OFDMA the estimator has a worse performance than for interleaved OFDMA, since the former one is subchannel-dependent. A reasonable but not verified speculation is that if an adaptive subcarrier assignment scheme is adopted, under the same assumptions, the modified ML CFO estimator may provide a MSE performance between those in conventional OFDMA and interleaved OFDMA.

Chapter 7

Summary and Conclusions

This thesis has dealt with frequency synchronization in OFDM-based systems, which include OFDM, MC-CDM, and the corresponding multiple access techniques, OFDMA, CDM-OFDMA, and MC-CDMA. The study is basically on the basis of the vector-valued transmission models.

The essential contributions of the thesis include

- Modeling of OFDM-based systems under the assumption of perfect time and frequency synchronization. This is the topic of Chapter 3. The principle of OFDM-based transmission schemes has been described. OFDM is a multi-carrier transmission method which allows a bandwidth efficient data transmission with low implementation complexity. MC-CDM can improve the performance of OFDM by spreading the symbols over not fully correlated subcarriers and thus obtaining diversity gain. Three spreading schemes, full spreading, sub-band spreading, and interleaved spreading are proposed for MC-CDM. For multiuser scenarios, OFDMA is taken instead of OFDM, while CDM-CDMA and MC-CDMA are taken instead of MC-CDM. Two fixed subcarrier assignment schemes have been proposed for OFDMA, and accordingly we have defined conventional and interleaved OFDMA, as well as conventional and interleaved CDM-OFDMA. The essential difference between CDM-OFDMA and MC-CDMA is that the former is based on OFDMA, and the latter is based on CDMA. This is the source of their differences in system structure, parameter estimation, and so on. Also MC-CDMA transmission can be realized with different spreading schemes. The vector-valued transmission model has been derived for each system.
- Modeling of OFDM-based systems in the presence of carrier frequency offset (CFO). In Chapter 4, the impacts of CFO on OFDM-based systems have been investigated in detail. In OFDM, a CFO will give rise to amplitude reduction and phase rotation of the desired signals, as well as intercarrier interference (ICI) between the subcarriers. These effects can be modeled by a matrix denoted by $\hat{\mathbf{E}}$. The derivation of the matrix $\hat{\mathbf{E}}$ is one of the important contributions of this work. As a consequence, vector-valued models have been derived for OFDM and MC-CDM transmissions with a CFO. A time-variant phase increment $i\theta$ (i is the vector index) due to CFO is also included in the model. The impacts of a CFO on MC-CDM has been considered for a simple situation where only one-tap ZF equalization and despreading are performed on received symbols. We have

also derived signal to interference and noise ratio (SINR) for the cases of OFDM and MC-CDM. Moreover, based on the investigation to the uplink transmission in the presence of multiple CFOs, simplified uplink transmission models are derived for OFDMA and CDM-OFDMA. For MC-CDMA, however, no simplification can be made.

- Frequency-domain carrier frequency offset compensation by using vector equalization approaches. This is particularly suited for the uplink, where frequency synchronization cannot be accomplished by adjusting the oscillator frequency. Separate frequency compensation is suggested in the case of pure OFDMA, for it has a relatively simple structure, whereas joint equalization is preferred for CDM-OFDMA and MC-CDMA, to eliminate interference caused by the joint influence of the CFOs and imperfect channels. Furthermore, we also proposed a complexity-reduction method for OFDMA, in which the interference entries in the matrix $\hat{\mathbf{E}}$ of a small magnitude are replaced by zeros. Simulations have been made for evaluating this method, and comparing the CDM-OFDMA and MC-CDMA for different scenarios.
- Frequency offset estimation for OFDMA systems. In Chapter 6 an overview of CFO estimation algorithms for pure OFDM has been given first. These algorithms basically can be classified into two categories: data-aided and non-data-aided. A particular derivation of data-aided one-shot maximum likelihood CFO estimator has been given for the estimation in the frequency domain. Compared with other algorithms, this estimator offers a best performance for fine (fractional) CFO estimations in that it attains the Cramer-Rao lower bound (CRLB). As all available subcarriers are used for estimation, the estimator is robust to frequency selective fading. Furthermore, under some assumptions, we proposed a modified version of this ML CFO estimator for the uplink of the OFDMA systems. As known, in the uplink receiver the estimation accuracy of a frequency offset will be strongly affected by the multiuser interference. The proposed estimator improves the MSE performance by restoring the orthogonality among the users, which is realized by means of the partially frequency compensation. It is worth noting that most of the CFO estimation methods proposed for OFDMA can also be used for CDM-OFDMA.

The following conclusions may be drawn from this work:

- OFDM-based systems are sensitive to frequency offset. In the case of multiple access, the ICI due to CFOs will further lead to multiuser interference (MUI), even for ideal channels.
- When OFDMA, CDM-OFDMA, and MC-CDMA are applied for multiuser scenarios, at least a coarse frequency synchronization should be implemented in the downlink, in order to avoid the subcarrier-shift caused by an integer CFO.
- For a quasi-synchronous OFDM-based system where the maximum timing offset at the uplink receiver is assumed to be not larger than that part of the guard interval which is reserved for time offsets, compensation of the residual frequency offset can be performed in the uplink. No extra bandwidth loss will occur, since no feedback control channel is needed.
- With the derived vector-valued models which include the influence of CFOs we can take vector equalization techniques to compensate for frequency offsets. In systems like CDM-OFDMA and MC-CDMA, joint equalization of frequency offsets and channel distortion are preferred.

- With reasonably designed parameters, the complexity-reduction method proposed in Chapter 5 provides an acceptable performance in the uplink of OFDMA systems. Nevertheless, the full $\hat{\mathbf{E}}$ matrix is preferred to be used when the values of the frequency offsets are distributed in a relatively large range.
- For CFO estimation in the uplink of OFDMA and CDM-OFDMA, the orthogonality among users should be at least approximately restored, in order to keep the estimate accurate.
- Both interleaved CDM-OFDMA and fully-spread MC-CDMA may be the promising candidates for future communication systems. However, due to the parameter estimation complexity in the uplink, interleaved CDM-OFDMA instead of MC-CDMA is preferred to be applied for the uplink transmission.

Some challenges remain for future work:

- One problem that is not solved in this work is frequency offset estimation in the uplink of MC-CDMA. The research on this topic is still under way.
- Coded performance of MC-CDMA and CDM-OFDMA systems should be investigated for the downlink and the uplink transmission. Furthermore, more vector detection methods should be evaluated in the future.
- The matrix decomposition methods are expected to reduce further the computational complexity of frequency compensation algorithms in the OFDMA uplink.

Appendix A

Linear Vector Equalization

The following derivation is made referring to [33].

A.1 The Linear Least Squares Approach

In the *least squares* (LS) approach we attempt to minimize the squared difference between the given data and the assumed signal or noiseless data. Consider a linear vector-valued model without the usual noise PDF assumption

$$\mathbf{s} = \mathbf{H}_c\mathbf{x}, \tag{A.1}$$

where $\mathbf{x}$ is a complex-valued vector of dimension $P \times 1$, $\mathbf{H}_c$ is a known $N \times P$ matrix ($N > P$) of full rank P, and the received signal $\mathbf{s} = [s_0, s_1, ..., s_{N-1}]^T$. Due to observation noise or model inaccuracies we observe a perturbed version of $\mathbf{s}$, which we denoted by $\mathbf{r} = [r_0, r_1, ..., r_{N-1}]^T$. Note that no probabilistic assumption have been made about the data $\mathbf{r}$. The *least square estimate* (LSE) is found by minimizing

$$\begin{aligned} J(\mathbf{x}) &= \sum_{n=0}^{N-1}(r_n - s_n)^2 \\ &= (\mathbf{r} - \mathbf{H}_c\mathbf{x})^H(\mathbf{r} - \mathbf{H}_c\mathbf{x}). \end{aligned} \tag{A.2}$$

Since

$$J(\mathbf{x}) = \mathbf{r}^H\mathbf{r} - \mathbf{r}^H\mathbf{H}_c\mathbf{x} - \mathbf{x}^H\mathbf{H}_c^H\mathbf{r} + \mathbf{x}^H\mathbf{H}_c^H\mathbf{H}_c\mathbf{x} \tag{A.3}$$

(note that $\mathbf{r}^H\mathbf{H}_c\mathbf{x}$ is a scalar), the gradient is

$$\frac{\partial J(\mathbf{x})}{\partial \mathbf{x}} = 0-(\mathbf{H}_c^H\mathbf{r})^* - 0+(\mathbf{H}_c^H\mathbf{H}_c\mathbf{x})^*. \tag{A.4}$$

Setting the gradient equal to zero yields the LSE

$$\tilde{\mathbf{x}} = (\mathbf{H}_c^H\mathbf{H}_c)^{-1}\mathbf{H}_c^H\mathbf{r}. \tag{A.5}$$

The equations $\mathbf{H}_c^H\mathbf{H}_c\mathbf{x} = \mathbf{H}_c^H\mathbf{r}$ to be solved for $\tilde{\mathbf{x}}$ are termed the *normal equations*. The assumed full rank of $\mathbf{H}_c$ guarantees the invertibility of $\mathbf{H}_c^H\mathbf{H}_c$.

A.2 Linear Minimum Mean Square Error (LMMSE) Approaches

A.2.1 The Scalar LMMSE

In this section the *linear minimum mean square error* (LMMSE) equalizer is derived. we begin our investigation with the case where a complex-valued scalar parameter x is to be estimated based on a data set in vector form $\mathbf{r} = [r_0, r_1, ..., r_{N-1}]^T$. The unknown parameter x is modeled as the realization of a random variable. We assume that a knowledge of the first two moments of the joint PDF $p(\mathbf{r}, x)$ is known. A further assumption is the statistical dependence of x on $\mathbf{r}$. For a linear equalizer we rely on the correlation between x and $\mathbf{r}$. The general expression of linear estimator of x is of the form

$$\tilde{x} = \sum_{n=0}^{N-1} d_n r_n + d_N. \tag{A.6}$$

The weighting coefficients d_n's have to be chosen to minimize the Bayesian MSE

$$\text{Bmse}(\tilde{x}) = E[(x - \tilde{x})^2], \tag{A.7}$$

where the expectation is with respect to the PDF $p(\mathbf{r}, x)$. Now we derive the optimal weighting coefficients for use in (A.6). Substituting (A.6) into (A.7) and differentiating

$$\begin{aligned}
&\frac{\partial}{\partial d_N} E\left[(x - \sum_{n=0}^{N-1} d_n r_n - d_N)^2\right] \qquad\qquad \text{(A.8)}\\
&= \frac{\partial}{\partial d_N} E\left[(x - \mathbf{d}^T\mathbf{r} - d_N)(x - \mathbf{d}^T\mathbf{r} - d_N)^*\right]\\
&= \frac{\partial}{\partial d_N} E\left[(x - \mathbf{d}^T\mathbf{r})^2 - (x - \mathbf{d}^T\mathbf{r})d_N^* - d_N(x - \mathbf{d}^T\mathbf{r})^* + d_N d_N^*\right]\\
&= E[-(x - \mathbf{d}^T\mathbf{r})^* + d_N^*],
\end{aligned}$$

where $\mathbf{d} = [d_0, d_1, ..., d_{N-1}]^T$. Setting this equal to zero produces

$$d_N = E[x] - \mathbf{d}^T E[\mathbf{r}], \tag{A.9}$$

which is zero if the means are zero. Continuing, we need to minimize

$$\text{Bmse}(\tilde{x}) = E\left\{\left[\mathbf{d}^T(\mathbf{r}-E[\mathbf{r}]) - (x - E[x])\right]^2\right\} \tag{A.10}$$

over the remaining d_n's, where d_N has been replace by (A.9). Further we have

$$\begin{aligned}
\text{Bmse}(\tilde{x}) &= E\left\{\left[\mathbf{d}^T(\mathbf{r}-E[\mathbf{r}]) - (x-E[x])\right]^2\right\} \qquad\qquad \text{(A.11)}\\
&= E\left\{\left[\mathbf{d}^T(\mathbf{r}-E[\mathbf{r}]) - (x-E[x])\right]\left[\mathbf{d}^T(\mathbf{r}-E[\mathbf{r}]) - (x-E[x])\right]^H\right\}\\
&= E\left[\mathbf{d}^T(\mathbf{r}-E[\mathbf{r}])(\mathbf{r}-E[\mathbf{r}])^H\mathbf{d}^*\right] - E\left[\mathbf{d}^T(\mathbf{r}-E[\mathbf{r}])(x-E[x])^*\right]\\
&- E\left[(x-E[x])(\mathbf{r}-E[\mathbf{r}])^H\mathbf{d}^*\right] + E[(x-E[x])^2]\\
&= \mathbf{d}^T\mathbf{\Phi}_{\mathbf{rr}}\mathbf{d}^* - \mathbf{d}^T\mathbf{\Phi}_{\mathbf{r}x} - \mathbf{\Phi}_{x\mathbf{r}}\mathbf{d}^* + \Phi_{xx}\\
&= (\mathbf{d}^*)^H\mathbf{\Phi}_{\mathbf{rr}}\mathbf{d}^* - (\mathbf{d}^*)^H\mathbf{\Phi}_{\mathbf{r}x} - \mathbf{\Phi}_{x\mathbf{r}}\mathbf{d}^* + \Phi_{xx},\\
&= \mathbf{d}^H\mathbf{\Phi}_{\mathbf{rr}}^*\mathbf{d} - \mathbf{d}^H\mathbf{\Phi}_{\mathbf{r}x}^* - \mathbf{\Phi}_{x\mathbf{r}}^*\mathbf{d} + \Phi_{xx},
\end{aligned}$$

where $\mathbf{\Phi_{rr}}$ is the $N \times N$ covariance matrix of r, and $\mathbf{\Phi}_{x\mathbf{r}}$ is the $1 \times N$ cross-covariance vector having the property that $\mathbf{\Phi}_{x\mathbf{r}}^H = \mathbf{\Phi}_{\mathbf{r}x}$, and Φ_{xx} is the variance of x. Note that Bmse($\tilde{x}$) is real-valued such that $[\text{Bmse}(\tilde{x})]^*$ =Bmse($\tilde{x}$), and $\mathbf{\Phi}_{\mathbf{rr}}^* = \mathbf{\Phi}_{\mathbf{rr}}^T$. We can minimize (A.11) by taking the gradient to yield

$$\frac{\partial \text{Bmse}(\tilde{x})}{\partial \mathbf{d}} = (\mathbf{\Phi}_{\mathbf{rr}}^T \mathbf{d})^* - \left(\mathbf{\Phi}_{x\mathbf{r}}^T\right)^* \tag{A.12}$$

which when set to zero results in

$$\mathbf{d} = \left(\mathbf{\Phi}_{x\mathbf{r}} \mathbf{\Phi}_{\mathbf{rr}}^{-1}\right)^T . \tag{A.13}$$

Using (A.9) and (A.13) in (A.6) produces

$$\begin{aligned} \tilde{x} &= \mathbf{d}^T \mathbf{r} + d_N \\ &= \mathbf{\Phi}_{x\mathbf{r}} \mathbf{\Phi}_{\mathbf{rr}}^{-1} \mathbf{r} + E[x] - \mathbf{\Phi}_{x\mathbf{r}} \mathbf{\Phi}_{\mathbf{rr}}^{-1} E[\mathbf{r}], \end{aligned} \tag{A.14}$$

or finally the LMMSE estimator is

$$\tilde{x} = E[x] + \mathbf{\Phi}_{x\mathbf{r}} \mathbf{\Phi}_{\mathbf{rr}}^{-\mathbf{1}} (\mathbf{r} - E[\mathbf{r}]). \tag{A.15}$$

If the means of x and r are zero, then

$$\tilde{x} = \mathbf{\Phi}_{x\mathbf{r}} \mathbf{\Phi}_{\mathbf{rr}}^{-\mathbf{1}} \mathbf{r}. \tag{A.16}$$

The minimum Bayesian MSE is finally given by

$$\text{Bmse}(\tilde{x}) = \Phi_{xx} - \mathbf{\Phi}_{x\mathbf{r}} \mathbf{\Phi}_{\mathbf{rr}}^{-1} \mathbf{\Phi}_{\mathbf{r}x}. \tag{A.17}$$

A.2.2 The Vector LMMSE

The vector LMMSE estimator is a straightforward extension of the scalar one. Now we wish to find the linear estimator that minimizes the Bayesian MSE for each element. We assume that

$$\tilde{x}_i = \sum_{n=0}^{N-1} d_{in} r_n + d_{iN} \tag{A.18}$$

for $i = 1, 2, ..., P$ and choose the weighting coefficients to minimize

$$\text{Bmse}(\tilde{x}_i) = E[(x_i - \tilde{x}_i)^2] , \tag{A.19}$$

where the expectation is with respect to $p(\mathbf{r}, x_i)$. For each x_i we have

$$\tilde{x}_i = E[x_i] + \mathbf{\Phi}_{x_i\mathbf{r}} \mathbf{\Phi}_{\mathbf{rr}}^{-\mathbf{1}} (\mathbf{r} - E[\mathbf{r}]) \tag{A.20}$$

and the minimum Bayesian MSE

$$\text{Bmse}(\tilde{x}_i) = \Phi_{x_i x_i} - \mathbf{\Phi}_{x_i\mathbf{r}} \mathbf{\Phi}_{\mathbf{rr}}^{-1} \mathbf{\Phi}_{\mathbf{r}x_i}. \tag{A.21}$$

The scalar LMMSE estimators can be combined into a vector estimator as

$$\begin{aligned}\tilde{\mathbf{x}} &= \begin{bmatrix} E[x_1] \\ E[x_2] \\ \vdots \\ E[x_P] \end{bmatrix} + \begin{bmatrix} \boldsymbol{\Phi}_{x_1\mathbf{r}}\boldsymbol{\Phi}_{\mathbf{rr}}^{-1}(\mathbf{r}-E[\mathbf{r}]) \\ \boldsymbol{\Phi}_{x_2\mathbf{r}}\boldsymbol{\Phi}_{\mathbf{rr}}^{-1}(\mathbf{r}-E[\mathbf{r}]) \\ \vdots \\ \boldsymbol{\Phi}_{x_P\mathbf{r}}\boldsymbol{\Phi}_{\mathbf{rr}}^{-1}(\mathbf{r}-E[\mathbf{r}]) \end{bmatrix} \\ &= \begin{bmatrix} E[x_1] \\ E[x_2] \\ \vdots \\ E[x_P] \end{bmatrix} + \begin{bmatrix} \boldsymbol{\Phi}_{x_1\mathbf{r}} \\ \boldsymbol{\Phi}_{x_2\mathbf{r}} \\ \vdots \\ \boldsymbol{\Phi}_{x_P\mathbf{r}} \end{bmatrix} \boldsymbol{\Phi}_{\mathbf{rr}}^{-1}(\mathbf{r}-E[\mathbf{r}]) \\ &= E[\mathbf{x}]+\boldsymbol{\Phi}_{\mathbf{xr}}\boldsymbol{\Phi}_{\mathbf{rr}}^{-1}(\mathbf{r}-E[\mathbf{r}])\end{aligned} \tag{A.22}$$

where now $\boldsymbol{\Phi}_{\mathbf{xr}}$ is a $P \times N$ matrix. By a similar approach we find that the Bayesian MSE matrix is

$$\begin{aligned}\mathbf{M}_{\tilde{\mathbf{x}}} &= E[(\mathbf{x}-\tilde{\mathbf{x}})(\mathbf{x}-\tilde{\mathbf{x}})^H] \\ &= \boldsymbol{\Phi}_{\mathbf{xx}} - \boldsymbol{\Phi}_{\mathbf{xr}}\boldsymbol{\Phi}_{\mathbf{rr}}^{-1}\boldsymbol{\Phi}_{\mathbf{rx}}\end{aligned} \tag{A.23}$$

Bayesian Gaussian-Markov Theorem for Complex-valued Parameters

If the data are described by the Bayesian linear model form

$$\mathbf{r} = \mathbf{H}_c\mathbf{x} + \mathbf{n}, \tag{A.24}$$

where $\mathbf{r}$ is an $N \times 1$ complex-valued data vector, $\mathbf{H}_c$ is a known $N \times P$ observation matrix with complex-valued entries, $\mathbf{x}$ is a $P \times 1$ random vector of complex parameters whose realization is to be estimated and has mean $E[\mathbf{x}]$ and covariance matrix $\boldsymbol{\Phi}_{\mathbf{xx}}$, and $\mathbf{n}$ is an $N \times 1$ complex-valued random vector with zero mean and covariance matrix $\boldsymbol{\Phi}_{\mathbf{nn}}$ and is uncorrelated with $\mathbf{x}$. The LMMSE estimator of $\mathbf{x}$ is

$$\begin{aligned}\tilde{\mathbf{x}} &= E[\mathbf{x}]+\boldsymbol{\Phi}_{\mathbf{xx}}\mathbf{H}_c^H(\mathbf{H}_c\boldsymbol{\Phi}_{\mathbf{xx}}\mathbf{H}_c^H + \boldsymbol{\Phi}_{\mathbf{nn}})^{-1}(\mathbf{r}-\mathbf{H}_cE[\mathbf{x}]) \\ &= E[\mathbf{x}] + (\boldsymbol{\Phi}_{\mathbf{xx}}^{-1} + \mathbf{H}_c^H\boldsymbol{\Phi}_{\mathbf{nn}}^{-1}\mathbf{H}_c)^{-1}\mathbf{H}_c^H\boldsymbol{\Phi}_{\mathbf{nn}}^{-1}(\mathbf{r}-\mathbf{H}_cE[\mathbf{x}]).\end{aligned} \tag{A.25}$$

It is because

$$\begin{aligned}E[\mathbf{r}] &= \mathbf{H}_cE[\mathbf{x}], \\ \boldsymbol{\Phi}_{\mathbf{rr}} &= \mathbf{H}_c\boldsymbol{\Phi}_{\mathbf{xx}}\mathbf{H}_c^H + \boldsymbol{\Phi}_{\mathbf{nn}}, \\ \boldsymbol{\Phi}_{\mathbf{xr}} &= \boldsymbol{\Phi}_{\mathbf{xx}}\mathbf{H}_c^H,\end{aligned} \tag{A.26}$$

where $\boldsymbol{\Phi}_{\mathbf{rr}}$ and $\boldsymbol{\Phi}_{\mathbf{xr}}$ are calculated by

$$\begin{aligned}\boldsymbol{\Phi}_{\mathbf{rr}} &= E[(\mathbf{H}_c\mathbf{x}+\mathbf{n})(\mathbf{H}_c\mathbf{x}+\mathbf{n})^H] \\ &= E[\mathbf{H}_c\mathbf{x}\mathbf{x}^H\mathbf{H}_c^H]+E[\mathbf{n}\mathbf{x}^H\mathbf{H}_c^H]+E[\mathbf{H}_c\mathbf{x}\mathbf{n}^H]+E[\mathbf{n}\mathbf{n}^H] \\ &= \mathbf{H}_c\boldsymbol{\Phi}_{\mathbf{xx}}\mathbf{H}_c^H + \boldsymbol{\Phi}_{\mathbf{nn}},\end{aligned}$$

and

$$\begin{aligned}\boldsymbol{\Phi}_{\mathbf{xr}} &= E[\mathbf{x}(\mathbf{H}_c\mathbf{x}+\mathbf{n})^H] \\ &= \boldsymbol{\Phi}_{\mathbf{xx}}\mathbf{H}_c^H.\end{aligned}$$

Application for unknown but deterministic variables

The transmit symbols are selected from an alphabet, e.g. QPSK modulation. These symbols has the mean $E[x] = 0$ and the variance $E[x^2] = \sigma_x^2$. In case of vector transmission, we have then $E[\mathbf{x}] = \mathbf{0}$ and $\Phi_{\mathbf{xx}} = \sigma_x^2\mathbf{I}$. On the other hand, we assume that $\mathbf{n}$ is complex Gaussian and $\Phi_{\mathbf{nn}} = \sigma_n^2\mathbf{I}$. The LMMSE estimator in (A.25) is therefore simplified to be

$$\begin{aligned}\tilde{\mathbf{x}} &= \mathbf{H}_c^H(\mathbf{H}_c\mathbf{H}_c^H + \frac{\sigma_n^2}{\sigma_x^2}\mathbf{I})^{-1}\mathbf{r} \\ &= (\mathbf{H}_c^H\mathbf{H}_c + \frac{\sigma_n^2}{\sigma_x^2}\mathbf{I})^{-1}\mathbf{H}_c^H\mathbf{r}.\end{aligned} \tag{A.27}$$

Appendix B

Mathematical Notation and List of Symbols

$a_{l,k}(t)$	time-variant equivalent low-pass tap weighting of kth path with delay $\tau_l(t)$
$\mathbf{a}$	training symbol vector used for ML CFO estimation in the frequency domain
$\mathbf{b}$	short training sequence used for ML CFO estimation in the time domain
B	bandwidth of a band-pass filter
B_c	coherence bandwidth of the channel
B_D	Doppler spread
c	velocity of light
$c_l(t)$	time-variant equivalent low-pass tap weighting of lth path
$\lvert c_l(t)\rvert$	amplitude of $c_l(t)$
$\mathbf{c}_j$	a spreading sequence
$\mathbf{e}$	a vector standing for the influence of CFO in the time domain
$\mathbf{E}$	a matrix with $\mathbf{e}$ on the main diagonal
$\dot{\mathbf{E}}$	a matrix standing for the influence of CFO in the the domain: matrix $\mathbf{E}$ after removing prefix
$\hat{\mathbf{E}}$	a matrix standing for the influence of CFO in the frequency domain
$\hat{\mathbf{E}}^{(k)}$	a matrix standing for the influence of CFO in the frequency domain for user k
$\bar{\mathbf{E}}^{(k)}$	a submatrix of $\hat{\mathbf{E}}^{(k)}$, only consisting of entries associated subcarriers assigned to user k
$\bar{\mathbf{E}}_{\mathrm{UL}}$	combined $\hat{\mathbf{E}}$ matrix in the uplink, consisting of effects of CFOs of all users
f_c	carrier frequency
f_d	Doppler shift
$f_{d\,\max}$	maximum Doppler shift
f_g	cutoff frequency of a bandlimited low-pass filter
f_n	subcarrier frequency in an multicarrier system
f_s	symbol rate on a subcarrier
f_ϵ	absolute carrier frequency offset
Δf	subcarrier frequency spacing in an OFDM system
$\mathbf{F}$	normalized Fourier matrix
$\mathbf{F}^{-1}$	normalized inverse Fourier matrix
$g(t)$	received signal at the input of the receiver

g_{ij}	entries of $\mathbf{H}$ at row i, column j
g_m	equalization coefficient on subcarrier m
$\mathbf{G}$	equalization matrix
$\mathbf{G}_{ap}$	matrix used for adding cyclic prefix
$\mathbf{G}_{pp}$	matrix used for removing cyclic prefix
$h(t,\tau)$	time-variant channel impulse response
$h_T(t)$	transmit filter
$h_R(t)$	receive filter
$h_K(t)$	impulse response of a time-invariant channel
h_{ij}	entries of $\mathbf{H}_c$ at row i, column j
$\mathbf{h}$	discrete-time equivalent low-pass channel impulse response vector
H_m	transfer function of subcarrier m
$H_m^{(k)}$	transfer function on subcarrier m which is assigned to user k
$\mathbf{H}$	channel transfer function matrix
$\mathbf{H}_c$	channel matrix
$\mathbf{H}_i^{(k)}$	channel transfer function matrix of user k at time index i
$\mathbf{H}^{(k)}$	$\mathbf{H}_i^{(k)}$ when channel is time invariant
$\mathbf{H}_{\mathrm{DL}}^{(k)}$	downlink channel transfer function matrix of user k
$\mathbf{H}_{\mathrm{UL}}^{(k)}$	uplink channel transfer function matrix of user k
$\bar{\mathbf{H}}_{\mathrm{UL}}$	combined uplink channel transfer function matrix
$\hat{\mathbf{H}}_i$	channel impulse response matrices at time index i
$I_{ICI,0}^{(m)}$	inter-carrier interference (ICI) on the subcarrier m in an ideal channel
$\lvert I_{m,m'}\rvert^2$	normalized power of the ICI from the subcarrier m' to subcarrier m under the
$\mathbf{I}$	identity matrix
K	maximum number of users in a multiuser system
L_b	length of $\mathbf{b}$
L_s	number of repeated training sequence $\mathbf{b}$
m_δ	subcarrier shift due to integer normalized CFO δ
M	the cardinality of the alphabet
$n(t)$	complex-valued low-pass white Gaussian noise
$n_{m,i}$	noise variable on subcarrier m at time index i
$\mathbf{n}$	noise vector
$\mathbf{n}_i$	frequency-domain noise vector at time index i
$\dot{\mathbf{n}}_i$	time-domain noise vector at time index i
$\mathbf{n}_i^{(k)}$	frequency-domain noise vector of user k at time index i
N_0	one-side power spectral density (PSD) of band-pass white Gaussian noise (real-valued)
N_{ch}	guard interval for multipath propagation
N_g	guard interval
N_s	number of symbols in an OFDM-symbol
N_f	length of DFT
N_{toff}	guard interval for small time offset
N_Q	size of submatrix $\mathbf{W}_q$ in $\mathbf{U}$ in the case of MC-CDM
$P_h(\tau)$	power delay profile (PDP) of $h(t,\tau)$
P_m	the zeroth-order moment of $P_h(\tau)$
P_{sv}	variance of the diagonal entries in MC-CDM due to a CFO
$P_{I_{\mathrm{in}}}$	interference from the transmit symbols transmitted on the desired subchannel

	in MC-CDM due to a CFO
$P_{I_{\text{out}}}$	interference from other subchannels in MC-CDM due to a CFO
$r_m(t)$	received signal at the carrier f_m
$r_{m,i}$	received symbol at the carrier f_m at time index i
$r_{m,i}^{(k)}$	received symbol of user k at the carrier f_m at time index i
$\mathbf{r}$	received symbol vector
$\mathbf{r}_i$	frequency-domain received symbol vector at time index i
$\mathbf{r}_{i,\text{DL}}$	overall received symbol vector at downlink receiver
$\mathbf{r}_{i,\text{UL}}$	overall received symbol vector at uplink receiver
$\mathbf{r}_{i,\text{DL}}^{(k)}$	downlink received symbol vector of user k at time index i
$\tilde{\mathbf{r}}_i$	received symbol vector after frequency offset compensation
R	code rate
$\mathbf{R}_i$	an equivalent channel matrix at time index
$s(t)$	time-domain transmit signal
$s_{k,i}$	kth time-domain transmit symbol at time index i
$\dot{s}_{k,i}$	time-domain transmit symbol
$\mathbf{s}_i$	time-domain transmit symbol vector with cyclic prefix
$\dot{\mathbf{s}}_i$	time-domain transmit symbol vector without cyclic prefix
S_0	diagonal entry of $\hat{\mathbf{E}}$
$S_0^{(k)}$	diagonal entry of $\hat{\mathbf{E}}^{(k)}$
$S_{m'-m}$	entry at row m, column m' of $\hat{\mathbf{E}}$
$S_{m'-m}^{(k)}$	entry at row m, column m' of $\hat{\mathbf{E}}^{(k)}$
$S_D(f_d)$	Doppler power spectral density
$S_\varphi(f)$	jitter power spectral density of $\varphi(t)$
$S_\xi(e^{j2\pi fT_s})$	jitter spectrum of ξ
$\delta(t)$	Dirac function
Δt	sampling time
T	duration of a single sample of an OFDM-symbol
T_s	OFDM-symbol duration
$\mathbf{T}$	permutation matrix in MC-CDM
$\mathbf{T}_c$	permutation matrix in CDM-OFDMA
$\mathbf{T}_m$	permutation matrix in MC-CDMA
$u(t)$	basic waveform at the transmitter
$\mathbf{U}$	(overall) spreading matrix
$\mathbf{U}^{(k)}$	user-specific spreading matrix of user k
$\bar{\mathbf{U}}_{\text{UL}}$	combined uplink spreading matrix in the case of MC-CDMA
v	velocity of movement
$v(t)$	matched filter of $u(t)$ at the receiver
$v_{m,i}$	colored noise
$V_{jj}^{(k)}$	diagonal entries of $\mathbf{V}^{(k)}$
V_γ	$2^\gamma \times 2^\gamma$ Hadamard matrix formed by using the Hadamard matrix $V_{\gamma-1}$
$\mathbf{V}^{(k)}$	user-specific subchannel division matrix for user k
$w(k)$	a Gaussian random variable (r.v.) with zero-mean and variance $4\pi\beta T$
w_m	the real-valued noise component
$\mathbf{w}$	the real-valued noise vector
W	total available bandwidth of a multicarrier system

$\mathbf{W}_{k,p}$	user-specific spreading submatrix of user k on the pth subchannel in the case of MC-CDMA
$\mathbf{W}_q$	submatrix in $\mathbf{U}$ in the case of MC-CDM
$\mathbf{W}_k$	user-specific spreading submatrix of user k in the case of CDM-OFDMA
$x(t)$	frequency-domain transmit signal
$x_{m,i}$	mth elements of $\mathbf{x}_i$, the transmit symbol on subcarrier m
$x_{m,i}^{(k)}$	mth elements of $\mathbf{x}_i$, the transmit symbol of user k on subcarrier m
$\hat{x}$	decided symbol
$\mathbf{x}$	transmit symbol vector
$\mathbf{x}_i$	transmit symbol vector at time index i, or overall transmit symbol vector
$\mathbf{x}_i^{(k)}$	transmit symbol vector of user k at time index i
$\tilde{\mathbf{x}}$	symbol vector after equalization
X_P	a given pilot symbol used for CFO tracking
$X_{p,i}^{(k)}$	one transmit symbol of user k at time index i
$y(t)$	time-domain received signal (after receive filter)
$y_{k,i}$	received time-domain discrete-time symbol on subcarrier k at time index i
$\mathbf{y}_i$	received time-domain symbol vector
$z_{m,i}$	variable designed for frequency-domain CFO estimation
α	a threshold used for the robust estimation of CFO, $\alpha \in [1, L_s - 3]$
β	phase increment due to a CFO during the transmission of a short training sequence
β_Δ	two-side 3dB linewidth of the Lorentzian power density spectrum of the oscillator
δ	integer part of ϵ
δ_{mn}	Kronecker delta
Δ_m	angle of $z_{m,i}$
$\boldsymbol{\Delta}$	a vector consisting of Δ_m
ϵ	normalized carrier frequency offset
ϵ_k	normalized CFO of user k
$\hat{\epsilon}$	estimate of ϵ
η	normalized clock frequency offset
γ	the average SNR at the output of a fading channel
γ_0	signal-to-noise ratio (SNR) in an AWGN channel
γ_a	average SNR when training symbol vector $\mathbf{a}$ is transmitted
λ	threshold for sub-optimal LMMSE
μ	threshold for complexity-simplification frequency offset compensation
ν	normalized constant time offset
ν_k	constant time offset of user k
$\nu_{\max}$	maximum constant time offset in the uplink
$\boldsymbol{\Pi}$	$\boldsymbol{\Pi}=\hat{\mathbf{E}}$
$\boldsymbol{\Pi}_I$	submatrix of $\boldsymbol{\Pi}$ used for complexity-simplification frequency offset compensation
$\boldsymbol{\Pi}_n$	submatrix of $\boldsymbol{\Pi}$
ϕ_0	phase of S_0
$\phi_{m'-m}$	phase of $S_{m'-m}$
$\phi_{nn}(\tau)$	autocorrelation function of $n(t)$
$\Phi_{nn}(f)$	power spectral density of $n(t)$
$\boldsymbol{\Phi}_{\mathbf{xx}}$	covariance matrix of $\mathbf{x}$
$\boldsymbol{\Phi}_{\tilde{\mathbf{n}}\tilde{\mathbf{n}}}$	covariance matrix of $\tilde{\mathbf{n}}$

$\mathbf{\Phi_{ww}}$	covariance matrix of $\mathbf{w}$
$\bar{\Psi}_i^{(k)}$	a diagonal matrix with instantaneous phase of user k at time index i
$\bar{\Psi}_{i,\mathrm{UL}}$	combined matrix in the uplink consisting of instantaneous phase of all users at time index i
σ_a^2	variance of training symbols in $\mathbf{a}$
σ_n^2	variance of white Gaussian noise
σ_x^2	variance of transmit symbol
σ_τ	rms delay spread
σ_φ^2	jitter variance of $\varphi(t)$
σ_ξ^2	jitter variance of ξ
$\tau_l(t)$	time-variant propagation delay
$\triangle\tau_l(t)$	delay difference between $\tau_l(t)$ and $\tau_{l-1}(t)$
τ_l	time-invariant propagation delay
$\bar{\tau}$	mean excess delay
$\frac{1}{\Delta\tau}$	sampling rate
θ	phase increment due to frequency offset during transmission of one OFDM vector
$\theta(t)$	time-variant carrier phase error
$\theta_l(t)$	time-variant phase of $c_l(t)$
$\theta_\Delta(t)$	time-variant phase noise
θ_0	constant phase offset
θ_k	phase increment due to frequency offset of user k
$\theta_{r,i}$	overall instantaneous phase error by reason of the CFO ϵ at the vector index i
θ_ν	phase shift caused by a constant time offset ν
$\hat{\theta}$	an estimate of θ
ε	fractional part of ε
$\varphi_{l,k}(t)$	time variant phase of $a_{l,k}(t)$
$\varphi(t)$	carrier phase jitter, modeled as a zero-mean stationary random process
$\xi(t)$	timing jitter
ζ	the azimuthal angle between direction of wave and direction of relative receiver movement.
$\mathcal{A}_x$	modulation alphabet
$\mathcal{G}_k$	ensemble of subcarriers assigned to user k
$(\cdot)^H$	vector/matirx complex conjugate transposition (Hermitian)
$(\cdot)^T$	vector/matrix transpose
$(\cdot)^*$	complex conjugate of a variable
$\mathrm{Im}\{\cdot\}$	imaginary part of the argument
$\mathrm{Re}\{\cdot\}$	real part of the argument
$\arg(\cdot)$	angle of the argument
$\mathrm{rect}(\cdot)$	rectangular window
$\mathrm{var}(\cdot)$	variance of an argument
$\hat{\Theta}(\cdot)$	symbol-wise decision function
$\Lambda(\cdot)$	log-likelihood function
SIR_0	signal-to-interference ratio (SIR) in an ideal or an AWGN channel

$SINR_0$ signal-to-interference-and-noise ratio (SINR) in an AWGN channel

$SINR_{\text{MC-CDM},0}$
SINR in MC-CDM over an AWGN channel

$SINR_{\text{MC-CDM, ZF}}$
SINR after ZF equalization in MC-CDM over a fading channel

$SINR_{\text{MC-CDM, 0}}|_{W_q}$
$SINR_{\text{MC-CDM},0}$ associated with the subchannel q

$SINR_{\text{MC-CDM, ZF}}|_{W_q}$
$SINR_{\text{MC-CDM, ZF}}$ associated with the subchannel q

Appendix C

List of Abbreviations

AWGN	Additive White Gaussian Noise
ACI	Adjacent Channel Interference
BER	Bit Error Rate
BPSK	Binary Phase Shift Keying
BS	Base Station
CDM	Code Division Multiplexing
CDMA	Code Division Multiple Access
CDM-OFDMA	Code Division Multiplexing - Othogonal Frequency Division Multiple Access
CFO	Carrier Frequency Offset
CIR	Channel Impulse Response
C-OFDMA	Conventional Othogonal Frequency Division Multiple Access
CP	Cyclic Prefix
CPO	Common Phase Error
CSI	Channel State Information
DA	Data-Aided
DAB	Digital Audio Broadcasting
DET	Detector
DFT	Discrete Fourier Transform
DVB-T	Digital Video Broadcasting - Terrestrial
EGC	Equal Gain Combining
ESPRIT	Estimation of Signal Parameters by Rotational Invariance Techniques
FDM	Frequency Division Multiplexing
FDMA	Frequency Division Multiple Access
FFT	Fast Fourier Transform
HF	High Frequency
HIPERLAN/2	HIgh PErformance Radio Local Area Network/2
ICI	Inter-Carrier Interference
IDFT	Inverse Discrete Fourier Transform
IFFT	Inverse Fast Fourier Transform
I-OFDMA	Interleaved Othogonal Frequency Division Multiple Access
ISI	Inter-Symbol Interference
LMMSE	Linear Minimum Mean Square Error
LO	Local Oscillator

LOS	Line-of-Sight
MC	Multicarrier
MCM	Multicarrier Modulation
MC-SS	Multicarrier - Spread Spectrum
MC-CDM	Multiarrier - Code Division Multiplexing
MC-CDMA	Multiarrier - Code Division Multiple Access
MF	Matched Filtering
ML	Maximum Likelihood
MLE	Maximum Likelihood Estimation
MS	Mobile Station
MSE	Mean Square Error
MUI	Multi User Interference
MUSIC	MUltiple SIgnal Classification
NDA	Non-Data-Aided
NLOS	Non-Line-of-Sight
MRC	Maximum Ratio Combining
OFDM	Othogonal Frequency Division Multiplexing
OFDMA	Othogonal Frequency Division Multiple Access
PAPR	Peak-to-Average Power Ratio
PDF	Probability Density Function
PDP	Power Delay Profile
PLL	Phase-Locked Loop
PN	Pseudo-Noise
QAM	Quadrature Amplitude Modulation
QPSK	Quadrature Phase Shift Keying
QS	Quasi-Synchronous
RF	Radio Frequency
RHS	Right-Hand Side
SI	Self-Interference
SIR	Signal to Interference Ratio
SINR	Signal to Interference and Noise Ratio
SNR	Signal to Noise Ratio
TDM	Time Division Multiplexing
TDMA	Time Division Multiple Access
US	Uncorrelated Scattering
WLAN	Wireless Local Area Network
WSS	Wide Sense Stationary
ZF	Zero-Forcing

Bibliography

[1] "http://grouper.ieee.org/groups/802/15/arc/802/wpanlist/msg00305.html."

[2] "IEEE Std 802.11a-1999 Part11: Wireless LAN Medium Access Control (MAC) and Physical Layer (PHY) Specifications High-speed Physical Layer in the 5G Band."

[3] "IEEE Std 802.16-2004: IEEE Standard for Local and Metropolitan Area Networks–Part 16: Air Interface for Fixed Broadband Wireless Access Systems," Oct. 2004.

[4] J. Armstrong, "Analysis of New and Existing Methods of Reducing Intercarrier Interference Due to Carrier Frequency Offset in OFDM," in *IEEE Transactions on Communications*, vol. 47, March 1999, pp. 365–369.

[5] S. Barbarossa, M. Pompili, and G. B. Giannakis, "Time and Frequency Synchronization of Orthogonal Frequency Division Multiple Access Systems," in *Processing of International Conference on Communications*, vol. 6, Helsinki, Finland, June 11-15 2001, pp. 1674–1678.

[6] ——, "Channel Independent Synchronization of Orthogonal Frequency Division Multiple Access Systems," in *IEEE Journal on Selected Areas in Communications*, vol. 20, No.2, Feb. 2002, pp. 474–486.

[7] J. A. C. Bingham, "Multicarrier Modulation for Data Transmission: an Idea Whose Time Has Come," in *IEEE Communications Magazine*, vol. 28, May 1990, pp. 5–14.

[8] M. Bossert, *Channel Coding for Telecommunications.* B. G. Teubner Stuttgart, 1992.

[9] A. Bury, *Efficient Multi-Carrier Spread Spectrum Transmission.* Dissertation. VDI Verlag GmbH, 2001.

[10] Z. Cao, U. Tureli, and Y.-D. Yao, "Analysis of Two Receiver Schemes for Interleaved OFDMA Uplink," in *Conference Record of the Thirty-Sixth Asilomar Conference on Signals, Systems, and Computers*, vol. 2, Nov. 2002, pp. 1818–1821.

[11] ——, "Efficient Structure-based Carrier Frequency Offset Estimation for Interleaved OFDMA Uplink," in *IEEE International Conference on Communications*, vol. 26, May 2003, pp. 3361–3365.

[12] ——, "Deterministic Multiuser Carrier-Frequency Offset Estimation for Interleaved OFDMA Uplink," in *IEEE Transaction on Communications*, vol. 52, No.9, Sept. 2004, pp. 1585–1594.

[13] ——, "Frequency Synchronization for Generalized OFDMA Uplink," in *GLOBECOM'04. IEEE Telecommunications Conference*, vol. 2, Nov./Dec. 2004, pp. 1071–1075.

[14] R. W. Chang, "Synthesis of Band-limited Orthogonal Signals for Multichannel Data Transmission," in *The Bell System Technical Journal.*, vol. 45, Dec. 1966, pp. 1775–1976.

[15] C. Chen, J. Li, and L. Zhao, "Comparison of Integer Frequency Offset Estimators for OFDM Systems," in *Proceeding of IEEE Global Telecommunications Conference,2004. GLOBECOM'04*, vol. 4, Nov./Dec. 2004, pp. 2371–2375.

[16] J. Chin and A. Cantoni, "Phase Jitter $\bar{\text{T}}$ime Jitter ?" in *IEEE Communications letters*, vol. 2, Feb. 1998, pp. 54–56.

[17] J. Choi, C. Lee, H. W. Jung, and Y. H. Lee, "Carrier Frequency Offset Compensation for Uplink of OFDM-FDMA Systems," in *IEEE Communication Letters*, vol. 4, No.12, December 2000, pp. 414–416.

[18] A. J. Coulson, "Maximum Likelihood Synchronization for OFDM Using a Pilot Symbol: Algorithms," in *IEEE Journal on Selected Areas in Communications*, vol. 19, No. 12, Dec. 2001, pp. 2486–2494.

[19] ——, "Maximum Likelihood Synchronization for OFDM Using a Pilot Symbol: Analzsis," in *IEEE Journal on Selected Areas in Communications*, vol. 19, No. 12, Dec. 2001, pp. 2495–2503.

[20] J. Egle, *Detection Methods for Power and Bandwidth Efficient Single Carrier Block Transmissions.* Dissertation. VDI Verlag GmbH, 2004.

[21] C. Eklund, R. B. Marks, K. L.Stanwood, and S. Wang, "IEEE Standard 802.16: A Technical Overview of the WirelessMAN Air Interface for Broadband Wireless Access," in *IEEE Transactions on Communication Technology*, vol. 40, June 2002, pp. 98–107.

[22] A. Engelhart, *Vector Detection Techniques with Moderate Complexity.* Dissertation. VDI Verlag GmbH, 2003.

[23] X. Gui and T. S. Ng, "Performance of Asynchronous Orthogonal Multicarrier CDMA System in Frequency Selective Fading Channel," in *IEEE Transactions on Communications*, vol. 47, July 1999, pp. 1084–1091.

[24] L. Haering, A. Czylwik, and M. Speth, "Analysis of Synchronization Impairments in Multiuser OFDM Systems," in *9th International OFDM-Workshop*, Sept. 2004.

[25] L. Hanzo, M. Münster, B. J. Choi, and T. Keller, *OFDM and MC-CDMA for Broadband Multi-user Communications, WLANs and Broadcasting.* England, John Wiley & Sons, Ltd., 2003.

[26] S. Haykin, *Adaptive Filter Theory*, 3rd ed. Prenstice Hall. Inc., 1996.

[27] D. D. Huang and K. B. Letaief, "Carrier Frequency Offset Estimation for OFDM Systems Using Null Subcarriers," in *IEEE Transactions on Communications*, vol. 54, No. 5, May 2006, pp. 813–823.

[28] J. Jang and B. E. Lee, "Effects of Frequency Offset on MC-CDMA System Performance," in *IEEE Communication Letters*, vol. 3, No.7, July 1999, pp. 196–198.

[29] S. Kaiser, "Performance Effects of the Uplink Asynchronism in a Spread Spectrum Multi-Carrier Multiple Access System," in *European Transactions on Telecommunications (ETT)*, vol. 10, No.4, July/Aug. 1999, pp. 399–406.

[30] ——, "OFDM Code-Division Multiplexing in Fading Channels," in *IEEE Transactions on Communications*, vol. 50, No.8, Aug. 2002, pp. 1266–1273.

[31] S. Kapoor, D. J. Marchok, and Y.-F. Huang, "Adaptive Interference Suppression in Multiuser Wireless ofdm Systems Using Antenna Arrays," in *IEEE Transaction on Signal Processing*, vol. 47, No.12, Dec. 1999, pp. 3381–3391.

[32] S. Kay, "A Fast and Accurate Single Frequency Estimator," in *IEEE Transactions on Acoustics. and Signal Processing*, vol. 37, No.12, Dec. 1989, pp. 1987–1990.

[33] S. M. Kay, *Fundamentals of Statistical Signal Processing I: Estimation Theory.* Prentice Hall PTR, 1993.

[34] N. Lashkarian and S. Kiaei, "Class of Cyclic-based Estimators for Frequency-Offset Estimation of OFDM Systems," in *IEEE Transaction on Communications*, vol. 48, No.12, Dec. 2000, pp. 2139–2149.

[35] B. P. Lathi, *Modern Digital and Analog Communication Systems.* Oxford Univ. Press, 1998.

[36] J.-H. Lee and S.-C. Kim, "Residual Frequency Offset Compensation Using the Approximate SAGE Algorithm for OFDM System," in *IEEE Transactions on Communications*, vol. 54, No. 5, May 2006, pp. 765–769.

[37] J. Lei and T.-S. Ng, "A Consistant ofdm Carrier Frequency Offset Estimator Based on Distinctively Spaced Pilot Tones," in *IEEE Transactions on Wireless Communications*, vol. 3, No.2, March 2004, pp. 588–599.

[38] G. Li and H. Liu, "Throughout Maximination with Buffer Constrains in Broadband OFDMA Networks," in *Proceedings of IEEE International Conference on Acoustics, Speech, and Signal Processing (ICASSP' 03)*, vol. 4, April 2003, pp. 197–200.

[39] Y. G. Li and N. R. Sollenberger, "Clustered OFDM with Channel Estimation for High Rate Wireless Data," in *IEEE Transactions on Communications*, vol. 49, December 2001, pp. 2071–2076.

[40] J. Lindner, "MC-CDMA in the Context of General Multiuser/Multisubchannel Transmission Methods," in *Europen Trans. Telecomm.*, July 1999, pp. 351–367.

[41] ——, *Informationsübertragung.* Springer - Verlag, 2004.

[42] H. Liu and U. Tureli, "A High-Efficiency Carrier Estimator for OFDM Communications," in *IEEE Communication Letters*, vol. 2, No.4, April 1998, pp. 104–106.

[43] M. Luise and R. Reggiannini, "Carrier Frequency Recovery in All-Digital Modems for Burst-Mode Transmissions," in *IEEE Transactions on Communications*, vol. 43, No. 2/3/4, February/March/April 1995, pp. 1169–1178.

[44] ——, "Carrier Frequency Aquisition and Tracking for OFDM Systems," in *IEEE Transactions on Communications*, vol. 44, No. 11, Nov. 1996, pp. 1590–1598.

[45] X. Ma, G. B. Giannakis, and S. Barbarossa, "Non-Data-Aided Carrier Offset Estimators for OFDM with Null Subcarriers: Identiability, Alorithms and Performance," in *IEEE Journal on Selective Areas in Communications*, vol. 19, No.12, Dec. 2001, pp. 2504–2515.

[46] ——, "Non-Data-Aided Frequency-Offset and Channel Estimation in OFDM and Related Block Transmissions," in *Processing of International Conference on Communications*, vol. 6, Helsinki, Finland, June 11-15 2001, pp. 1866–1870.

[47] U. Mengali and M. Morelli, "Data-Aided Frequency Estimation for Burst Digital Transmission," in *IEEE Transactions on Communications*, vol. 45, No.1, Jan. 1997, pp. 23–25.

[48] H. Minn, V. K.Bhargava, and L. B. Letaief, "A Rubost Timing and Frequency Synchronization for OFDM Systems," in *IEEE Transactions on Wireless Communications*, vol. 2, No. 4, July 2003, pp. 822–839.

[49] A. F. Molisch, *Wireless Communications.* John Wiley & Sons Ltd., 2005.

[50] P. H. Moose, "A Technique for Orthogonal Frequency-Division Multiplexing Frequency offset correction," in *IEEE Transactions on Communications*, vol. 42, Oct. 1994, pp. 2908–2914.

[51] M. Morelli, "Time and Frequency Synchronization of an OFDMA System," in *IEEE Transactions on Communications*, vol. 52, No.2, Feb. 2004, pp. 296–306.

[52] M. Morelli and U.Mengalli, "An Improved Frequency Offset Estimator for OFDM Applications," in *IEEE Communication Letters*, vol. 3, No.3, Mar. 1999, pp. 75–78.

[53] ——, "Carrier-Frequency Estimation for Transmissions over Selective Channels," in *IEEE Transaction on Communications*, vol. 48, No.9, Sep. 2000, pp. 1580–1589.

[54] B. R. N. Murthy, "Effect of Carrier Mistracking and Phase Jitter in a QPRS Receiver," in *IEEE Transactions on Communications*, vol. 25, Oct. 1977, pp. 1244–1247.

[55] M. Olosson and H. Johansson, "Blind OFDM Carrier Frequency Offset Estimation by Locating Null Subcarriers," in *9th International OFDM-Workshop*, Dresdon, Germany, Sept. 2004.

[56] R. N. Petersen, *Performance Considerations of OFDMA Radio Communication Systems.* Dissertation. VDI Verlag GmbH, 1998.

[57] T. Pollet, M. V. Bladel, and M. Moeneclaey, "BER Sensitivity of OFDM Systems to Carrier Frequency Offset and Wiener Phase Noise," in *IEEE Transactions on Communications*, vol. 43, Feb./Mar./April 1995, pp. 191–193.

[58] J. G. Proakis, *Digital Communications*, 4th ed. New York, McGraw-Hill Book Company, 2001.

[59] T. S. Rappaport, *Wireless Communications Principles & Practice.* Prentice Hall, Inc., 1996.

[60] E. Rosnes and A. Vahlin, "Frequency Estimation of a Single Complex Sinusoid Using a Generalized Kay Estimator," in *IEEE Transaction on Communications*, vol. 54, No.3, Mar. 2006, pp. 407–415.

[61] T. M. Schmidl and D. C. Cox, "Robust Frequency and Timing Synchronization for OFDM," in *IEEE Transaction on Communications*, vol. 45, No.12, Dec. 1997, pp. 1613–1621.

[62] B. Sklar, "Rayleigh Fading Channels in Mobile Digital Communication Systems Part i: Characterization," in *IEEE Communication Magazine*, vol. 35, July 1997, pp. 90–100.

[63] ——, "Rayleigh Fading Channels in Mobile Digital Communication Systems Part ii: Mitigation," in *IEEE Communication Magazine*, vol. 35, Sept. 1997, pp. 148–155.

[64] H.-K. Song, Y.-H. You, J.-H. Paik, and Y.-S. Cho, "Frequency-Offset Synchronization and Channel Estimation for ofdm-Based Transmission," in *IEEE Communications Letters*, vol. 4, March 2000, pp. 95–97.

[65] A. Springer and R. Weigel, *UMTS The Universal Mobil Telecommunications Systems.* Springer - Verlag, 2002.

[66] H. Steendam, *The Effect of Synchronization Errors on Multicarrier Systems.* Dissertation. University of Gent, 2001.

[67] H. Steendam, H. Bruneel, and M. Moeneclaey, "A Comparison between Uplink and Downlink MC-DS-CDMA Sensitivity to Static Timing and Clock Frequency Offsets," in *IEEE Transactions on Signal Processing*, vol. 53, OCT. 2005, pp. 3869–3979.

[68] H. Steendam and M. Moeneclaey, "The Effect of Carrier Phase Jitter on MC-CDMA Performance," in *IEEE Transactions on Communications*, vol. 47, Feb. 1999, pp. 195–198.

[69] ——, "Sensitivity of Multicarrier Systems to Stnchronization Errors," in *International Syposium on Signals, Systems and Electronics, ISSSE'01,*, Tokoy, July 2001, pp. 66–69.

[70] ——, "The Effect of Carrier Frequency Offsets on Downlink and Uplink MC-DS-CDMA," in *IEEE Journal on selected areas in Communications*, vol. 19, December 2001, pp. 2528–2536.

[71] P. Stoica and R. Moses, *Introduction to Spectral Analysis.* Prentice Hall, 1997.

[72] J. H. Stott, "The Effects of Frequency Errors in OFDM," in *BBC Research and Developement Report NO.RD*, 1995/15.

[73] ——, "The Effects of Phase Noise in COFDM," in *EBU Technical Review*, Summer 1998.

[74] ——, "The How and Why of COFDM," in *EBU Technical Review*, Winter 1998.

[75] O. Takyu, T. Ohtsuki, and M. Nakagawa, "Frequency Offset Compemsation with MMSE-MUD for Multi-Carrier CDMA in Quasi-Synchronous Uplink," in *IEEE International Communication Conference*, vol. 4, May 2003, pp. 2485–2489.

[76] L. Tomba, "On the Effect of Wiener Phase Noise in OFDM System," in *IEEE Transactions on Communications*, vol. 46, May 1998, pp. 580–583.

[77] S. A. Tretter, "Estimating the Frequency of a Noisy Sinusoid by Linear Regression," in *IEEE Transactions on Information Theory*, vol. IT-31, No.6, Nov. 1985, pp. 832–835.

[78] U. Tureli, H. Liu, and M. D. Zoltowski, "OFDM Blind Carrier Offset Estimation: ESPRIT," in *IEEE Transaction on Communications*, vol. 48, No.9, Sept. 2000, pp. 1459–1461.

[79] J.-J. van de Beek, P. O. Börjesson, M.-L. Boucheret, D. Landström, J. M. Arenas, P. Ödling, C. Östberg, M. Wahlqvist, and S. K. Wilson, "A Time and Frequency Synchronization Scheme for Multiuser OFDM," in *IEEE Journal on selected areas in Communications*, vol. 17, November 1999, pp. 1900–1914.

[80] J.-J. van de Beek, M. Sandell, and P. O. Börjesson, "ML Estimation of Time and Frequency Offset in OFDM Systems," in *IEEE Transactions on Signal Processing*, vol. 45, July 1997, pp. 1800–1805.

[81] S. Verdu, *Multiuser Detection.* Cambridge University Press, 1998.

[82] H. Wang and B. Chen, "A Comparison of the Subcarrier Allocation Schemes for the Uplink OFDMA System," in *2004 Conference on Information Sciences and System*, March 2004, pp. 345–350.

[83] L. Wei and C.Schlegel, "Synchronization Requirements for Multi-User OFDM on Satellite Mobile and Two-Path Rayleigh-Rading Channels," in *IEEE Transactions on Communications*, vol. 43, Feb./Mar./Apr. 1995, pp. 887–895.

[84] S. B. Weinstein and P. M. Ebert, "Data Transmission by Frequency-Division Multiplexing Using the Discrete Fourier Transform," in *IEEE Communications Magazine*, vol. 19, No. 5, Oct. 1971, pp. 628–634.

[85] S. Wu and Y. Bar-Ness, "OFDM Systems in the Presence of Phase Noise: Consequences and Solutions," in *IEEE Transactions on Communications*, vol. 52, Nov. 2004, pp. 1988–1996.

[86] ——, "OFDM Systems in the Presence of Phase Noise: Consequences and Solutions," in *IEEE Transaction on Communications*, vol. 52, No.11, Nov. 2004, pp. 1988–1996.

[87] Z. Wu and B. Caron, "Digital Television Terrestrial Broadcasting," in *IEEE Communications Magazine*, vol. 32, May 1994, pp. 46–52.

[88] G. Xu, Y. Ji, J. Zhang, and P. Zhang, "Adaptive OFDMA Subcarrier Assignment for QoS Guaranteed Services," in *IEEE 61st Vehicular Technology Conference (VTC 2005-Spring)*, vol. 3, Stockholm, Sweden, May/June 2005, pp. 1817–1820.

[89] B. Yang, K. B. Letaief, R. S. Cheng, and Z. Cao, "Time Recovery for OFDM Transmission," in *IEEE Journal on Selective Areas in Communications*, vol. 18, No.11, Nov. 2000, pp. 2278–2291.

[90] W. Zhang, M. A. Dangl, and J. Lindner, "Performance Analysis of the Downlink and Uplink of MC-CDMA with Carrier Frequency Offset," in *Proceeding of Fourth International Workshop on Multi-Carrier Spread Spectrum (MC-SS 2003)*, Oberpfaffenhofen, Germany, Sept. 2003, pp. 259–267.

[91] W. Zhang and J. Lindner, "MC-CDMA in the Uplink: A Transmission Scheme Which Tolerates Frequency Offsets and Frequency Selective Channels," in *Proceeding of PIMRC 2004, 15th IEEE International Symposium on Personal, Indoor and Mobile Radio Communications*, vol. 1, Bacelona, Spain, Sept. 2004, pp. 677–681.

[92] ——, "A Comparative Analysis of CDM-OFDMA and MC-CDMA Systems," in *Proceeding of Fifth International Workshop on Multi-Carrier Spread Spectrum (MC-SS 2005)*, Oberpfaffenhofen, Germany, Sept. 2005, pp. 385–392.

[93] ——, "A Frequency Tracking Scheme for the Uplink of OFDMA Systems," in *10th International OFDM-Workshop*, Hamburg, Germany, Aug./Sept. 2005.

[94] ——, "Modeling of OFDM-based Systems with Frequency Offset and Frequency Selective Fading Channels," in *IEEE 61st Vehicular Technology Conference (VTC 2005-Spring)*, vol. 5, Stockholm, Sweden, May/June 2005, pp. 3072–3076.

[95] Y. Zhao and S. Höggman, "Intercarrier Interference Self-Cancellation Scheme for OFDM Mobile Communication Systems," in *IEEE Transactions on Communications*, vol. 49, July 2001.